A Poloidal Divertor Model for Tokamak Fusion Reactors

A. Mense

January 1977

UWFDM-219

Ph.D. Thesis.

FUSION TECHNOLOGY INSTITUTE

UNIVERSITY OF WISCONSIN

MADISON WISCONSIN

A Poloidal Divertor Model for Tokamak Fusion Reactors

A. Mense

Fusion Technology Institute
University of Wisconsin
1500 Engineering Drive
Madison, WI 53706

http://fti.neep.wisc.edu

January 1977

UWFDM-219

Ph.D. Thesis.

A POLOIDAL DIVERTOR MODEL

FOR

TOKAMAK FUSION REACTORS

by

Allan Tate Mense*

A thesis submitted in partial fulfillment of the
requirements for the degree of

DOCTOR OF PHILOSOPHY

(Nuclear Engineering)

at the

UNIVERSITY OF WISCONSIN

1977

*Present address: Oak Ridge National Laboratory, Fusion Energy Division, P. O. Box Y, Oak Ridge, Tennessee 37830.

A POLOIDAL DIVERTOR MODEL FOR TOKAMAK FUSION REACTORS

Abstract

The work presented here represents a study on magnetic field divertors for fusion reactors. In particular, a model was developed to try to simulate the particle collection effects of a divertor. The model incorporates the effects of an electrostatic sheath at the particle collector plates. This model was incorporated into the plasma transport equations. The entire coupled set of time dependent, nonlinear, particle and energy transport equations, including the divertor model and Maxwell's equations, was solved numerically. The numerical technique used to solve these equations was a Crank-Nicholson differencing algorithm combined with a linearization scheme proposed by Widner and Dory. The fusion reactor plasmas investigated were assumed to have transport properties characterized by the so-called "dissipative trapped particle" modes. The cross field transport in the divertor zone was taken to be Bohm.

The results of the above assumptions are that the plasma edge (separatrix) density is held very low, ≈ 100 times smaller than the center density. The separatrix temperatures are $\simeq 10$ times smaller than center temperatures. The plasma density and electron temperature drop very rapidly in the divertor zone. The ion temperature drops more slowly. The ratio of plasma flux incident onto the wall was $< 10^{-3}$ of the plasma flux diffusing into the divertor zone from the plasma core region. The primary sputtering mechanism of the walls

in the fusion reactor was fast charge exchange neutrals. An entire neutral transport calculation was performed and for the fusion reactors studied, it was found that most of the neutrals (fuel and impurity) coming off of the wall were ionized in the divertor zone, indicating a high shielding efficiency even to hydrogen atoms. In addition, a calculation was made which indicates that the mean residency time of an impurity in the divertor zone may be reasonably short, thus reducing the number which can diffuse into the hot central plasma region. This implies a good "unload" divertor.

The models investigated all had very short particle confinement times and produced exceedingly large particle fluxes to the divertor collectors. No mechanically viable scheme was found to handle such large particle fluxes.

The conclusions drawn from this work are that (ignited) equilibrium solutions can be found to the plasma transport equations even when trapped particle modes are assumed to cause the diffusion and the separatrix density is held low by a divertor. The problems which must now be addressed are: 1) How does one really fuel such a device (pellet injection, DT liquid jets, etc.): and 2) How does one design a mechanically sound particle collection system for the divertor burial chamber?

APPROVED:

_____ _____

Date Major Professor

ACKNOWLEDGMENTS

I have had the pleasure and good fortune to be involved with the fusion technology studies at the University of Wisconsin since its inception in 1970. It was indeed a unique experience to sit through "lectures" on different phases of plasma physics, strength and materials, radiation damage, superconductor technology, etc. with fellow "students" such as D. W. Kerst, H. K. Forsen, C. W. Maynard, R. G. Boom, K. R. Symon, W. Stewart, M. A. Abdou, D. G. McAlees, and the like! To all of these, my fellow explorers in fusion technology, I owe a debt of thanks. Through their questions, and the answering of mine, I have learned a great deal.

During the course of my research work I had the opportunity to work at the Princeton Plasma Physics Laboratory. My studies there were on MHD equilibrium and magnetic field design. Messrs. G. V. Sheffield, U. Christensen, and Drs. John L. Johnson and Dale Meade were instrumental in my learning these areas correctly from the start. I must also extend my sincere appreciation to Dr. Robert G. Mills, a great physicist and engineer, who worked closely with me and helped me through more than one cloudy problem—not all of which were scientific!

At the University of Wisconsin a number of my fellow compatriots deserve mention. They are Drs. J. G. Martín, A. El Nadi, J. Drake and B. Feinberg. In addition, W. Houlberg, M. Khelladi and J. Kesner worked closely with me on the 1-D transport code which was used extensively throughout the latter part of my research. For their

numerical analysis assistance, I am indebted to Drs. Warren Stewart (Chemical Engineering Department), Donald Greenspan (Computer Sciences Department), Louis Rall (Mathematics Research Center), and Glen Myers (Mechanical Engineering Department), all at the University of Wisconsin. I acknowledge also the help provided by the staff of the Madison Academic Computer Center at the University of Wisconsin.

I wish to acknowledge helpful discussions with Drs. H. C. Howe, J. T. Hogan, and J. D. Callen at the Oak Ridge National Laboratory and with Drs. G. L. Schmidt, J. A. Schmidt, and W. M. Tang at the Princeton Plasma Physics Laboratory.

I acknowledge the help and assistance provided by Drs. R. W. Conn, C. W. Maynard, J. Donhowe, R. Boom, and H. Barschall, all of the Nuclear Engineering Department at the University of Wisconsin.

To my thesis advisor, Dr. Gilbert A. Emmert, I owe more than I can repay. His patience, understanding, and critical questioning have aided me immeasurably in my understanding of plasma phenomena. His friendship has meant as much to me as his technical knowledge, and has been an important influence in my life. Nothing more need be said.

My wife, Marcia, who typed the preliminary drafts of this thesis twice, persevered through both her schooling, my schooling, her working, my working, our moving, and my writing. This was an ordeal I am sure she never wants to go through again. She has willingly and lovingly provided the understanding so necessary for the completion of my work. I love her very much.

Thanks must go to Mr. Gene Watkin, technical illustrator, at the Oak Ridge National Laboratory, and most of all to Ms. Caila Cox who deciphered, corrected, punctuated, encoded, decoded, and typed this entire final copy of my thesis, equations and all. Her attention to detail was masterful.

I acknowledge the assistance and support provided by the Wisconsin Electric Utilities Research Foundation, the Oak Ridge National Laboratory, Union Carbide Corporation-Nuclear Division, and the U.S. Energy Research and Development Administration.

TABLE OF CONTENTS

TABLE OF CONTENTS (Cont.)

CHAPTER I

Introduction

One of the key objectives in current tokamak fusion research is impurity control.[1] By control, one means the production, ionization, transport and collection of all $z > 1$ ions and atoms. In present day devices impurities are thought to have both good and bad effects on tokamak discharges.[2] For future reactors one cannot say for sure what overall effects impurities may have until one unravels their transport characteristics, i.e., diffusion, thermal conduction, resistance effects, etc., but, undoubtedly, it is safe to infer that their control will be essential!

There have been postulated a number of possible impurity control techniques. Some methods, such as inverting the fuel ion density gradient at the plasma edge, represent somewhat transient types of solutions.[3] Other methods are of the more steady state variety: the magnetic field divertor[4] and the cold neutral blanket[5] are the most thought of examples along this line. The research and findings presented herein represent a theoretical study of one possible impurity control method for tokamaks—the poloidal magnetic field divertor.

Before proceeding with a detailed description of how one envisions a divertor and its workings, a brief outline of the contents of this report is in order.

The remainder of this chapter will be devoted to defining terminology and outlining salient divertor features. Chapter II then gives

a brief review of current thoughts on how impurities appear to affect tokamak plasmas both from a stability and an energy balance point of view. Chapter III outlines the MHD equilibrium and stability considerations and the magnetic field design. Chapter IV describes some early (circa 1969-1970) transport models used in divertor analysis. Solutions, mostly analytic, are given and discussed. Chapter V presents the more advanced one-dimensional work on plasma transport with a divertor. It includes a description of the numerical technique chosen to solve the problems as well as the initial and boundary conditions used. Chapter VI displays the results of this computer code for three types of tokamak fusion reactors: 1) UWMAK-II, the model of a large (5000 MW_{th}) fusion power reactor,[6] 2) UWMAK-III, a scaled down in size (but not in power) version of UWMAK-II,[7] and 3) a typical EPR (few hundred MW_{th}) prototype fusion reactor.[8] In Chapter VII the work is summarized, conclusions are formulated, and recommendations for future work are discussed.

Divertor Descriptions

Historically, the first divertor was a device, proposed by Lyman Spitzer, Jr.,[9] for avoiding contact between the hot plasma and the first material wall surrounding the plasma. Spitzer's idea, as shown in Fig. I-1 illustrates how this was accomplished in a stellerator. A set of external coils were programmed in such a manner as to produce a locus of nulls in the toroidal magnetic field. This locus of nulls generates what is called a separatrix surface. Field lines outside

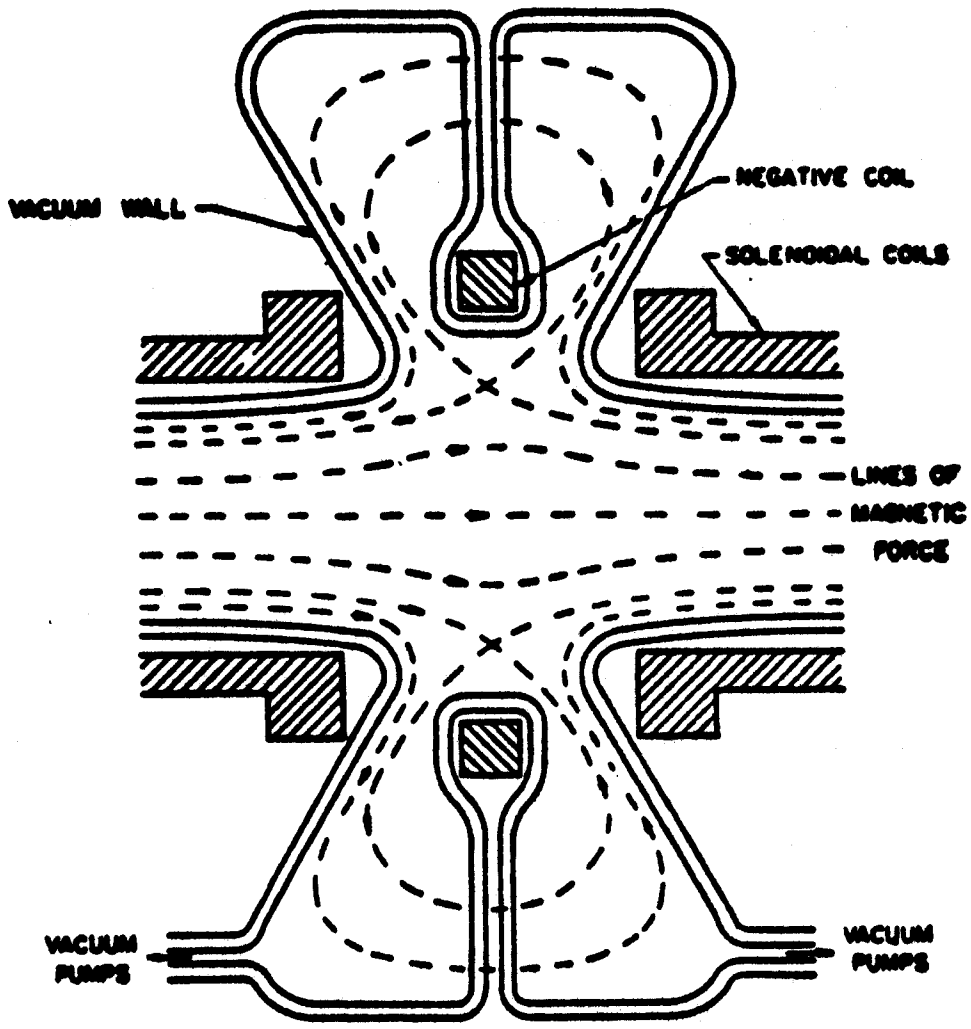
VACUUM WALL
NEGATIVE COIL
SOLENOIDAL COILS
LINES OF
MAGNETIC
FORCE
VACUUM
PUMPS
VACUUM
PUMPS

Figure I-1

this separatrix are 'diverted' away from the proximity of the plasma core region (away from the first wall too!) and into a chamber where plasma collection and neutral gas pumping can be more readily managed. Magnetic flux surfaces on the inside of the separatrix remain closed within the main plasma volume.

The separatrix is sometimes referred to as a magnetic limiter, but it should be emphasized that it does not define the edge of the plasma in terms of density. It only denotes a demarcation surface beyond which there is no current flow, i.e., $\vec{J}=0$. The region between the separatrix and the first wall is often called the scrape-off zone. In this report it will be called simply the divertor zone. The plasma density in this zone is established by a balance between 1) the plasma diffusing across the separatrix from the plasma core region plus the ionization of neutrals coming off of the walls and refluxing back from the particle collection chamber, and 2) the loss of plasma due to flow (called effusion) along the field lines to the collectors.

Several different types of divertors are shown in Fig. I-2. The first is a toroidal divertor. This type of divertor is produced by generating a null in the toroidal magnetic field. It was used on stellerators in the 1960's. The chief advantage of this type of divertor is that it does not depend on the presence of a plasma current in order to function as a particle collector. The following disadvantages present themselves. First, to preserve topology one must have coils encircle the plasma in the poloidal direction. This places hardware in the central core of the torus where things are already crowded. Since one wishes to position the plasma as close to

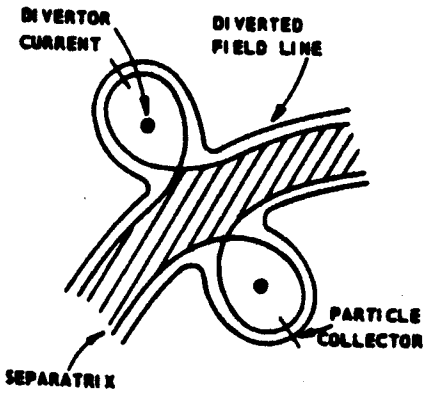

TOROIDAL DIVERTOR
(TOP VIEW OF TORUS)

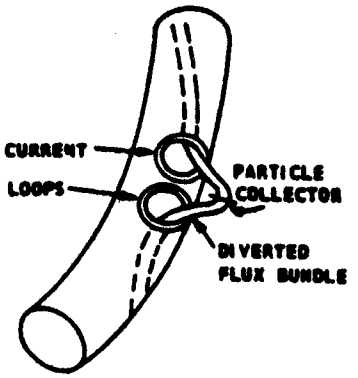

BUNDLE DIVERTOR

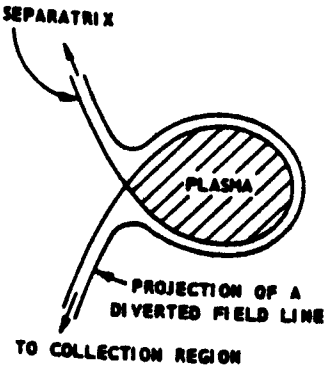

SINGLE NEUTRAL POINT
(CURRENTS NOT SHOWN)

POLOIDAL DIVERTORS

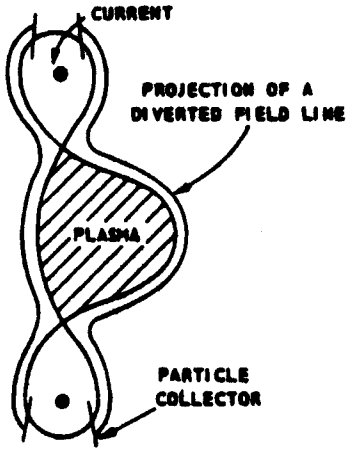

DOUBLE NEUTRAL POINT
(NOT ALL CURRENTS SHOWN)

Figure I-2

the maximum toroidal magnetic field as possible for cost effectiveness and this type of divertor arrangement forces the plasma to a larger major radius, one is lead by implication to greater expense. Also, the coils, to be economically operated in a (low β) fusion reactor, must be superconducting. Once placed behind a one to two meter thick neutron/gamma-ray shield, the current requirements for these coils are extremely large which, in turn, dictates a large coil cross section, high stresses and bending moments, and thus high cost. A toroidal divertor also destroys, in the strongest way possible, the axisymmetry of the tokamak. As higher temperatures are reached, the breaking of axisymmetry leads to unconfined particle orbits and thus particle loss. [10] This loss usually produces 'hot spots' on the surfaces where the particles deposit. This may not only adversely affect the plasma purity, but can be deleterious to first wall lifetime. Thus, toroidal divertors initially appear unattractive for tokamaks.

A variation of the toroidal field divertor is the so-called bundle divertor (Fig. I-2) recently installed on the DITE tokamak. [11] Two opposing current loops adjacent to each other divert a 'bundle' of magnetic flux. The main additional advantages (over that already outlined for a toroidal divertor) of this approach are that only minor perturbation ($\sim 1\%$) is produced in the magnetic field at the center of the plasma, and the coils for producing the separatrix null are on the outer side of the torus and thus away from the already crowded central region. However, its disadvantages are that, in addition to destroying the tokamak's asixymmetry, theoretically this type of

divertor also unravels the nested flux surfaces because it destroys the topology of a torus entirely.[12] This may or may not bother the plasma and remains to be seen. Its use on a fusion reactor can be questioned due to the large currents necessary to drive the toroidal field null. These currents, even if allowed to reside close to the reactor first wall, may produce significant structural problems. If the coils are to be of the superconducting variety, they would have to be well shielded which may be impossible to do at a reasonable cost.

Figures I-2c and I-2d represent cross sections of two proposed poloidal magnetic field divertor configurations.[6,13] The poloidal divertor, as its name implies, diverts the poloidal magnetic field (which is typically a factor of 10 smaller than the toroidal field) using toroidal current carrying coils. They may or may not be located outside the blanket and shield region.* This type of divertor has been used on the DIVA [14] tokamak and on the FM-1 spherator.[15] The configuration in Fig. I-2c is presently used on DIVA with no deleterious effects.[16] Recent studies tend to favor the double null design of Fig. I-2d,[17] which has been the favored design for the UWMAK reactors. In addition, it is one of the many possible configurations to be tried on PDX.[18]

The poloidal field divertor has the advantage of preserving, as well as one can, the axisymmetry of the tokamak. It also provides a comparatively large particle collector area. A major disadvantage

*One may even be able to place them outside of the TF coils.

is that it requires that the plasma current be present in order to drive a null in the poloidal field to produce the diverted field lines. During start up, the plasma near the wall recycles many times before any type of 'steady state' is reached and since this recycling can release impurities which can move into the plasma, one must still ascertain experimentally whether or not a poloidal divertor can be 'switched on' soon enough to effectively control the initial surge of impurities into the system. This is discussed in more detail in Chapter II.

With the above brief outline of the different divertor classes, it can be seen that, provided poloidal divertors are effective enough to allow the plasma discharge to ignite, then they are the natural choice for tokamak reactors. The engineering problems involved in including such a device inside the toroidal field coils are formidable. Detailed mechanical design studies are only now getting under way.[19]

[12] J. B. Taylor, Culham Rept. CLM-R132 (1974).

[13] R. G. Mills, Princeton Plasma Physics Lab. Rept. MATT-1050 (1974).

[14] H. Maeda et al., Nuc. Fusion 16, 148 (1976); see also M. Yoshikawa et al., listed in Ref. [4].

[15] J. A. Schmidt, private communication on FM-1.

[16] H. Meada, loc. cit.

[17] A. M. M. Todd, S. L. Gralnick, H. E. Dalhed, "Sixth Symp. on Eng. Prob. of Fusion Research," San Diego (Nov. 1975); see also Princeton Plasma Physics Lab. Rept. MATT-1199.

[18] See D. M. Meade, listed in Ref. [4].

[19] Mechanical design work is currently being carried out by an ORNL/ Westinghouse team as part of ORNL TNS study group.

CHAPTER II

Impurities

When one considers impurities in a tokamak reactor, one must be concerned with their origin, rate of influx into the hot plasma core, and their effect on plasma behavior. The study of impurity behavior in tokamaks is only in its infancy and a great deal more must be learned before accurate quantitative estimates can be made of their effects.[1] Nevertheless, it is appropriate to outline briefly some of what is presently known about impurity evolution with the understanding that this knowledge is somewhat ephemeral in nature. For a more complete review than will be presented here, the papers of Behrisch,[1] Behrisch and Kadomtsev,[2], Colchin, et al., [3] and Schwirzke[4] are recommended.

The present state of knowledge as to exactly how impurities behave in a tokamak discharge is meager. The reasons for the meagerness have mostly to do with the experimental detection techniques for impurities. Colchin, et al.[3] describe fairly lucidly where the experimental uncertainties lie and come to the conclusion that the impurity content in the plasma (particularly of high Z material such as Au, Mo, and W) is not discernible to within a factor of 5. Also, experimental results reported by different groups differ in their belief of whether impurities build up in the plasma as a function of time or whether they diffuse out rapidly enough to maintain some steady value. Hogan contends that one can explain both these

observations (self-consistently) when the levels of MHD turbulence brought about by the impurity effects themselves are included in the analysis.[5] This will be discussed more thoroughly later. A forthcoming document[4] from ERDA entitled, "Impurities in Tokamaks," which was compiled and edited by F. Schwirzke addresses most of the relevant impurity problems (but gives few if any solutions) and should stand as the authoritative review for the near future at least.

Rather than paraphrase this report, which is over 60 pages in length, only the most salient features will be covered. They are: 1) impurity groupings, 2) impurity effects, 3) impurity origins, 4) impurity release mechanisms, 5) impurity levels in present day experiments, 6) proposed impurity control methods, and 7) impurity accumulation questions.

Impurity Groupings

The impurities which appear in present day tokamaks can conveniently be broken into roughly three groups. Low Z impurities such as carbon and oxygen fall into the first group. Intermediate Z materials such as Si, Al, Ni, and Fe compose a second group, and higher Z elements like molybdenum, gold, and tungsten make up the third group. These groupings are prompted by energy balance considerations, i.e., the low Z materials can be fully stripped in present day tokamaks, most of the intermediate Z atoms are not (or just barely) fully stripped in present devices, but will certainly be so in the centers of future high temperature reactors, and the high Z materials will, in all likelihood, never be fully stripped

even in future reactor grade plasmas.

Impurity Effects

Impurities can affect the plasma in many ways. They can 1) enhance bremsstrahlung radiation, 2) produce line and recombination radiation, 3) produce a "fuel ion defect" for a given maximum allowable β, 4) produce current channel shrinkage and thus promote MHD turbulence, 5) increase plasma collisionality which can reduce some microinstability turbulence and 6) create the possibility for new microinstabilities due to the impurity density gradient itself. All of the above effects can ultimately affect both the ignition requirements* for a tokamak and whether or not the requirements can be met with a reasonable amount of input power.

The most easily explained impurity effect is the enhancement of the classical bremsstrahlung radiation rate [6]

$$P_{Brem} = \frac{4}{\pi\sqrt{3}} g_{ff}\left\{\frac{4}{3}\pi^2\left(\frac{2}{\pi}\right)^{1/2}\left(\frac{e^2}{4\pi\epsilon_0 C}\right)^3 \frac{n_e \sum_{j}^{ions} n_j z_j^2}{m_e^{3/2}\hbar}(kT_e)^{1/2}\right\}\frac{w}{m^3} \qquad (2.1)$$

$$= 1.5 \times 10^{-32} Z_{eff}\, n_e^2\, T_e^{1/2} \text{ watts/cm}^3$$

where n_e is in units of $\#/cm^3$ and T_e in eV in the last expression in (2.1). This Z_{eff} enhancement is usually of negligible importance in the overall plasma energy balance compared to other loss channels.

*Ignition is taken to mean the condition whereby the fusion alpha particle energy plus ohmic heating just balances all the energy losses from the plasma.

The second effect impurities produce in the energy loss category is line (de-excitation) and recombination radiation. In principle, one should determine the charge state and excitation state within that charge state for each impurity species in the plasma as a function of position in the plasma and time. Unfortunately, even if the required reaction rates and transition probabilities were available, and they are not,[7] one would have a tremendous "bookkeeping" problem in keeping track of all the states in order to determine the power loss. In actual fact, one makes some approximations. Time dependent modeling of low Z impurity radiation has been done for C and O.[8] Some coronal equilibrium work with iron has also been reported.[8] The transitions for Au, Mo, and W are not well known and little has been done to date in including these impurities radiation losses except in some very approximate ways. One approximation is to use the work of Hopkins.[9] He reviewed earlier works and came up with a "fit" to the data for $Z < 18$ impurities. His expression is

$$P_{Rad} = P_{Brem}\left(1 + \underbrace{\frac{37.9\,\xi_z Z^4}{Z_{eff}\,T_e}}_{\text{recomb.}} + \underbrace{\frac{855\,\xi_z Z^6}{Z_{eff}\,T_e^2}}_{\text{line}}\right)\frac{\text{watts}}{\text{cm}^3} \qquad (2.2)$$

where P_{Brem} is given by (2.1). The factor of unity in (2.2) represents the classical bremsstrahlung. The terms in the parentheses are recombination and line radiation, respectively. Formula (2.2) is only valid for impurities in coronal equilibrium. Hopkins stipulates that (2.2) is probably only good to within 100% or so and has been derived based on results for atoms having $Z < 18$. Merts, et al.[10] have done

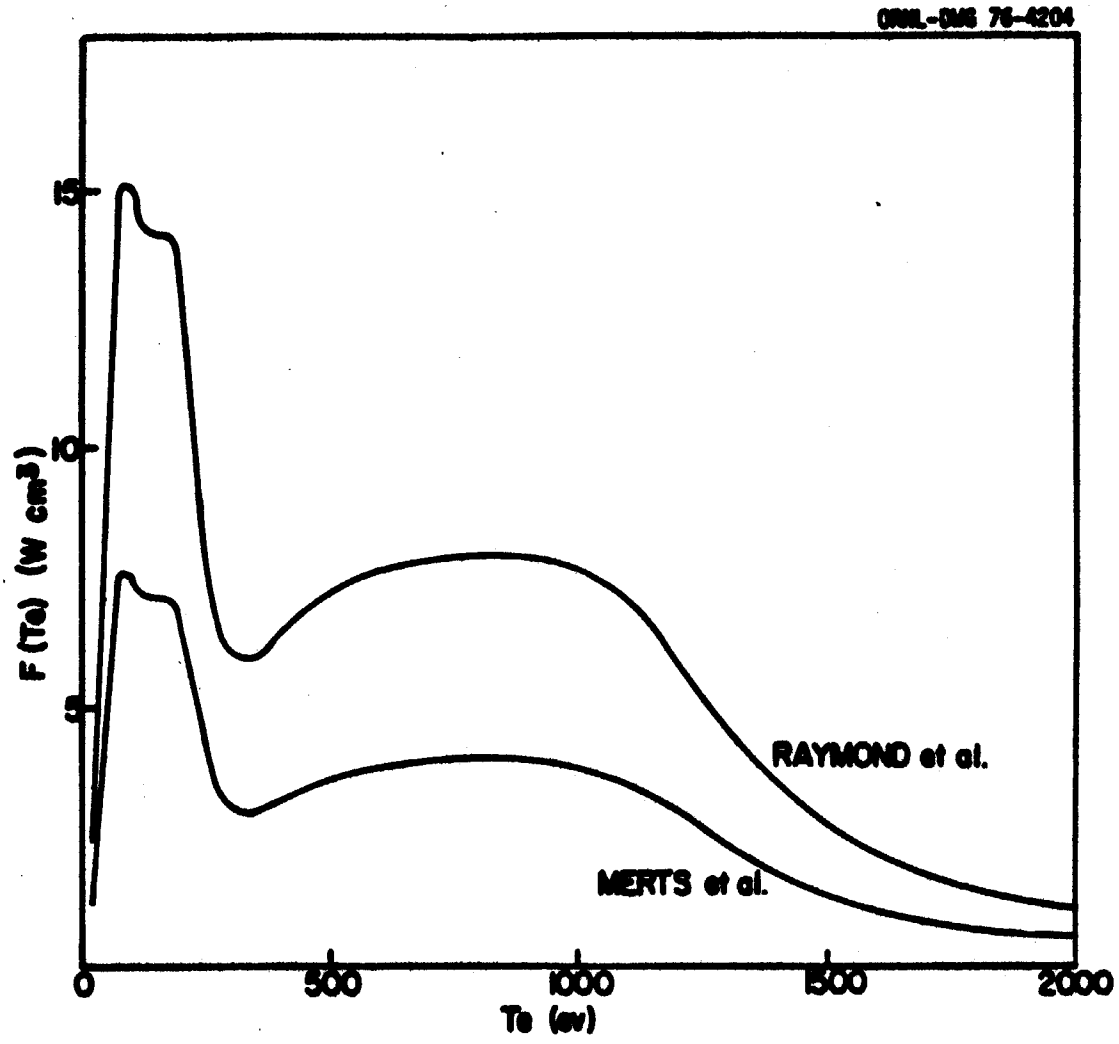
ORNL-DWG 76-4204
15
10
5
F (Te) (W cm³)
RAYMOND et al.
MERTS et al.
0
500
1000
1500
2000
Te (ev)

Figure II-1

some work on iron and using some experimental and some theoretical data have produced a (coronal equilibrium) radiation loss formula for iron of the form

$$P_{Rad} = 10^{-26}\, n_e n_{Fe}\, F(T_e)\, \frac{\text{watts}}{\text{cm}^3} \qquad (2.3)$$

where n_e, n_{Fe} are the electron and iron (sum of all charge states) densities in $\#/\text{cm}^3$. The function $F(T_e)$ is shown in Fig. II-1 and is ≈ 4 for 1 eV $< T_e <$ 1 keV and drops to 1 for $T_e >$ 1.5 keV. Hinnov has tended to propose the formula

$$P_{Rad} \simeq 1.2 \times 10^{-26}\, n_e n_Z$$

for use with high Z materials in general. There is, to this author's knowledge, no such formula comparable to (2.3) for the high Z atoms such as Au, Mo, and W. Some of the most recent DIVA (JFT-2a) data does, however, seem to indicate that Au may be responsible for essentially all of the electromagnetic radiation leaving the plasma.[11] This would indicate a need for a formulation such as (2.3) for high Z materials.

In fusion grade plasmas there are other impurity effects of interest. In order for ignition to occur, $n_i^2\langle\sigma v\rangle/4$ must be sufficiently large to produce a sustaining reaction. If one agrees that there must be some maximum allowable β^*(≡ average plasma pressure

*There may be some disagreement as to what the maximum value of β can be, but there is certainly no doubt that there is some maximum allowable value.

divided by $B_0^2/2\mu_0$ where B_0 = vacuum toroidal field at the magnetic axis) at which the plasma can stably operate, then since

$$\bar{p} \equiv \frac{1}{v}\int_{\substack{\text{volume}\\ \text{of}\\ \text{plasma}}} (n_e T_e + n_i T_i + n_\alpha \frac{2}{3}\bar{E}_\alpha + \sum_{j}^{\text{impurities}} n_j T_j)dv$$

one easily sees that if a reasonable fraction of $\bar{p}$ is due to species other than the fuel ions that $n_i^2\langle\sigma v\rangle/4$ is correspondingly reduced. This reduction in the fuel ion density (for a fixed maximum β) is called the "proton defect" and if this defect becomes too large, the power production capability of the plasma can be considerably diminished.

Another impurity effect which may already be manifesting itself in present day discharges is MHD turbulence. As impurities enter the discharge, they tend to cool the edge region. Since most of the current flow in low β_p devices is due to conduction current ($J = \sigma E \propto T_e^{3/2}$), a lowering of T_e due to radiation tends to cause the "current channel" to shrink in radially. This shrinkage changes the $q(\psi)$ profile and can cause $q(r=0)$ to drop below 1 which may cause MHD oscillations (turbulence) to set in. If the impurities can reach the center of the discharge, due to diffusion, before they strip to a charge state in which they radiate ferociously then the central electron temperature can be diminished and hollow T_e profiles can develop. This would flatten out the $q(\psi)$ profile and possibly ameliorate the MHD behavior. Hogan contends that a slow impurity influx rate may not cause severe current channel shrinking and therefore

inward diffusive effects may outweigh any fine scale MHD turbulence which would tend to spread the impurities out.[5] On the other hand, large impurity influx rates would tend to cause severe edge cooling, sharp current channel shrinkage, and stimulate stronger MHD turbulence whose consequence is to cause the impurities to be spread out across the plasma counteracting any neoclassical peaking effects.

The collisionality of the plasma is of course effected by the presence of impurities. Increasing the collisionality in regions where there are many trapped particles should tend to retard the onset and reduce the consequences of the so-called dissipative trapped particle modes.

As there seems to be an instability for every purpose, there is the potential at least to have an impurity-drift instability when the fuel ion density gradient is opposite to the impurity density

The consequences of such a mode have been the topic of some fairly recent work.[13] It may help transport out impurities.

All of the above mentioned effects can alter the achievement of an ignition condition in a tokamak. Radiation losses effect the electron energy balance which, due to the reasonably high density operation of a tokamak reactor ($\bar{n} \approx 10^{14}$ #/cm^3), couples to the ion energy balance very quickly. The enhancement of MHD turbulence affects both the particle and energy containment times in the plasma which, of course, implies an increased need for fusion events to balance the energy losses and high fueling rates to keep the density up. The "proton defect" problem is one which will be addressed later

in connection with divertor shielding, but it is clear that any "proton defect" is bad in the sense that there is less available power for a given allowable plasma pressure.

During beam heating, or if operated in a TCT mode, a high impurity content near the plasma edge can cause unfavorable beam deposition profiles.[14] This can lead to an ineffective operation scenario and/or a total lack of sufficient central plasma heating to ignite the reactor.

In addition to the unfavorable effects of impurities which have been mentioned above, there are a few "good" impurity effects. First, electromagnetic radiation is probably the least detrimental way of putting the plasma (alpha particle) energy onto the walls. With the exception of photon desorption of oxygen and/or photo-electron emission from the walls, which could release some adsorbed gases, the consequences of EM energy on the walls are mild. In fact, EM radiation will be "uniformly" incident on the walls and this avoids local "hot spots" as might occur in some types of particle transport. A second beneficial effect is the added collisionality which may help to prevent or reduce microinstability turbulence and the resultant transport processes. Thirdly, the impurity content may be one of the most effective agents in preventing a "skin effect" during start up although the charge exchange and hydrogen ionization process may also keep the edge temperatures low enough to prevent a skin condition.

With the above facets in mind, it is best to proceed on to the understanding of where the impurities may evolve.

Impurity Origin

Carbon and Oxygen: These are the most prevalent impurities in present day tokamaks. They are thought to reside on the metallic surfaces (walls and limiter) as carbides and oxides. They can evolve from metallic surfaces as CO_2, O_2, CO, H_2O, or CH_4 to note just a few. Both carbon and oxygen appear in a typical discharge at very early times.* The carbon concentration can be reduced to negligible levels (< .1%) through the use of discharge cleaning techniques.[3] H_2O can be pumped out by baking the chamber walls and ports.[3] As oxygen binds very tightly to stainless steel, it is very hard to remove even using discharge cleaning. As a consequence, oxygen is usually the most abundant low Z impurity in present day tokamaks. It is not accurately known at what rate oxygen impurities accumulate in the plasma during the course of a discharge. In fact, ORMAK data can be interpreted to indicate that they may not collect at all,[15] but may enter, ionize, and once having reached a high charge state (say O VIII) they may leave the discharge (by an as yet unknown mechanism), recombine at or near the wall, and reenter the plasma as neutral oxygen. There is no evidence to either confirm or deny this hypothetical recycling behavior! This hypothesis may, however, be used to explain the low edge electron temperatures.

*They can be released by any one or many of the following mechanisms: 1) plasma bombardment, 2) charge exchange neutral bombardment, 3) direct photon desorption, 4) photo-electron desorption, 5) thermal desorption due to local heating of the surface.

Lithium: This element is not seen in present tokamaks, but is likely to appear in future devices if magnetic field divertors are used whose field lines terminate in lithium collection plates. Since Z = 3, lithium would be less of a problem than oxygen even if some does get into the hot plasma core. In any case, it is unlikely, with a properly engineered particle collection chamber, that anything but ionized lithium could escape the "burial" chamber. Once ionized, the probability is high that it will be heated and returned (along the field lines) to the collection plates rather than diffuse across the B field lines into the plasma core. This will be discussed in Chapter VI.

Silicon: Only trace amounts of Si appear in present day devices, but much more may appear (along with more carbon) if SiC is used as a wall and/or limiter material. This has been proposed by the people at General Atomic.[16]

Aluminum, Nickel, Iron: These intermediate Z materials are the major or minor constituents of the most commonly proposed structural materials. They can be released to the plasma due to sputtering either by plasma or (more probably) charge exchange neutrals. The sputtering threshold energies are usually O(70 eV) so that it is hard to believe that present day plasma "edge" temperature ions ($T_i < 100$ eV) would be responsible for sputtering much of this from the walls. Charge exchange neutrals from the plasma interior, runaway electrons, or untrapped neutrals from neutral beam heating do have enough energy to cause sputtering. If Fe can be tied up as $Fe[CO]_X$ gas, then Fe can

get in by desorptive processes! Once Fe, for example, enters the discharge, it can produce very large amounts of line radiation. This cools the electron population.

Molybdenum, Tungsten: These materials are used as limiter materials primarily due to their low sputtering yields (from proton bombardment), high heat capacities, and high melting points. Limiters are usually found experimentally to "take a beating" in that runaway electrons whose orbits shift outwards from the plasma center have been known to intercept the limiter and produce "hot spots."[17] This local vaporization of high Z material and its subsequent entrance into the discharge could prevent ignition.[18] In addition, since the limiter material apparently gets "plated" onto the chamber walls,[3] one must be concerned with whether or not it can be more easily released from the wall surfaces than it could have been residing in its own structural matrix. This information is apparently not readily available at this time. One way of alleviating the problem of surface vaporization of the limiter due to runaway electrons is to use some type of low Z material, such as graphite. The range of runaway electrons ($E > 1$ MeV) in low Z materials is such that their energy can be deposited throughout the limiter volume and not just at the surface. The use of a divertor may also alleviate the need for a limiter and thus resolve this problem. Having touched upon the (assumed) origins of some of the impurities in tokamaks, it seems appropriate to indicate how present day experiments fair with regard to impurity content.

Experimental Devices

Present day devices seem to fall into one of two classes: the "clean machines" (Alcator and Microtor) and "all others."[4] Alcator is the best diagnosed of the clean machines and its x-ray spectra show prominent lines at low densities ($n_e \sim 1\text{-}3 \times 10^{13}$ cm^{-3}) but less prominent lines at higher densities. ORMAK scaling[19] seems to imply that $Z_{eff} \sim 1/n_e$ so Alcator's cleanliness may be due to its high density operation. TFR has attempted to run up to Alcator densities but without success.[20] The Z_{eff} values claimed in Alcator are between 1 and 2. Most other machines have $3 < Z_{eff} < 10$ although ATC was able to attain $Z_{eff} < 2$ after evaporating titanium onto 25% of its first wall. The Impurities Studies Experiment (ISX), being built at the Oak Ridge National Laboratory, has been designed with enough flexibility so as to allow careful diagnosis of impurity influx and testing of control techniques.

Impurity Control Techniques

A number of possible techniques have been proposed for controlling impurity influx into the hot plasma core region. The "passive" techniques will be discussed first.

Honeycomb Walls - This concept has been investigated in a preliminary manner at the Oak Ridge National Laboratory.[21] It entails producing (by etching, for example) a surface with "pockets" in it such that most of the incident charge exchange neutrals (and plasma ions) produce sputtered material which tends to replate inside the "pocket" rather than escape. It was shown by Monte Carlo calculations

that a reduction in the effective sputtering yield of as much as 4 to 5 might be achievable. Whether or not the walls of the honeycomb will be preferentially erroded away has not been analyzed to date

Carbon Curtain - The concept of using a woven carbon fibre curtain draped in front of the first wall in a fusion reactor was proposed at the University of Wisconsin.[22] The underlying premise which goes with the idea is that is is more advantageous (from an energy loss point of view) to have low Z impurities in the discharge than to have high Z ones. What really must be assessed is the product of the number of carbon atoms which enter the discharge times their effect on the discharge energy balance versus the same product for the case where no curtain is used. The total impurity sputtering rate depends on the plasma (electron + ion + cx neutral) energy flux* to the first wall (and limiter if a divertor is not used).[23] The energy flux in turn depends on the plasma "edge" temperature which is effected through the energy balance equations (i.e., radiation, charge exchange, etc.) by the impurity content. One thus finds that the determination of whether one should use a low Z on higher Z first wall cannot be determined short of solving (self consistently) the plasma plus impurity particle and energy balance equations. This is no simple problem!

*By energy flux, one means the product of the energy of each incident particle on the wall times its velocity and integrated over all incident particles.

Silicon Carbide on First Wall - This idea was proposed by the study group at General Atomics.[16] Again it must be assessed in the same vein as the carbon curtain concept outlined above. Silicon Carbon does, however, have some structural integrity and possibly a lower sputtering yield.

Discharge Dynamics - By discharge dynamics, one means the careful control of the physical position of the plasma column during all phases of the reactor cycle,* e.g., startup, burn, and shutdown. It is presently believed that during the breakdown phase of the discharge when the plasma is not yet in mechanical equilibrium with the magnetic fields, that plasma incident onto the walls produces the initial "charge" of impurities which are seen spectroscopically from the earliest times in the discharge cycle.

Careful positioning during the breakdown phase may reduce the initial impurity content in the reactor. Careful control during the shutdown may prevent vaporization of metallic impurities which could subsequently be tied up in some type of gas phase that could be easily released during the breakdown phase of the next cycle. In other words, poor initial control can lead to ever-worsening impurity problems.

Wall Conditioning - A point to be learned from Alcator is that preparation of the first wall before a discharge is ever created may be significant in reducing impurity influx. The importance of this

*In addition, if one has a magnetic field divertor, one must control the position of the diverted field lines.

is only now being investigated. Wall preconditioning by baking and discharge cleaning appears very important.[4]

There are a number of other measures which one can take (or the plasma itself will take) to control impurity influx. The following techniques take advantage of certain properties of the plasma itself, i.e., its transport behavior, etc.

Inverted Plasma Ion Density Gradient - As has been proposed,[24] one might at least on a transient basis cause the fuel ion density gradient to reverse in sign, i.e., point toward larger minor radius values. This is accomplished by puffing neutral gas in at the "edge." The subsequent ionization of these neutrals can cause an inverted ion density gradient and if the impurity ions behave neoclassically, they should diffuse up this ion gradient and thus be carried out of the hot plasma core region. If there is significant turbulence present, then diffusion due to the turbulence may completely override any neoclassical effects. This, however, remains to be seen.

Gradient T Screening - In performing neoclassical kinetic theory calculations using three species (electrons, ions, one impurity charge state), one finds in the particle and energy balance equations that the particle flux, for example, contains terms proportional to ∇T_i. These terms appear only when terms on the order of (ion mass/impurity mass) are retained in the expansion procedure used to solve for the fluxes.[25] These ∇T_i terms also appear in such a fashion that for a normal temperature gradient ($\nabla T < 0$), they cause the inward impurity flux to be reduced or even reversed if ∇T is strong

enough. This temperature screening may aid, but again only if turbulent transport processes are not dominant.

Impurity Flow Reversal - Ohkawa[26] has noted that if the fuel ions could maintain a net parallel flow velocity in the proper direction that the ion-impurity friction force balance (i.e., fuel ion-impurity ion collisions) would cause a net outward flow of the impurities. This is again based on neoclassical theory and, of course, depends on being able to create the net ion flow. This concept will be the first major experiment on ISX.[27]

Dense Cold Gas Blanket - The cold gas blanket idea has been around for a number of years.[28] From the published work it appears that very high plasma densities ($n > 10^{15}$ #/cm^3) are required and high neutral densities also. For a power producing (ignited) fusion reactor, this poses considerable problems in terms of fueling to maintain ignition, and at these high densities, an ignition machine ($T > 6$ keV) would be very high β for most reasonable magnetic fields. In all fairness the concept has not been closely scrutinized in terms of application on a high density tokamak reactor and probably does deserve more attention.

RF Heating - In theory, one might be able to selectively heat impurities using RF heating and thus cause them to preferentially leave the discharge. If these impurities can be collected in some manner (say, by a divertor) so that impurity sputtering of the metallic surfaces in the near vicinity of the plasma core could be minimized, then this scheme may be of some value. Nothing has been

published on this scheme to date.

Divertors - Finally, one notes that magnetic field divertors (toroidal, "bundle," and poloidal) present one possible alternative for cleaning the plasma. Not only might it be effective in transporting ionized impurities to collector chambers remotely positioned from the plasma, but it also can serve the function of incident impurity shield (as will be demonstrated in Chapter VI) and collector of runaway electrons. These features will all be covered in Chapters V, VI, and VII.

Finally, a few words should be said on the question of impurity accumulation. As was noted earlier, one can supply a plausible explanation for the apparent diversity of experimental results on whether or not impurities tend to accumulate in present day tokamaks. The argument, based on weak (or strong) excitation of MHD turbulence, depends on whether "small" (or "large" amounts of impurities influx in a short period of time. If turbulence does spread out the impurity concentration, it does us some good to collect those impurities (i.e., divertor) rather than allow them to impinge on nearby metallic surfaces. It has been shown by Emmert[22] that one can effect the principle eigenvalue in the particle diffusion equation through the insertion of a divertor collection term (not too surprising) and this equation should lead to an overall lower steady state level of impurities. If the level can be kept "low enough" in the central portion of the plasma where most of the fusion events are taking place and if adequate replenishment of spent fuel can be supplied

(either by inward diffusion of fuel ions or by pellet or beam injection) then ignition can be maintained. This implies that the alphas produced by fusion events must diffuse with some reasonable multiple of the fuel ions (central) containment time. The question of exactly how long a reactor would remain ignited (and stable) if the alphas did not diffuse depends on the details of the reactor design geometry (e.g., minor radius), but some estimates show that a 1.5 meter minor radius, reasonably high density ($\bar{n} \sim 10^{14}$ #/cm^3) ignited reactor would burn for on the order of 100 to 200 seconds before deigniting.[29] This result was based on the assumption that the fuel ions diffuse on a time scale consistent with the use of the so-called trapped particle mode diffusion coefficients, but at 1/10 of their "published values."[30] This is only one possible model of plasma behavior, however, and should be judged as such.

In general, one can say that impurities should not be allowed to accumulate in the central core region of the plasma. If by some magic, one could contain the impurities near the plasma edge so as to form a radiation "halo"[31] then some of the alpha energy can be harmlessly deposited on the first wall. This high Z halo, however, must not be allowed to form if beam heating is to be used as it would then produce very unacceptable heating profiles and may, in fact, lead to instability.[14] Much remains to be learned in this area before accurate (numerical) predictions can be made of reactor behavior.

CHAPTER II

Bibliography

[1] R. Behrisch, Nuc. Fusion 12, 695 (1972).

[2] R. Behrisch and B. B. Kadomtsev in "Fifth IAEA Int. Conf. on Plasma Physics and Controlled Fusion Research," Tokyo (1974), paper #CN-38/S2.

[3] R. J. Colchin et al., "Proc. of Int. Conf. on Surface Effects in Controlled Fusion Devices," San Francisco (1976), to be published in J. Nuc. Mat.

[4] F. Schwirzke, Ed., "Impurities in Tokamaks," to be published as ERDA report.

[5] J. T. Hogan, private communication.

[6] G. V. Marr, Plasma Spectroscopy, (Elsevier Pub. Co., London, 1968), p. 223.

[7] R. Isler, private communications; see also references with E. C. Crume in 1975 Annual Report of the Thermonuclear Division, ORNL-5154, Oak Ridge (June 1976).

[8] D. Duchs, H. R. Griem, Phys. Fluids 9, 1099 (1966); see also H. R. Griem in "Atomic Data for Fusion," 1, 9 (1975); also private communication with E. C. Crume, ORNL; see also A. L. Merts, R. D. Cowan and N. H. Magee, Jr., Los Alamos Rept LA-7220-MS (March 1976); see also J. C. Raymond et al., Wisconsin Astro. Rept. 12 (1975).

[9] G. Hopkins, General Atomics Rept. GGA-12374 (Oct. 1972); see also "Fifth Int. Conf. on Plasma Physics and Controlled Nuclear Fusion Research," Tokyo, 1974 (IAEA, Vienna, 1975), Vol. II, p. 275.

[10] A. L. Merts, Los Alamos Rept. LA-6220-MS (March 1976).

[11] H. Meada et al., in "Proc. of Sixth Int. Conf. on Plasma Physics and Controlled Nuclear Fusion Research," Berchtesgaden (1976), Paper #CN-35/A-18.

[12] B. Coppi et al., Phys. Rev. Lett. 17, 377 (1966); see also K. T. Tsang, ORNL/TM-5287 (May 1976 - submitted to Nuc. Fusion).

[13] J. D. Callen and K. T. Tsang, private communication.

[14] J. T. Hogan and H. C. Howe, to be published in J. Nuc. Materials.

[15] R. Isler, private communication.

[16] General Atomics Co. Rept. GAA-13870 (April 1, 1976).

[17] D. A. Spong, Ph.D. Thesis, U. of Michigan, ORNL/TM-5147 (1976).

[18] D. M. Meade, Nuc. Fusion 14, 289 (1974).

[19] Thermonuclear Division Annual Progress Report for Period Ending December 31, 1975, ORNL-5154, Oak Ridge National Lab. (June 1976); also H. C. Howe, private communication.

[20] TFR group, private communication.

[21] S. N. Cramer and E. M. Oblow, Nuc. Fusion 15, 339 (1975) and Nuc. Fusion 16, 158 (1976).

[22] UWMAK-II Report, Ref. [6], Chapter I.

[23] H. Vernickel, Nuc. Fusion 12, 386 (1972).

[24] Ref. [3], Chapter I.

[25] K. T. Tsang and E. C. Crume, ORNL/TM-5366 (April 1976).

[26] T. Ohkawa, Kakuyugo Kenkyu 32, 67 (1974); see also K. H. Burrell and T. Ohkawa, GA-A14116, Gen. Atomics Co. (August 1976).

[27] R. J. Colchin and T. C. Jernigan, ORNL/TM-5434 (May 1976).

[28] Ref. [5], Chapter I.

[29] D. G. McAlees, private communication.

[30] S. O. Dean et al, "Status and Objectives of Tokamak Systems for Fusion Research," USAEC Rept. WASH-1295 (1974).

[31] H. C. Howe and E. C. Crume, private communication.

CHAPTER III

MHD and $\vec{B}$ Field Considerations

The purpose of this chapter is to outline the MHD equilibrium and stability considerations which were investigated in the design of the UWMKA-I,II reactors and, in particular, emphasize those properties believed unique to divertor configurations. The field of MHD analysis has grown rapidly over the last few years, particularly in the field of MHD stability where nonlinear time dependent computer codes are being used.[1]

The topics to be covered herein are: 1) a brief discussion of MHD equilibrium in general, 2) MHD equilibrium problems in the presence of a divertor null (X-point), 3) a brief discussion of the MHD stability criteria applied to UWMAK-II, and 4) a discussion of how one might proceed in the magnetic field design for a diverted tokamak. There will be no discussion of the "disruptive instability"[2] and "sawtooth" oscillations[3] since they were not extensively investigated in the context of UWMAK-I,II,III and, of course, are not settled issues even at the date of this thesis writing.

MHD Equilibrium

Very simply stated, when the summation of all forces on a body are zero, it is by definition in mechanical equilibrium.[4] It cannot translate through space. In addition, the summation of torques must be equal to zero. Plasma rotation is still an allowable, though possibly not preferred, avenue of motion for the plasma. Thus, when an equilibrium is sought, one should, in principle, allow for a steady state rotation of the plasma.

The study of MHD equilibrium usually begins with the 1-fluid MHD equations. The equations are just the moments of the Vlasov equation and are listed below for future reference.[5]

$$\frac{\partial \rho}{\partial t} + \nabla \cdot \rho \vec{V} = 0 \tag{3.1}$$

$$\rho \frac{d}{dt} \vec{V} = - \nabla \cdot \vec{\vec{P}} + \rho_c \vec{E} + \vec{J} \times \vec{B} \tag{3.2}$$

$$\rho \frac{d}{dt} U = \vec{V} \cdot (\nabla \cdot \vec{\vec{P}}) - \nabla \cdot (\vec{\vec{P}} \cdot \vec{V}) \tag{3.3}$$

$$- \nabla \cdot \vec{Q} + \vec{J} \cdot (\vec{E} + \vec{V} \times \vec{B})$$

$$- \rho_c \vec{E} \cdot \vec{V}$$

where ρ = mass density of plasma

ρ_c = net electrical charge density (usually $\simeq 0$ in a plasma)

$\rho \vec{V}$ = kinetic momentum density

$\vec{\vec{P}}$ = pressure tensor

$\rho U = \frac{1}{2}$ Trace $\{\vec{\vec{P}}\}$ = internal energy density

$\vec{J}$ = net electrical current density

$\vec{Q}$ = heat flux vector, and

$\frac{d}{dt} \equiv \frac{\partial}{\partial t} + \vec{V} \cdot \nabla$.

In addition to the above equations, one must include (for self consistency) Maxwell's equations.

$$\nabla \times \vec{B} = \mu_0 \vec{J} \tag{3.4}$$

$$\nabla \times \vec{E} = - \frac{\partial \vec{B}}{\partial t} \tag{3.5}$$

$$\nabla \cdot \vec{B} = 0 \tag{3.6}$$

$$\nabla \cdot \vec{E} = \frac{1}{\epsilon_0} \rho_c \tag{3.7}$$

Equations (3.1) through (3.7) are often supplemented with Ohm's Law.

$$\vec{E} + \vec{V} \times \vec{B} = \vec{\vec{\eta}} \cdot \vec{J} + \text{"other terms"} \tag{3.8}$$

where $\vec{\vec{\eta}}$ is the resistivity tensor and the "other terms" indicate in (3.8) include the Hall effect, pressure driven terms, etc. which can in certain instances be very important,[5] but are most often excluded in a preliminary equilibrium analysis for reasons of simplicity.[6]

The set of equations most often used are the so-called "ideal" 1-fluid MHD euqations. They are

$$\nabla p = \vec{J} \times \vec{B} \tag{3.9}$$

$$\nabla \times \vec{B} = \mu_0 \vec{J} \tag{3.4}$$

$$\nabla \cdot \vec{B} = 0 \tag{3.6}$$

Implicit to these equations are that the $(V \cdot \nabla)\vec{V}$ term and off-diagonal terms of $\vec{\vec{P}}$ are negligible and that $\vec{\vec{P}}$ is isotropic. In a tokamak, $\vec{\vec{P}}$ is certainly not isotropic and, in fact, it is the anisotropy that is responsible for trapped particle effects.[7] However, again for simplicity, one uses the above equations as a starting point. Substituting (3.4) into (3.9) and using (3.6), one can show that these three equations can be cast into the form

$$\nabla \cdot \vec{\vec{T}} = 0 \tag{3.10}$$

where

$$\vec{\vec{T}} \equiv \left\{p + \frac{B^2}{2\mu_0}\right\} (\vec{\vec{I}} - \hat{n}\hat{n}) + \left\{p - \frac{B^2}{2\mu_0}\right\} \hat{n}\hat{n} \tag{3.11}$$

$$\hat{n} \equiv \vec{B}/|\vec{B}|$$

and

$$\vec{\vec{I}} = \text{identity tensor}$$

Equation (3.10) is, of course, still a set of three equations, one for each orthogonal direction. In some instances (3.10) can be integrated over the volume of the plasma

$$\vec{F} = \int_{\substack{\text{plasma} \\ \text{volume}}} \nabla \cdot \vec{\vec{T}}\, d^3r = \oint_{\substack{\text{plasma} \\ \text{surface}}} \vec{\vec{T}} \cdot d\vec{A} = 0 \tag{3.12}$$

and solved explicitly.[4] The solutions which result involve only integral parameters of the plasma such as the average pressure $\bar{p}$ or internal self inductance ℓ_i, etc. Their applicability is usually restricted to low β, large aspect ratio (R/a) plasmas and a typical

result is the minor radius force balance[8]

$$\bar{p} + \frac{\overline{(B_T^{int})^2}}{2\mu_0} = \frac{\overline{(B_T^{ext})^2}}{2\mu_0} + \frac{B_p^2(a)}{2\mu_0} \tag{3.13}$$

where the bar ($\bar{\ }$) indicates an integration over the plasma volume and $B_p(a)$ is the poloidal field evaluated at the plasma edge.* Another result which comes from solving (3.12) is the required vertical field needed to maintain the plasma column in balance in the major radius direction. It is given by [8]

$$B_\perp = \frac{a}{2R} B_p(a) \left[\ell n\,(8\,\frac{R}{a}) - 1.5 + \bar{\beta}_p + \frac{\ell_i}{2}\right] \tag{3.14}$$

where

$$\bar{\beta}_p \equiv \frac{2\mu_0}{\pi a^2 B_p^2(a)} \int_0^a 2\pi r p(r) dr \tag{3.15}$$

$$\ell_i \equiv \frac{1}{\pi a^2 B_p^2(a)} \int_0^a B_p^2(r)\, 2\pi r dr = \frac{\text{plasma inductance per unit length of plasma}}{(\mu_0/4\pi)} \tag{3.16}$$

For the plasma column (assumed circular) to remain in equilibrium if perturbed as a rigid body, the field index n defined as

$$n \equiv -\frac{R}{B_\perp}\frac{\partial B_\perp}{\partial R} \tag{3.17}$$

must fall within certain bounds. $n > 0$ insures vertical stability

*Plasma edge in the context of MHD work is the line of demarcation beyond which no electrical current is allowed to flow, i.e., $\vec{J} = 0$ beyond the plasma "edge" by definition. Also $B_p(a)$ is to lowest order taken to be independent of poloidal angle, θ.

while $n < 3/2$* insures horizontal stability. If the plasma is non-circular, the criteria are more complex.[11] Also if the plasma is not treated as a rigid body during the perturbation, one has a much more difficult analysis procedure, and MHD stability analyses do treat the plasma in just this manner.

These simple equations (3.13), (3.14), and (3.17) can be used to obtain a feel for the required parameters, but usually a more sophisticated analysis is called for. To do this in a tokamak, one can take advantage of the axisymmetry to reduce the number of equations (3.10) which must be solved down to one scalar equation in which one needs to specify two arbitrary functions. To understand exactly what is meant by this, a derivation is presented below.

There are many ways to perform the derivation we are about to do. It can be done in very general coordinates (such as ψ and χ) but to keep the mathematics straight and simple, the derivation will be performed in cylindrical geometry where the z-axis coincides with the axis of symmetry of the tokamak (i.e., the center of the machine, not the center of the plasma). The plasma forms a torus of arbitrary cross sectional shape about this symmetry axis.

From axisymmetry and $\nabla \cdot \vec{B} = 0$, we note that $\vec{B}_p$, the poloidal field, can be represented by

$$\vec{B}_p = \nabla \times (A_\varphi \hat{e}_\varphi) \tag{3.18}$$

*The 3/2 number comes from Shafranov's analysis.[9] Johnson, et al. came up with a number somewhat lower in value.[10]

where A_φ = magnetic vector potential, $\hat{e}_\varphi$ = unit vector in the $+\varphi$ direction. Equation (3.18) has components in a right-handed coordinate system

$$B_r = -\frac{\partial A_\varphi}{\partial z} = -\frac{1}{r}\frac{\partial}{\partial z}(rA_\varphi) \tag{3.19}$$

and

$$B_z = \frac{1}{r}\frac{\partial}{\partial r}(rA_\varphi) \tag{3.20}$$

from which one can verify that $\nabla \cdot \vec{B}_p = 0$. The streamlines for $\vec{B}_p$ are found by solving

$$\frac{dz}{B_z(r,z)} = \frac{dr}{B_r(r,z)} \tag{3.21}$$

and is, in general, nonlinear. A property of interest is that

$$\begin{aligned} d(rA_\varphi) &\equiv \frac{\partial}{\partial z}(rA_\varphi)dz + \frac{\partial}{\partial r}(rA_\varphi)dr \\ &= -rB_r dz + rB_z dr \\ &= -rB_r\left(\frac{B_z}{B_r}dr\right) + rB_z dr \\ &= 0 \end{aligned}$$

This means that the magnetic field lines lie on surfaces of constant rA_φ. It is customary to define the function ψ as

$$\psi \equiv \pm 2\pi rA_\varphi(r,z) \tag{3.22}$$

where the 2π factor is sometimes omitted from the definition, and the selection of a + or - sign is strictly a matter of personal preference. The advantage of including the 2π is that the poloidal magnetic flux

$$\underset{\text{flux}}{\text{poloidal}} \equiv \int \vec{B}_p \cdot d\vec{s} = \oint \vec{A} \cdot d\vec{\ell}$$

$$= 2\pi r A_\varphi = \psi$$

can be identified directly with ψ. The function ψ is then a legitimate way to identify a surface on which magnetic field lines lie.* From the force balance equation $\nabla p = \vec{J} \times \vec{B}$ we can see that $\vec{B} \cdot \nabla p = \vec{B} \cdot (\vec{J} \times \vec{B}) = 0$ which indicates that if we follow a $\vec{B}$ field line around the plasma, it will stay on a surface of constant pressure. This is only true when the plasma is in static ($\vec{v} = 0$) equilibrium. At least that is all that can be inferred from using Eqs. (3.9), (3.4), and (3.6). To collect our thoughts then, we see that $\vec{B}$ field lines lie in surfaces of constant ψ (due to axisymmetry) and also in surfaces of constant pressure (due to equilibrium and scalar pressure assumptions).

Using these properties we note that

$$\vec{B}_p = \nabla \times (A_\varphi \hat{e}_\varphi) = \nabla \times (rA_\varphi \nabla\varphi)$$

$$= rA_\varphi \nabla \times \nabla\varphi + \nabla(rA_\varphi) \times \nabla\varphi = \nabla(rA_\varphi) \times \nabla\varphi$$

using $\psi = +2\pi r A_\varphi$, one has

$$\vec{B}_p = \frac{\nabla\psi \times \nabla\varphi}{2\pi} = \frac{\nabla\psi \times \hat{e}_\varphi}{2\pi r} \tag{3.23}$$

For convenience the toroidal field may be written in the form

*Due to axisymmetry B_φ the toroidal field cannot vary in the φ direction so that $\nabla \cdot \vec{B}_\varphi \equiv 1/r\ \partial B_\varphi/\partial\varphi = 0$ independently and so the entire field line $B = \vec{B}_p + \vec{B}_\varphi$ lies on the torus labeled by ψ.

$$B_\varphi = B_\varphi^*(r,z) + \frac{B_0 r_0}{r} \tag{3.24}$$

where $B_\varphi^* = 0$ implies $B_\varphi = 1/r$ toroidal field. Writing out Ampere's Law in component form gives

$$-\frac{\partial B_\varphi^*}{\partial z} = \mu_0 J_r \tag{3.25a}$$

$$\frac{\partial B_r}{\partial z} - \frac{\partial B_z}{\partial r} = \mu_0 J_\varphi \tag{3.25b}$$

$$\frac{1}{r}\frac{\partial}{\partial r}(rB_\varphi^*) = \mu_0 J_z \tag{3.25c}$$

Using (3.19) and (3.20) we have

$$B_r = -\frac{1}{2\pi r}\frac{\partial \psi}{\partial z} \tag{3.26a}$$

$$B_z = \frac{1}{2\pi r}\frac{\partial \psi}{\partial r} \tag{3.26b}$$

The force balance equation $\nabla p = \vec{J} \times \vec{B}$ in component form becomes

$$\frac{\partial p}{\partial r} = J_\varphi B_z - J_z B_\varphi \tag{3.27a}$$

$$\frac{1}{r}\frac{\partial p}{\partial \varphi} = 0 = J_z B_r - J_r B_z \tag{3.27b}$$

$$\frac{\partial p}{\partial z} = J_r B_\varphi - J_\varphi B_r \tag{3.27c}$$

Using Eqs. (3.25b), (3.26a), and (3.26b), one obtains

$$\frac{\partial^2 \psi}{\partial z^2} + r\frac{\partial}{\partial r}\left(\frac{1}{r}\frac{\partial \psi}{\partial r}\right) = -2\pi r \mu_0 J_\varphi \tag{3.28}$$

The operator on the left hand side of (3.28) is often given a special

symbol, Δ^*, defined by

$$\Delta^* \equiv \frac{\partial^2}{\partial r^2} - \frac{1}{r}\frac{\partial}{\partial r} + \frac{\partial^2}{\partial z^2} \tag{3.29}$$

and $(\nabla \times \vec{B}_p) = \mu_0 J_\varphi \hat{e}_\varphi$ can be rewritten as

$$\Delta^* \psi = -2\pi r \mu_0 J_\varphi \tag{3.30}$$

We now wish to incorporate the plasma force balance $\nabla p = J_\varphi \hat{e}_\varphi \times \vec{B}_p + \vec{J}_p \times B_\varphi \hat{e}_\varphi$ into Eq. (3.30). Taking the φ component of the force balance equation and using (3.25a), (3.25c), (3.26a), and (3.26b), we discover the following relationship.

$$\frac{\partial}{\partial z}(rB_\varphi^*)\frac{\partial \psi}{\partial r} - \frac{\partial}{\partial r}(rB_\varphi^*)\frac{\partial \psi}{\partial z} = 0 \tag{3.31}$$

but this is just the Jacobian, $\partial(rB_\varphi^*, \psi)/\partial(r,z)$, for the transformation from (rB_φ^*, ψ) to (r,z). The Jacobian being zero indicates that rB_φ^* is not functionally independent of ψ, i.e.,

$$rB_\varphi^*(r,z) = g(\psi(r,z)) \tag{3.32}$$

where $g(\psi)$ is some yet to be prescribed arbitrary function of ψ only.

From the r and z components of the force balance, we have

$$B_r \frac{\partial p}{\partial r} = J_\varphi B_z B_r - J_z B_\varphi B_r$$

$$B_z \frac{\partial p}{\partial r} = J_r B_\varphi B_z - J_\varphi B_r B_z$$

Adding these equations gives

$$B_r \frac{\partial p}{\partial r} + B_z \frac{\partial p}{\partial z} = B_\varphi (J_r B_z - J_z B_r) = 0$$

and substituting (3,26a,b) for B_r and B_z gives

$$\frac{\partial \psi}{\partial r} \frac{\partial p}{\partial z} - \frac{\partial \psi}{\partial z} \frac{\partial p}{\partial r} = 0 = \frac{\partial(\psi, p)}{\partial(r,z)} \tag{3.33}$$

which is the Jacobian for $(p,\psi) \rightarrow (r,z)$. Equation (3.33) implies that $p = p(\psi)$ only. Thus

$$p = p(\psi)$$

$$rB_\varphi^* = g(\psi)$$

as a consequence solely of axisymmetry. Using the r and z components of the force balance coupled with our knowledge that rB_φ^* and p are functions only of ψ, one finds

$$\frac{\partial p}{\partial r} = \frac{dp}{d\psi} \frac{\partial \psi}{\partial r} = 2\pi r B_z \frac{dp}{d\psi}$$

and

$$\frac{\partial p}{\partial z} = \frac{dp}{d\psi} \frac{\partial \psi}{\partial z} = -2\pi r B_r \frac{dp}{d\psi}$$

which when substituted into (3.27a) and (3.27c) give

$$2\pi r \frac{dp}{d\psi} = J_\varphi - \left(\frac{J_z}{B_z}\right) B_\varphi \tag{3.34}$$

$$2\pi r \frac{dp}{d\psi} = J_\varphi - \left(\frac{J_r}{B_r}\right) B_\varphi$$

and adding (3.34) and (3.35), and dividing by 2, one obtains

$$2\pi r \frac{dp}{d\psi} = J_\varphi - \frac{B_\varphi}{2} \left(\frac{J_r}{B_r} + \frac{J_z}{B_z}\right) \tag{3.36}$$

From axisymmetry in the force balance equation [i.e., (3.27b)], we know that

$$\frac{J_r}{B_r} = \frac{J_z}{B_z} = \frac{\frac{1}{\mu_0}\frac{1}{r}\frac{\partial}{\partial r}(rB_\varphi^*)}{\frac{1}{2\pi r}\frac{\partial \psi}{\partial r}} = \frac{2\pi}{\mu_0}\frac{d(rB_\varphi^*)}{d\psi} \tag{3.37}$$

where (3.25c) and (3.26b) have been used.

Equation (3.36) becomes

$$2\pi r \frac{dp}{d\psi} = J_\varphi - \frac{B_\varphi}{2}\left(\frac{4\pi}{\mu_0}\frac{d(rB_\varphi^*)}{d\psi}\right)$$

or rewritten to solve for J_φ, it becomes

$$J_\varphi = 2\pi r \frac{dp}{d\psi} + \frac{2\pi}{\mu_0}\frac{rB_\varphi}{r}\frac{d}{d\psi}(rB_\varphi) \tag{3.38}$$

where use is made of the fact that $d/d\psi(B_0 r_0/r) = 0$. Defining a new function

$$I(\psi) \equiv \frac{2\pi r B_\varphi}{\mu_0} \tag{3.39}$$

Eq. (3.38) can be rewritten as

$$\begin{aligned} J_\varphi &= 2\pi r \frac{dp}{d\psi} + \frac{\mu_0 I}{2\pi r}\frac{dI}{d\psi} \\ &= r\left(2\pi \frac{dp}{d\psi}\right) + \frac{1}{r}\left(\frac{\mu_0}{4\pi}\frac{d(I^2)}{d\psi}\right) \\ &= A(\psi)r + \frac{C(\psi)}{r} \end{aligned}$$

where the latter form is that used by Shafranov[12] to demonstrate explicitly the dependencies of J_φ on ψ and r.

Substituting (3.40) into (3.30) the "famous" elliptic MHD equilibrium equation is obtained

$$\boxed{\Delta^* \psi = - 2\pi r \mu_0 \left\{ 2\pi r P' + \frac{\mu_0}{2\pi r} II' \right\}} \qquad (3.41)$$

where P', I' indicates $d/d\psi$. $I(\psi)$ describes physically the current flowing in the poloidal direction on each ψ surface.

When applying (3.41) in practice, $P(\psi)$ and $I(\psi)$ must be prescribed. One would like to be able to specify a $P(\psi)$ and an $I(\psi)$ which represent the actual profiles in an experimental device. This is much easier said than done. In fact, we should never have expected to reduce seven equations to one equation and get away with it! In reality, (3.41) should be solved in conjunction with the particle continuity equation and energy balance equation.* This type of procedure is only now beginning to appear.[13]

Obviously $P(\psi)$ and $I(\psi)$ are chosen to be analytically tractable expressions of if one wishes to solve (3.41) analytically.[14] They can be taken to be more involved when applying a numerical solution scheme. In UWMAK-II,III, $P(\psi)$ and $I(\psi)$ were specified to have the form

$$P(\psi) = (P_0 - P_b) \left| \frac{\psi_b - \psi}{\psi_b - \psi_{ma}} \right|^{\alpha} + P_b \qquad (3.42)$$

and

$$I(\psi) = 1 + g_P \left| \frac{\psi_b - \psi}{\psi_b - \psi_{ma}} \right|^{\gamma} \qquad (3.43)$$

*Sometimes Ohm's Law in a simplified form is also included.

where

ψ_b = ψ value at the plasma edge (separatrix)

ψ_{ma} = ψ value at the magnetic axis

P_b = plasma pressure at the plasma edge (input variable)

P_0 = plasma pressure at the magnetic axis (input variable)

α, γ = arbitrary real, positive numbers which are adjusted to represent physically reasonable profiles (input variables).

The factor g_p is iterated internally during the solution procedure to insure that the total current flowing in the toroidal direction (I_φ^{total}) is always equal to a prescribed value which is an input variable to the program; i.e., we solve (3.41) subject to the integral constraint

$$\int_{plasma} J_\varphi dzdr = 2\pi \int P'(\psi(r,z))r'drdz + \frac{\mu_0}{4\pi} \int \frac{dI^2(\psi(r,z))}{d\psi} \frac{drdz}{r}$$

$$= \left(2\pi\alpha(P_0 - P_b) \int \left| \frac{\psi_b - \psi}{\psi_b - \psi_{ma}} \right|^{\alpha-1}_{rdrdz} \right)$$

$$+ \left(\frac{\mu_0}{2\pi} \gamma \int \left| \frac{\psi_b - \psi}{\psi_b - \psi_{ma}} \right|^{\gamma-1} \frac{drdz}{r} \right) g_p$$

$$+ \left(\frac{\mu_0}{2\pi} \gamma \int \left| \frac{\psi_b - \psi}{\psi_b - \psi_{ma}} \right|^{2\gamma-1} \frac{drdz}{r} \right) g_p^2$$

$$= C_1 + C_2 g_p + C_3 g_p^2$$

$$= I_\varphi^{total} = \text{specified input parameter}$$

This is a quadratic equation from g_p in terms of integrals which are evaluated during each iteration.

Studies have been conducted using the forms (3.42) and (3.43) for P and I.[15] It was found that the parameters α and γ can crucially affect the equilibrium profile[16] and they must be chosen with an eye to what seems physically reasonable in terms of the J_φ and P profiles. For stability reasons, one must also try to keep the safety factor $q(\psi) > 1$ throughout the plasma. The reason for this has to do with preventing an internal king instability which might under certain conditions trigger a global "external" kink mode and cause the plasma to go disruptive.[17] More will be said of this in a later section, but one notes for reference that

$$q(\psi) = \frac{\mu_0 I(\psi)}{2\pi} \oint_{\psi \text{ surface}} \frac{d\ell}{r|\nabla\psi|}$$

where the integration is in the poloidal direction around the ψ surface of interest.

Some of the graphical output produced by the code used at the University of Wisconsin is shown in Figs. III-1 and III-2. The plots are for UWMAK-II parameters.[18] The first figure shows the ψ contours. Note the "D" shape; this is a natural consequence of going to a double null divertor with the nulls on the inside of the major radius. The "D" shape is also a natural shape for high β plasmas[19] since the plasma and magnetic field pressures want the plasma ring to expand outward. Figure III-2 shows the components of the force

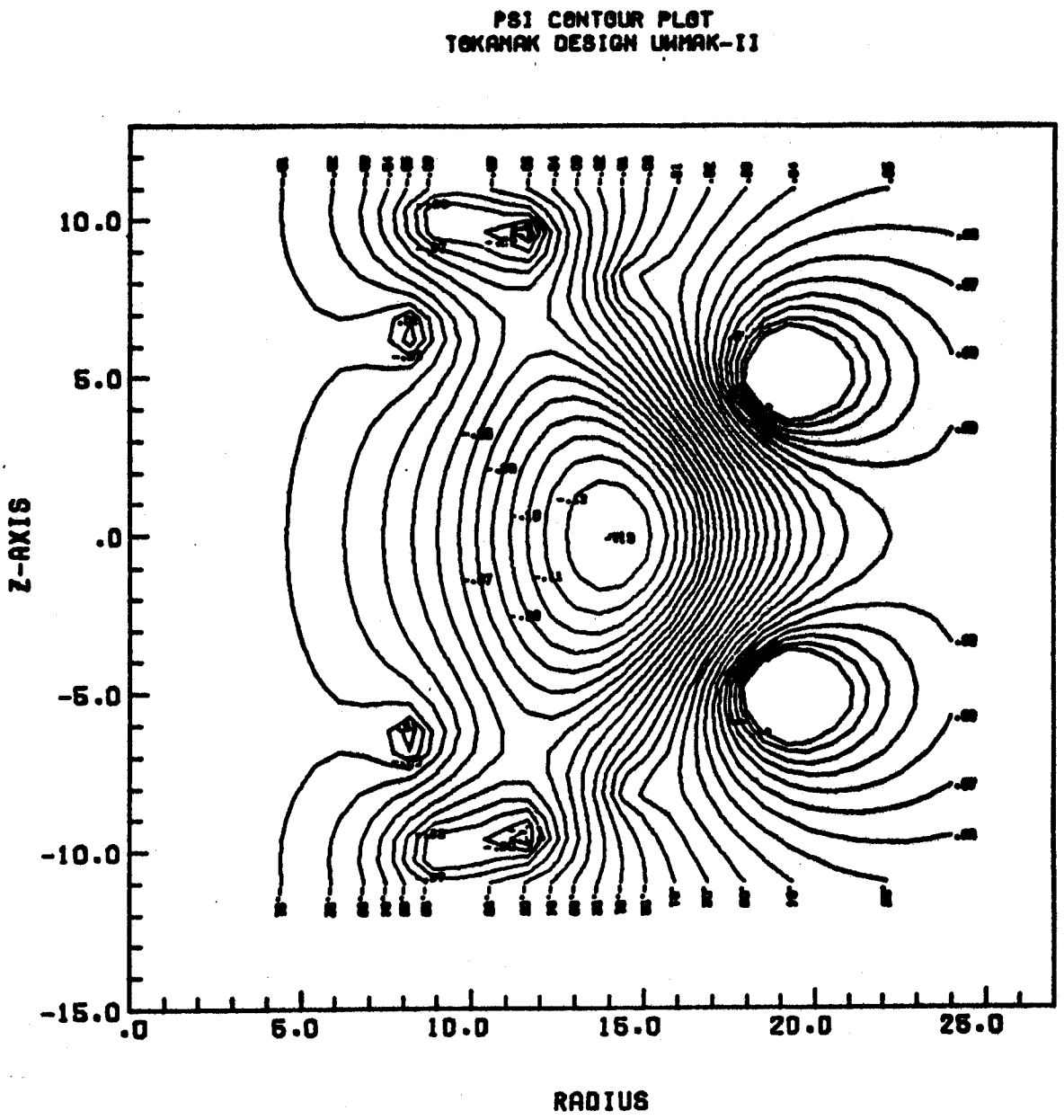
PSI CONTOUR PLOT
TOKAMAK DESIGN UWMAK-II
10.0
5.0
.0
-5.0
-10.0
-15.0
Z-AXIS
.0
5.0
10.0
15.0
20.0
25.0
RADIUS

Figure III-1

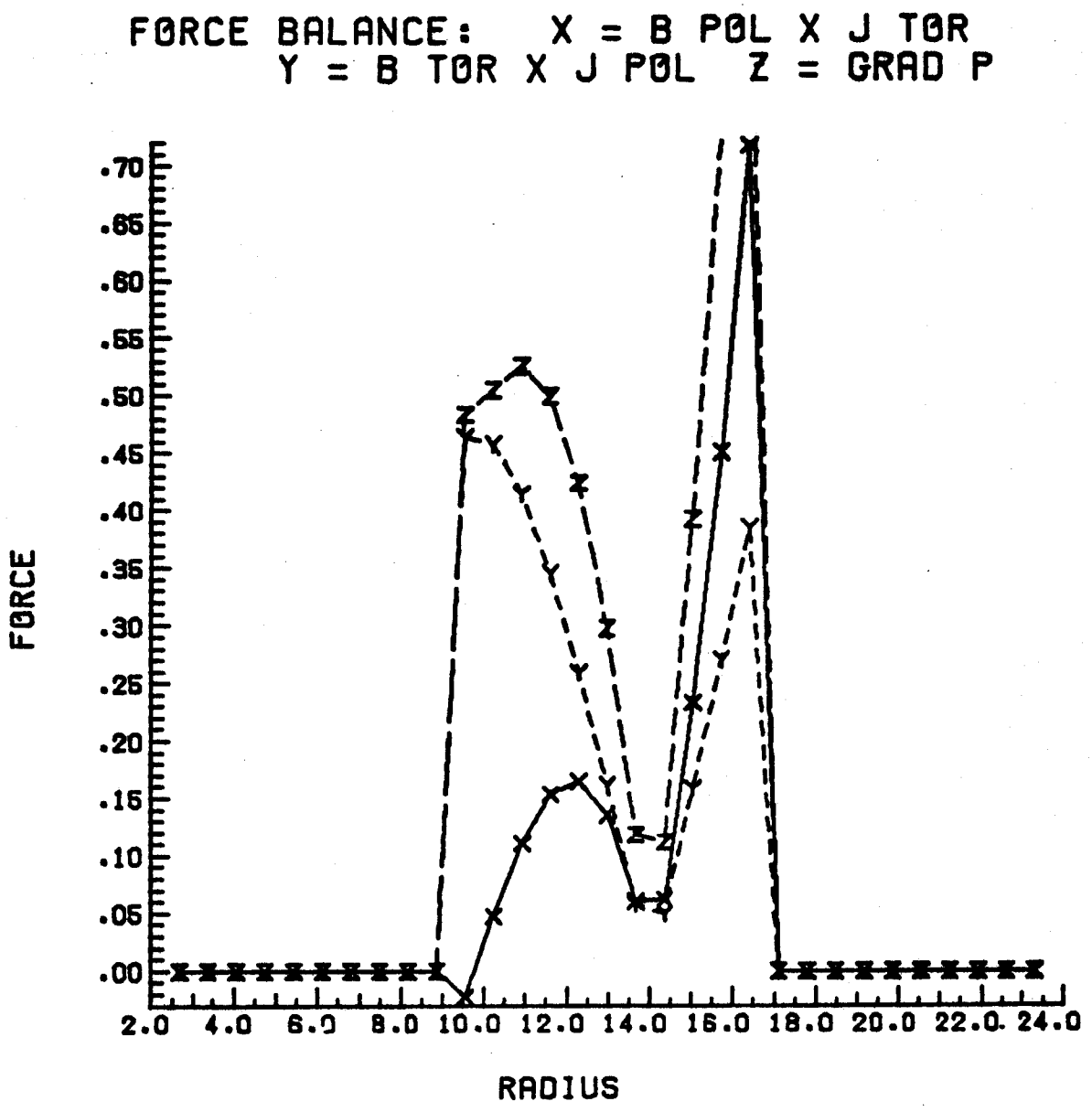
FORCE BALANCE: X = B POL X J TOR
Y = B TOR X J POL Z = GRAD P
FORCE
.70
.65
.60
.55
.50
.45
.40
.35
.30
.25
.20
.15
.10
.05
.00
2.0 4.0 6.0 8.0 10.0 12.0 14.0 16.0 18.0 20.0 22.0 24.0
RADIUS

Figure III-2

balance: i) ∇p, ii) $J_{toroidal} \times B_{poloidal}$, and iii) $J_{poloidal} \times B_{toroidal}$. The graph is taken at the $Z = 0$ plane sweeping across the center of the plasma. One notes that the poloidal magnetic field crossed with the toroidal current seems to be holding most of the plasma pressure on the outside of the plasma while the toroidal field crossed with the poloidal current is holding ∇p on the inner side of the plasma. This is a natural consequence of high β. In high β the plasma leans toward the outside creating a large ∇p. This, in turn, produces a large magnetization current $\nabla \times \vec{M}$. At high β a larger vertical field is needed to maintain the plasma centered in the chamber. This larger B_v increases the pitch of the field lines on the outside of the plasma ($r > R_0$). This increased pitch means that more of the magnetization current is in the toroidal direction. This is exactly what is reflected in Fig. III-2.

Divertor MHD Problems

There are several points which are of concern in plasma configurations containing null points* in the poloidal magnetic field. As can be seen from Fig. III-3, there are three such points in the plasma region for a double-null configuration such as UWMAK-II. One of these nulls is at the magnetic axis. The structure of the poloidal field about this null point is elliptical in nature (i.e., poloidal field lines encircle the null point) and is called a O-type null point.

*A null point is defined here to be any point where the magnetic field component of interest is identically zero.

Symmetrically placed above and below the Z = 0 plane are the other two "divertor" null points. These are referred to as X-type null points since the field lines map away from the null like a hyperbola.

One worries about the stability of the X-type null points. By stability, one means the spatial wandering of the null point about some central position. This wandering could be due to perturbations (axisymmetric) of the plasma current, eddy currents in the walls, or coil currents. The wandering of this null point would tend to "smear-out" the separatrix as a function of time. This would not happen if the plasma were a perfect conductor. However, the plasma is somewhat resistive and probably more so at the separatrix (and in the divertor region) than in the inner core of the plasma so that a wandering of the null point may be inescapable.

A second worry is the problem of how asymmetric effects will bother the divertor nulls. Morozov and Solov'ev[20] discuss somewhat the behavior of field lines in cases like the one presented here. They address the problem of field lines mapping from one quadrant about the null point to another. Their work has strictly to do with fields where $\nabla \times \vec{B} = 0$ in the region of interest. That is not the case in a tokamak. The portion of $\vec{J}$ due to externally applied EMF may be small near the separatrix since the $\vec{E}$ field in a high temperature plasma is very small and the field is essentially shorted out by electron motion to the divertor collector plates in the divertor zone. However, $\vec{J}$ also has a component due to ∇p and this is always present even in the absence of an external EMF. This $\vec{J}$ can affect $\vec{B}$ if ∇p is

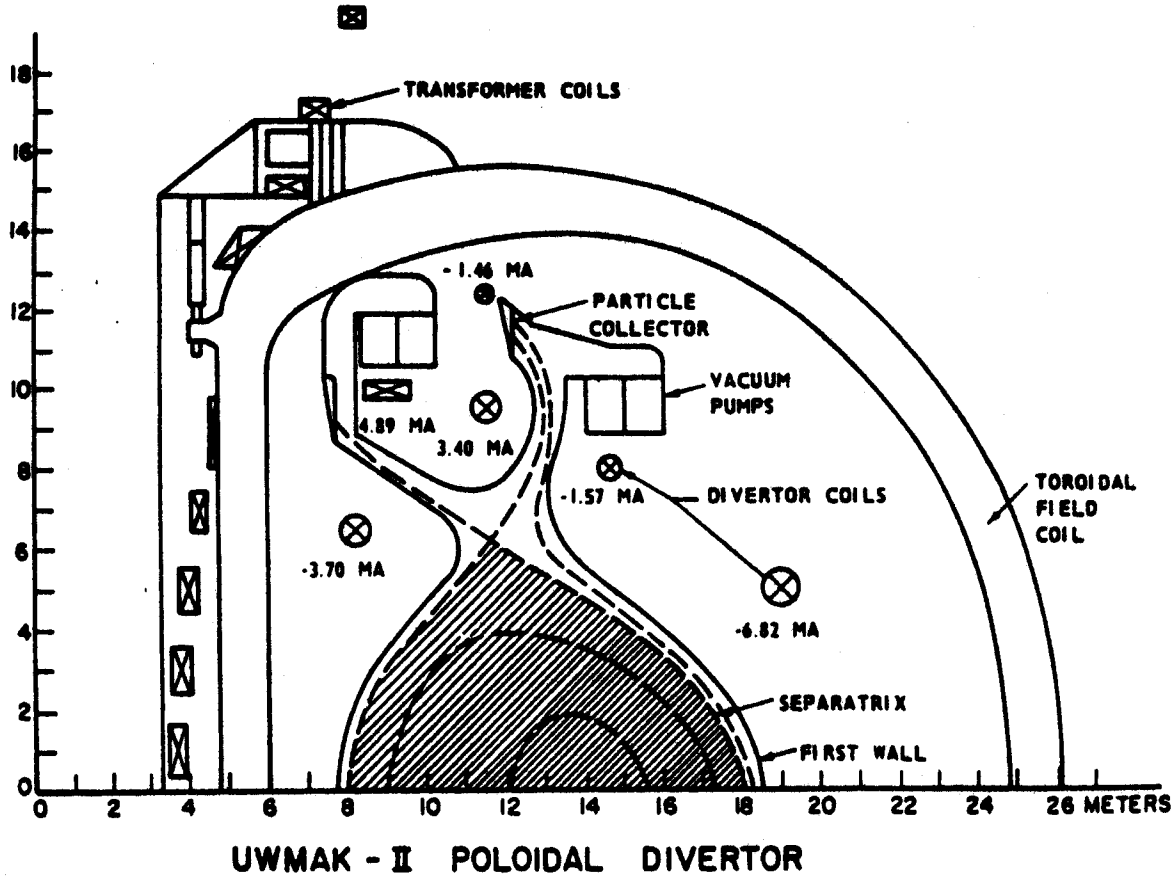
TRANSFORMER COILS
-1.46 MA
PARTICLE COLLECTOR
VACUUM PUMPS
4.89 MA
3.40 MA
-1.57 MA
DIVERTOR COILS
TOROIDAL FIELD COIL
-3.70 MA
-6.82 MA
SEPARATRIX
FIRST WALL
0 2 4 6 8 10 12 14 16 18 20 22 24 26 METERS
UWMAK - II POLOIDAL DIVERTOR

Figure III-3

steep enough! A suitable study of the problem for the case $\nabla \times \vec{B} \neq 0$ has not been done to this author's knowledge.

In the context of what has just been said, it has been conjectured[21] that if one has a toroidal current flowing in the plasma up to and including the separatrix and if one requires that no current flow outside the separatrix, the determination of the magnetic field configuration is not a physically well-posed problem, i.e., one would always need a surface current at the separatrix in order to match the vacuum fields to the field inside the plasma. This is pure nonsense physically because there will always be some $\vec{J}$ in the divertor zone outside the separatrix and when this is taken into consideration, one does not have a matching problem with the boundary conditions.

MHD Stability

The area of MHD stability analyses has grown considerably since 1972-73 when the author's work was performed. Due to this, there will be no attempt to bring one abreast of the latest concepts and solution techniques in the field. Instead, the interested reader is referred to the literature.[22] A few criteria were, however, investigated and the results of these will be presented along with a discussion of what we believe to be problems of concern in the divertor region itself.

To prevent the onset of localized (Mercier) modes, a Mercier criteria was applied numerically to the ψ profiles generated by the equilibrium code. The code uses the criteria as derived by Johnson, et al. and can be formulated (see Appendix D) as follows. The

necessary condition for stability against ideal localized modes is that the quantity

$$D_I < 0 \quad .$$

The necessary condition for stability against resistive localized modes is that the quantity

$$D_R \equiv D_I + (H - \tfrac{1}{2})^2 < 0 \quad .$$

The quantities H and D_I are defined in Appendix D. Their form is not needed for what remains to be said in this section. In Appendix D, Fig. D-1 shows a plot of both D_I and D_R for UWMAK-II and the large negative values near the magnetic axis are indicative of a favorable minimum average $|B|$ well.

Also plotted in Fig. D-4 is the $q(\psi)$ profile for UWMAK-II. One tries to choose $P(\psi)$ and $I(\psi)$ so that $q(\psi)$ does not drop below one anywhere in the plasma. This is the Kruskal-Shafranov criteria[23] for kink mode stability.

With the exception of the three tests outlined above, little else in the way of stability analysis was applied. The results of all these calculations did not appear sensitive to the divertor field line configuration. The computer codes ran into some numerical difficulties near the magnetic axis and the separatrix surface. This is to be expected when one uses a finite size spatial grid to represent the plasma currents. It is of interest to note that, to the best of this author's knowledge, all of the work published to date on MHD equilibria

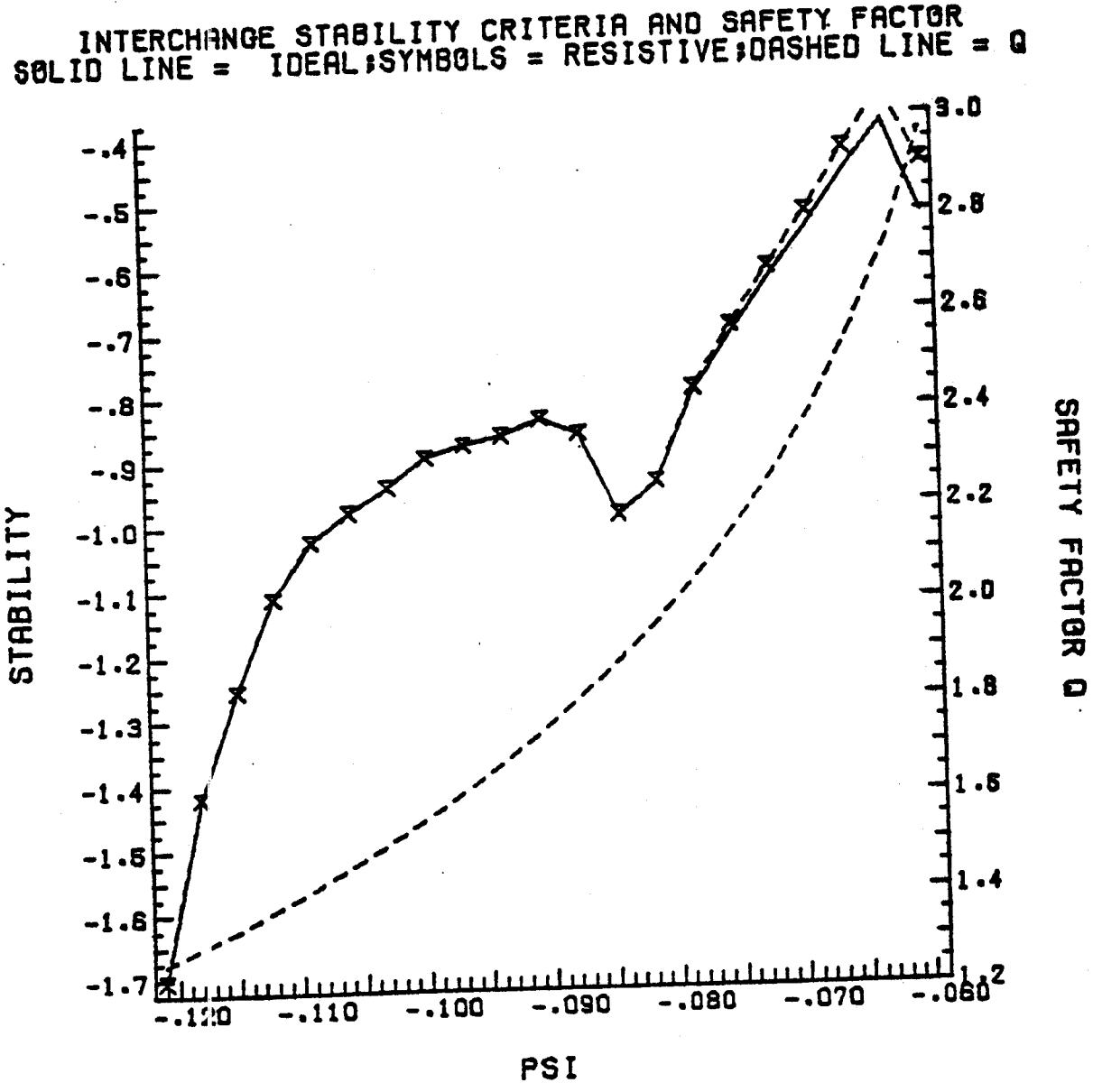
INTERCHANGE STABILITY CRITERIA AND SAFETY FACTOR
SOLID LINE = IDEAL;SYMBOLS = RESISTIVE;DASHED LINE = Q
STABILITY
-.4
-.5
-.6
-.7
-.8
-.9
-1.0
-1.1
-1.2
-1.3
-1.4
-1.5
-1.6
-1.7
SAFETY FACTOR Q
3.0
2.8
2.6
2.4
2.2
2.0
1.8
1.6
1.4
1.2
-.120
-.110
-.100
-.090
-.080
-.070
-.060
PSI

Figure III-4

in the presence of a divertor field has not allowed current to flow in the divertor region, i.e., J_φ was set to zero outside the separatrix during the iterative solution procedure for Eq. (3.40). What effect having current flowing in the divertor region has on the equilibrium profiles has yet to be numerically assessed. It needs to be done.

A worry is sometimes voiced that since the plasma in the outer divertor zone is always in a region of bad curvature, it is susceptible to a number of MHD modes (flute and ballooning). The pure flute modes may be shorted out by the divertor collector plates, but the ballooning mode might be present. The pressure in the divertor region appears reasonably low (although ∇p may be large) and the shear in the divertor zone may be high enough to prevent the mode from going or at least localize its region of growth.

The reason for lack of detailed study of the MHD effects in the divertor zone can be traced directly to the geometry problem. It appears that only a three-dimensional code that can somehow encorporate the processes at the divertor collector plates can be used to perform a detailed analysis. This has not been done to date.

Magnetic Field Design

Deciding on where to place external coils and what currents they must carry in order to achieve a desired plasma configuration is very much a combination of science and art. There is usually a lot of trial and error involved. In particular, one needs to interface closely with the rest of the engineering design of the reactor; otherwise, mechanical credibility is sacrificed. In many instances, the

engineering problems in placing coils inside vacuum vessels with divertor channels around them are almost insurmountable.

It has been found useful in the design of the UWMAK reactors to replace the distributed plasma current by a filament still carrying I_{φ}^{total} and place this filament in the general vicinity of the plasma magnetic axis. One can then do field line integrations much more economically, particularly when one is not concerned with the fields inside the plasma itself.

Y-K. M. Peng at the Oak Ridge National Laboratory has developed a coil configuration which does not require any coils to carry extremely large currents in order to produce the nulls in the poloidal field to achieve a divertor configuration. The results of this are forthcoming.[24] If one can achieve his proposed configuration in a mechanically sound way, then it is an encouraging sign in terms of building one into a power producing fusion reactor.

CHAPTER III

Bibliography

[1] G. Bateman in COMPAS Rept, Ed. by W. L. Sadowski, to be issued by ERDA (1976-77); see also J. U. Brackbill in Meth. of Comp. Phys., Vol. 16, Acad. Press, New York (1976).

[2] B. B. Kadomtsev in "Proc. Sixth European Conf. on Controlled Fusion and Plasma Physics," Moscow (1973); see also "Proc. Sixth Int. Conf. on Plasma Physics and Controlled Nuclear Fusion Research," Berchtesgaden FR6, (1976), papers #CN-35/A7-A9.

[3] S. V. Mirnov, I. B. Semenov, Nuc. Fus. Supp., p 189 (1972); see also S. V. Mirnov, JETP 33, 6 (1971); see also S. V. Mirnov, Sov. Atomic Energy 30, 1 (1971).

[4] A. T. Mense, UWFDM-71, Nuc. Eng. Dept., Univ. of Wiscon (Sept. 1973) and references therein.

[5] N. A. Krall, A. W. Trivelpiece, Principles of Plasma Physics, (McGraw-Hill, New York, 1973), pp. 82-99.

[6] J. M. Greene and J. L. Johnson in Advances in Theroetical Physics, Vol. 1, K. A. Brueckner, Ed., (Academic Press, New York, 1965).

[7] R. D. Hazeltine, in Advances in Plasma Physics, Vol. 6, (Interscience, John Wiley and Sons, New York, 1976), p. 273; see also F. L. Hinton and R. D. Hazeltine, Rev. Mod. Phys. 48, 239 (1976).

[8] V. D. Shafranov in Reviews of Plasma Physics, Vol. 2, (Consultants Bureau, New York , 1970), pp. 103-150; see also V. S. Mukhovatov and V. D. Shafranov, Nuc. Fusion 11, 605 (1971); see also I. A. Artsimovich, Nuc. Fusion 12, 215 (1972); see also Ref. [4].

[9] V. S. Mukhovatov, et al., in Ref. [8] above.

[10] J. M. Greene, J. L. Johnson, and K. E. Weimer, Phys. Fluids 14, 671 (1971).

[11] E. Rebhan, Nuc. Fusion 15, 277 (1975).

[12] V. D. Shafranov, in Ref. [8] above.

[13] J. T. Hogan, private communication; G. Bateman, private communication.

[14] Y. Suzuki, Inst. of Plasma Physics Rept. IPPJ-159, Nagoya Univ., (May 1973); see also Ref. [8].

[15] See Ref. [7], Chapter I and Ref. [17], Chapter I.

[16] See Ref. [7], Chapter I.

[17] G. Bateman and B. V. Waddell, private communication; see also Ref. [2].

[18] Ref. [6], Chapter I.

[19] Y-K. M. Peng, R. A. Dory, ORNL/TM-5555 (1976), to be published in Nuclear Fusion.

[20] A. I. Morozon and L. S. Solov'ev, in Reviews of Plasma Physics, Vol. 2, (Consultants Bureau, New York, 1966) pp. 1-100; see also L. S. Solov'ev and V. D. Shafranov in Vol. 5 of the above series.

[21] R. A. Dory, private communication.

[22] H. P. Furth, Nuc. Fusion 15, 487 (1975); see also Ref. [1].

[23] B. B. Kadomtsev, in Reviews of Plasma Physics, Vol. 2, (Consultants Bureau, New York, 1966) p. 179.

[24] Y-K. M. Peng, private communication.

CHAPTER IV

Simple Divertor Models

In this chapter several simplified models for charged particle transport in the divertor zone of a tokamak reactor will be developed. The models will be based upon the assumption that the plasma present in the divertor zone undergoes a diffusive process across the magnetic field lines and leaves convectively* along the direction of the field lines. In addition, a source of plasma in the divertor volume due to ionization of neutrals will be included. The purpose of this type of analysis is two-fold. First, it will allow one to obtain a qualitative feel for how the plasma density may vary in the divertor region assuming a variety of diffusion coefficients and parallel flow terms. Secondly, one will see explicitly the effect of the boundary conditions at the first wall on the behavior of the plasma density near the separatrix. This will be an important concept later in Chapter VI when numerical techniques are applied.

To develop a model incorporating the features mentioned above, one may consider the zeroth moment of the Boltzmann equation to be the basis. In time independent form, it may be written as

$$\nabla_{\perp} \cdot (n\vec{V}_{\perp}) = - \nabla_{\parallel} \cdot (n\vec{V}_{\parallel}) + n\, n_0 \langle \sigma v \rangle_{iz} \qquad (4.1)$$

where $n\vec{V}$ is the plasma flux and $n\, n_0 \langle \sigma v \rangle_{iz}$ is the ionization rate/volume. Equation (4.1) is merely the particle continuity equation

*This convection motion is sometimes called "effusion."

with a source term. For the models to be solved in this chapter, Eq. (4.1) will be written in slab geometry and, with reference to Fig. IV-1, one can write equation (4.1) as

$$\frac{d}{dx}\Gamma_x(x) = -\nabla_{\parallel} \cdot \vec{\Gamma}_{\parallel} + n(x)\, n_0(x)\langle\sigma v\rangle_{iz} \tag{4.2}$$

where $\vec{\Gamma} \equiv n\vec{V}$ is the plasma flux.

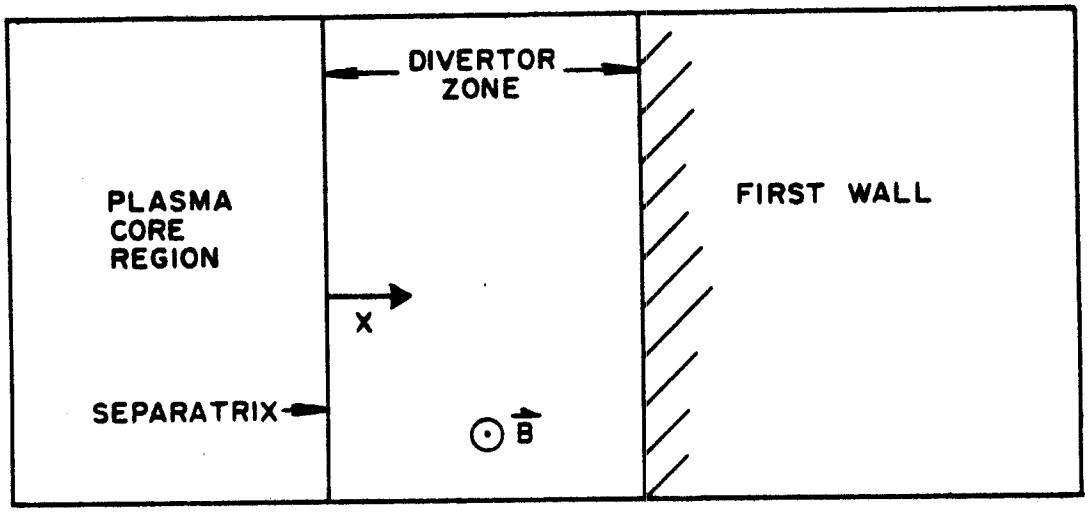

Figure IV-1

The assumption that the cross field motion is strictly diffusive is tantamount to taking Γ_x to be defined by a Fick's Law such as

$$\Gamma_x(x) \equiv -D_{\perp}\frac{dn}{dx} \tag{4.3}$$

where $D_{\perp}$ is the cross field diffusion coefficient and all other possible "off-diagonal" terms due to, say, temperature gradients, electric fields, etc. have been ignored.[1] $D_{\perp}$ will, however, be allowed to depend on density and x itself for some cases of interest. The most troublesome term in (4.2) is the $\nabla_{\parallel} \cdot \vec{\Gamma}_{\parallel}$ term which

represents the net particle loss along the field lines to the divertor collector plates. In order to keep the equations one-dimensional (i.e., dependent only on the coordinate x), the $\nabla_{\parallel} \cdot \Gamma_{\parallel}$ term is "modeled" by replacing it as shown below

$$\nabla_{\parallel} \cdot \vec{\Gamma}_{\parallel} \rightarrow \frac{\Gamma_{\parallel}(x)}{L(x)} \simeq \frac{n(x)\ v(x)}{L(x)} \simeq \frac{n(x)}{\tau_{\parallel}(x)} \tag{4.4}$$

In essence, one is replacing $\nabla_{\parallel} \cdot \vec{\Gamma}_{\parallel}$ with an adsorption or sink term which indicates that the density n(x) is lost (i.e., adsorbed, collected by the divertor) from a unit volume in a time $\tau_{\parallel}(x)$. Combining (4.2) through (4.4), one obtains

$$\frac{d}{dx}\left(-D_{\perp}\frac{dn}{dx}\right) = -\frac{n}{\tau_{\parallel}} + n\, n_0 \langle \sigma v \rangle_{iz} \tag{4.5}$$

and this is the equation which shall be used for the remainder of this chapter's analysis.

Using (4.5), one can make some interesting estimates of divertor behavior. It will not be until Chapter VI that we discover how close the quantitative results of using (4.5) come to the "more exact" results which arise when both particle and energy transport equations are solved simultaneously. In what follows, assumptions will be made as to the form of $D_{\perp}, \tau_{\parallel}$ and $n_0 \langle \sigma v \rangle_{iz}$. Let us begin with a look at the ionization term $n_0 \langle \sigma v \rangle_{iz}$.

Ionization Term

One can write $n\, n_0 \langle \sigma v \rangle_{iz}$ in the form

$$\frac{n}{\tau_{iz}} \equiv n\, n_0 \langle \sigma v \rangle_{iz} \tag{4.6}$$

which serves to define τ_{iz}, the characteristic time scale over which the plasma density can be built up due to the ionization of neutrals of density $n_0(x)$. To correctly solve (4.5) with this term (4.6) present, a transport equation for the neutral density $n_0(x)$ should be simultaneously solved. This is not "in the spirit" of a simple model and, indeed, for the qualitative behavior we are seeking, τ_{iz} will usually be taken as a constant.

To evaluate $\langle\sigma v\rangle_{iz}$ for hydrogen, one can use a rather popular approximation for $\langle\sigma v\rangle_{iz}$ given by[2]

$$\langle\sigma v\rangle_{iz} = \frac{10^{-5}[T_e/13.6]^{1/2}}{(13.6)^{3/2}[T_e/13.6 + 6]} \exp\left(-\frac{13.6}{T_e}\right) \frac{cm^3}{sec} \qquad (4.7)$$

where T_e is in eV. For $T_e \simeq 30$ gives $\langle\sigma v\rangle_{iz} \simeq 6 \times 10^{-9}$ cm^2/sec and for neutral density on the order of 2×10^{10} $\#/cm^3$, one finds a

$$\tau_{iz} \simeq [(2 \times 10^{10})(6 \times 10^{-9})]^{-1} \simeq 8 \text{ milliseconds}$$

Let us now turn our attention to the parallel loss terms.

Parallel Loss Terms

There are two possible characteristic times which can be used (separately or in combination with one another) to determine $\tau_{\|}$, the plasma loss rate to the divertor. The first time is merely that time which it takes the plasma to stream along the field lines to the collectors. To find this time scale, let us suppose that L is the average distance which the plasma must travel along the field lines in the divertor zone before it is away from the proximity of

the central plasma core* (i.e., into a region where it can no longer help shield the plasma core region from first wall originated neutrals and/or neutral impurities. Obviously, right on the separatrix ψ surface L would be infinite since $\vec{B}_p = 0$ at the null point. In fact, L varies rapidly as one moves from the separatrix towards the wall as is illustrated in Fig. IV-2. In order to make the solutions of (4.5) analytically tractable, we shall take L to be a constant and its value shall be chosen from a more detailed study of how the field lines behave in an actual divertor configuration. Using the ion

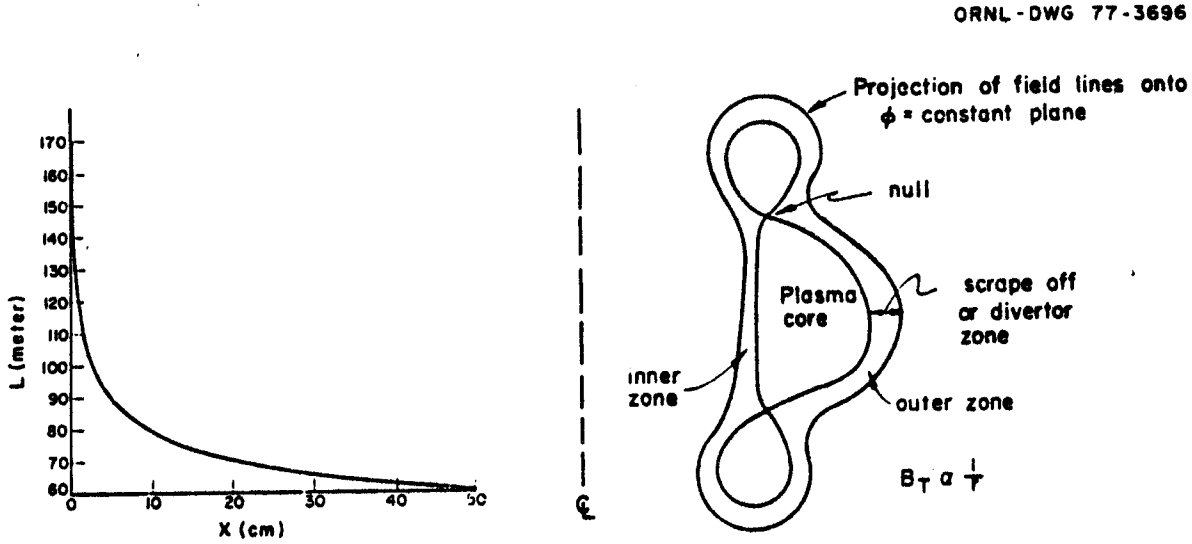

Figure IV-2

velocity, or in some cases the ion sound speed, as the characteristic flow speed for the plasma along the field lines, one finds a $\tau_{\|}$

*L shall be measured starting from the z = 0 plane.

given by

$$\tau_{\parallel} = L/v_{th} \equiv \tau_s \tag{4.8}$$

where $v_{th} \equiv 1/4\ (8/\pi\ k/m_i\ \max\ [T_i,T_e])^{1/2}$. Equation (4.8) can be thought of as a minimum characteristic time for plasma density loss along the field lines. If there were no impeding influences along the particle's path to the divertor collector plates, then $\tau_{\parallel}$ as given above would probably be correct to within a factor of 2 or 3.

As mentioned, there is another possible characteristic time for plasma loss in the divertor zone. This second time scaling is thought to come about if a fraction of the plasma in the divertor zone is impeded by a magnetic field gradient along the way to the collector. This is precisely the case one would suppose for the plasma diffusing into the "outer" divertor zone in a double null divertor as shown in Fig. IV-2. The plasma diffusing out at the z = 0 plane will see a magnetic mountain (due mostly to $\nabla B_{Toroidal}$) as it follows the field lines. The question then becomes one of how quickly this trapped plasma (which executes "banana orbits" in the divertor zone) will be untrapped or, to use the vernacular of the mirror "machinists," how fast will the loss cone be filled? The true answer is that no one yet knows. There are two extremes, however. If the loss cone fills classically* then $\tau_{\parallel} \sim \tau_{ii}$ which is the classical ion-ion collision

*Obviously, only a fraction of f_T of the plasma diffusing across the separatrix into the scrape-off zone will have velocity vectors which cause them to be trapped. Therefore, one would have $f_T n/\tau_{ii} + (1-f_T)\ n/\tau_s$ as a more correct term. Usually, however, $f_T \simeq .7$ so that for all practical purposes, Eq. (4.9) will suffice.

time. More exactly,

$$\tau_{ii} \leq \left(\frac{\theta_{LC}}{\pi/2}\right)^2 \left\{\frac{3}{4\sqrt{\pi}} \frac{(4\pi\,\epsilon_0)^2\, m_i^{1/2} (kT_i)^{3/2}}{q_i^4\, \ell n\, \Lambda_{ii}}\right\}$$

$$\simeq 2 \times 10^7\, (T_i(ev))^{3/2}\, \sqrt{AMV}/Z^4\, n_i(\#/cm^3)\, \ell n\, \Lambda_{ii} \text{ sec.} \tag{4.9}$$

where θ_{LC} = loss cone angle = $\sin^{-1}\left(\sqrt{B_{min}/B_{max}}\right)$. On the other hand, one may suspect that loss cone microinstabilities may develop. This possibility was investigated by Mense, Emmert, and Callen.[3] The essence of their calculations revealed that almost all loss cone microinstabilities should be unstable in the divertor region. Due to the short wavelengths of these modes ($k_\perp \rho_i \simeq \theta(1)$), they will produce little cross field diffusion. The $\vec{E}$ fields for these waves have growth rates $\gamma \approx \omega_{ci}$ which is considerably faster than the bounce frequency of a trapped ion ($\omega_{bi} \sim \sqrt{\epsilon}\, v_{thi}/qR_0$). The nonlinear consequence of such an unstable plasma is that if a loss cone develops (which takes time $(\omega_{bi})^{-1}$) it should be almost immediately filled. This filling would imply that $\tau_\parallel$ would be on the order of a few bounce periods for the ions, i.e.,

$$\tau_\parallel \sim 3\,(\omega_{bi})^{-1} \approx \frac{3\sqrt{\epsilon \frac{2T_i}{m_i}}}{qR_0} \sim \tau_s \tag{4.10}$$

which is the minimum characteristic loss time given by (4.8). Both (4.8) and (4.9) will, however, be used in this chapter in order to ascertain the limiting forms for $\tau_\parallel$ under these two extreme assumptions.

Cross Field Diffusion Coefficients

A cross field diffusion coefficient, $D_\perp$, is not easily determined from present day tokamak experiments, although the claim in ORMAK is that the particle density profile can be modeled using a reasonable multiple (~ 20) of the neoclassical value.[4] Rather than become involved in the pros and cons of cross field diffusion scaling, let us take, as we did with $\tau_\parallel$, a couple of extreme scalings. For example, one might expect that the smallest value for $D_\perp$ would come about using neoclassical scaling, i.e.,

$$(D_\perp)_{NC} \simeq \alpha_c D_c = \alpha_c \left\{\frac{8}{3}\left(\frac{2\pi m_e}{kT_e}\right)^{1/2} \frac{Z_{eff}\, n_e\, e^2\, \ell n\, \Lambda}{(4\pi\epsilon_0)^2\, B^2}\right\} \equiv A^* \frac{n}{T_e^{1/2}} \tag{4.11}$$

$$\simeq \alpha_c\, 3.55 \times 10^{-5} Z_{eff} n_e(\#/cm^3) \ell n\, \Lambda_e / B^2(\text{gauss}) T_e^{1/2}(\text{ev}) cm^2/\text{sec}$$

where $Z_{eff} \equiv \sum_j n_j z_j^2 / n_e$ and the sum is over all ion species in the plasma. In general, α_c is a function of space and the collisionality of the plasma. Its exact formulation will, however, not be of concern in this chapter. Therefore, α_c can be chosen as some constant and the resulting density profile can be parameterized by α_c values. $\alpha_c \simeq 100$ to 1000 would not be unusual.

The opposite extreme to neoclassical diffusion is usually judged to be Bohm diffusion. The Bohm value is taken (arbitrarily) to be

$$(D_\perp)_{Bohm} = \frac{kT_e}{16eB} = 6.25 \times 10^6 \frac{T_e(eV)}{B(\text{Gauss})} \frac{cm^2}{sec} \tag{4.12a}$$

and, in order to obtain a similar parameterization for $(D_\perp)_{Bohm}$ as α_c gives to $(D_\perp)_{NC}$, we shall arbitrarily multiply (4.12a) by a

constant α_B so that the value used for $D_\perp$ will be

$$D_\perp = \alpha_B \, 6.25 \times 10^6 \frac{T_e}{B} \frac{cm^2}{sec} \qquad (4.12b)$$

Values of α_B from 1 to 1/100 would not be unusual.

Solutions

Having two choices for $\tau_\parallel$ given by

$$(\tau_\parallel)_{min} = \tau_s \qquad \text{Eq. (4.8)}$$

and

$$(\tau_\parallel)_{max} = \tau_{ii} \qquad \text{Eq. (4.9)}$$

and two choices for $D_\perp$ given by

$$(D_\perp)_{min} = \alpha_c D_c \qquad \text{Eq. (4.11)}$$

and

$$(D_\perp)_{max} = \alpha_B D_{Bohm} \qquad \text{Eq. (4.12)}$$

one can proceed to try and solve Eq. (4.5) for n(x). Before doing so it is worthwhile to discuss the boundary conditions to be placed on Eq. (4.5).

In this chapter the boundary condition to be placed on (4.5) at the separatrix will be to require that the flux leaving the plasma core region (presumed known) and given by Γ_s should be balanced at the separatrix by $- D_\perp dn/dx$, i.e.,

$$- D_\perp \frac{dn}{dx}\bigg|_{separatrix} = \Gamma_s \qquad (4.13)$$

The boundary condition at the wall, however, needs to be discussed carefully. Intuitively one would expect that (given a reasonably wide separation between the separatrix and first wall) the plasma density in the scrape off zone should e-fold down relatively fast, thus allowing very little plasma to directly hit the first wall. This is obviously true as long as the ionization (source) term n/τ_{iz} in Eq. (4.5) is of negligible importance near the wall. It will be demonstrated in more detail in Chapter VII that this should indeed be the case at least near the wall since the plasma electrons will usually be cold in that region.* In any case, one can picture the plasma diffusing up to within an ion gyroradius of the wall and then the ions gyrate directly into the wall where they will be assumed to neutralize and return as neutrals. The electrons can be pictured to stream along the field lines near the wall until they eventually come in contact with a metallic surface which thus provides a closed current path, or they may be assumed to somehow leave across the field lines (magically) and hit the wall at the same rate as the ions. This type of "no return" boundary condition can be written in terms of the random and diffusive particle fluxes as

$$\Gamma_w^- \equiv \underbrace{\left(\frac{n\bar{v}_i}{4}\right)}_{\substack{\text{random}\\ \text{flux}}} + \underbrace{\frac{D_\perp}{2}\left(\frac{dn}{dx}\right)_{wall}}_{\substack{\text{diffusive}\\ \text{flux}}} = 0 \qquad (4.14)$$

*There may be some heating of the electrons by synchrotron radiation[5] or else one may wish to intentionally cause a warm plasma build up there by injecting and heating that zone.

Unfortunately, this type of boundary condition is difficult to apply numerically due to the fact that $\bar{v}/2D_\perp$ is usually so large that one must have a very fine grained special mesh to show how dn/dx drops off near the wall. To get around this numerical problem (which will show up in Chapter VI), we will investigate two other possible substitute boundary conditions. The first of these is to merely take the density of plasma at the wall to be zero or at least some extremely small number.

$$n(x_w) \simeq 0 \tag{4.15}$$

This condition is the handiest to use numerically. To get a feel for how good this is, we will compare (4.14) and (4.15) to the b.c. $n(x_w) \to 0$ and $x_w \to \infty$, i.e.,

$$\lim_{x_w \to \infty} n(x_w) = 0 \tag{4.16}$$

The results may appear surprising! This can be seen by working out a simple problem.

Case #1

$$D_\perp = \alpha_B D_{Bohm}, \quad \tau_\parallel = \tau_s$$

Writing out (4.5) using (4.8) and (4.12) and ignoring, for the moment, the ionization term $n\, n_0 \langle \sigma v \rangle$, one obtains

$$-\frac{d}{dx}\left(A\, T_e(x)\, \frac{dn}{dx}\right) = -\frac{n}{c}\,(T_i(x))^{1/2} \tag{4.17}$$

where $A = \alpha_B\, 6.25 \times 10^6/B(G)$ and $c = 2.5 \times 10^{-6}\ L(cm)\sqrt{AMU}$, which can easily be discerned from (4.8) and (4.12). Before n(x) can be found,

$T_e(x)$ and $T_i(x)$ must be known. In Chapter VI we will solve simultaneous equations for n, T_e, T_i, as well as $J_{Toroidal}$ and $B_{Poloidal}$. For now, however, we must content ourselves with a guess for T_e and T_i. The guess taken here (a rather well educated guess, too) for $T_e(x)$ and $T_i(x)$ is

$$T_e(x) = T_{es}\, e^{-x/\lambda_e}$$
$$T_i(x) = T_{is}\, e^{-x/\lambda_i} \tag{4.18}$$

where $x = 0$ will be taken as the separatrix and $x = d_w$ will be the first wall. With these choices (4.17) becomes

$$\frac{d^2n}{dx^2} - \frac{1}{\lambda_e}\frac{dn}{dx} = \frac{n}{(d_s)^2}\, e^{x/\lambda} \tag{4.19}$$

where

$$d_s \equiv \sqrt{D_\perp(0)\tau_s(0)} = \sqrt{\frac{A}{c}\, T_{es}T_{is}}^{1/2} \tag{4.20}$$

and

$$\frac{1}{\lambda} \equiv \frac{1}{\lambda_e} - \frac{1}{2\lambda_i} \tag{4.21}$$

Case #1a

Let us look at a special case of (4.19). As $\lambda_e, \lambda_i \to \infty$ which is the T_e = constant, T_i = constant case, one easily obtains

$$n(x) = c_1\, e^{-x/d_s} + c_2\, e^{x/d_s} \tag{4.22}$$

Applying (4.13) at $x = 0$, one obtains

$$n(x) = \frac{\Gamma_s}{D_s/d_s}\left\{R_w \cosh\left(\frac{x}{d_s}\right) - \sinh\left(\frac{x}{d_s}\right)\right\} \tag{4.23}$$

and $D_s \equiv D_\perp(0)$

$$\Gamma(x) = \Gamma_s \left\{ \cosh\left(\frac{x}{d_s}\right) - R_w \sinh\left(\frac{x}{d_s}\right) \right\} \tag{4.24}$$

where R_w depends on the boundary condition chosen at $x = d_w$. The possibilities are

$$R_w = \frac{\bar{v} \sinh (d_w/d_s) + 2D_s/d_s \cosh (d_w/d_s)}{\bar{v} \cosh (d_w/d_s) + 2D_s/d_s \sinh (d_w/d_s)} \tag{4.25a}$$

if one uses b.c. (4.14),

$$R_w = \frac{\sinh (d_w/d_s)}{\cosh (d_w/d_s)} \qquad \text{using (4.15)}, \tag{4.25b}$$

and

$$R_w = 1 \qquad \text{using } n(x_w \to \infty) = 0. \tag{4.25c}$$

Computing the flux of plasma incident onto the first wall divided by the flux entering the divertor gives a measure of how effective the divertor is in "unloading" the plasma into the collection chamber. For the case considered here (T_e, T_i = constants) one has

$$\begin{aligned} \frac{\Gamma(d_w)}{\Gamma(0)} &= \cosh (d_w/d_s) - R_w \sinh (d_w/d_s) \\ &\to \exp (- d_w/d_s) \text{ for } \frac{d_w}{d_s} \gg 1 \end{aligned} \tag{4.26}$$

A graphical display of (4.23) appears in Fig. IV-3. The important point to notice about n(x), which is demonstrated clearly in Fig. IV-3, is how the two boundary conditions $(n\bar{v}/4 + D/2\ dn/dx)_{d_w} = 0$ and $n(d_w) = 0$ give almost exactly the same n(x). In fact, they only differ when one gets within a fraction of a centimeter of the wall.

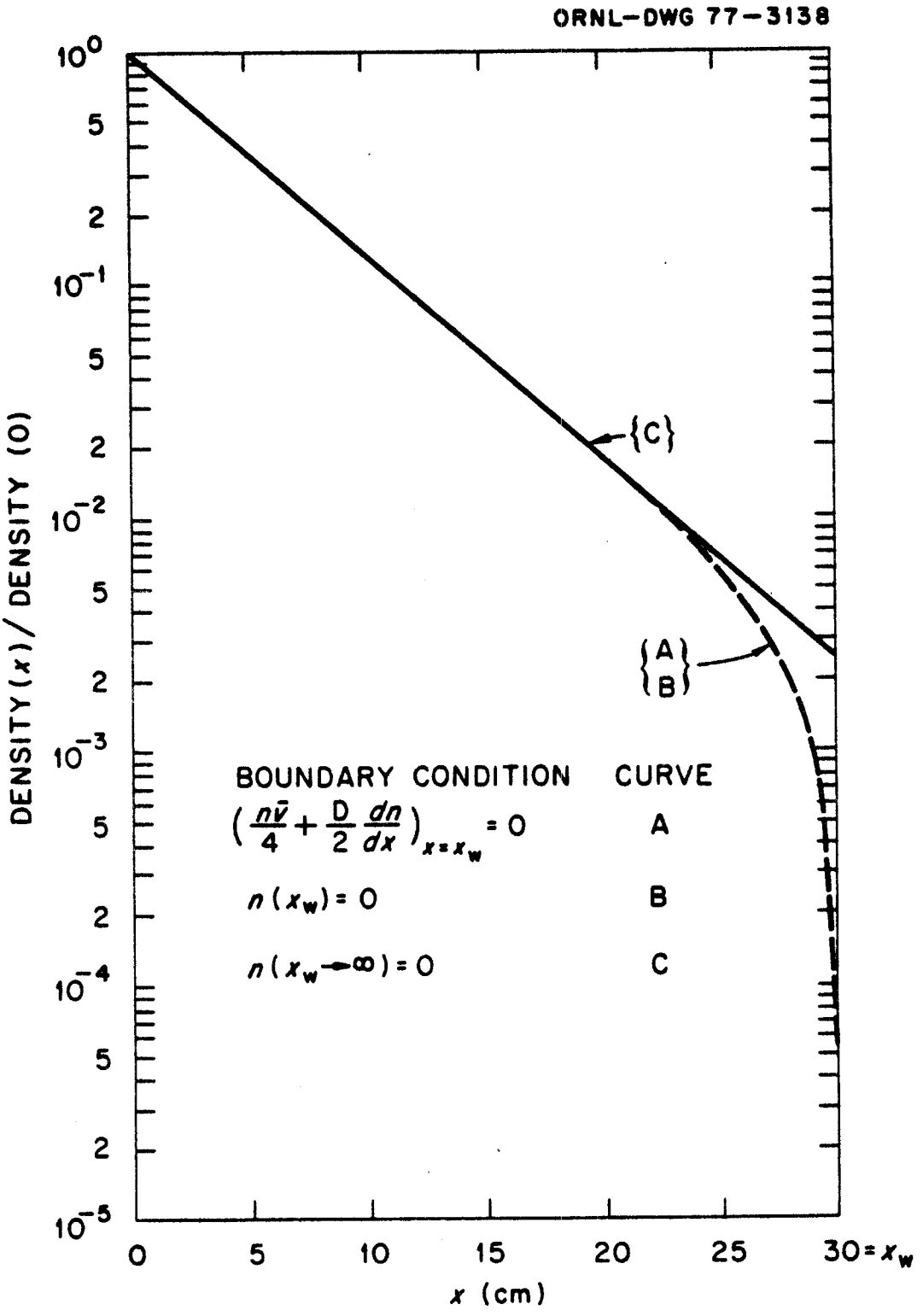
ORNL-DWG 77-3138
DENSITY (x) / DENSITY (0)
10^0
5
2
10^{-1}
5
2
10^{-2}
5
2
10^{-3}
5
2
10^{-4}
5
2
10^{-5}
{C}
{A}
{B}
BOUNDARY CONDITION
CURVE
$\left(\frac{n\bar{v}}{4} + \frac{D}{2}\frac{dn}{dx}\right)_{x=x_w} = 0$
A
$n(x_w) = 0$
B
$n(x_w \to \infty) = 0$
C
0
5
10
15
20
25
$30 = x_w$
x (cm)

Figure IV-3

The $n(d_w \to \infty) = 0$ solution coincides up to 9 cm from the wall so that one could use e^{-x/d_s} as a good approximation to the true solution over most of the scrape off zone.

To allow a fair comparison, all numerical examples will be solved using the data shown in Table IV-1. This data should not, however, be looked upon as data absolutely characteristic of a "real" divertor.

TABLE IV-1

PLASMA PARAMETERS

$T_{es} = 720$ eV	$\lambda_e = 3.25$ cm
$T_{is} = 3000$ eV	$\lambda_i = 16.25$ cm
$B = 3 \times 10^4$ Gauss	$f_T = .4$
$L = 2 \times 10^4$ cm	$\bar{v} = 10^7$ cm/sec
$\alpha_B = .1$	$\tau_{iz} = .01$ sec
$\alpha_c = 100$	$d_s = 3.25$ cm
$Z_{eff} = 1.0$	$d_{cs} = .15$ cm
$\ell n\, \Lambda = 10$	$\lambda = \lambda_e/.9 = 3.6$ cm
$(\theta_{LC}\, 2/\pi)^2 = T/4$	$\tau^*_{\parallel s} = 7.5 \times 10^{-4}$ sec

Case #1b

The previous example assumed T_e and T_i were constants (i.e., $\lambda_e, \lambda_i \to \infty$). Keeping λ_e, λ_i at some fixed finite values such that $\lambda > 0$ leads one to solve (4.19) through the use of the obvious coordinate transformation

$$y = e^{x/\lambda} \tag{4.27}$$

This transformation applied to (4.19) produces the equation

$$y \frac{d^2n}{dy^2} - \left(\frac{\lambda}{\lambda_e} - 1\right) \frac{dn}{dy} - \left(\frac{\lambda}{d_s}\right)^2 n = 0 \qquad (4.28)$$

which can be transformed using $z = 2i\, \lambda/d_s \sqrt{y}$ into a form of Bessel's equation which gives a solution

$$n(y) = y^{p/2} \left[A\, I_p(2p\sqrt{y}) + B\, K_p(2p\sqrt{y})\right] \qquad (4.29)$$

where $p \equiv \lambda/\lambda_e$ If $\lambda < 0$, one has the J_{-p} and Y_{-p} functions instead of I_p and K_p.

For simplicity, let us look at the case $\lambda = \lambda_e$ which implies that the ion temperature in the divertor zone stays constant while the electron temperature exponentially decays. In this case, $\lambda/\lambda_e = 1$, $p = 1$ and one obtains the solution for $n(x)$ and $\Gamma(x)$ in the form

$$n(x) = \frac{\Gamma_s}{D_s/d_s} \sqrt{y} \left\{ \frac{K_1(\xi) - R_w^* I_1(\xi)}{K_{Os} - R_w^* I_{Os}} \right\} \qquad (4.30)$$

and

$$\Gamma(x) = \Gamma_s \left(\frac{y}{y_s}\right) \left\{ \frac{K_O(\xi) + R_w^* I_O(\xi)}{K_{Os} + R_w^* I_{Os}} \right\} \qquad (4.31)$$

where

$$\xi \equiv 2 \frac{\lambda_e}{d_s} \sqrt{y} = 2 \frac{\lambda_e}{d_s} e^{x/2\lambda_e} \qquad (4.32)$$

and

$$I_{O\alpha} \equiv I_O \left(2 \frac{\lambda_e}{d_s} e^{x_\alpha/\lambda_e}\right) \text{ and } y_s = e^0 = 1$$

The form of R_w^* depends on the boundary condition applied at the first wall.

$$R_w^* = \begin{cases} \dfrac{\bar{v}\, K_{1w} - \xi_w\, D_s/\lambda_e\, K_{0w}}{\bar{v}\, I_{1w} + \xi_s\, D_s/\lambda_e\, I_{0w}} & \text{using (4.14)} \\ \dfrac{K_{1w}}{I_{1w}} & \text{using (4.15)} \\ 0 & \text{for } n(d_w \to \infty) = 0 \end{cases} \tag{4.33}$$

As with the $\lambda_e, \lambda_i \to \infty$ cases, we have plotted n(x) for Eq. (4.31) in Fig. IV-4. For comparison, the form of the solution to the T_e, T_i = constant case [Eq. (4.23)] is also plotted in Fig. IV-4. Note the very close agreement of the solutions independent of the boundary condition applied at the wall. The more rapid drop off is obviously due to the T_e dependence in the Bohm diffusion coefficient. If we had kept λ_i finite so that $\lambda > \lambda_e > 0$, we would have had I_p and K_p functions with $p = \lambda/\lambda_e \neq 1$ which is, in general, non-integral. The qualitative appearance differs little from I_1 and K_1 except that $p > 1$ would give a faster drop off in density than $p = 1$. If $\lambda < 0$ due to the improbable case that $2\lambda_i < \lambda_e$, then one would have J_{-p} and Y_{-p} functions which would give a more convex appearing drop off, i.e., one would have more cross field diffusion than effusion along the field lines and this would produce a broader region of density in the scrape off zone.

Case #1c

If we had chosen $T_i(x)$ = constant, added an ionization term $n(n_0\langle\sigma v\rangle_{iz})$, and had taken $n_0\langle\sigma v\rangle_{iz} \simeq$ constant, then one would also have an equation similar to (4.17). It would look like

$$-\frac{d}{dx}\left(A\, T_e(x)\, \frac{dn}{dx}\right) = -n\left(\frac{T_i^{1/2}}{c} - n_0\langle\sigma v\rangle_{iz}\right) = -n\left(\frac{1}{\tau_s} - \frac{1}{\tau_{iz}}\right) \tag{4.34}$$

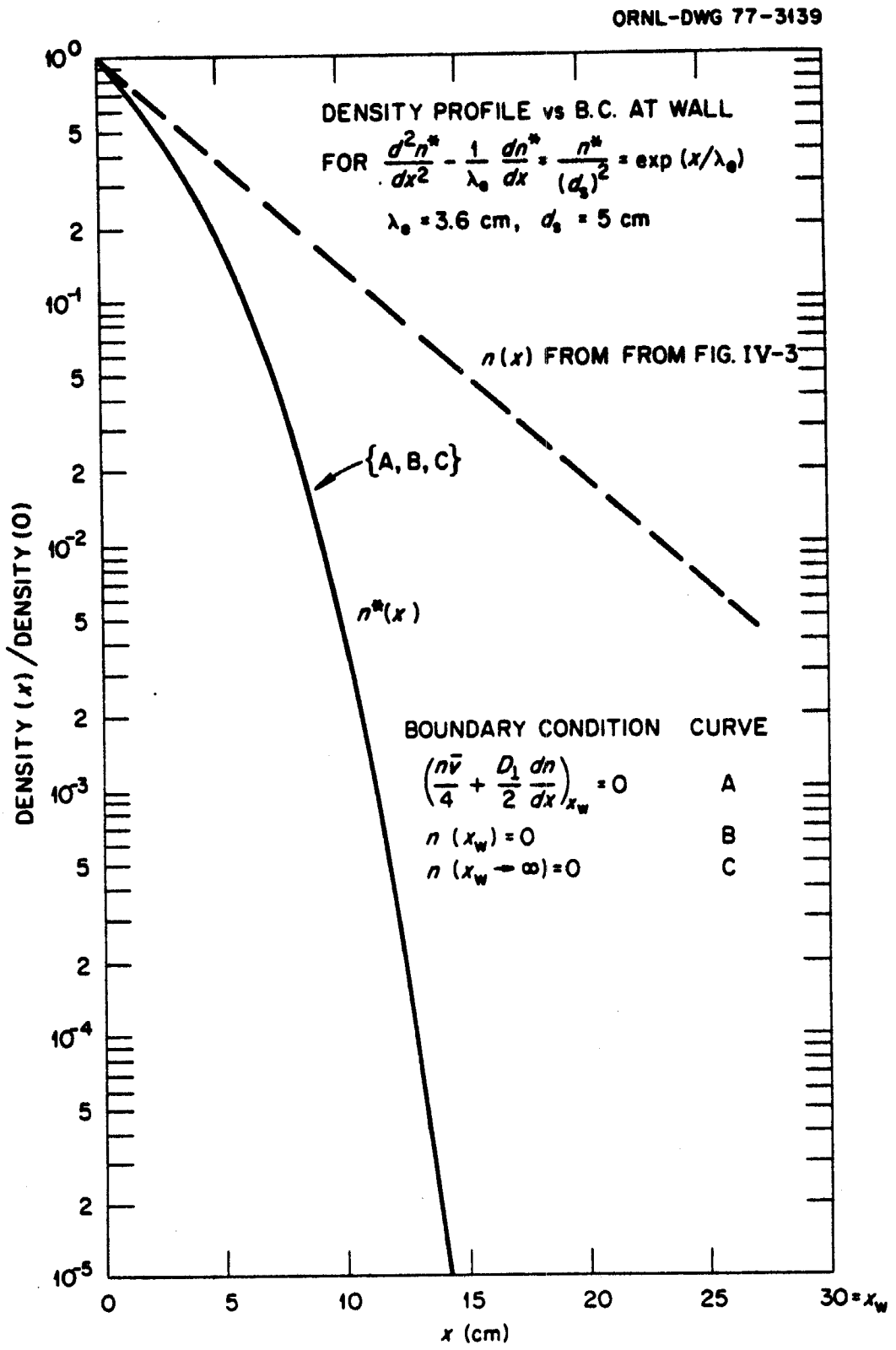
ORNL-DWG 77-3139
DENSITY PROFILE vs B.C. AT WALL
FOR $\frac{d^2n^*}{dx^2} - \frac{1}{\lambda_e}\frac{dn^*}{dx} = \frac{n^*}{(d_s)^2} = \exp(x/\lambda_e)$
$\lambda_e = 3.6$ cm, $d_s = 5$ cm
$n(x)$ FROM FROM FIG. IV-3
{A, B, C}
$n^*(x)$
BOUNDARY CONDITION CURVE
$\left(\frac{n\bar{v}}{4} + \frac{D_1}{2}\frac{dn}{dx}\right)_{x_w} = 0$ A
$n(x_w) = 0$ B
$n(x_w \to \infty) = 0$ C
DENSITY (x) /DENSITY (0)
10^0
5
2
10^{-1}
5
2
10^{-2}
5
2
10^{-3}
5
2
10^{-4}
5
2
10^{-5}
0
5
10
15
20
25
30 = x_w
x (cm)

Figure IV-4

which (assuming $T_e = T_{es}\, e^{-x/\lambda_e}$) becomes

$$\frac{d^2n}{dx^2} - \frac{1}{\lambda_e}\frac{dn}{dx} = \frac{n\, e^{x/\lambda_e}}{D_s\, \tau^*} \tag{4.35}$$

where

$$\frac{1}{\tau^*} \equiv \frac{1}{\tau_s} - \frac{1}{\tau_{iz}} \tag{4.36}$$

The solutions would be I_1 and K_1 functions as long as $\tau^* > 0$. This implies physically that the time scale for loss along the field lines is shorter than the ionization time scale. For $\tau^* < 0$, one would obtain the more convex looking functions which indicate that the ionization source term is stronger than the parallel loss term. This would broaden the divertor density profile and therefore "call upon" the cross field diffusion term to transport some of the plasma to the walls in order to establish a steady state. The solution of (4.35) would then be in terms of J_1 and Y_1 functions.

Having just looked at the two fastest time scales, $D_\perp = D_{Bohm}$ and $\tau_\parallel = \tau_s$, it is worthwhile now to consider the other extreme.

Case #2

$$D_\perp = D_{NC},\ \tau_\parallel = \tau_{ii}$$

Assuming T_e, T_i have constant values, one can use (4.9) for τ_{ii} and (4.11) for $D_\perp$ in Eq. (4.5). This produces the equation

$$-\frac{A^*}{2T_{es}^{1/2}}\frac{d^2}{dx^2}n^2 = -\frac{n^2}{C^* T_{is}^{3/2}} - n\, n_0 \langle\sigma v\rangle_{iz} \tag{4.37}$$

when $A^* \simeq 3.55 \times 10^{-4}\, \alpha_c\, Z_{eff}/(B(\text{Gauss}))^2$, $C^* = 1.9 \times 10^6 (2\theta_{LC}/\pi)^2$,

and $\ln \Lambda \simeq 10$. Ignoring the ionization term gives a simple solution for $n^2(x)$, i.e.,

$$n^2(x) = C_1 e^{-x/d_{cs}} + C_2 e^{x/d_{cs}} \tag{4.38}$$

where

$$d_{cs}^2 = \frac{A^* C^* T_{is}^{3/2}}{2T_{es}^{1/2}} = \frac{D_{NC}(x=0)\tau_{ii}(x=0)}{2} = \alpha_c \rho_{Le}\rho_{Li}\left(\frac{T_i}{4T_e}\right) \tag{4.39}$$

Applying b.c. (4.13) at $x = 0$ (the separatrix) and imposing for simplicity the b.c. $n(x_w \to \infty) = 0$ produces the solutions

$$n(x) = \sqrt{\frac{\Gamma_s d_{cs}}{\alpha_s}}\ e^{-x/2d_{cs}} \tag{4.40}$$

and

$$\Gamma(x) = -\alpha_s \frac{d}{dx} n^2 = \Gamma_s e^{-x/d_{cs}} \tag{4.41}$$

For the parameters listed in Table IV-1, one finds that

$$d_{cs} = \sqrt{\frac{(1.3 \times 10^{-4})(10^2)(1)(1.9 \times 10^6)(1/4)(3000)^{3/2}}{(3 \times 10^4)^2(2)(720)^{1/2}}}$$

$$\simeq .15 \text{ cm} \tag{4.42}$$

$$\alpha_s = \frac{(1.3 \times 10^{-4})(10^2)(1)}{(3 \times 10^4)^2(2)(720)^{1/2}} = 2.7 \times 10^{-13}$$

and if $\Gamma_s = 10^{17}$ #/cm^2/sec leaving the plasma, then the separatrix density would rise to

$$n_s = \sqrt{\frac{(10^{17})(.15)}{2.7 \times 10^{-19}}} \simeq 2.4 \times 10^{14} \text{ cm}^{-3} \tag{4.43}$$

Comparing this value with n_s obtained from (4.23) which is for Bohm diffusion and streaming loss term, one has (again using Table IV-1

where $d_s \simeq 4.65$ cm) $n_s \simeq 2 \times 10^{13}$ cm^{-3} which is an order of magnitude lower.

Thus, as would have been suspected all along, $D = 1/10\ D_{Bohm}$, $\tau_{\parallel} = \tau_s$ produces a lower density ($n_s \sim 2 \times 10^{13}$) broader ($\lambda_n \sim 3$ cm) scrape off zone than does $D = 100\ D_{NC}$, $\tau_{\parallel} = \tau_{ii}$ where $n_s \sim 2.4 \times 10^{14}$, $\lambda_n \sim .15$ cm. A comparison will be made of the "shielding" capabilities of their two plasma profiles later in this chapter. Before this is done, however, a few words are necessary concerning the other two possible pairings of $D_{\perp}$ and $\tau_{\parallel}$, i.e., $D_{\perp} = D_{Bohm}$, $\tau_{\parallel} = \tau_{ii}$ and $D_{\perp} = D_{NC}$, $\tau_{\parallel} = \tau_s$.

Case #3

$$D_{\perp} = D_B, \quad \tau_{\parallel} = \tau_{ii}$$

The resulting equation after taking $T_e(x) = T_{es}$, $T_i(x) = T_{es}$, and τ_{iz} = constant is

$$\underbrace{\frac{d^2n}{dx^2}}_{\text{diffusion}} = \underbrace{\frac{n^2}{\gamma^2}}_{\parallel\text{-loss}} - \underbrace{\frac{n}{\lambda^2}}_{\text{ionization}} \tag{4.44}$$

where $\gamma^2 \equiv AT_{es}C^*T_i^{3/2}$ and $\lambda^2 = AT_{es}\tau_{iz}$. This transforms into

$$\int_{n_s}^{n} \frac{dn}{\sqrt{n^2(n-\xi)+C_0}} = -\sqrt{\frac{2}{3}} \int_0^x \frac{dx}{\gamma} \tag{4.45}$$

where $\xi \equiv \frac{3}{2}(\gamma/\lambda)^2$ and n_s, C_0 are the two constants which must be evaluated by applying the appropriate boundary conditions. Unfortunately, this is easier said than done. The solution to (4.45) can be expressed in terms of elliptic functions.[6] The problem is that

one does not know which elliptic function until C_0 is known, and C_0 is the solution to a transcendental equation involving the elliptic function itself. Thus one can, in principle, find an analytic solution, but in practice it is easier to solve (4.44) numerically.

Qualitatively, we can see from Eq. (4.44) itself that as long as $n > (\nu/\lambda)^2 \equiv n_c$, the second derivative is always positive. This implies an "exponential-like" decay or concave profile for n(x). At $n = n_c, n'' = 0$ and for $n < n_c$, one will find a more convex ("cosine-like") profile down to $n = 0$. The solution to (4.44) using b.c. (4.13) is shown in Fig. IV-5. The b.c. at the wall was $n \geq 0$. It clearly shows that one obtains a wider region of reasonably high density. This is to be expected since even 1/10 Bohm diffusion produces relatively large transport rates on the time scale of τ_{ii} which is the loss time in this case. An important point to note from Fig. IV-5 is that the ionization rate does not affect the separatrix density very much as long as τ_{iz} is reasonably long (> 10 millisec). This indicates that if mirror detrapping was the governing mechanism for parallel ion loss (i.e., $\tau_{\parallel} \simeq \tau_{ii}$) in the divertor zone, then $D_\perp$ = 1/10 Bohm would provide a relatively wide plasma density profile which would shield the plasma core region relatively well. However, as Mense, et al.[3] have pointed out, one may find that loss cone microinstabilities may make $\tau_{\parallel}$ significantly smaller than τ_{ii}!

As a last example, we can investigate the consequences of assuming $D_\perp = D_{NC}$ and $\tau_{\parallel} = \tau_s$.

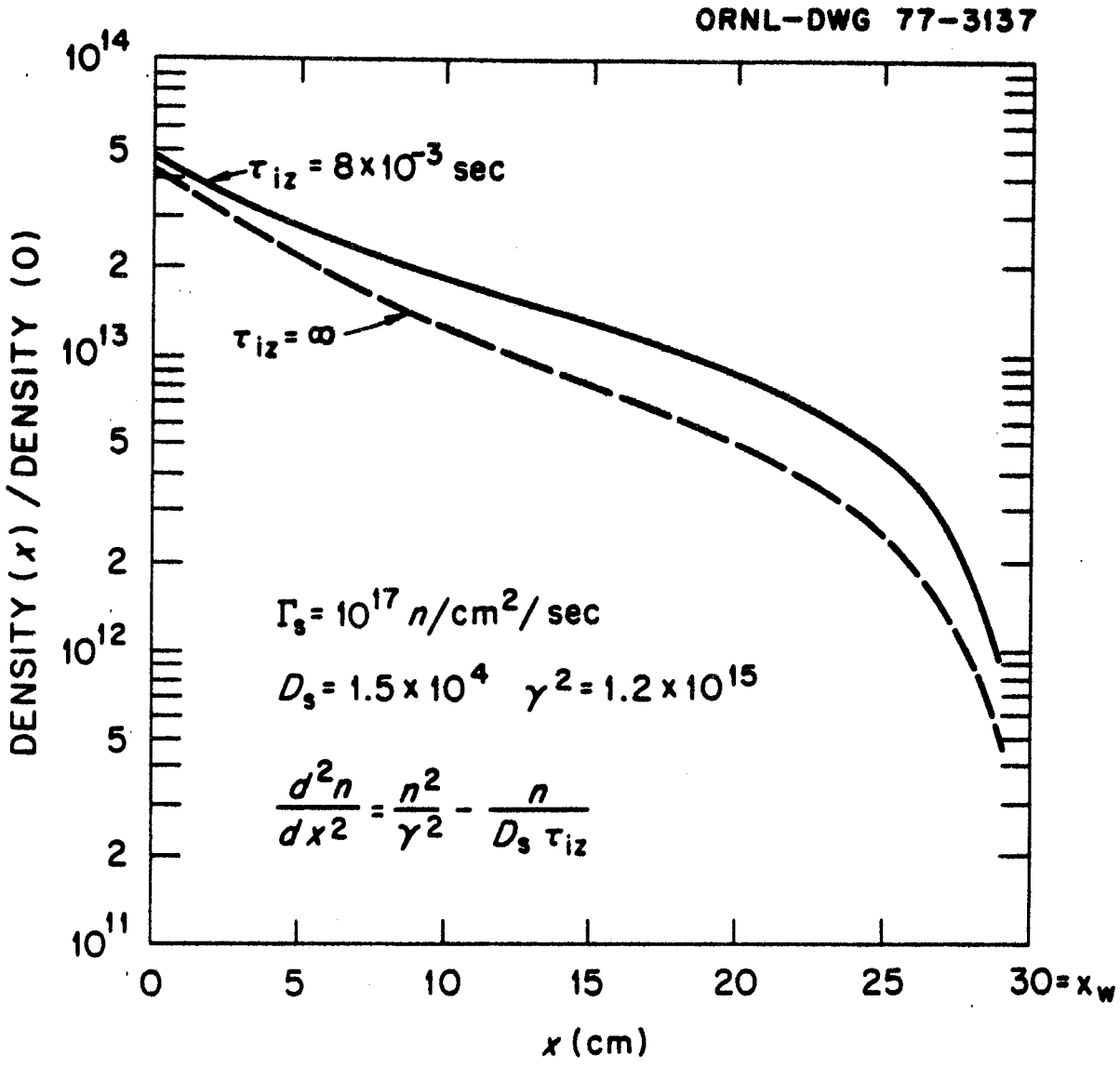
ORNL-DWG 77-3137
DENSITY (x) / DENSITY (0)
10^{14}
5
2
10^{13}
5
2
10^{12}
5
2
10^{11}
$\tau_{iz} = 8 \times 10^{-3}$ sec
$\tau_{iz} = \infty$
$\Gamma_s = 10^{17}\ n/cm^2/sec$
$D_s = 1.5 \times 10^4 \quad \gamma^2 = 1.2 \times 10^{15}$
$\frac{d^2n}{dx^2} = \frac{n^2}{\gamma^2} - \frac{n}{D_s \tau_{iz}}$
0
5
10
15
20
25
30 = x_w
x (cm)

Figure IV-5

Case #4

$$D_\perp = D_{NC},\ \tau_\parallel = \tau_s$$

The equation to be solved in this case is

$$-\frac{d}{dx}\left(\frac{A^*}{T_e^{1/2}}\, n\, \frac{dn}{dx}\right) = -\frac{n}{C}\, T_i^{1/2} + \frac{n}{\tau_{iz}} \tag{4.46}$$

where $A^* = 3.55 \times 10^{-4}\ \alpha_c\ Z_{eff}/B_G^2$, $C = 2.5 \times 10^{-6}\ L(cm)\ \sqrt{AMU}$. Taking T_e and T_i as constants, this equation transforms into

$$\frac{d^2}{dx^2}\,(n^2) = \frac{n}{\lambda^2} \tag{4.47}$$

where $1/\lambda^2 = 1/D_s^*\ (1/\tau_s - 1/\tau_{iz})$ and $D_s^* \equiv A^*/2T_{es}^{1/2}$. Using the transformation $p = dn^2/dx$, one can rewrite (4.47) as

$$\frac{p}{2n}\,\frac{dp}{dn} = \frac{n}{\lambda^2} \tag{4.48}$$

which has as its first integral

$$\frac{d(n^2)}{dx} = -\sqrt{\frac{4}{3\lambda^2}\, n^3 + C} = 2n\,\frac{dn}{dx} \tag{4.49}$$

Since $\Gamma = D_s^*\ d(n^2)/dx$, one notes that if $n \to 0$ anywhere short of the first wall ($x < x_w$), then Γ should be zero there also. This is obvious from physical reasoning. If, however, $n \to 0$ <u>at</u> the first wall, then Γ does not have to be zero there. Let us search for that special class of solutions where $\Gamma \to 0$ when $n \to 0$. They are analytically tractable solutions. The more general case involves elliptic functions much as in Case #3 which was just discussed.

The requirement that $\Gamma = 0$ when $n = 0$ implies that $C = 0$ in (4.49). This produces

$$2n \frac{dn}{dx} = - \frac{2}{\sqrt{3\lambda^2}} n^{3/2} \tag{4.50}$$

which has the solution

$$n = n_s \left(1 - \frac{x}{\xi}\right)^2 \tag{4.51}$$

where

$$\xi \equiv 2\sqrt{3D_s^* n_s \tau} = 3\left(\frac{4}{3} D_s^* \Gamma_s \tau^2\right)^{1/3}$$

$$n_s = \left(\frac{3}{4} \frac{\tau}{D_s^*} \Gamma_s^2\right)^{1/3} \tag{4.52}$$

$$\tau^{-1} \equiv \tau_s^{-1} - \tau_{iz}^{-1}$$

and Γ_s is the flux entering the divertor from the central plasma core.

We note the following characteristics about the solution given by (4.51). First $n = 0$ at $x = \xi$. ξ depends on $(\tau_{iz} - \tau_s)^{-1}$ through τ. As $\tau_{iz} \to \tau_s$, then $\tau \to \infty$, $\xi \to \infty$, $n_s \to 0$ and the density drop off in the divertor zone is very broad. This occurs since the ionization rate is becoming comparable to the parallel loss rate.

A more general class of solutions than those requiring $\Gamma \to 0$ as $n \to 0$ can be found by transforming (4.49) using b.c. (4.13) to determine C.

$$\Gamma_s = - D_s^* \frac{d}{dx} (n_s^2) = D_s^* \sqrt{\frac{4}{3\lambda^2} n_s^3 + C}$$

which implies

$$C = \left(\frac{\Gamma_s}{D_s^*}\right)^2 - \frac{4}{3\lambda^2} n_s^3$$

$$= \frac{4 n_s^4}{3 D_s^* n_s \tau} \left(\frac{3\tau}{4 D_s^* n_s} \left(\frac{\Gamma_s}{n_s}\right)^2 - 1\right) \qquad (4.53)$$

Then (4.49) can be expressed as

$$\int_{n_s}^{n} \frac{n dn}{\sqrt{n^3 + n_s^3 K}} = - \frac{x}{\sqrt{3 D_s^* \tau}} \qquad (4.54)$$

and

$$K \equiv \frac{3}{4} \frac{\tau_s}{D_s^* n_s} \left(\frac{\Gamma_s}{n_s}\right)^2 - 1 \qquad (4.54)$$

Using the transformation to $y = n_s$, one has

$$\int_{1}^{(n/n_s)} \frac{y dy}{\sqrt{y^3 + K}} = - \frac{x}{\eta} \qquad (4.55)$$

where η is defined as $\sqrt{3 D_s^* n_s \tau}$. The solution is an elliptic function. The remaining undetermined constant K or n_s, if you prefer, is determined by setting a boundary condition at $x = x_w$, the wall. If one takes $n \to 0$ at $x = x_w$, then (4.55) can be solved for K by iteration, i.e., solve

$$\int_{0}^{1} \frac{y dy}{\sqrt{y^3 + K}} = \frac{x_w}{\eta} \qquad (4.56)$$

The problem which occurs in solving (4.56) for K is the same one run into in Case #3. The integral on the left hand side of (4.56) can be expressed as an elliptic function(s) whose type and arguments depend

on the roots of $y^3 + K = 0$, but K is unknown!

Numerical solutions to (4.47) are shown in Fig. IV-6. There it is clearly seen that as $\tau_{iz} \to \infty$, the density drops off very rapidly. In fact, one usually has numerical difficulties due to the "steepness" of the solutions when $\tau_{iz} \to \infty$ and τ_s is short. To obtain some analytic feel for this, let us examine the value of ξ as used in (4.51). Taking values from Table IV-1 with $\tau_{iz} = \infty$, one finds

$$D_s^* = \frac{(3.55 \times 10^{-4})(100)(1)}{(3 \times 10^4)^2\, 2(720)^{1/2}} = 7.35 \times 10^{-13}$$

$$\tau = \tau_s = \frac{(2.5 \times 10^{-6})(2 \times 10^4)(2.5)^{1/2}}{(3000)^{1/2}} = 1.44 \times 10^{-3}$$

and taking $\Gamma_s = 10^{17}$ #/cm^2/sec, ξ becomes

$$\xi = 3\left(\frac{4}{3}(7.35 \times 10^{-13})(10^{17})(1.44 \times 10^{-3})^2\right)^{1/3} = 1.77 \text{ cm}$$

which is extremely small and implies very steep density gradients. Note that $n_s = 2.45 \times 10^{14}$ using (4.52) for the case where $\xi = 1.77$ cm. One can see that high edge densities are a general result of neoclassical cross field transport in the divertor zone. In fact, even if $\tau = 10^{-4}$ seconds, n_s would only drop to 1×10^{14} #/cm^3 which is still very high.

We have now looked at the four possible pairings of the transport coefficients $(D_\perp, \tau_\parallel)$. In general, one finds from the solutions to the equations the following properties of interest.

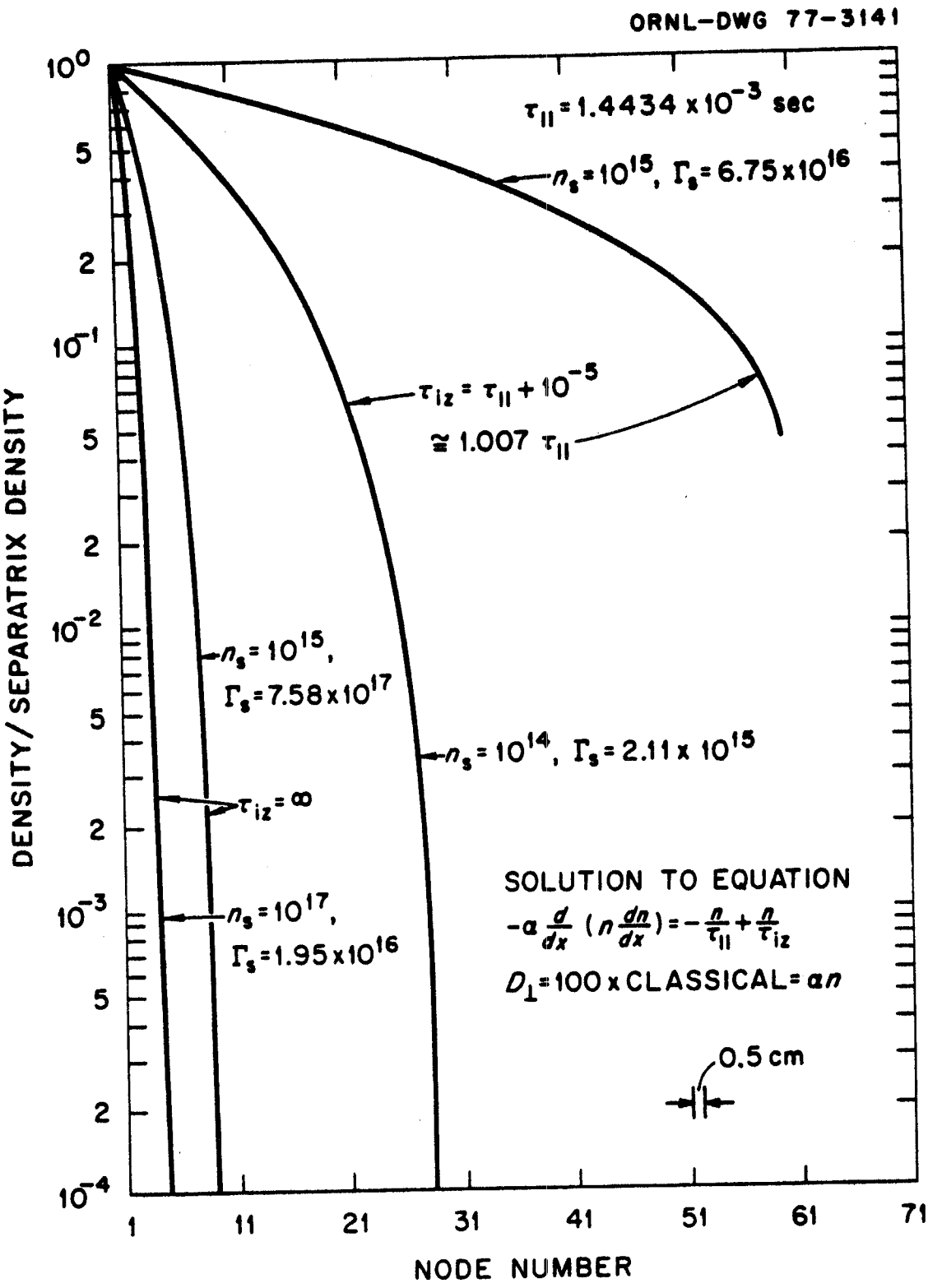
ORNL-DWG 77-3141
$\tau_{||} = 1.4434 \times 10^{-3}$ sec
$n_s = 10^{15}$, $\Gamma_s = 6.75 \times 10^{16}$
$\tau_{iz} = \tau_{||} + 10^{-5}$
$\cong 1.007\ \tau_{||}$
$n_s = 10^{15}$, $\Gamma_s = 7.58 \times 10^{17}$
$n_s = 10^{14}$, $\Gamma_s = 2.11 \times 10^{15}$
$\tau_{iz} = \infty$
$n_s = 10^{17}$, $\Gamma_s = 1.95 \times 10^{16}$
SOLUTION TO EQUATION
$-\alpha \frac{d}{dx}\left(n \frac{dn}{dx}\right) = -\frac{n}{\tau_{||}} + \frac{n}{\tau_{iz}}$
$D_\perp = 100 \times$ CLASSICAL $= \alpha n$
0.5 cm
DENSITY/SEPARATRIX DENSITY
NODE NUMBER
10^0
5
2
10^{-1}
5
2
10^{-2}
5
2
10^{-3}
5
2
10^{-4}
1
11
21
31
41
51
61
71

Figure IV-6

1) The boundary condition at the wall ($x = x_w$) does not sensitively effect the density profile near the separatrix nor, in fact, over much of the scrape off zone as long as x_w is moderately large, e.g., $x_w \geq 3\lambda_n$.

2) Low $D_\perp$ values cause thin density drop off regions in the divertor and high separatrix densities for a given fixed incident plasma flux Γ_s.

3) If $T_e(x)$ decreases more rapidly than $T_i(x)$ using $D_\perp = D_{Bohm}$ and $\tau_\parallel = \tau_s$, then one can still have a reasonably thin scrape off zone (see Case #1).

4) Ionization of neutrals in the divertor zone does act to broaden the density profile in that zone.

Let us now discern the consequences of having different density profiles in the divertor zone in terms of its impurity shielding efficiency.

Impurity Shielding

One figure of merit for a divertor in the ratio of the impurity neutral flux which crosses the separatrix and enters the hot plasma core to the same flux leaving the first wall. Since the neutral impurities are usually produced by various and sundry means (sputtering, photo-electron desorption, vaporization) one can expect the impurity neutrals to leave the wall with some type of angular distribution. If we consider a slab geometry and assume the impurities to come off of the first wall isotropically, then it is an easy problem

in transport theory to show that the probability of an impurity neutral reaching the separatrix (x = 0) having left the wall ($x = x_w$) with speed v_0 is

$$p(x=0) = \int_0^1 \exp\left\{-\frac{1}{\mu}\left|\int_{x_w}^{x=0}\frac{dx}{\lambda_T}\right|\right\} d\mu \qquad (4.57)$$

and $\lambda_T^{-1} = n_e(x)\langle\sigma v\rangle_{iz}^z(x)/v_0$. The integral over μ is recognized as E_2, an exponential integral.[1] To obtain some feel for how much $E_2(x)$ differs from e^{-x} one can look at Fig. IV-7. It is easily seen that the integration over solid angle can produce a reasonable reduction in the probability of impurity entrance into the hot plasma core region. A brief numerical illustration is in order.

Case #1

$$D_\perp = 1/10\ D_{Bohm},\quad \tau_\parallel = \tau_s$$

Using (4.23) and the b.c. $n(x_w \to \infty) = 0$, one finds (assuming $\langle\sigma v\rangle_{ix}$ = constant):

$$\left|\int_{x_w}^{0}\frac{n_e\langle\sigma v\rangle_{iz}}{v_0}\,dx\right| = \frac{\Gamma_s d_s}{v_0 D_s}\langle\sigma v\rangle_{iz}\left|\int_{x_w}^{0} e^{-x/d_s}\,dx\right|$$

$$= \frac{\Gamma_s d_s^2}{v_0 D_s}\langle\sigma v\rangle_{iz}\left(1 - e^{-x_w/d_s}\right)$$

for $x_s/d_s \gg 1$

$$\simeq \frac{\Gamma_s d_s^2}{v_0 D_s}\langle\sigma v\rangle_{iz} \equiv A_1 \qquad (4.58)$$

and thus

$$p(0) = \int_0^1 d\mu\ e^{-A_1/\mu}$$

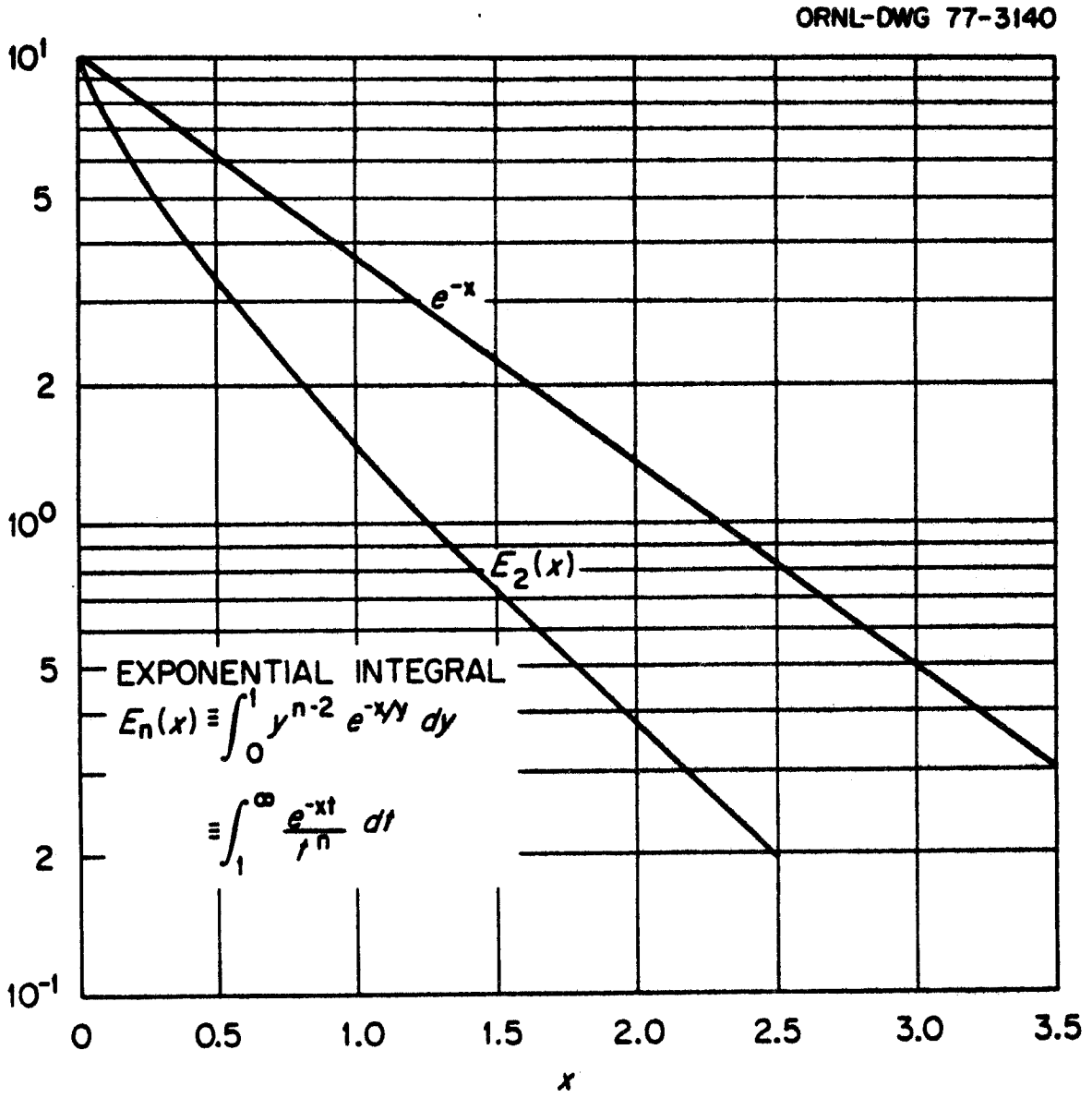
ORNL-DWG 77-3140
10^1
5
2
10^0
5
2
10^{-1}
0
0.5
1.0
1.5
2.0
2.5
3.0
3.5
x
e^{-x}
$E_2(x)$
EXPONENTIAL INTEGRAL
$E_n(x) \equiv \int_0^1 y^{n-2} e^{-x/y}\, dy$
$\equiv \int_1^\infty \frac{e^{-xt}}{t^n}\, dt$

Figure IV-7

Case #2

$$D_\perp = 100\, D_c,\quad \tau_\parallel = \tau_{ii}$$

$$\left| \int_{x_w}^{0} \frac{n_e \langle\sigma v\rangle_{iz}}{v_0}\, dx \right| = \sqrt{\frac{\Gamma_s d_{cs}}{\alpha_s}}\, \frac{\langle\sigma v\rangle_{iz}}{v_0} \left| \int_{x_w}^{0} e^{-x/2d_{cs}}\, dx \right|$$

$$= 2\sqrt{\frac{\Gamma_s d_{cs}^3}{\alpha_s}}\, \frac{\langle\sigma v\rangle_{iz}}{v_0} \left(1 - e^{-\gamma w/2d_{cs}}\right)$$

for $x_w/2d_{cs} \gg 1$

$$\simeq \frac{2\langle\sigma v\rangle_{iz} d_{cs}}{v_0} \sqrt{\frac{\Gamma_s d_{cs}}{\alpha_s}} \equiv A_2 \qquad (4.59)$$

and

$$p(0) = \int_0^1 d\mu\, e^{-A_2/\mu}$$

Numerically, using values from Table IV-1, and taking carbon as the impurity (AMU = 12, $E_0 \simeq 20$ eV), one finds

$$A_1 = \frac{(10^{17})(4.65)^2}{(1.3 \times 10^6)(1.5 \times 10^4)} (5 \times 10^{-8}) \simeq 5.7\ ,$$

and for A_1, $p(0) = 4.47 \times 10^{-4}$,

$$A_2 = \frac{2(5 \times 10^{-8})(.15)}{1.3 \times 10^6} \sqrt{\frac{10^{17}(.15)}{2.7 \times 10^{-13}}} \simeq 2.7$$

and for A_2, $p(0) = 1.54 \times 10^{-2}$.

For this particular set of data values the $D_\perp = 1/10\, D_{Bohm}$, $\tau_\parallel = \tau_s$ transport properties will increase the shielding efficiency by about a factor of 20 or more!

Given everything computed up to now, one would prefer to have a broad density profile in the divertor zone, at least from the impurity shielding standpoint. We will examine the effects of taking

the electron and ion energy balance equations into consideration in Chapter VI. Before moving on to the more inclusive 1-D, time dependent, numerical methods, it seems worthwhile to investigate how these shielding probabilities and other such figures of merit come into use in tokamak impurity analysis.

Simple Impurity Model

In keeping with the "spirit" of this chapter, a simple time dependent, spatial independent, impurity buildup equation will be presented and its characteristics discussed.

Defining $\bar{n}_{im} v_c$ to be the total number of impurities in the central plasma core region which has a volume v_c, one can write an equation for the time evolution of $\bar{n}_{im}$. It is

$$\frac{\partial}{\partial t}(\bar{n}_{im} v_c) = \text{impurity influx} - \text{impurity outflux} \tag{4.60}$$

and

$$\text{impurity influx} = \alpha \left\{ \Gamma^*_{He} \frac{\bar{n}_{He}}{\tau_{He}} S_{He} + \Gamma^*_{p} \frac{\bar{n}_{p}}{\tau_{p}} S_{DT} + \Gamma^*_{im} \frac{\bar{n}_{im}}{\tau_{im}} S_{im} \right\} v_c$$

$$+ \alpha \left\{ \Gamma_{fn} A_w S_{DT} + \varphi_n A_w S_n \right\} \tag{4.61}$$

$$\text{impurity outflux} = \frac{\bar{n}_{im}}{\tau_{im}} v_c \tag{4.62}$$

where all terms are as defined below.

$\bar{n}_{im}$ = average impurity density.

v_c = volume of central plasma core.

$\bar{n}_{He}, \bar{n}_{p}$ = average He and fuel ion densities.

$S_{He}, S_{DT}, S_{im}, S_n$ = sputtering yields due to α's, fuel ions, impurities (self-sputtering), and neutrons.

$\Gamma^*_{He}, \Gamma^*_p, \Gamma^*_{im}$ = flux of He, fuel ions, and impurities which hit the first wall divided by their respective fluxes leaving the plasma (i.e., crossing the separatrix and entering the divertor zone).

A_w = area of the first wall.

α = shielding inefficiency [p(0) as defined in (4.57)]
= impurity neutral flux entering plasma/flux leaving first wall. ($\alpha = 1 \Rightarrow$ no shielding of impurities.)

Γ_{fn} = flux of fast (charge exchange) neutrals hitting first wall.

φ_n = flux of neutrons hitting first wall which causes sputtering of material on the plasma side of the first wall.

$\tau_{He}, \tau_p, \tau_{im}$ = average particle confinement times for He, fuel ions, and impurities, respectively.

The terms in Eqs. (4.60), (4.61), and (4.62) are almost self-explanatory. The terms in the first brackets { } in (4.61) represent the first wall sputtering rates due to alphas, D and T ions, and ionized wall impurities, respectively, and in reality the sputtering yields (S_{He}, S_{DT}, S_{im}) should be weighted with the energy dependence of the incident particles. The terms in the second bracketed { } term in (4.61) represent the sputtering due to charge exchange neutrals and the neutron flux, respectively. The quantity α represents the

probability that the impurities sputtered off of the wall escape capture in the divertor zone. Equation (4.62) gives the net impurity outflow from the plasma core and the fraction $(1 - \Gamma^*_{im})$ of this outflow is assumed collected by the divertor collectors, and once collected never to return!

Defining terms $\tau_{He} \equiv C_{He}\tau_p$ and $\tau_{im} \equiv C_{im}\tau_p$, one can rewrite (4.60) as

$$\frac{\partial \bar{n}_{im}}{\partial t} + \left\{\frac{1 - \alpha\, \Gamma^*_{im}\, S_{im}}{C_{im}\, \tau_p}\right\} \bar{n}_{im} = \frac{\alpha}{\tau_p} \left\{\frac{\Gamma^*_{He}\, \bar{n}_{He}}{C_{He}}\, S_{He} + \Gamma^*_p\, \bar{n}_p\, S_{DT}\right\} + \alpha \frac{A_w}{V_c} \left\{\Gamma_{fn}\, S_{DT} + \psi_n S_n\right\} \tag{4.63}$$

In a steady state

$$(\bar{n}_{im})_\infty = C_{im}\, \alpha\, \frac{\left\{\Gamma^*_{He}\, \dfrac{\bar{n}_{He}}{C_{He}}\, S_{He} + \Gamma^*_p\, \bar{n}_p\, S_{DT}\right\}}{\{1 - \alpha\, \Gamma^*_{im}\, S_{im}\}} + C_{im}\, \tau_p\, \alpha\, \frac{A_w}{V_c}\, \frac{\{\Gamma_{fn}\, S_{DT} + \psi_n\, S_n\}}{\{1 - \alpha\, \Gamma^*_{im}\, S_{im}\}} \tag{4.64}$$

and the "time constant" to reach this steady state is

$$\tau \equiv C_{im}\, \frac{\tau_p}{1 - \alpha\, \Gamma^*_{im}\, S_{im}} \tag{4.65}$$

which is essentially the "net" impurity confinement time since it is weighted to reflect the influx of impurities due to self-sputtering of the wall. If perchance $\alpha\, \Gamma^*_{im}\, S_{im} \geq 1$, then the impurity density would increase continuously as a function of time and no steady state is possible. In practice, Γ^*_{He}, Γ^*_p, and Γ^*_{im} are small for a divertor

with any reasonable scrape off thickness ($|x_w - x_s| > 10$ to 20 cm). In fact, the primary culprit in a plasma with a divertor is the charge exchange neutral flux. Thus, the steady state impurity density in the plasma core region should approach the value

$$(\bar{n}_{im})_\infty = \alpha \frac{[C_{im}\ \tau_p]\{\Gamma_{fn}\ A_w\}S_{DT}}{V_c} \tag{4.66}$$

One can estimate Γ_{fn} if one were to assume some fraction (say, 10%) of the plasma ions collected by the divertor were really recycled back as neutrals; then

$$\Gamma_{fn} = .1 \left\{\frac{\bar{n}_p\ V_c}{\tau_p}\right\} \frac{1}{A_w} \frac{f}{1-f} \tag{4.67}$$

where f accounts for the fact that only a fraction (f) of these recycled neutrals will charge exchange with the plasma and end up hitting the wall ($f < .5$). The $1/(1-f)$ factor accounts for the continued recycling of these neutrals which come from the wall charge exchange in the plasma and create another cx neutral which subsequently hits the wall. Using $f = .5$ as an upper limit, one has

$$(\bar{n}_{im})_\infty = .1\ \alpha\ C_{im}\ S_{DT}\ \bar{n}_p\ \frac{1-f}{f} \tag{4.68}$$

$$= .1\ \alpha\ C_{im}\ S_{DT}\ \bar{n}_p$$

and

$$\frac{(\bar{n}_{im})_\infty}{\bar{n}_p} \equiv \xi_{im} = .1\ C_{im}\ \alpha\ S_{DT} \tag{4.69}$$

Using $S_{DT} \simeq .08$ (relatively high), one finds

$$\xi_{im} = .008\ \alpha\ C_{im} \tag{4.70}$$

Since we have no real idea of how quickly impurities will diffuse in a fusion reactor, a meaningful value of C_{im} is not at hand. If one only had 50% shielding, then $\xi_{im} \simeq .004\ C_{im}$ and

$$\frac{\bar{n}_{im}}{\bar{n}_e} = \frac{\xi_{im}}{1 + \bar{z}\ \xi_{im}} \tag{4.71}$$

Meade[8] and others[9] have shown that the maximum permissible concentration of carbon, for example, in a plasma is

$$\frac{\bar{n}_{carbon}}{\bar{n}_e} < 7\%$$

or else ignition becomes impossible. Noting from (4.71) that for $\bar{n}_{im}/\bar{n}_e < C_{max}$ that

$$\xi_{im} < \frac{C_{max}}{1 - \bar{z}\ C_{max}}$$

which for carbon ($\bar{z} = 6$) gives

$$\xi_{im} < \frac{.07}{1 - (6)(.07)} = .12$$

which means that the maximum allowable proton defect (when carbon is the impurity) is

$$\text{"proton defect"} \equiv \frac{\bar{n}_e - \bar{n}_p}{\bar{n}_e} = 1 - \frac{\bar{n}_{im}/\bar{n}_e}{\xi_{im}}$$

which is $\simeq 42\%$. This translates into a requirement on the impurity confinement time τ_{im}, i.e., for carbon when $\alpha = .5$ and $S_{DT} \simeq .08$

$$.004\ C_{im} < .12$$

or

$$C_{im} \equiv \frac{\tau_{im}}{\tau_p} < 30$$

This indicates that if the carbon confinement time is less than 30 times the fuel ion confinement time that ignition is achievable.

Obviously, the value of α, the fraction of impurities which are not trapped by the divertor, can only be determined after some self-consistent analysis of the divertor zone physics. This will be done in Chapter VI. One can, however, place "reasonable" estimates on α and these range in the neighborhood of $.05 < \alpha < .5$ which is not very enlightening!

The choice of impurity is important also. Meade[7] again has indicated that only a fraction of a percent of W, for example, present in a plasma would prevent ignition. This reasoning would indicate that one would like low Z wall materials or coatings or curtains which would release less detrimental impurities upon bombardment by the plasma. The factor often overlooked, as was pointed out in Chapter II, is that due to the slower velocity, lower ionization potential, and usually lower sputtering yield, one may, due to trapping in the divertor zone, produce a much lower influx of impurities if higher Z (and mass) walls were used compared to the proposed low Z liners.

CHAPTER IV

Bibliography

[1] Ref. [7], Chapter III.

[2] R. W. P. McWhirter, in Plasma Diagnostic Techniques, Eds. R. H. Huddlestone and S. L. Leonard (Academic Press, New York, 1965) p. 222; see also NRL-Plasma Forulary, Ed. D. L. Book, Naval Res. Lab., Washington, D. C., p. 17.

[3] See Appendix E for reproduction of Nuclear Fusion Letter.

[4] Ref. [7], Chapter III.

[5] H. K. Forsen and J. C. Sprott, Nuclear Fusion 12, 126 (1972).

[6] H. Hanock, Elliptic Integrals (Dover Pub. Co., 1958)p. 24.

[7] K. H. Beckurts and K. Wirtz, Neutron Physics, (Springer-Verlag, Berlin, 1964) p. 241.

[8] Ref. [18], Chapter II.

[9] Ref. [2], Chapter II.

CHAPTER V

1-D TRANSPORT CODE

The purpose of this chapter is to describe in fairly complete detail the equations used to model the particle and energy transport in a tokamak reactor with a magnetic field divertor. The equations used to model the transport behavior are 1) the particle (fuel ion) continuity equation, 2) the electron (internal) energy transport equation, 3) the ion (internal) energy transport equation, 4) a simple Ohm's Law $E = \eta J$, and 5) Maxwell's equations $\nabla \times \vec{E} = - \partial B/\partial t$ and $\nabla \times B = \mu_0 J$.

These equations have been used by others to model the central core region (inside the separatrix) of a tokamak and have met with varying degrees of success.[1] What has been added in this research is a model for the divertor transport processes, both particle and energy transport. The divertor model is incorporated into the above equations and the entire set (plasma core region plus divertor zone) is solved as a two region problem. At the separatrix where the plasma core region interfaces with the divertor region, the particle and energy fluxes are matched. This matching procedure circumvents the perplexing problem of exactly what boundary conditions should be supplied at the "edge" of the plasma core region. With suitable boundary conditions imposed at the plasma center and wall (see Chapter IV), one can solve the entire set of coupled, nonlinear, second order, partial differential plus algebraic equations using any one of

several numerical schemes.[1]

Before proceeding to outline the method used to do this, it seems worthwhile to make a remark or two as to the applicability of a one-dimensional (cylindrical), fluid analysis for predicting tokamak behavior. Hogan[1] has noted, and rightly so, that to obtain reasonable agreement (using a 1-D code) between experiment and "theory" on present day tokamaks, one must introduce into these transport equations a good deal of empiricism.* This introduction of semi-empirical terms into the transport equations in order to model the experimental behavior then tends to tie the equations to a particular device. This in turn diminishes the prognosticative value of the model for determining the properties of future experiments, particularly when the future experiment is required to have operational characteristics very dissimilar to those of the experiment to which the code was modeled. Thus transport codes can presently only be reliably used as an avenue to give quantitative assurances in machine designs when the extrapolations required above the experimentally well modeled devices are small, as in an extrapolation from ORMAK to ORMAK Upgrade.[2]

Transport codes do, however, have their use in reactor systems studies. First, they allow one to compare different theoretical models for plasma behavior versus the requirements imposed for

---

*For example, experiments on ORMAK have lead to the need for an electron thermal conductivity of the form $\chi_e = A\ I/\bar{n}_e\ (I + 40\ (r/a))$ where I is the total plasma current, $\bar{n}_e$ is the average electron density, and a = limiter radius.[ ]

ignition.* Secondly, a 1-D code can demonstrate plasma parameter (n, T_e, T_i, B, J, etc.) profile sensitivities which would otherwise go unnoticed in a 0-D model.[3] This will be demonstrated in Chapter VI. Thirdly, 1-D codes are the stepping stone to more exotic 2-D codes.

The code to be described here assumes the plasma to be a cylinder with circular concentric Ψ surfaces. This geometry may be representative of low β, large aspect ratio devices, but may not be an accurate representation of high β, non-circular, low aspect ratio tokamaks such as are conceived to be demonstration power reactors.[4] Nevertheless, one may still be able to obtain a feel for the reactor physics implications as long as the phenomena of interest are on diffusive time scales. Some transport codes now coming on line use Ψ instead of r as the "spatial" coordinate and then couple the transport and MHD equilibrium codes together in an iterative fashion in order to represent more faithfully the plasma behavior.[5] One may be able to represent some effects from non-circular cross sectioned devices using a circular cylindrical code by weighting the transport coefficients ($D_\perp$, χ_e, χ_i) with a Jacobian which reflects the geometric differences in diffusive behavior.[5] This has not been done for the work to be presented here.

---

*Ignition is defined as the condition when the alpha heating power from the fusion events is sufficient to balance out all the energy loss channels from the plasma.

The starting point for solving any transport problem is some type of kinetic equation.[1] We will not be quite so interested in the kinetic equation itself as in its moments. Of particular interest are its lowest 5 moments which produce the equations of continuity, conservation of momentum, and energy balance. Formally, the moments of the Boltzmann equation can be written as[6]

$$\frac{\partial n_j}{\partial t} + \nabla \cdot (n_j \vec{V}_j) = S^j_{\text{ources}} - S^j_{\text{inks}} \tag{5.1}$$

$$m_j n_j \frac{d_j \vec{V}_j}{dt} = - \nabla p_j - \nabla \cdot \vec{\pi}_j + Z_j |e| n_j (\vec{E} + \vec{V}_j \times \vec{B}) + R_j \tag{5.2}$$

$$\frac{3}{2} n_j \frac{d_j T_j}{dt} + p_j \nabla \cdot \vec{V}_j = - \nabla \cdot \vec{q}_j - \vec{\vec{\pi}}_j : \nabla V_j + Q_j \tag{5.3}$$

where the index j denotes the species of the particle.

$$\frac{d_j}{dt} \equiv \frac{\partial}{\partial t} + \vec{V}_j \cdot \nabla$$

p_j = scalar pressure, $\vec{\vec{\pi}}_j$ = off diagonal stress tensor, $\vec{B}$ = electric field in lab frame, $\vec{V}_j$ = species averaged particle velocity, $\vec{R}_j$ = frictional force due to collisions (elastic + inelastic) with other species, Q_j = net energy generation term which includes all plasma heating terms, bremsstrahlung, recombination, and line radiation, and even charge exchange losses.

As can plainly be seen, Eqs. (5.1)–(5.3) are not closed (more unknowns than equations) even when one imposes symmetries (i.e., cylindrical symmetry) and includes Maxwell's equations. The method used here to close the set is to assume that one can relate the

"fluxes" $n\vec{V}_j$, $\vec{q}_j$, and $\vec{J}$ to the available "driving forces" such as ∇p_j, ∇T_j, and $\vec{E}$ linearly. Written in more general terms

$$J^{(K)} = \sum_{\ell} L_{K\ell} F^{(\ell)} \tag{5.4}$$

where

$$J^{(K)} = \left\{\Gamma_r,\ q_{er},\ q_{ir},\ J_z\right\}$$

and

$$F^{(\ell)} = \left\{\frac{\partial n}{\partial r},\ \frac{\partial T_e}{\partial r},\ \frac{\partial T_i}{\partial r},\ E_z\right\}$$

Relationships such as shown in Eq. (5.4) are known in non-equilibrium thermodynamics. Those used here are similar to those used by Rosenbluth, et al.[7] and their derivation (and applicability) have traditionally depended on the plasma being Local Thermodynamic Equilibrium (LTE) and possessing "weak" gradients. How weak "weak" must be before the relations (5.4) are no longer valid cannot be easily determined.

The processes which will be dealt with in this research are assumed to occur on time scales much longer than those required to maintain the plasma in MHD equilibrium. On these long time scales Eq. (5.2) reduces to (when summed over species)

$$\nabla p = \vec{J} \times \vec{B} \tag{5.5}$$

where $p = p_e + p_i$. Equation (5.5) is the MHD equilibrium equation and is implicitly present in the Onager relations.

Of all the elements in the $L_{K\ell}$ array, only the diagonal elements will be used in the research presented here. Specifically, we will assume

$$\Gamma_r \equiv nV_r = - D_\perp \frac{\partial n}{\partial r} \tag{5.6}$$

$$q_{er} = - n\chi_e \frac{\partial T_e}{\partial r} \tag{5.7}$$

$$q_{ir} = - n\chi_i \frac{\partial T_i}{\partial r} \tag{5.8}$$

$$J_z = \sigma E_z \tag{5.9}$$

where $D_\perp$ = cross field diffusion coefficient, $\chi_{e,i}$ is the electron (ion) thermal diffusivity, and σ is the parallel electrical conductivity. In general, equations such as (5.6) would have other driving forces such as $\Gamma \propto - D_T \partial T_e/\partial r$ where D_T is called the thermal diffusion coefficient. In classical and neoclassical theory the entire transport array ($L_{K\ell}$) has been worked out. We, however, will be using a transport model based on microinstability turbulence and to date the off-diagonal elements have not been worked out. This is not to imply that diffusion due to temperature gradients is not important,* it merely is a statement of the present state of ignorance as to what the transport coefficient relating Γ to ∇T should be.

Transport Coefficients

The transport coefficients to be used in quantitatively assessing tokamak plasma behavior in this report are taken from the five-regime trapped particle instability model, sometimes called 'anomalous' diffusion model. Possibly the best concise discussion of this model

*For example, the diffusion coefficient itself will be dependent on ∇T for the trapped electron mode.

can be found in the UWMAK-II report itself,[8] or in WASH-1295.[9] The essence of the evaluation procedure is to ascertain the linear growth rates (γ_L) and appropriate ($k_\perp$) values which represent the fastest growing mode based upon the plasma properties in each particular spatial location (r value).* By looking at Fig. V-1 one can see that values taken using these modes create $D_\perp$, $\chi_\perp$ values far in excess of 'neoclassical' values. These coefficients are given explicitly in Appendix A. The functional dependence of these coefficients ($D_\perp$, χ_e, χ_i) can be described through a rather general formula.

$$\left.\begin{matrix} D \\ \chi_e \\ \chi_i \end{matrix}\right\} = C\, T_e^{S1}\, T_i^{S2}\, n_i^{S3}\, B^{S4} (\nabla n)^{S5} (\nabla T)^{S6} (\nabla q)^{S7} (1 + T_e/T_i)^{S8} \qquad (5.10)$$

and the code used for this report handles coefficients of the above form. In fact, the whole algebraic nightmare in coding the transport equations is in handling terms such as $\partial D/\partial r$ and $\partial D/\partial \nabla n\ \partial(\nabla n)/\partial r$, etc. This will be described in more detail later.

Transport Equations in Cylindrical Geometry

The particle (fuel ion) continuity equation used in the work presented here is written as:

*Houlberg[27] has questioned the validity of the assumption (particularly in the trapped ion mode regime) that the mode with the fastest growth rate $\gamma(k_\perp, \omega)$ should be the one which produces the largest diffusion, i.e., $D = \gamma/k_\perp^2$.

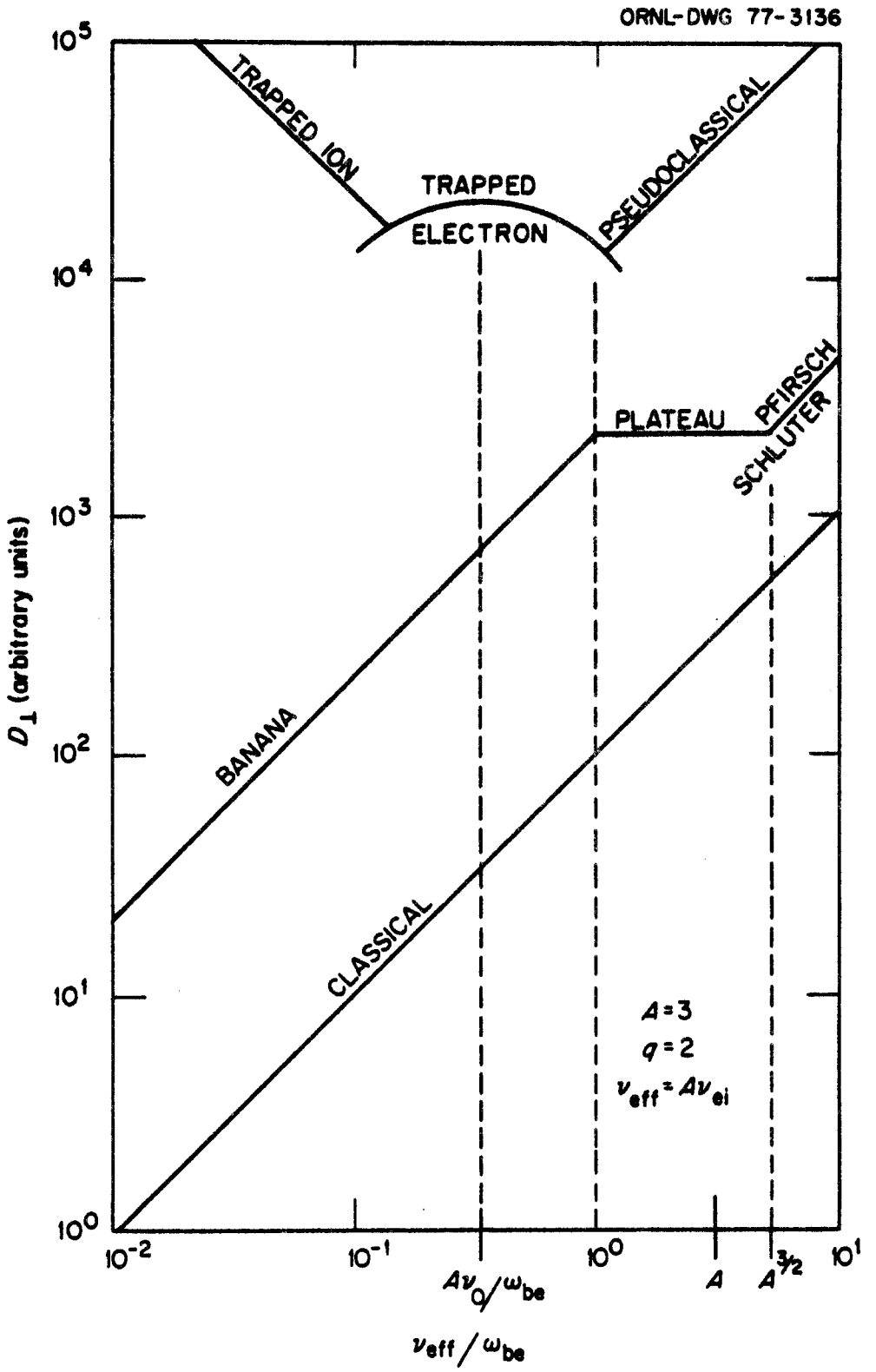
ORNL-DWG 77-3136
TRAPPED ION
TRAPPED ELECTRON
PSEUDOCLASSICAL
PLATEAU
PFIRSCH SCHLUTER
BANANA
CLASSICAL
A=3
q=2
$\nu_{eff} = A\nu_{ei}$
$D_\perp$ (arbitrary units)
10^5
10^4
10^3
10^2
10^1
10^0
10^{-2}
10^{-1}
10^0
10^1
$A\nu_0/\omega_{be}$
A
$A^{3/2}$
ν_{eff}/ω_{be}

Figure V-1

$$\frac{\partial n}{\partial t} + \frac{1}{r}\frac{\partial}{\partial r}\left(r\Gamma_{\perp}\right) = S_n + n_e n_o \langle\sigma v\rangle_{iz} - \nabla_{\parallel} \cdot \Gamma_{\parallel} - 2\left(\frac{n^2\langle\sigma v\rangle_{DT}}{4}\right)$$

$$+ \dot{n}_{beam} - n_{beam}\, n_T\, \sigma^b_{DT}\, V_{beam} \qquad (5.11)$$

where

n = ion density

n_e = electron density = ion density if $Z_{eff} = 1$

$\Gamma_{\perp}$ = diffusion flux $\equiv -D\, \partial n/\partial r$; $\perp$ to $\vec{B}$

n_o = neutral density

n_{beam} = density of fast ions from beam injection

$\dot{n}_{beam}$ = neutral beam ion deposition rate (#/cm^3/msec)

$\langle\sigma v\rangle_{iz}$ = ionization rate (cm^3/sec) coefficient

S_n = pellet (cold plasma) volumetric deposition profile

$= S_o(t)\,(1 - C(r/a)^2)$ = assumed form

V_{beam} = velocity of beam ions

$\vec{\Gamma}_{\parallel}$ = particle flux leaving along field lines in divertor zone

$\langle\sigma v\rangle_{DT}$ = fusion reaction rate coefficient

σ^b_{DT} = fusion cross section evaluated at beam energy

and the electron density is determined by

$$n_e = n + \sum_j^{\text{impurities}} Z_j n_j = \text{electron density.}$$

The terms on the left hand side of Eq. (5.11) are self explanatory. The terms on the right hand side give the sources ($S_n + n_e n_o \langle\sigma v\rangle_{iz} + \dot{n}_{beam}$) of plasma ions due to pellet injection, neutral ionization and beam injection and the sinks ($n^2\langle\sigma v\rangle_{DT}/2 + n_{beam}\, n_T\, \sigma^b_{DT}\, V_{beam}$) due to thermal Maxwellian fusions and beam-plasma fusions. The remaining

term on the right hand side is $-\nabla_{\|} \cdot \Gamma_{\|}$ and is zero for the central plasma core region, but assumes some value in the divertor zone since it represents the loss of particles along the field lines to the divertor collector. It is the inclusion of $\nabla_{\|} \cdot \Gamma_{\|}$ that makes the divertor transport equations intrinsically two dimensional. The description of how this is dealt with in practice will be saved until after the electron and ion energy transport equations are presented.

The electron (internal) energy balance equation used in this work is written as

Electron Temperature Equation:

$$\begin{aligned}\frac{\partial T_e}{\partial t} = \frac{1}{\frac{3}{2} n_e} \Big[& - \frac{1}{r} \frac{\partial}{\partial r} (r \tilde{Q}_{e_\perp}) - \frac{3}{2} \Gamma_\perp \frac{1}{r} \frac{\partial}{\partial r} (r T_e) \\ & - \frac{3}{2} T_e (S_n + n_e n_0 \langle \sigma v \rangle_{iz} - \frac{n^2}{2} \langle \sigma v \rangle_{DT}) \\ & - \nabla_{\|} \cdot \vec{Q}_{e_{\|}} + \frac{3}{2} T_e \nabla_{\|} \cdot \Gamma_{\|} \\ & + P_{\alpha e} + P_{Be} + P_{\Omega} \\ & - P_{Rad} - P_{ei} - (P_e)_{other} \Big] \quad , \end{aligned} \tag{5.12}$$

where

$\tilde{Q}_{e_\perp}$ = electron <u>heat</u> flux $\equiv - n_e \chi_e \frac{\partial T_e}{\partial r}$; $\perp$ to $\vec{B}$

$\vec{Q}_{e_{\|}}$ = total net electron energy flux leaving along field lines in divertor zone

P_{Ω} = ohmic heating power

$= \eta(r, T_e) J_z^2$ (5.12a)

η = resistivity[1]

$$= \frac{3.27 \times 10^{-9}\ \ell n\,\Lambda}{T_e^{3/2}\, f_{TR}} \left[.29\, Z_{eff} + \frac{.457\, Z_{eff}}{1.077 + Z_{eff}}\right] \qquad (5.12b)$$

$$f_{TR} \equiv 1 - \frac{1}{1 + \nu_e^*}\left(1.95\left(\frac{r}{R_0}\right)^{1/2} - .95\left(\frac{r}{R_0}\right)\right)$$

$$\nu_e^* \equiv 6.92 \times 10^{-24} \frac{R_0^{3/2}\, B_T\, n_e\, \ell n\,\Lambda}{r^{1/2} T_e^{3/2} B_\theta(r)} \qquad (5.12c)$$

$$P_{Rad} = P_{Brems} + P_{Sync} + P_{Imp}$$

$$P_{Brem} = 1.5 \times 10^{-32}\, Z_{eff}\, n_e^2 [T_e(eV)]^{1/2}\ \text{watts/cm}^3\ [10] \qquad (5.12d)$$

$$Z_{eff} \equiv \sum_{\text{all ions}} n_j Z_j^2 / n_e$$

$$P_{Sync} = 1.6 \times 10^{-28}(1 - .013A)^3 B_0^{5/2}(1-\beta)^{5/4} \left(\frac{n_e}{a}\right)^{1/2} T_e^{2.1} \sqrt{1-R}\ \frac{\text{watts}}{\text{cm}^3}\ [11] \qquad (5.12e)$$

where

B_0 = vacuum magnetic field (gauss), a = plasma minor radius (cm)

R = effective wall reflectivity, $n(\#/\text{cm}^3)$, $T_e(eV)$, $A = R_0/a$

$$P_{Imp} = P_{Recomb} + P_{Deexc}$$

$$\cong P_{Brem}\left(\frac{3.97 \times 10^{-2}\, \xi_z Z^4}{Z_{eff}\, T_e} + \frac{8.6 \times 10^{-4}\, \xi_z Z^6}{Z_{eff}\, T_e^2}\right) \frac{\text{watts}}{\text{cm}^3} \qquad (5.12f)$$

$P_{Imp} = 1.2\, \xi_z n_e^2 \times 10^{-26}$ (for low temperatures), $\xi_z \equiv n_z/n_e$ (5.12g)

P_{ei} = electron-ion (classical) equilibration term

$$= \left[\sum_{j}^{\text{ion species}} 2 \frac{m_e}{m_j} \frac{3}{2} \frac{n_e(T_e - T_j)}{\tau_{ej}}\right] C_{eQ} \qquad (5.12h)$$

where

m_j = ion mass of j^{th} species

τ_{ej} = electron - j^{th} species ion (90°) collision time

T_j = temperature of j^{th} ionic species

C_{eQ} = coefficient to account for any anomalous equilibration effects

$P_{\alpha e}$ = alpha particle energy imparted to electrons

$= f_\alpha \frac{n^2}{4} \langle\sigma v\rangle_{DT} E_\alpha$

E_α = 3.5 MeV

f_α = function of E_α/T_e which determines what fraction of E_α goes to the electrons

P_{Be} = beam energy imparted to electrons

$= g(r, T_e, T_i, n) f_b E_{beam}$

f_b = similar to f_α except as function of E_{beam}/T_e

$g(r,T_e, T_i,n)$ = beam deposition profile

$(P_e)_{other}$ = power lost due to ionization of incoming neutrals (i.e., $13.6\, n_0 n_e \langle\sigma v\rangle_{iz}$)

+

power lost due to ionization of impurities which is not accounted for in P_{Rad}

The terms in (5.12) are self explanatory, but again it should be noted that the net energy loss due to other than particle loss (i.e.,

$-(\nabla_{\parallel} \cdot Q_{e\parallel} - 3/2\ T_e\ \nabla_{\parallel} \cdot \Gamma_{\parallel}))$ makes the equation inherently two dimensional.

The ion (internal) energy balance equation looks very much like the one for the electrons and is given by

Ion Temperature Equation:

$$\frac{\partial T_i}{\partial t} = \frac{1}{\frac{3}{2} n}\left[-\frac{1}{r}\frac{\partial}{\partial r}(r\tilde{Q}_{i_\perp}) - \frac{3}{2}\Gamma_\perp \frac{1}{r}\frac{\partial}{\partial r}(rT_i)\right.$$
$$- \frac{3}{2} T_i (S_n + n_e n_0 \langle\sigma v\rangle_{iz} - \frac{n^2}{2}\langle\sigma v\rangle_{DT})$$
$$- \nabla_{\parallel} \cdot \vec{Q}_{i_\parallel} + \frac{3}{2} T_i\ \nabla_{\parallel} \cdot \vec{\Gamma}_{\parallel}$$
$$\left. + P_{\alpha i} + P_{Bi} - P_{CX} - (P_i)_{other}\right] , \qquad (5.13)$$

where

$$P_{\alpha i} = \frac{n^2}{4}\langle\sigma v\rangle_{DT} E_\alpha - P_{\alpha e} \qquad (5.13a)$$

= alpha power to fuel ions. It is assumed that the impurity ions do not share this energy which is allowed if n_{Imp}/n_i is small.

$P_{Bi} = P_{Beam} - P_{Be}$

P_{CX} = net local power loss due to charge exchange events in the plasma.

$(P_i)_{other}$ = power taken from ions to heat any cold impurities which enter the plasma.

The other terms have meanings similar to those in the electron temperature equation.

Equations (5.8)–(5.9) along with Ohm's Law

$$E_z = \eta(r,T_e(r,t))J_z \tag{5.14}$$

and Maxwell's equations in the form

$$\frac{\partial B}{\partial t} = + \frac{\partial E_z}{\partial r} \quad , \tag{5.15}$$

where B is in the theta direction (i.e., poloidal field only) and

$$\mu_0 \frac{\partial J_z}{\partial t} = + \frac{1}{r} \frac{\partial}{\partial r} \left(r \frac{\partial E_z}{\partial r} \right) \tag{5.16}$$

are solved simultaneously using a Crank-Nicholson[1] finite differencing technique and a specially coded matrix inversion technique[12] which takes advantage of the sparseness of the coefficient matrix involved in the equational formulation. This will be elaborated upon in more detail later. First, a discussion of the boundary conditions applied to the equations is necessary and this will lead naturally into formulating how one treats the $\nabla_{\|} \cdot \Gamma_{\|}$, $\nabla_{\|} \cdot Q_{e\|}$, $\nabla_{\|} \cdot Q_{i\|}$ terms and still maintains a one-dimensional code.

Boundary Conditions

Codes in the past which just try to solve the transport equations in a single region, e.g., the plasma core region have always had the perplexing problem of how to determine self consistently what the "edge" temperatures and plasma density should be.* When modeling a

*Hogan's article on Multifluid Transport Codes is probably the most authoratative review on these one-region codes and their boundary conditions.[1]

specific experiment, one can look to the experimental data to give a $T_e(\text{edge})$, $T_i(\text{edge})$, and $n_e(\text{edge})$, where "edge" is usually taken to be the limiter radius. One could then vary these boundary conditions within a reasonable range of values and look at what effects these variations had on the plasma profiles $T_e(r)$, $T_i(r)$, and $n(r)$. This technique, however, is of little help when one wishes to extrapolate into a much different operating regime such as might occur if a divertor were to define the "edge," or if a strong heating source is present as occurs near the ignition point in a fusion reactor. Hotston[13] and Hotston and McCraken[14] have tried to model self-consistently the "edge" boundary conditions by taking the plasma-wall interactions into account. With a two-region model (plasma core/divertor), this "edge" condition is circumvented since at the separatrix one merely requires the particle and energy fluxes to match, $B(a) = \mu_0 I_p(t)/2\pi a$ and $J(a) = \nabla \times B(a)/\mu_0$. The boundary conditions at $r = 0$ are $\Gamma_r = q_{er} = q_{ir} = B = \partial E/\partial r = 0$. The boundary conditions to be used at the first wall have been discussed in Chapter IV where it was pointed out that the more physically appropriate no return current boundary conditions which are formulated as

$$(\alpha\, n + \beta\, \partial n/\partial r)_{r=r_{wall}} = 0 \tag{5.17}$$

can be replaced by the condition

$$n\big|_{r=r_{wall}} = \gamma \approx \text{small number} \simeq 0 \tag{5.18}$$

and conditions similar to (5.17) and (5.18) can be derived for the T_e and T_i equations.

with no noticeable effect on the profile particularly near the separatrix. The physical significance reflected by this lack of profile sensitivity to the boundary conditions at the wall is that the volumetric effect arising from the $\nabla_{\|} \cdot \Gamma_{\|}$ in the divertor particle equation is so strong that it essentially governs the behavior away from the wall leaving only a thin "boundary layer" near the wall that is sensitively effected by the boundary conditions. This is fortuitous because when conditions such as (5.17) were applied numerically to the transport equations (particularly to the particle continuity equation), density oscillations in space and time developed. Using a condition such as (5.18) these oscillations did not occur and fortunately using (5.18) does not affect the important parts of the solution profiles. The exact reason why a condition such as (5.17) should produce such an oscillation was never investigated.

Parallel Flow Terms

As was just mentioned the divergence terms, such as $\nabla_{\|} \cdot \Gamma_{\|}$ in the density transport equation for the divertor region, seem to govern the plasma behavior in that zone to such a degree that the "divertor essentially uncouples the plasma core region from the first wall." To see rigorously how this was made to happen, a detailed description of how one models $\nabla_{\|} \cdot \Gamma_{\|}$, $\nabla_{\|} \cdot Q_{e\|}$, and $\nabla_{\|} \cdot Q_{i\|}$ must be given. We need to make an assumption in order to reduce Eqs. (5.11) to (5.13) to one-dimensional form in the divertor region and we do so much like we did in Chapter IV; we assume a mathematical model.

Assumption: Replace $\nabla_{\parallel} \cdot \Gamma_{\parallel}$ as shown below

$$\nabla_{\parallel} \cdot \Gamma_{\parallel} \rightarrow \frac{\Gamma_{\parallel}(r)}{L(r)} \simeq \frac{n_i(r)\bar{V}_i(r)}{L(r)} = \frac{n_i(r)}{\tau_{\parallel}(r)} \tag{5.19}$$

and similarly replace

$$\nabla_{\parallel} \cdot Q_{e\parallel} \rightarrow \frac{Q_{e\parallel}(r)}{L(r)} \tag{5.20}$$

and

$$\nabla_{\parallel} \cdot Q_{i\parallel} \rightarrow \frac{Q_{i\parallel}(r)}{L(r)} \tag{5.21}$$

where $L(r)$ = average distance a particle (in the divertor region) must travel along a $\vec{B}$ field line before it escapes the close proximity of the plasma core (see discussion in Chapter IV). One can find $L(r)$ for any given plasma/magnetic field configuration by integrating along a field line from the $Z = 0$ plane (at some given radial value) to the divertor collector plate, or what is more appropriate, from a shielding point of view integrating up to the Z = constant plane which passes through the $\vec{B}_p = 0$ null point. This integration is repeated for different radial starting positions on the $Z = 0$ plane. The curve generated tends to look like Fig. V-2 which is for UWMAK-II. In reality, $L(r)$ is not sharply defined within a cm or so of the separatrix due to the fact that the $\vec{B}_p = 0$ nulls will probably move about somewhat. This motion should tend to smear out $L(r)$ near the separatrix. This smearing was not taken into account in the equations whose solutions will be presented in Chapter VI.

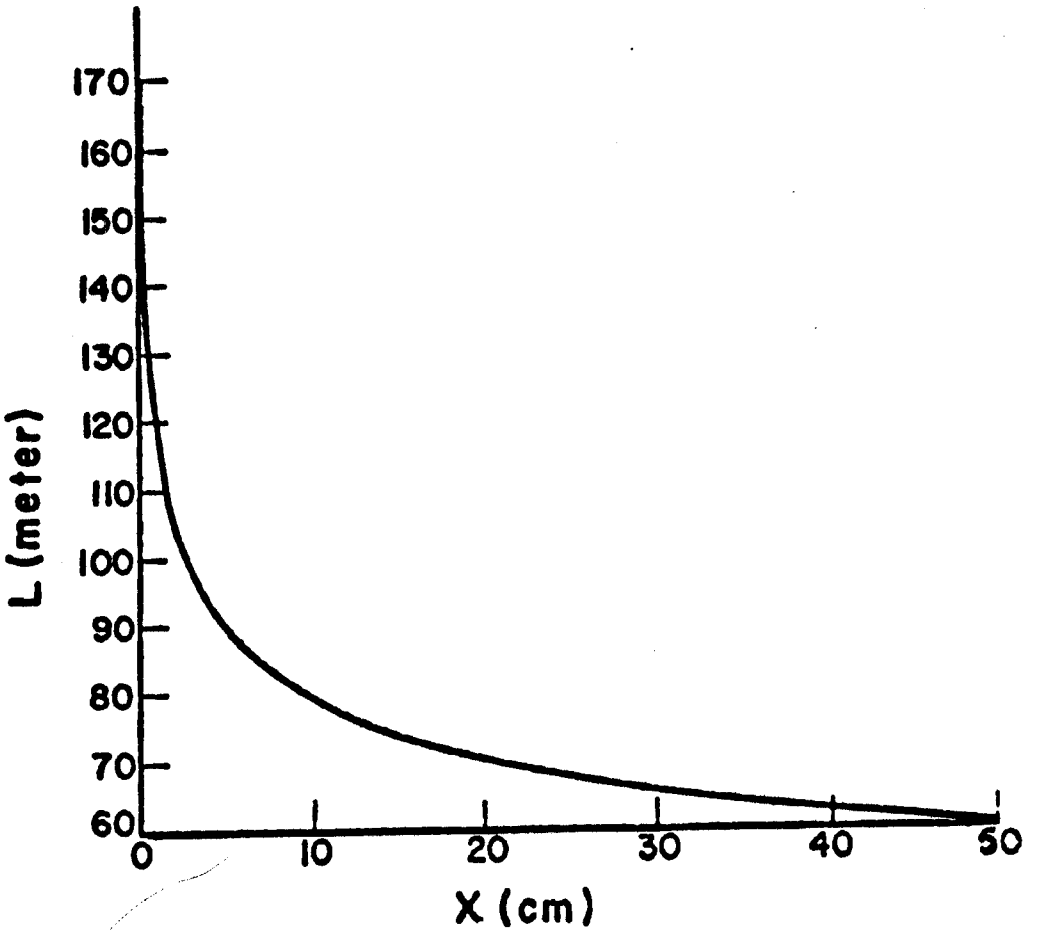
170
160
150
140
130
120
110
100
90
80
70
60
L (meter)
0
10
20
30
40
50
X (cm)

Figure V-2

Once $L(r)$ has been determined, $\Gamma_{\parallel}(r)$, $Q_{e\parallel}(r)$, and $Q_{i\parallel}(r)$ must be found. In the work presented here, the assumption was made that "trapping" of the plasma in the divertor zone due to $|\nabla B|$ along the field lines can be neglected. This neglect was based upon the semi-quantitative arguments put forth by Mense, et al.[15] in which it was pointed out that almost all known mirror microinstabilities have the potential for being unstable in the divertor zone. The nonlinear consequences of these instabilities are believed (not proved) to be that the plasma will flow out on a time scale comparable to the ion flow speed in the absence of any $|\nabla B|$. There is some experimental evidence to substantiate this model.[16]

If the ions have a net loss rate proportional to $n_i\bar{V}_i/4$ where $\bar{V}_i \equiv (8\ kT/\pi m_i)^{1/2}$ and since the electrons want to try to leave at a rate proportional to $n_e\bar{V}_e/4$, the collector plate in the divertor zone must have a potential built up on it until the net electrical current incident on the plate (at each position on the plate) is zero.* Thus we assume:

> "Ions and electrons stream to the collector plates unimpeded by the B field gradient. An electrostatic potential develops at the divertor particle collector plates which causes the net electrical current collected by the plate to be zero."

*Account has not been made for the unipolar arc phenomena. This may or may not be important on divertor collector plates.[17] However, the plates will probably be kept quite clean by the incident plasma.

The effect of the electrostatic sheath is to preferentially cool the electrons.[18] This will be shown quantitatively in just a moment, but first one must ascertain what potential one believes will build up at the collectors.

With reference to Fig. V-3, we can determine Φ_{max} (the potential of the collector plate) by equating the ion and electron (charge) fluxes at the collector plate. If we assume for the moment no secondary electron emission, then $\Gamma^{+}_{\|i}(Z_A)$ must be equal to $\Gamma^{+}_{\|e}(Z_A)$ in order for J, the electrical current, to be zero. If one draws an imaginary plane at the location $Z = Z_B$, where the electric field is believed to be essentially zero, then one knows the following two facts:

1. The ions, which cross the $Z = Z_B$ plane, $\Gamma^{+}_{\|i}(Z_B)$, heading towards the collector plate at $Z = Z_A$, will all be absorbed.
2. The electrons, which cross the $Z = Z_B$ plane, $\Gamma^{+}_{\|e}(Z_B)$, heading towards the collector plate, will <u>not</u> all be absorbed. Indeed, most will be reflected back due to $\Phi(r)$, so only some fraction $\Gamma^{+\#}_{\|e}(Z_B)$ will actually be collected and this flux must be equal to $\Gamma^{+}_{\|i}(Z_B)$ in order for $J = 0$.

Since the electric field is assumed nearly zero at $Z = Z_B$, the flux of ions heading toward the collector plate is given by

$$\Gamma^{+}_{\|i}(Z_B) = \int_{-\infty}^{+\infty}\int dV_x dV_y \int_{0}^{\infty} V_z f_i(V_x,V_y,V_z,Z_B,r,t)dV_z \qquad (5.22)$$

The electron flux crossing $Z = Z_B$ heading for the collector plate is similar to (5.22) except using f_e, the electron distribution function.

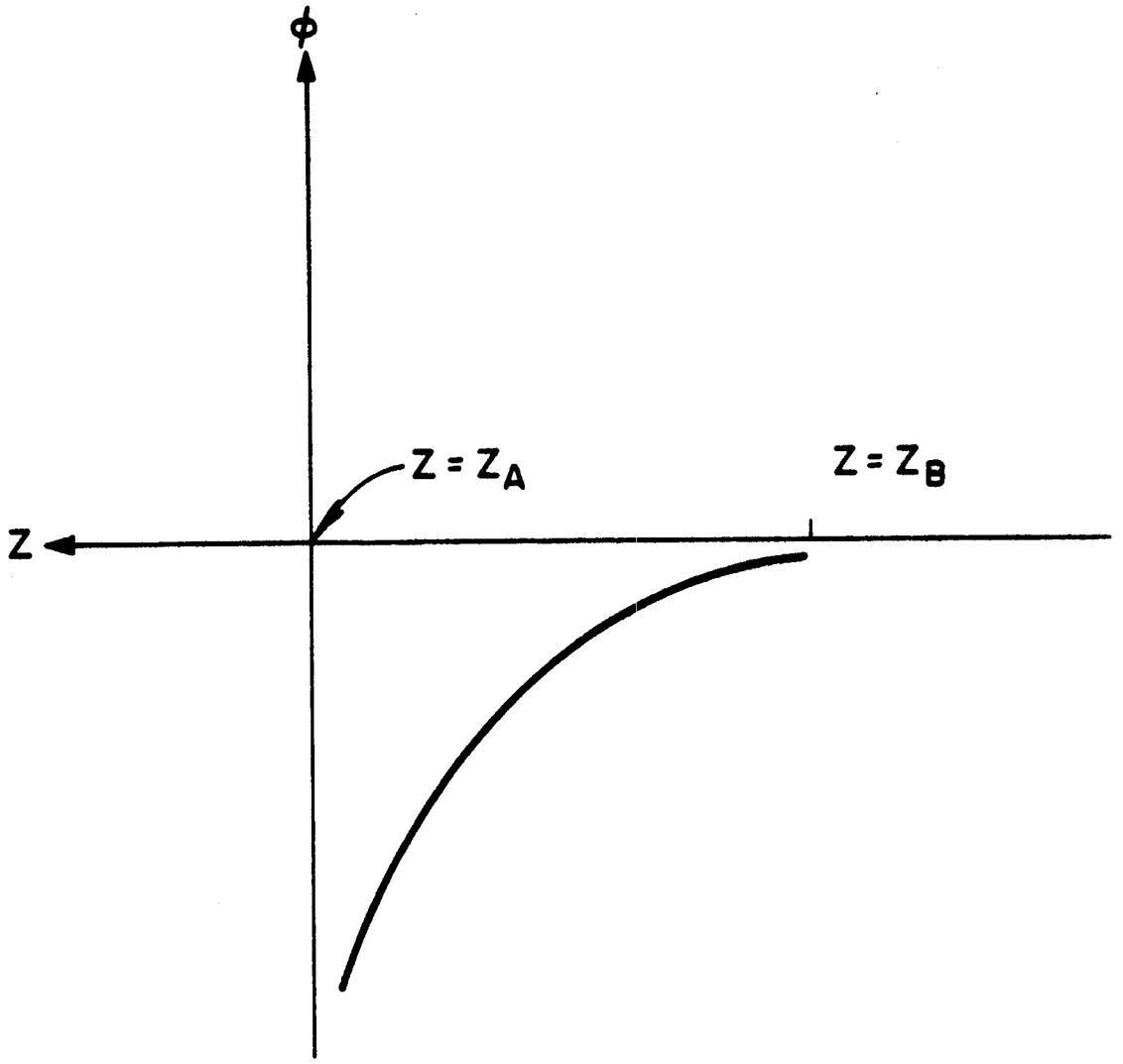

Figure V-3

However, the flux of these electrons which are actually collected by the plate is given by

$$\Gamma^{+\#}_{\|e}(Z_B) = \int_{-\infty}^{+\infty} \int dV_x dV_y \int_{V^e_{max}}^{\infty} V_z f_e(V_x, V_y, V_Z, Z_B, r, t) dV_z \qquad (5.23)$$

At this point one needs to know f_i and f_e which actually should be found from some rigorous kinetic theory analysis, but which will be assumed to take on a Maxwellian form to lowest order, i.e., assume that

$$f_i = n_{0i}(r,t) \left(\frac{m_i}{2\pi k T_i(r,t)}\right)^{3/2} \exp\left\{-\frac{m_i(V_x^2 + V_y^2 + V_z^2)}{2kT_i(r,t)}\right\} \qquad (5.24)$$

and

$$f_e = n_{0e}(r,t) \left(\frac{m_e}{2\pi k T_e(r,t)}\right)^{3/2} \exp\left\{-\frac{m_e(V_x^2 + V_y^2 + V_z^2)}{2kT_e(r,t)}\right\} \qquad (5.25)$$

Inserting (5.21) into (5.19) gives

$$\Gamma^{+}_{\|i}(Z_B) = \frac{n_{0i}(r,t)}{4} \left(\frac{8}{\pi} \frac{kT_i(r,t)}{m_i}\right)^{1/2} \qquad (5.26)$$

Inserting (5.22) into (5.20) gives

$$\Gamma^{+\#}_{\|e}(Z_B) = \frac{n_{0e}(r,t)}{4} \left(\frac{8}{\pi} \frac{kT_e}{m_e}\right)^{1/2} \exp\left\{-\frac{m_e(V^e_{max}(r,t)^2}{2kT_e(r,t)}\right\} \qquad (5.27)$$

The assumption of quasi-neutrality in the plasma outside the sheath region ($Z_A \geq Z \geq Z_B$ in sheath region) implies that $n_{0e}(r,t) = n_{0i}(r,t) \equiv n(r,t)$ for a $Z_{eff} = 1$ plasma. In order for the net electrical current to be zero at $Z = Z_A$, the condition (5.27) = (5.26)

must be true* at $Z = Z_B$. Equations

$$\Gamma^{+}_{\|i}(Z_B) = \Gamma^{+\#}_{\|e}(Z_B) \tag{5.28}$$

produces an equation for V^e_{max} given by

$$\frac{1}{2} m_e (V^e_{max})^2 = kT_e(r,t) \, \ell n \left[\left(\frac{m_i T_e}{m_e T_i} \right)^{1/2} \right] \tag{5.29}$$

and knowing that $-|e|\Phi_{max}$ must be equal to $1/2\ m_e(V^e_{max})^2$, one has an expression for Φ_{max}.

If one wishes to include secondary electron emissions from the collector plates due to ion, electron, and photon bombardment, then instead of (5.28), the condition that $J = 0$ becomes

$$\Gamma^{+}_{\|i} + \langle \beta_i \rangle_{eff} \Gamma^{+}_{\|i} + \langle \beta_e \rangle_{eff} \Gamma^{+}_{\|e} + \langle \Phi_\gamma \beta_\gamma \rangle_{eff} = \Gamma^{+}_{\|e} \tag{5.30}$$

and this can be recast into the form

$$\Gamma^{+}_{\|e}(Z_B) = \Gamma^{+}_{\|i}(Z_B) \left\{ \frac{1 + \langle \beta_i \rangle_{eff}}{1 - \langle \beta_e \rangle_{eff}} \right\} \left\{ 1 - \frac{S}{\Gamma^{+}_{\|i}} \right\} \tag{5.31}$$

where

$$S \equiv \langle \Phi_\gamma \beta_\gamma \rangle_{eff} \tag{5.32}$$

and

$\langle \beta_j \rangle_{eff}$ = secondary electron emission coefficient due to bombardment of species j integrated over the energy distribution of species j. The "eff" indicates that since the $\vec{B}$ field lines will not be at normal (90°)

*We assume here that no ionization or recombination occurs in the region between $Z = Z_A$ and $Z = Z_B$.

incidence to the collector plates that some fraction of the secondary e^- emitted will spiral back onto the plate and be recaptured. This effect obviously reduces the net emission rate as far as the main plasma is concerned.

$\langle \Phi_\gamma \beta_\gamma \rangle_{eff}$ = effective rate of secondary e^- emission due to incident photon flux integrated over the photon energy distribution function.

The expression for $1/2\ m_e(V^e_{max})^2$ is now given by

$$\frac{1}{2} m_e (V^e_{max})^2 = kT_e \ln\left[\left(\frac{m_i T_e}{m_e T_i}\right)^{1/2} \left\{\frac{1 - \langle \beta_e \rangle_{eff}}{1 + \langle \beta_i \rangle_{eff}}\right\} \left\{\frac{1}{1 - S/\Gamma^*_{\|i}}\right\}\right] \quad (5.33)$$

Using (5.33) one can compute the energy flux carried to the collector plates by the electrons

$$Q^{+\#}_{\|e}(Z_B) = \int_{-\infty}^{+\infty}\int dV_x dV_y \int_{V^e_{max}}^{\infty} \frac{1}{2} m_e (V_x^2 + V_y^2 + V_z^2) V_z f_e(V_x, V_y, V_z, Z_B, r, t) dV_z$$

$$= 2kT_e\ \gamma_E\ \Gamma^+_{\|i} \quad (5.34)$$

where (5.25) was taken for f_e, $\Gamma^+_{\|i}$ is given by (5.26), and γ_E is the function

$$\gamma_E = \frac{1 + \langle \beta_i \rangle_{eff}}{1 - \langle \beta_e \rangle_{eff}} \left\{1 - \frac{S}{\Gamma^+_{\|i}}\right\} \left\{1 + \ln\left[\left(\frac{m_i T_e}{m_e T_i}\right)^{1/4} \left(\frac{1 - \langle \beta_e \rangle_{eff}}{1 + \langle \beta_i \rangle_{eff}}\right)\right]\right\} \quad (5.35)$$

In a similar manner the total energy flux due to the ions is given by

$$Q^{+}_{\|i}(Z_B) = \int_{-\infty}^{+\infty}\int dV_y dV_x \int_0^{\infty} \frac{1}{2} m_i (V_x^2 + V_y^2 + V_z^2) V_z f_i(\vec{V}, Z_B r, t) dV_z$$

$$= 2kT_i \, \Gamma^{+}_{\|i} \tag{5.36}$$

Thus, the equations (factor of two accounts for loss in both directions along $\vec{B}$ lines)

$$\Gamma_{\|}(r) = 2\Gamma^{+}_{\|i} = \frac{n}{2}\left(\frac{8}{\pi}\frac{kT_i}{m_i}\right)^{1/2} \tag{5.37}$$

$$Q_{\|i}(r) = 2Q^{+}_{\|i} = 2kT_i \, \Gamma_{\|}(r) \tag{5.38}$$

$$Q_{\|e}(r) = 2Q^{+\#}_{\|e} = 2kT_e \, \gamma_E \, \Gamma_{\|}(r) \tag{5.39}$$

and γ_E as taken from (5.35) will be used in combination with L(r) to model the parallel particle and energy loss in the divertor zone of a tokamak reactor. Substitution of these expressions, (5.37)-(5.39), into equations (5.11), (5.12), and (5.13) constitutes the transport equations for the divertor zone. The results from using these equations to model UWMAK-II, UWMAK-III, and a typical EPR design are shown in Chapter VI. Before the solutions are discussed, the numerical solution procedure, which is central to the solution of these equations, must be discussed.

Numerical Methods

Once the equations are formulated and boundary conditions determined, the remaining problem is to choose a suitable numerical technique. By suitable, one means stable, reasonably accurate, easily

coded to prevent algebraic errors, and inexpensive to run. One can hardly ever find a technique which satisfies all four of these requirements. The technique to be used here will provide stable and reasonably accurate solutions, but it is not easily coded. It is fairly inexpensive to run when consideration is taken of the fact that in fusion reactor calculations (i.e., large reactors) one must usually carry the calculation out for three or four central particle confinement times (i.e., five seconds of reactor time) before one can be assured of finding a 'quasi-equilibrium' solution. Due to round off errors, one can never really find an 'equilibrium' solution to the time-dependent equations.

Before describing the numerical technique which was actually used, it is worthwhile to discuss briefly why an attempt was not made to solve the time-independent (or steady state) transport equations. One might think that solving a coupled set of ordinary differential equations would be easier to solve than a coupled set of partial differential equations. In general, however, this belief can be shown to be false. Early work performed by the author on trying to solve a somewhat more simplified set of steady state transport equations using several of the standard methods (e.g., 'shooting technique,' Newton's method, etc.) proved to be dismal failures. As a guide, one can also look back at the lack of success in the field of fluid mechanics in finding steady state solutions to the Navier-Stokes equations. The last point to note about the transport equations, which is primarily due to the presence of the divertor, is

that in the divertor zone the equations can be characterized as being numerically 'stiff.' By 'stiff,' one means the equations possess either exponentially increasing or decreasing solutions. Numerical techniques for solving ordinary differential equations usually experience trouble when 'stiff' regions are encountered, and this leads to very long calculation times and, thus, great expense.

After many failures, it was judged that the best approach was to solve the time-dependent transport equations as an initial boundary value problem. Proceeding with this idea, one is immediately confronted with what to do about the nonlinearity in the equations, e.g., the diffusion coefficient in the trapped ion mode regime scales as $D \sim T_e^{7/2} (\partial n/\partial r)^2 n^{-3} (1 + T_e/T_i)^{-2} r^{-1/2}$ and D appears in a term $\partial/\partial r(r\, D\, \partial n/\partial r)$. One has an equation (or set of equations) of the type

$$\frac{\partial y}{\partial t} = f\left(x,t,y, \frac{\partial y}{\partial r}, \frac{\partial^2 y}{\partial r^2}\right) \qquad (5.40)$$

where f may be any function of its arguments. There is one equation like (5.40) for each variable (n, T_e, T_i, etc.) at each spatial node ($i = 1, 2, \cdots N$). Thus, if we divide the spatial (r) axis into (N-1) zones with N nodal points, and if there are V variables, then there will be NV coupled equations to solve simultaneously.

Denoting by $\underline{Y}^{(s)}$ the solution vector whose components are the dependent variable values at each spatial nodal point at the s^{th} time step, one may more generally write (5.40) in the form

$$\frac{\partial}{\partial t}\,\underline{Y} = \underline{f}(r,\ t,\ \underline{Y},\ \underline{Y}',\ \underline{Y}'') \tag{5.41}$$

where the primes ($'$) indicate $\partial/\partial r$. Formally, integrating (5.41) produces

$$\underline{Y}^{(s+1)} = \underline{Y}^{(s)} + \int_{t}^{t+\Delta t} \underline{f}(r,\tau,\underline{Y}(\tau),\underline{Y}'(\tau),\underline{Y}''(\tau))d\tau \tag{5.42}$$

where $\underline{Y}^{(s+1)} \equiv \underline{Y}(t+\Delta t)$, $\underline{Y}^{(s)} \equiv \underline{Y}(t)$. The essence of all the numerical techniques seems to be how to handle the integration of $\underline{f}$. If one applies the trapezoidal rule to the integral, one obtains

$$\begin{aligned}\underline{Y}^{(s+1)} = \underline{Y}^{(s)} + \frac{\Delta t}{2}\,[&\underline{f}(r,s\Delta t,\underline{Y}^{(s)},\underline{Y}'^{(s)},\underline{Y}''^{(s)}) \\ &+ \underline{f}(r,(s+1)\Delta t,\underline{Y}^{(s+1)},\underline{Y}'^{(s+1)},\underline{Y}''^{(s+1)})]\end{aligned} \tag{5.43}$$

This is given the name Crank-Nicholson Method[19] and is the method we have used. The method requires, in order to obtain good accuracy, that all the first (spatial) derivations be approximated by central differences, e.g., $Y'_k \equiv Y_{k-1} - Y_{k+1}/2\Delta r$, and $Y''_k \equiv Y_{k-1} - 2Y_k + Y_{k+1}/(\Delta r)^2$.

It should be noted that we as yet have not done anything about the nonlinearity in $\underline{f}$. Since all terms with $^{(s)}$ superscripts are known, we need only concern outselves with $\underline{f}^{(s+1)}$, the second term in the square brackets in (5.43). This term is, in general, nonlinear in $\underline{Y}^{(s+1)}$. We have recourse to one of two techniques. We can keep f in its nonlinear form and perform an iterative sequence of calculations to find $\underline{Y}^{(s+1)}$, or we can linearize $\underline{f}^{(s+1)}$ about the

values of its arguments at the s^{th} time step.[1] We shall use the latter (linearization) approach for reasons which will become clear in a moment.

The primary advantages offered by the Crank-Nicholson Method are that it is a two (time) level formulation, i.e., uses values at only the s and s+1 time steps, and that it has a fairly high order of accuracy.* If $\underline{f}$ is linear, it is also fairly easily coded for the computer. If $\underline{f}^{(s+1)}$ were linear in $\underline{Y}^{(s+1)}$ then (5.43) could be written as

$$\underline{Y}^{(s+1)} = \underline{Y}^{(s)} + \frac{\Delta t}{2}\,\underline{f}^{(s)} + \frac{\Delta t}{2}\,\frac{\partial \underline{f}}{\partial \underline{Y}^{(s)}} \cdot \underline{Y}^{(s+1)} \qquad (5.44)$$

which has the formal solution

$$\underline{Y}^{(s+1)} = \left(\underline{\underline{I}} - \frac{\Delta t}{2}\,\frac{\partial \underline{f}}{\partial \underline{Y}}\right)^{-1} \cdot \left(\underline{Y}^{(s)} + \frac{\Delta t}{2}\,\underline{f}^{(s)}\right) \qquad (5.45)$$

where $(\underline{\underline{I}} - \Delta t/2\ \partial \underline{f}/\partial \underline{Y}^{(s)})^{-1}$ is obviously the inverse of the formal operations given in (5.44). There are many non-trivial but standard numerical methods for quickly performing the operations needed to produce (5.45). These will not be discussed here.

When $f^{(s+1)}$ is nonlinear, one can linearize using the following technique.[1] Replace $\underline{f}^{(s+1)}$ by

$$\underline{f}^{(s+1)} \simeq \underline{f}^{(s)} + \left[\left[\frac{\partial \underline{f}}{\partial \underline{Y}}\right]\right]^{(s)} \cdot \frac{(\underline{Y}^{(s+1)} - \underline{Y}^{(s)})}{\Delta t}\,\frac{\Delta t}{2} \qquad (5.46)$$

---

*By second order accuracy, one means that the solution to the differential equation differs from the solution to the finite differential equations by terms which are proportional to $\theta((\Delta t)^2) + \theta((\Delta r)^2)$.

where $[[\ ]]^{(s)}$ indicates the terms are to be evaluated at the s^{th} time step. Using (5.46) in (5.43) gives

$$\underline{Y}^{(s+1)} = \underline{Y}^{(s)} + \Delta t \left(\underline{\underline{I}} - \frac{\Delta t}{4} \left[\frac{\partial \underline{f}}{\partial \underline{Y}}\right]^{(s)}\right)^{-1} \cdot \underline{f}^{(s)} \qquad (5.47)$$

To show more explicitly how (5.47) was applied to the transport equations, one can consider $\underline{f}$ to represent the right hand sides of equations (5.11) through (5.13), for example, $\underline{f}$ then depends on a set of parameters $\{P_j\}$ where

$$\{P_j\} = \left\{T_e, T_i, n, B, \frac{\partial n}{\partial r}, \frac{\partial T}{\partial r}, \frac{\partial q}{\partial r}, \left(1 + \frac{T_e}{T_i}\right)\right\} \qquad (5.48)$$

and q is the safety factor $r/R_0\ B_T/B(r)$. At a particular nodal position, say node k, each parameter $(P_j)_k$ depends on one or more of the following set of variables $\{X_i\}_k$.

$$\{X_i\}_k = \{T_{ek-1}, T_{ek}, T_{ek+1};\ T_{ik-1}, T_{ik}, T_{ik+1};\ J_{k-1}, J_k, J_{k+1};$$

$$B_{k-1}, B_k, B_{k+1};\ E_{k-1}, E_k, E_{k+1};\ n_{k-1}, n_k, n_{k+1};$$

$$V_{k-1}, V_k, V_{k+1}\} \qquad (5.49)$$

where T_e, T_i are the electron and ion temperatures, respectively; J is the current density in the plasma in the Z direction; B is the poloidal magnetic field; E is the axial (Z) electric field; n is the plasma ion density; and V is the diffusion velocity = $- D_\perp/n\ \partial n/\partial r$.

The reasons for choosing this particular set, $\{P_j\}$, stems from our choice of diffusion coefficients (see Appendix A) and how they scale. The inclusion of only the k-1, k, and (k+1) nodal points stems

from the need for compactness, i.e., with the exception of certain types of boundary conditions, one can achieve second order accuracy ($\mathcal{O}(\Delta X)^2$) using only the nearest spatial neighbors.

To perform the linearization on $\underline{f}^{(s+\theta)}\,(P_j\{X_i\})$, one has[1]

$$\underline{f}^{(s+\theta)} = \underline{f}^{(s)} + \sum_j \Sigma \left[\frac{\partial \underline{f}}{\partial P_j}\frac{\partial P_j}{\partial X_i}\right]^{(s)} \left(\frac{X_i^{(s+1)} - X_i^{(s)}}{\Delta t}\right) \theta\, \Delta t \qquad (5.50)$$

where $\theta = 1/2$ gives the Crank-Nicholson algorithm, and, to be perfectly clear, a specific example is calculated below for reference.

Example: Let us linearize the term

$$\left[\frac{\partial}{\partial r}\left(r\, T_e \frac{\partial n}{\partial r}\right)\right]_k$$

and expand about the s+1 time using the scheme indicated above, where k indicates that the term is to be represented at the k^{th} special node.

$$\left[\frac{\partial}{\partial r}\left(r\, T_e \frac{\partial n}{\partial r}\right)\right]_k = \left[\frac{\partial}{\partial r}\left(r\, T_e \frac{\partial n}{\partial r}\right)\right]_k^{(s)}$$

$$+ \left[\frac{\partial}{\partial r}\left(r \frac{\partial n}{\partial r}\right)\right]_k^{(s)} \left\{\frac{T_{ek}^{(s+1)} - T_{ek}^{(s)}}{\Delta t}\right\} \Delta t$$

$$+ \left[\frac{\partial}{\partial r}\left(r\, T_e\right)\right]_k^{(s)} \left\{\frac{\left(\frac{\partial n}{\partial r}\right)^{(s+1)} - \left(\frac{\partial n}{\partial r}\right)^{(s)}}{\Delta t}\right\} \Delta t$$

$$+ \left[r \frac{\partial n}{\partial r}\right]_k^{(s)} \left\{\frac{\left(\frac{\partial T_e}{\partial r}\right)^{(s+1)} - \left(\frac{\partial T_e}{\partial r}\right)^{(s)}}{\Delta t}\right\} \Delta t$$

$$+ \left[r\, T_e\right]_k^{(s)} \left\{\frac{\left(\frac{\partial^2 n}{\partial r^2}\right)_k^{(s+1)} - \left(\frac{\partial^2 n}{\partial r^2}\right)^{(s)}}{\Delta t}\right\} \Delta t \qquad (5.51)$$

where (s) indicates evaluation using the properties as known at the s^{th} time step. One can see from (5.51) that when the time derivative of the above quantities becomes small (i.e., terms in curly { } brackets go to zero) the term on the left of (5.42) approaches the steady state solution of the nonlinear time-independent equation, which is the first term on the right of (5.51). Thus, if one can find an 'equilibrium' solution to the linearized (using the above method) transport equations by following it along in time from some initial value, then one knows that the solution found is a solution to the full nonlinear steady state set of equations. This is a very nice property of the above linearization procedure. Richtmyer and Morton[20] speak of this type of solution technique in their book; it was generalized by Widner and Dory[12] and discussed by Hogan.[1]

The Δt terms in (5.51) reflect the fact that we are taking the time derivative of the transport equations [like (5.4) through (5.6)] to be evaluated at the s+1 time step. If instead of s+1 we had chosen to expand out at the s+δ timestep ($0 \leq \delta \leq 1$), then one would have obtained, instead of (5.51), the terms shown below.

$$\left[\frac{\partial}{\partial r}\left(r\, T_e\, \frac{\partial n}{\partial r}\right)\right]_k = \left[\frac{\partial}{\partial r}\left(r\, T_e\, \frac{\partial n}{\partial r}\right)\right]_k^{(s)}$$

$$+ \left[\frac{\partial}{\partial r}\left(r\, \frac{\partial n}{\partial r}\right)\right]_k^{(s)} \left\{\frac{T_{ek}^{(s+1)} - T_{ek}^{(s)}}{\Delta t}\right\} \delta\, \Delta t$$

$$+ \left[\frac{\partial}{\partial r}(r\, T_e)\right]_k^{(s)} \left\{\frac{\left(\frac{\partial n}{\partial r}\right)_k^{(s+1)} - \left(\frac{\partial n}{\partial r}\right)_k^{(s)}}{\Delta t}\right\} \delta\, \Delta t$$

$$+\left[r\,\frac{\partial n}{\partial r}\right]_k^{(s)}\left\{\frac{\left(\frac{\partial T_e}{\partial r}\right)_k^{(s+1)}-\left(\frac{\partial T_e}{\partial r}\right)_k^{(s)}}{\Delta t}\right\}\delta\,\Delta t$$

$$+\left[r\,T_e\right]_k^{(s)}\left\{\frac{\left(\frac{\partial^2 n}{\partial r^2}\right)^{(s+1)}-\left(\frac{\partial^2 n}{\partial r^2}\right)^{(s)}}{\Delta t}\right.\delta\,\Delta t$$

and this can be rewritten as

$$\frac{\partial}{\partial r}\left[r\,T_e\,\frac{\partial n}{\partial r}\right]_k^{s+\delta}=\left[\frac{\partial}{\partial r}\left(r\,T_e\,\frac{\partial n}{\partial r}\right)\right]_k^{(s)}(1-\delta)$$

$$+\left[\frac{\partial}{\partial r}\left(r\,\frac{\partial n}{\partial r}\right)\right]_k^{(s)}\delta\,T_{ek}^{(s+1)}$$

$$+\left[\frac{\partial}{\partial r}(r\,T_e)\right]_k^{(s)}\delta\left\{\frac{n_{k-1}^{(s+1)}-n_{k+1}^{(s+1)}}{2\Delta r}\right.$$

$$+\left[r\,\frac{\partial n}{\partial r}\right]_k^{(s)}\delta\left\{\frac{T_{ek-1}^{(s+1)}-T_{ek+1}^{(s+1)}}{2\Delta r}\right\}$$

$$+\left[r\,T_e\right]_k^{(s)}\delta\left\{\frac{n_{k-1}^{(s+1)}-2n_k^{(s+1)}-n_{k+1}^{(s+1)}}{(\Delta r)^2}\right\}\qquad(5.52)$$

As can plainly be seen, (5.52) would be only one of the terms in the particle diffusion equation [(5.52) assumed $D_\perp \sim T_e$ only). Imagine the algebra necessary when one assumes that $D_\perp$ has some more complicated variation, e.g.,

$$D_\perp \sim T_e^{S1}\,T_i^{S2}\,n_i^{S3}\,B^{S4}\left(\frac{\partial n}{\partial r}\right)^{S5}\left(\frac{\partial T}{\partial r}\right)^{S6}\left(\frac{\partial q}{\partial r}\right)^{S7}\left(1+\frac{T_e}{T_i}\right)^{S8}$$

This is just exactly what has been assumed in the code now being used at Wisconsin. The initial modification of the code to handle such complicated dependences was done by Kesner and Khelladi in 1974 at Wisconsin and has been reported on elsewhere.[21]

This linearization procedure was applied not only to the transport equations, but also to Ohm's Law (5.14) and two of Maxwell's equations (5.15) and (5.16).

Once the equations are linearized, then all terms which are evaluated at the (s+1) time step are placed on the left hand side of the equations. These terms have coefficients which are evaluated at the s^{th} time step and are, therefore, known. The remaining terms which stand alone on the right hand side of the equations are evaluated at the s^{th} time step. One ends up with a matrix equation of the form

$$\underline{\underline{A}}\ \underline{Y}^{(s+1)} = \underline{B} \tag{5.53}$$

and a Gaussian elimination technique is used to invert the above equation.[22]

As we stated previously, the Crank-Nicolson Method ($\delta = 1/2$) is stable for any size time step Δt. There is, however, a limitation on how large Δt can be. The limitation comes about due to the linearization and the fact that one cannot allow some of the physical variables to become negative during the course of the numerical solution. To see this more clearly, consider Fig. V-4 which shows the exact solution to a simple diffusion equation ($\partial u/\partial t = \partial^2 u/\partial x^2$),

$$\frac{du_1}{d\theta} = -2u_1 \qquad u_1 = e^{-2\theta}$$

Euler: $u^{(v+1)} = (1 - 2p)u^{(v)}$

Crank-Nicolson: $(1 + p)u^{(v+1)} = (1 - p)u^{(v)}$ where $p = \Delta\theta/(\Delta x)^2$

Pure implicit: $(1 + 2p)u^{(v+1)} = u^{(v)}$

Each of these may be put in the following general form:

$u^{(v+1)} = \lambda u^{(v)}$

where λ has the following definitions:

Euler: $\lambda = 1 - 2p$

Crank-Nicolson: $\lambda = \dfrac{1 - p}{1 + p}$

Pure implicit: $\lambda = \dfrac{1}{1 + 2p}$

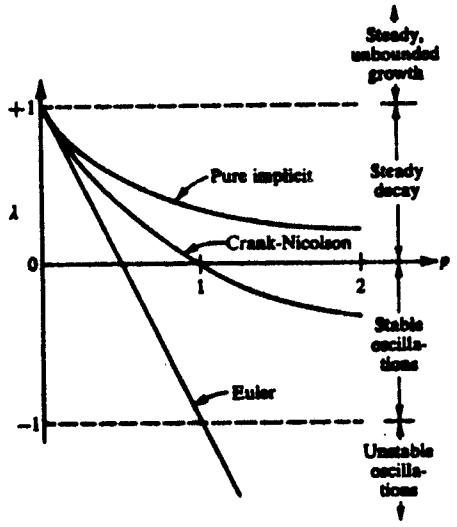

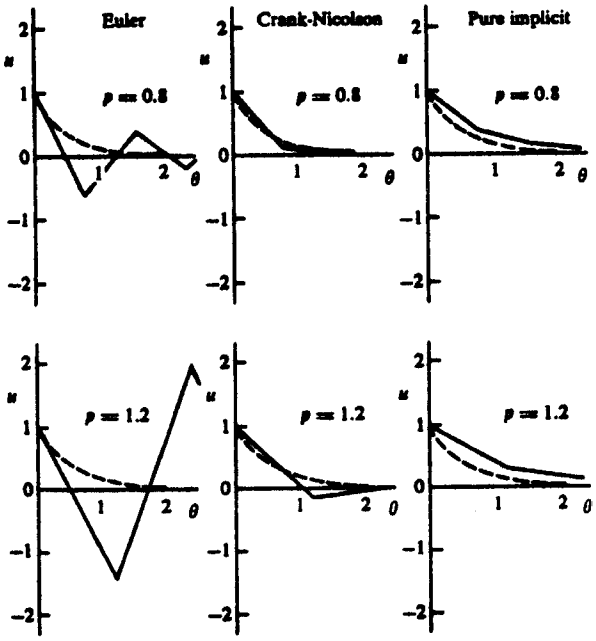

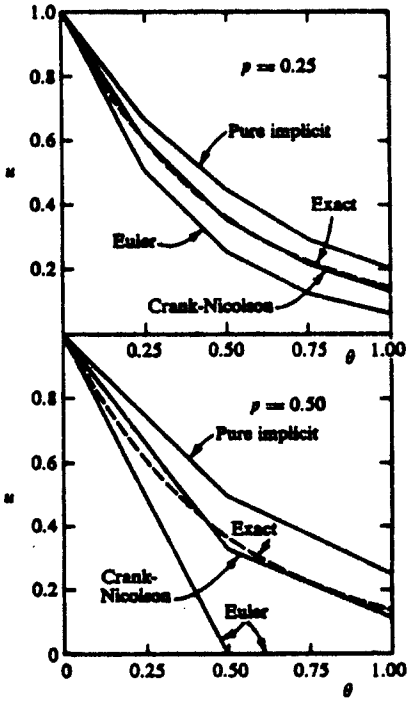

Figure V-4

and the approximate solution found using an Euler ($\delta = 0$), a Crank-Nicolson ($\delta = 1/2$), and a pure implicit ($\delta = 1$) numerical scheme. The solutions are shown for two separate ratios of $P \equiv \Delta t/(\Delta x)^2$. The example was taken with the author's permission from "Analytical Methods in Conduction Heat Transfer," by G. E. Myers.[23] One finds that the Euler technique produces oscillations which will continue to grow (i.e., become unstable) for $p > .5$. The Crank-Nicholson technique overshoots, and oscillates about the solution. These oscillations can become more severe, but they will never go unstable. Oscillations would never appear in the pure implicit technique, but it will continue to lose accuracy.

As is schematically indicated in Fig. V-4, the Crank-Nicolson technique does tend to follow more closely the exact solution curve than do the other methods shown. A problem occurs, however, when the temperatures or plasma density become small and time derivatives still remain reasonably large. In that case, one is limited to a Δt which is small enough to guarantee that the 'overshoot' on the approximate solutions is not so large as to drive n or T negative. If this condition occurs when initially starting the numerical calculation, it tends to indicate an inappropriate choice of initial conditions. It can also occur, however, right after one has performed some calculation extraneous to the transport (and Maxwell's) equations themselves, i.e., the neutral particle and impurity transport calculations are handled in a completely different manner than the plasma transport calculations. After one of these 'extraneous' procedures is performed,

the plasma sees itself (numerically) as having a new set of initial conditions put on it. If these conditions are severe, one can run into cases where the time derivatives, when evaluated through the linearized equations, are large. This forces the code to take very small time steps, and can, under these conditions, make the calculations very expensive. Some of the specific problems encountered in solving certain types of fusion reactor systems (including divertors) are presented in the next chapter. The solutions for each reactor shown in Chapter VI had its own numerical pitfalls!

Neutral Transport

In order to ascertain the ionization rate and charge exchange energy in the plasma (including the divertor zone) one must know $n_0(r)$, the density of neutral fuel atoms at each spatial position in the plasma. Due to the time scale for these neutrals to take on an "equilibrium" profile, one needs only to solve the time independent Boltzmann transport equation. This equation is resolved at a given set of predetermined times during the course of the plasma operating cycle.

In the work presented in Chapter VI the plasma is very large compared to most of the neutrals mean free paths. Thus, one can use a slab geometry to solve for n_0 instead of cylindrical geometry. This saves a considerable amount of time. Explicitly the equation that is solved is

$$v_x \frac{\partial f_0}{\partial x} = s\{f_0\} \qquad (5.54)$$

where $s\{f_0\}$ = ionization term + charge exchange term + elastic scattering term + plasma recombination term; $f_0 = f_0(x,v,\theta)$ = neutral distribution function; $v_x = v \cos\theta$. In practice, elastic scattering between neutrals and plasma ions and electrons is ignored as is recombination of fuel ions which would serve as a volumetric source of neutrals. The ionization term is

$$[s\{f_0\}]_{\text{ion iz}} = \int f_e(x,v')\sigma_{iz}^{e}(|\vec{v}'-\vec{v}|)|\vec{v}'-\vec{v}|f_0(x,v,\theta)d^3v' + \int f_i(x,v')\sigma_{iz}^{i}(|\vec{v}'-\vec{v}|)|\vec{v}'-\vec{v}|f_0(x,v,\theta)d^3v' \tag{5.55}$$

where $f_{e(i)}$ = electron (ion) distribution function and $\sigma_{iz}^{e(i)}$ = electron (ion) input ionization cross section.

The charge exchange term is

$$[s\{f_0\}]_{cx} = \int f_0(x,v',\theta')f_i(x,v)\sigma_{cx}(|\vec{v}'-\vec{v}|)|\vec{v}'-\vec{v}|d^3v' - \int f_0(x,v,\theta)f_i(x,v')\sigma_{cx}(|\vec{v}'-\vec{v}|)|\vec{v}'-\vec{v}|d^3v' \tag{5.56}$$

where the first term represents "in scattering" and the second term gives the loss due to "out scattering." Equation (5.54) can then be written as

$$v\cos\theta\frac{\partial f_0}{\partial x} + \frac{f_0}{\tau} = f_i(x,v)\int f_0(x,v',\theta')\sigma_{cx}(|\vec{v}-\vec{v}'|)|\vec{v}-\vec{v}'|d^3v' \tag{5.57}$$

where

$$\frac{1}{\tau} \equiv n_e\langle\sigma v\rangle_{iz}^{e} + n_i\{\langle\sigma v\rangle_{iz}^{i} + \langle\sigma v\rangle_{cx}\} \tag{5.58}$$

and

$$\langle \sigma_{j0} v \rangle_j \equiv \int f_j(x,v') \sigma_{j0}(|\vec{v}-\vec{v}'|) |\vec{v}-\vec{v}'| d^3v' \tag{5.59}$$

In the code used for the cases in Chapter VI, f_i and f_e were assumed to be Maxwellian at temperatures $T_i(x)$ and $T_e(x)$, respectively.

Equation (5.57) can be recast into integral equation form. This gives

$$f_0(x,v,\mu) = \exp\left\{-\frac{1}{v\mu}\int_a^x \frac{dx'}{\tau(x',v)}\right\} \left[c + \frac{1}{v\mu}\int_a^x I_s(f_0(x',v)) \exp\left\{-\frac{1}{v\mu}\int_a^{x'} \frac{dx''}{\tau(x'',v)}\right\} dx'\right] \tag{5.60}$$

where $I_s \equiv$ right hand side of (5.57). The unknown c is determined by the boundary condition applied at x = a. To find $n_0(x)$ one must integrate f_0 over v and μ. There are a number of ways one can proceed to solve for f_0 using (5.60).[24] They will not be elaborated here. The technique used here* is based upon a type of particle following technique.

If one ignores the integral term in (5.60) and proceeds from the boundary (x = a) inwards, the neutral density is seen to "drop off" exponentially. If one assumes a monoenergetic ($1/2\ mv_0^2 = E_0$), isotropic, neutral source at the plasma edge, then $f_0^{(0)}(x,v_0)$ can be determined. The superscript (0) indicates the initial "relaxation" of the neutrals, not accounting for charge exchange creation of energetic neutrals. Some fraction of $f_0^{(0)}$ given by

*Initially developed by M. Khelladi.[21]

$$\{n_e\langle\sigma v\rangle_{iz} + n_i\langle\sigma v\rangle_{iz}\}\tau\, f_0^{(0)} \qquad (5.61)$$

are ignored and contribute to the plasma density. The energy loss (or gain) due to this ionization process is also accounted for in the code. The fraction

$$n_i\langle\sigma v\rangle_{cx}\,\tau\, f_0^{(0)} \qquad (5.62)$$

undergoes charge exchange. Within each spatial region where f_o, n_i, T_e, T_i, etc. are calculated, one can determine (5.62). This charge exchange fraction is taken as a new source of neutrals. These new neutrals are assumed to have an energy equal to the ion temperature at that particular spatial location at which the cx occurred. Thus, the energy "spectrum" of the neutrals is a histogram with values only at the ion temperatures for each of the spatial cells used in the plasma calculations. These new sources of neutrals (one source for each spatial node) are then successively treated in the same manner as was done to the initial "edge" neutrals except now v would take on the value $\sqrt{2T_i(x_k)/m_i}$ of the source when originating at the k^{th} spatial node. Each generation of charge exchange neutrals are followed and account is taken of the net energy transfer in each spatial cell due to charge exchange reactions, and ionizations. The flux of neutrals (and their discrete energy spectrum) is computed and subsequently used to determine wall erosion rates.[25]

The subroutines used for this computation has been optimized to take a relatively small amount of time as long as the number of

spatial regions used is reasonable (< 20) and the number of charge exchange generations is small (< 10). For the large plasmas considered in Chapter VI, it was determined by trial and error that only the closest 20 spatial regions needed to be considered and only four generations of cx neutrals needed to be followed. Account was taken of the neutrals which escaped deeper into the plasma by renormalizing the particle ionization rates, and neutral fluxes out of the device, i.e., the neutral calculations always conserved particles so that the number into the plasma equaled the number hitting the wall, plus the number ionized.

Impurity Transport

Impurity transport equations and calculational procedures were saved for last for three reasons. First, impurity transport is not yet well diagnosed in present day plasmas so no good numerical model exists. Secondly, the numerical models which do exist are by necessity relatively complicated, particularly for high Z materials where one must account for the time dependent stripping and radiation effects. Thirdly, due to the above two reasons, impurity transport was not performed in the work presented herein. Impurity effects are important but it seemed advisable to try to separate out the energy and particle balance effects due to the divertor alone from those effects due to the presence of impurities, i.e., this is a research report on divertor behavior, not impurity behavior. It will be noted in the conclusion to this research that multispecies divertor zone equations

should be developed.

Hogan[1] outlines some of the codes currently used to study impurity evolution and his article should be consulted for further formulation of the impurity problem.

Calculational Procedure

The entire numerical procedure is modularized so that as each new model for plasma behavior is discovered, it can be inserted into the code. The skeletal structure used was that developed at the Oak Ridge National Laboratory by John Hogan, et al.[26] With reference to Figs. V-5 and V-6, the program cycle proceeds as follows:

1. Read in all parameters, set up initial profiles for density, temperature, current density, B field, electric field, and diffusion velocity.
2. Normalize data to specified average values.
3. Print out initial profiles.
4. Calculate initial power balance.
5. Begin simulation cycle by deciding on maximum number of time steps desired. (Program will exit on this value or on a given maximum time for plasma operation.)
6. Determine appropriate time step size.
7. Determine neutral density profile.
8. Determine impurity source profile.
9. Determine fusion alpha particle profile.

```
C        BEGINNING OF MAIN PROGRAM FLOW PROG:A.T.MENSE 1971/1976
C
C ********************************************************************
C **** THIS IS MAINSTREAM OF LOGIC IN PLASMA TRANSPORT PROGRAM.
C **** COMMON BLOCKS HAVE BEEN DELETED TO SIMPLIFY READING.
C **** ALMOST ALL PRINTING IS DONE IN ONE SUBROUTINE: SUB PRTOUT
C **** PRTOUT IS NEVER CALLED DIRECTLY. ONLY CALLED THROUGH ENTRY
C **** POINTS SUCH AS PROFIL.IMPRIN. ETC.
C ********************************************************************
C
C --- READ ALL INPUT PARAMETERS. INITIAL CONDITIONS AND BOUNDARY VALUES.
C --- THEN PRINT ALL THESE DATA.
C --- INITIALIZE TEMPERATURE. CURRENT DENSITY. PLASMA DENSITY. NEUTRAL D
C --- CURRENT DENSITY. ELECTRIC AND MAGNETIC FIELDS.
C --- AND IONIZATION TERM PROFILES.
      CALL GETSET
CC     IF(NJCT.GT.0)CALL BMSTRT(AB)
      IF (IHF.LT.-1.OR.IHF.GE.1) GO TO 1
      CALL STORE(1,IFILE)
  1   CONTINUE
C   ***** NORMALIZE DENSITY AND TEMPERATURE TO SPECIFIED VALUES
      IF(INORM.GT.0)CALL DENORM
C  **** PRINT OUT INITIALIZEING DATA
      CALL INIOUT
      IF(AB.GE.2.0.AND.NJCT.LT.0)CALL TCTGET
C   ******** TCTGET IS ENTRY INTO GETTSET WHICH CALLS TCTSET ******
C --- CALCULATE INITIAL POWER BALANCE.
      CALL INITPB(ZEFF)
C --- PRINT INITIAL POWER BALANCE COMPONENTS.
      CALL IPBOUT
C --- **** **** **** B E G I N   S I M U L A T I O N **** **** ****
      NSTEP=NT
      IF(NSTEP.EQ.0) NSTEP=1200
      DO 10 ITT=1,NSTEP
      IT=ITT
C   **** CALCULATE WHAT IS APPROPRIATE TIMSTEP
      CALL TIMSTP(IT)
C   **** CALCULATE THE NEUTRAL PROFILE AND CX FLUX TO WALL
       CALL NEUTRA(IT)
C   **** CALCULATE THE IMPURITY SOURCE RATE DUE TO SPUTERING ETC.
C     CALL SOURCE
C   TEMPORARY DELETION OF SOURCE  A.T. MENSE
C   **** CALCULATE THE ALPHA PARTICLE PROFILE
      IF (IT.GT. 25) CALL ALFDIF
C   **** CALCULATE THE IMPURITY CONTENT OF PLASMA.FIND DEN(I)
      CALL IMPRTY
   69 CONTINUE
C   **** K IS THE NUMBER OF EQUATIONS SOLVED
      K=7
  3   CONTINUE
C  **** DETERMINE WHICH BEAM INJECTION ROUTINE TO USE
      IF(NJCT)200,202,201
C   **** WHBEAM IS PENCIL BEAM ROUTINE
  200 CALL WHBEAM(AB)
      GO TO 202
C   **** INJECT IS A FINITE WIDTH BEAM ROUTINE OF J.ROME O.R.N.L.
  201 CALL INJECT(AB)
  202 CONTINUE
C   **** COMBINES RAD LOSS.INJECTION. AND NEUTRAL ENERGY LOSS TERMS
C   **** ALSO COMPUTES PELLET INJECTION RATE TO ACHIEVE SPECIFIED
```

Figure V-5

```
C    **** DENSITY.
       CALL BMSET
C************** CALCULATE ONE PLASMA TIMESTEP
       CALL PLASM1(IT)
C************** RESET TO NEW VALUES
       CALL RESET(IT,K,$8,$69)
C --- PRINT TEMPERATURE, DENSITY PROFILES
       CALL PROFIL(IT)
C --- CALCULATE LOCAL CONVECTION LOSS, THERMAL CONVECTION LOSS
C    MULTIFLE ENTRY IN ORMPWR:SAVPWR(FROM RESET)
C    AND NEWPWR HERE
    20 CALL NEWPWR
C --- CALCULATE PLASMA POWER BALANCE
       CALL PWRBAL(IT)
       CALL SUMARY
C    **** WRITE OUT BEAM INJECTION PARAMETERS
       IF(NJCT.NE.0)CALL BMWRIT
C    **** PRINT OUT IMPURITY PROFILES
       IF(IMOL.EQ.2.AND.PCIMP.NE.0.0)CALL IMPRTT
       CALL IMPRIN(0)
C    **** RENORMALIZE IF DESIRED
C       CALL DENORM
  8    CONTINUE
C    **** HISTORY IS NOW CALLED FROM SAVPWR A.T.M.
C       CALL HISTOR(IT)
C   **** CHECK TO SEE IF SHOULD END COMPUTATION
       IF ( TIM .LT. TMAX .AND. IT.LT.NSTEP)GO TO 10
 1001 CONTINUE
       WRITE(5,1020)IT,NSTEP,TIM,TMAX
 1020 FORMAT(5X,'LEAVING PROGRAM IT,NSTEP,TIM,TMAX',/,5X,
     & 2I5,1PE10.2,E10.2,//)
       CALL PROFIL(IT)
       CALL NEWPWR
       CALL SUMARY
       CALL IMPRIN(1)
       IF (IMOL.EQ. 2.AND.PCIMP.NE.0.0) CALL IMPRTT
       CALL HISTOR(IT)
  12   CONTINUE
C    **** FIND REQUIRED EMF AROUND PLASMA LOOP
       CALL VOLT(IT)
       IF(IHF.GT.2.OR.IHF.LT.0) GO TO 9999
C    **** STORE THE DATA ON A FILE CALLED FILE2
       IF(NNN.GE.0)CALL STORE(2,IFILE2)
       GO TO 9999
  10   CONTINUE
C --- **** **** **** E N D   S I M U L A T I O N **** **** ****
       CALL HISTOR(IT)
       WRITE(6,1000)
 1000 FORMAT(1X,'SAVS')
 9999 CONTINUE
       STOP
       END
```

Figure V-6

10. Determine impurity (other than alphas) profile and relate n_e to $n_i + zn_z$.
11. Determine power and particle input due to neutral beam injection and pellet ionization.
12. Determine energy loss due to radiation, ionization, and cx losses.
13. Compute plasma cycle by
    a. find diffusion coefficients and thermal conductivities.
    b. evaluate all terms in transport equation matrix.
    c. invert matrix to find n, T_e, T_i, B, J, E, V.
14. Check to see that n, T_e, T_i are not negative and if okay, replace old variable values by new values. Go back to 6. unless you wish to print, or time has run out, or number of iterations has exceeded maximum prescribed value.
15. If printing is called for, do so and return to cycle.
16. If time exceeds t_{max} or iterations exceed NSTEP, then exit, perform last printing, and save profiles in special output file.

Now that the basic program chain has been outlined and the equations which must be solved described, the actual results must be presented. This is done in Chapter VI for three cases of some interest to the Fusion Technology Study Group at the University of Wisconsin.

CHAPTER V

Bibliography

[1] J. T. Hogan, in Methods of Comp. Phys., Vol. 16, (Academic Press, New York, 1976) p. 131.

[2] H. C. Howe, private communication on ORMAK Upgrade proposal.

[3] J. Kesner and R. W. Conn, UWFDM-155, Nuc. Eng. Dept., Univ. of Wisconsin, Madison, WI (Dec. 1975).

[4] Ref. [19], Chapter III.

[5] J. T. Hogan and D. B. Nelson, private communications.

[6] Ref. [7], Chapter III.

[7] M. N. Rosenbluth, R. D. Hazeltine and F. L. Hinton, Phys. Fluids 15, 116 (1972).

[8] Ref. [6], Chapter I.

[9] Ref. [30], Chapter II.

[10] Ref. [6], Chapter I.

[11] T. F. Yang et al., FDM-49, Nuc. Eng. Dept., Univ. of Wiscon, Madison, WI (July 1973); see also Ref. [6], Chapter I.

[12] M. M. Widner and R. A. Dory, Bull. Am. Phys. Soc. 11, 1418 (1970); see also ORNL/TM-3498 (1971); see also J. K. Munro et al., ORNL/TM-5262 (1976-77).

[13] E. Hotston, CLM-P449, Culham Lab., England (Jan. 1976).

[14] E. Hotston and G. M. McCracken, CLM-P455, Culham Lab., England (Feb. 1976).

[15] See Appendix E for reproduction of Nuclear Fusion Letter.

[16] J. A. Schmidt, private communication on FM-1.

[17] See Appendix in Ref. [2] given in Chapter I.

[18] G. D. Hobbs and J. A. Wesson, Plasma Physics 9, 85 (1967).

[19] G. Dahlquist et al., Numerical Methods (Prentice-Hall, 1974); see also J. T. Hogan, loc. cit.

[20] R. D. Richtmyer and K. W. Morton, Difference Methods for Initial-Value Problems (Interscience Pub., John Wiley and Sons, New York, 1967).

[21] R. W. Conn, M. Khelladi, and J. Kesner, UWFDM-136, Nuclear Eng. Dept., Univ. of Wiscon, Madison, WI (1975).

[22] G. Dahlquist, loc. cit.

[23] G. E. Myers, Analytical Methods in Conduction Heat Transfer (McGraw-Hill, New York, 1971), pp. 281-289.

[24] M. M. R. Williams, Mathematical Methods in Particle Transport Theory, (Wiley-Interscience, New York, 1971).

[25] R. W. Conn and J. Resner, to be published in J. Nuc. Mat (1976); see also UWFDM-153, Nuc. Eng. Dept., Univ. of Wisconsin, Madison, WI (Feb. 1976).

[26] J. K. Munro et al., ORNL/TM-5262, "User's Manual for ORNL 1-D Transport Code."

[27] W. A. Houlberg, UWFDM-162, Nuc. Eng. Dept., Univ. of Wisconsin, Madison, WI, (June 1976).

CHAPTER VI

Numerical Solutions to Transport Equations with Divertor

The purpose of this chapter is to outline in detail the actual numerical results obtained from three fusion reactor designs. The first design studied was that of UWMAK-II[1] which is a large ($a \simeq 5$ m, $R_0 \simeq 13$ m, $P_{th} \simeq 5000$ MW_{th}), low β device. The second case covered was that of UWMAK-III[2] which is smaller than UWMAK-II ($a \simeq 2.7$ m, $b = 5.4$ m, $R_0 = 8.1$ m, $P_{th} \simeq 5000$ MW_{th}), vertically elongated, but of the same thermal output. The last case was that of a typical Experimental Power Reactor (EPR), which may be viewed as the step just before a full scale demonstration power reactor. The EPR designs[3] typically run somewhat smaller in size ($a \simeq 2.0$ m, $R_0 \simeq 8$ m, $P_{th} \simeq 1200$ MW_{th}) and have been designed at reasonably low β. Higher β systems are only now being investigated.[4]

Before discussing the points of difference between each of the three cases to be considered, it is worthwhile to note first their similarities.

1. All calculations used the divertor model outlined in Chapter V and all excluded secondary electron emission effects (see Appendix G).

2. All cases were solved under the assumption that the dissipative trapped particle modes produced the diffusion process. (See Appendix A for exact details.)

3. The boundary conditions at the center of the plasma core region were as outlined in Chapters IV and V (i.e., $\Gamma_r = \tilde{Q}_{er} = \tilde{Q}_{ir} =$

$B = \partial E_z/\partial r = 0$ at $r = 0$).

4. In all cases, equilibrium solutions were strived for within the bounds of the numerical errors associated with machine round off.[5] In each case this equilibrium was sought by starting with initial values on the plasma such that the device was above ignition.* From this set of initial values the profiles were followed temporally until they "relaxed" to a relatively constant set of values. The integrated parameters such as average density, average electron (ion) temperature, and average beta poloidal were used as indications of a steady operating condition. When these averages appear sensibly constant over a time span of several central particle confinement times, the solution was taken to be a steady state.

It should be noted that certain types of initial values, particularly if they were significantly different from the "steady state" solutions, caused the numerical solution procedure to slow down (i.e., take smaller time steps) to such a degree that it became economically unattractive to try and follow that set of values all the way to the steady state. Thus, the secret to finding a steady state without using extremely large amounts of computer time was to judiciously select the initial values for the problem.**

---

*(i.e., the power deposited by alphas and ohmic heating is greater than or equal to the sum of all the power losses from the plasma.)

**There have always been questions of uniqueness when one has a coupled set of very nonlinear equations. Empirically, we have never seen any situations occur where two or more solutions were attained with the same source functions and boundary conditions. This is not a proof, but merely reflects a few years of experience with the code.

5. The boundary conditions prescribed at the first wall were typically n ~ 1.0 to 10^4 #/cm^3, T_e ~ .001 to 1 eV, T_i ~ .01 to 10 eV. The plasma profiles in the plasma core region and over most of the divertor region were not particularly sensitive to the exact values chosen for the boundary conditions at the wall as long as the plasma density remained low. By this one means that if the plasma density in the divertor zone were high (say ~ 10^{13} #/cm^3), then the plasma can more sensitively couple to the wall at least on a transient basis. If one specifies initial values with high plasma densities in the divertor zone, then one must be more careful in specifying the first wall boundary conditions. In addition, however, one would normally have to go to a finer spatial grid in order to represent the plasma behavior near the first wall. From a computational point of view, this can become prohibitively expensive. One can construct situations where the density in the divertor zone is high and, therefore, the boundary conditions that have been used here would be inappropriate. We have chosen not to consider those cases for two basic reasons. First, they can become computationally expensive, as was noted above; and, secondly, because we have taken very large separation distances between the separatrix and first wall so that physically one would not expect to have these "boundary sensitive" cases present.

Some thought has been given to the idea of actually flowing plasma along the field lines in the divertor zone from one collector chamber to another. This plasma flow may help the shielding

efficiency of the divertor and, in addition, cause an impurity flow reversal as postulated by Ohkawa.[6] Modeling this type of divertor plasma may require a closer look at the boundary condition sensitivities. This idea was not pursued in the work presented here.

6. In each case to be presented the particle and energy fluxes were matched at the separatrix surface. There are several ways in which this may be done. First, one may solve the matching condition at the separatrix, e.g.,

$$- D_C \frac{dn}{dr}\bigg|_{\substack{\text{core}\\\text{region}}} = - D_D \frac{dn}{dr}\bigg|_{\substack{\text{divertor}\\\text{region}}}$$

where D_C, D_D are the diffusion coefficients in the core region and divertor regions, respectively, and $\partial n/\partial r\big|_{\text{core}}$ is taken as a backward difference while $\partial n/\partial r\big|_{\text{divertor}}$ is replaced by a forward difference. There are similar conditions for $\tilde{Q}_e$ and $\tilde{Q}_i$. These equations are solved instead of the transport equations (Chapter V). A second method is to write a balance equation for the volume element about the separatrix node. One then obtains an equation for $\partial \bar{n}_s/\partial t$, for example, where $\bar{n}_s$ is a volume averaged density at the separatrix.[7] The third, and easiest, way to assure the fluxes match is to make sure the diffusion coefficients and thermal conductivities match at the separatrix. This was the method used in the work presented here. The diffusion process in the divertor zone was assumed to scale like Bohm ($\propto T_e$). The actual diffusion coefficient used for the divertor region was multiplied by a factor α_β This α_β factor was determined at each

time step so that the divertor region diffusion coefficient at the separatrix was equal to the diffusion coefficient in the plasma core region at the separatrix. This was also done for the thermal conductivities. The reasons for choosing this latter procedure are threefold. First, it is very easy to implement numerically. Secondly, the separatrix is in all probability not going to be a well defined position and thus there is no reason to believe that a sharp change in cross field diffusion coefficients is any more appropriate than a continuous change. Thirdly, one does not know the real diffusion properties in either zone well enough to believe there should be a discontinuity, i.e., the use of trapped particle mode scalings is only a guess in the first place!

7. In order to maintain the plasma density against both diffusional losses and fusion losses, fresh (cold) fuel ions were assumed deposited within the plasma volume with some assumed spatial profile $\propto(1-.5(r/a)^2)$. This profile may be assumed to come from pellet injection. Since the study of pellet injection is only in its infancy[8] one must take this injection profile as only a guess. As will be pointed out later, the behavior of the plasma is critically tied to this cold fuel ion source profile. This is a sad state of affairs since we know so little about how pellets will ablate on their way through a hot plasma. The entire question of pellet injection must be carefully studied and it has not been done to date.

8. In addition to "pellet" injection, which has been legislated to provide the central plasma core with fresh fuel, 10% of all the

plasma which is collected by the divertor is recycled to the plasma boundary as cold H_2 molecules. These H_2 molecules are modeled to be released from the first wall. As they proceed across the divertor zone, many ionize and then produce Franck-Condon neutrals. These neutrals are followed using the code described in Chapter V. The source function $n_e(r)n_0(r)\langle\sigma v\rangle_{iz}(r)$ is computed. For all three cases to be presented here, it was found that most of the neutrals get ionized near the separatrix surface. The preponderance of the charge exchange neutrals which are incident onto the first wall also originate near the separatrix and, therefore, the energy spectrum of these neutrals is characterized by the separatrix temperature.[9]

9. Sputtering of the first wall due to neutrons, plasma ions, and charge exchange neutrals was calculated using sputtering yield vs energy curves fit to recent experimental data.[9] The impurities (taken to be carbon for the three cases to be presented here) are assumed to come off the first wall isotropically with an energy of 20 eV. No data was found on the energy spectrum of sputtered carbon atoms when bombarded by (low energy) deuterons and tritons. Therefore, one has to look for information based on other types of materials and bombarding particles where these energy measurements were made. A personal assessment of several sources[10] seemed to indicate that the figure of 20 eV might be a reasonable (upper) value for the energy of the average particle sputtered off of the wall. In fact, if carbon undergoes mostly chemical sputtering, one would imagine the energy of the ejected atom to be down in the 1 eV range.

The sputtered carbon atom flux was then "followed" using the same type of neutral transport code as was described in Chapter V for the neutral fuel atoms. With this code, an impurity deposition profile was determined. This profile will be shown in the subsequent figures. A useful calculation, outlined in Appendix B, demonstrates that impurities ionized in the divertor zone will most probably be heated and leave along the field lines rather than diffuse across the field lines into the plasma core region. Obviously, if the divertor particle collectors cannot trap these impurities, they will return to the plasma edge and must in a steady state raise the concentration of impurities in the plasma core region. Methods for assuring that high Z materials are trapped in the divertor collection chamber are now under development.[11] The effects of the deposited impurities on the plasma energy balance were not assessed in this study. The reason for the neglect was that the primary direction of the research presented here was to ascertain what properties were peculiar to divertors and how can they be modeled into a 1-D transport code. The whole impurity problem, which would involve a multispecies generalization of the divertor region equations, was deemed to be the next logical extension of the research presented here, and is so outlined in Chapter VII. Impurity effects are very important and must be incorporated for a complete analysis. This work is only now beginning.

10. Another pecularity of the computer model used here is how the synchrotron radiation loss is handled. The formula used was one developed by Yang[12] amd based on some of Trubnikov's work.[13]

It includes the effect of relativistic broadening and the presence of a 1/R toroidal field. The equation (5.12e) is only strictly valid when multiplied by the plasma volume and used as a total power loss. As one knows, it is difficult to treat exactly the energy (photon) transport problem in a nonlinear medium such as a plasma in a convenient (economical) fashion. The formulation of Yang does agree with more exact calculations[14] in terms of total power loss from the plasma volume, but, of course, it may not appropriately reflect the local net energy loss from any given volume element. The one qualitative effect that would be expected from an exact treatment would be a flattening of the plasma temperature profile. A method outlined by Clarke[15] and soon to be implemented by Mense will investigate the validity of this conjecture. In the meantime, there is but one saving grace about the inexact treatment of the synchrotron radiation and that is that it is negligible compared to the other energy loss channels (such as thermal conductance) for temperatures of reactor interest—particularly when one assumes trapped particle mode transport coefficients.

With the above factors in mind, we can proceed to describe the specific reactor designs to which the divertor transport model was applied.

Case I: UWMAK-II

The UWMAK-II conceptual tokamak reactor design was undertaken at the University of Wisconsin for the sole purpose of assessing potential problem areas in the road toward the technological development

of fusion power. The details of the design are to be found elsewhere[16] but a number of its plasma characteristics are reproduced from the UWMAK-II report in Figs. VI-1 and VI-2. The UWMAK-II design assumed the presence of a poloidal field divertor, but at the time of the issuance of that report the research reported herein had not been completed and so the report was incomplete. This will now be corrected.

The description of the equations which were solved was given in Chapter V and only certain details (and pecularities) involved in finding the solution remain along with, of course, a presentation of the findings. In order to understand the findings without the need to continually turn back to previous chapters, some of the previously presented information will be represented in the course of describing the solution.

The points which remain to be addressed in order to complete the calculational model for UWMAK-II are: 1) How was scrape-off zone thickness (separatrix-to-first wall) chosen?; 2) Was there a sensitivity in the numerical solution method to the initial conditions; if so how was it solved?

After a discussion of the above points, the results, given conveniently in graphical form, will be discussed including which "factors" were assessed to be the most critical in terms of determining whether or not one had an ignited (self-sustaining) fusion discharge. The answer, as will be seen, is not obvious, or at least was not so to the author!

Plasma Operating Parameters for UWMAK-II*

Based on a Point Reactor Model

Plasma Current, I	14.9 MA
Electron Poloidal Beta, β_θ^e	1.22
Total Poloidal Beta, β_θ	2.275
Total Toroidal Beta, β_ϕ	0.064
Stability Factor, q(a)	2.3
Plasma Radius, a	5 m
Major Radius, R_0	13 m
Axial Toroidal Magnetic Field, B_T°	3.57 T
Plasma Volume	6415 m^3
Energy Content of Plasma	2.95 GJ
Ion Temperature, T_i	13.2 keV
Electron Temperature, T_e	12.0 keV
Electron Density, n_e	$7.71 \times 10^{13}/cm^3$
Ion Density, n_{D+T}	$7.33 \times 10^{13}/cm^3$
Alpha Density, n_α	$1.87 \times 10^{12}/cm^3$
Particle Confinement Time,* τ_p	8.28 s
Energy Confinement Time,* τ_E	3.64 s
$n_e \tau_E$	2.8×10^{14} s-cm^{-3}
Fractional Burnup, f_b	4.85%

*Based on trapped particle mode estimates of the diffusion coefficient and thermal conductivity.

Figure VI-1

Power Parameters for UWMAK-II

Total energy per fusion	21.56 MeV
Thermal power during plasma burn	5000 MW(th)
Average power density in plasma	0.78 MW/m^3
14 MeV neutron wall loading	1.16 MW/m^2
Surface heat loading	0.0367 MW/m^2
Power to divertor	713 MW

Fueling Parameters for UWMAK-II

Tritium consumption rate	0.624 kg/d
Deuterium consumption rate	0.416 kg/d
Particle leakage rate (D + T + α)	5.82 x 10^{22}/s
Fueling rates	
Tritium	12.85 kg/d
Deuterium	8.57 kg/d

Figure VI-2

The criteria for determining how far the first wall should be spaced from the separatrix surface was based upon the maximum drift (banana) orbit of a 3.5 MeV (Z = 2) alpha particle which was started at the separatrix. In UWMAK-II, with the external coil/current arrangement as outlined in the UWMAK-II report, the maximum banana orbit of an alpha in the divertor zone was found to be $\simeq$ 50 cm. This was determined numerically by integrating the guiding center equations of motion of a 3.5 MeV alpha for many different initial velocity vectors measured with respect to the field lines. The scrape-off distance, determined in this manner, is probably an upper limit due to the fact that essentially all of the alpha particles in UWMAK-II* are born inside .4 of the plasma radius and, therefore, will probably slow down before they diffuse out.[17]

With a 50 cm scrape-off zone, the density in the divertor zone was seen to exponentiate down (see Fig. VI-3) to very low values before the first wall is encountered. This validates the use of a fixed (low) density b.c. at the wall. In fact, it was found that if the density was arbitrarily set at a higher value at the wall (say $n \simeq 10^{10}$ or 10^{11}) that a dip in the density was found in the divertor zone, i.e., the wall would be taken as a source of plasma which, of course, it is not—it is a source of neutrals.

*The exception being those born near the edge due to beam plasma fusions during the heating phase of the start-up cycle.

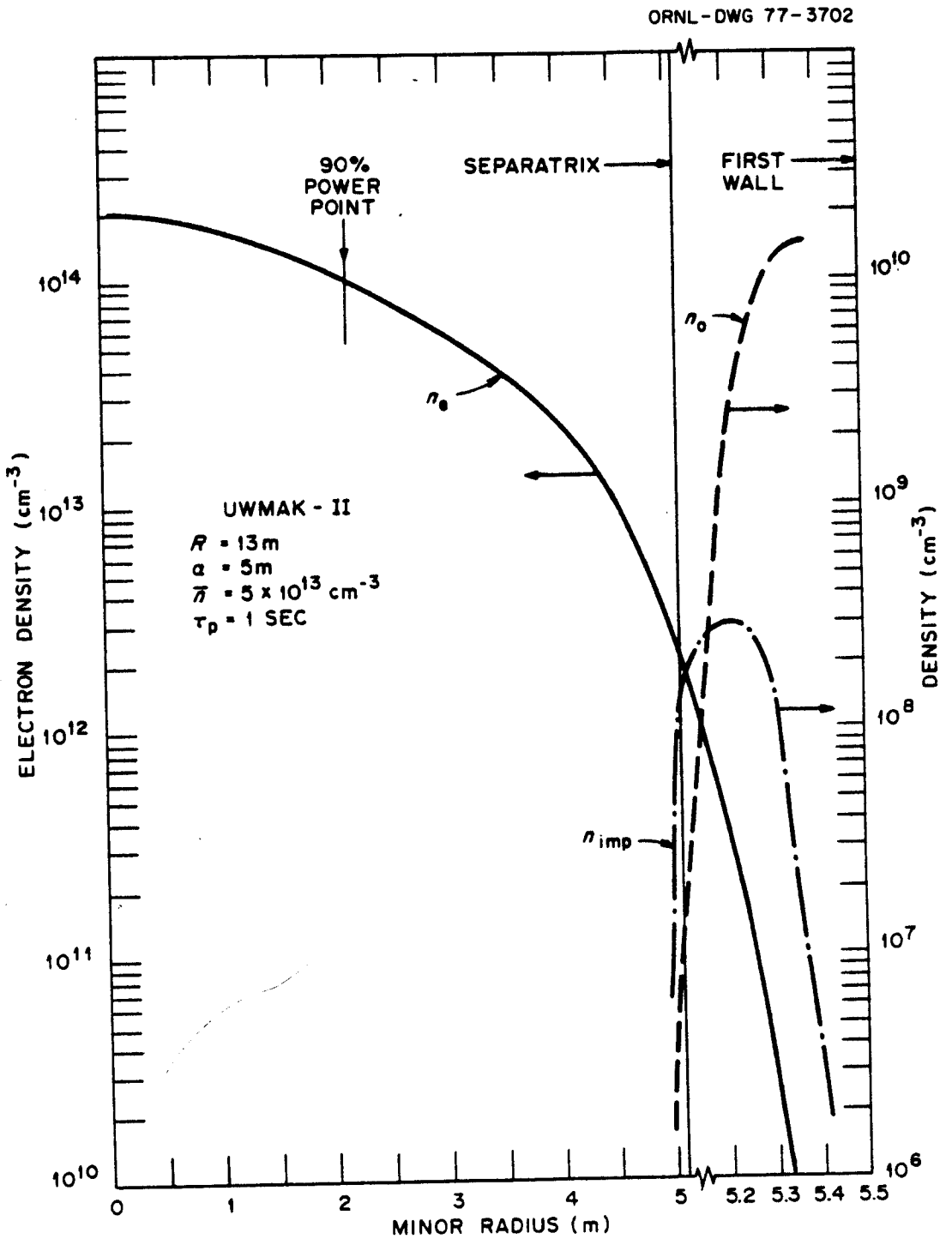
ORNL-DWG 77-3702
90% POWER POINT
SEPARATRIX
FIRST WALL
UWMAK - II
R = 13m
a = 5m
n̄ = 5 x 10^13 cm^-3
τp = 1 SEC
n_e
n_o
n_imp
ELECTRON DENSITY (cm^-3)
DENSITY (cm^-3)
MINOR RADIUS (m)
10^14
10^13
10^12
10^11
10^10
10^10
10^9
10^8
10^7
10^6
0
1
2
3
4
5
5.2
5.3
5.4
5.5

Figure VI-3

In numerically treating the UWMAK-II case, many different initial conditions (i.e., profiles for n(r), $T_e(r)$, $T_i(r)$, B(r), etc.) were tried. Most profiles, if they differed considerably (particularly in the divertor zone) from those shown in Figs. VI-3 and VI-5, required taking very small time steps ($\Delta t \leq 10^{-6}$ seconds) in order to maintain physically meaningful values for the variables n, T_e, and T_i. If too large a time step was taken, the electron temperature, for example, might go negative which is unallowable since we have terms such as Bremsstrahlung radiation ($\propto T_e^{1/2}$) to compute. The size of the time steps for the calculation were dictated by the divertor zone physics—which is very much a "tail-wagging-the-dog" kind of problem. No easy way of working around this problem was discovered except to continually readjust the initial conditions at each spatial location (for each of the variables) in the direction which the time derivatives seemed to indicate they wanted to go. This was both laborious and uninteresting to perform, particularly since it could not for economic reasons be done on a real time basis with the computer directly linked into the teletype! A possible solution to this problem may be not to use the Crank-Nicholson differencing algorithm, but use instead a more implicit method.[18]

Another numerical complication arose which deserves attention. This involved the fact that the transport coefficients due to the trapped particle modes depend explicitly on density gradients and sometimes temperature gradients. Having $D \propto (\nabla n)^{\alpha}$ can produce oscillations in the density and temperatures under some circumstances. When

∇n changes sign, the trapped particle modes are stabilized and some "other" diffusion process must be dominant. Depending on what one chooses this "other" process to be, there can be reasonably large changes in the diffusion properties from one spacial node to another. This tends to readjust ∇n and once again the assumed trapped particle modes control the diffusion. This type of behavior can cause havoc in finding a suitable automatic time stepping algorithm. Houlberg[19] has been looking into this effect in more detail in order to ascertain whether the oscillations occur due to the ∇n dependence in D, χ_e, etc. or whether it is due to the numerical solution technique (see Chapter V). The problem was dealt with here by smoothing the oscillations when they occurred. Once the plasma settled down close to its equilibrium, the oscillations never reappeared.

With the above notes well in mind, a description of the results can now be given. First, with reference to Fig. VI-3 we can see a density fall off from plasma center to separatrix of approximately 10^2. Half of this occurs in the outer .4 of the plasma core region. This drop is due to the fact that the divertor lowers the density and since no strong mechanism is provided for pulling the temperatures down near the separatrix, the trapped ion mode is prevalent in this region of the plasma. The net effect is a very large particle loss rate from the edge which must, of course, be balanced by an equally high fueling rate in that region. If the cold fuel ion (pellet) deposition profile were flat or peaked toward the outside, one could build up the edge density and in addition reduce the particle loss

rate due to the fact that $D \propto 1/n^3$ for the trapped ion mode (see Appendix A). With the pellet deposition profile $\propto (1-.5(r/a)^2)$ and with only 10% plasma recycling from the divertor, one will always see this large density drop. The particle confinement time for the 5 meter minor radius reactor was .74 seconds where τ_p is defined through the formula

$$\frac{\bar{n}V_c}{\tau_p} \equiv \oint_{\text{separatrix}} \Gamma \cdot dA = \Gamma(a)\, 2\pi a\, 2\pi R_0 \qquad (6.1)$$

where $V_c = (\pi a^2)(2\pi R_0)$ and $\bar{n}$ = average plasma density in core region. The confinement time for plasma in the center was, of course, longer, but since plasma crossing the separatrix leaves mostly along the field lines, the τ_p calculated from (6.1) is the correct one to use in estimating the required pumping speeds in the particle collection chambers. Note: present day tokamaks also have short τ_p values as defined by (6.1). The plasma which leaves is replenished by cold neutrals coming off the walls and limiter. Often experimental quotations of τ_p are central particle confinement times, ususally defined as $(n_0(0)\langle\sigma v\rangle_{iz}(0))^{-1}$ where n_0 = neutral density at the center of the plasma (r = 0).

Also shown in Fig. VI-3 are the neutral density and impurity (carbon) deposition profiles. As can plainly be seen, $n_e n_0 \langle\sigma v\rangle_{iz}$ will peak in the divertor zone for both hydrogen neutrals and carbon atoms. This indicates two things. First, UWMAK-II does appear to shield the central plasma core region from impurities, and,second, it also tends to shield the core from fuel atoms so that "edge"

fueling appears difficult and probably only pellet fueling can be used. However, before a definitive answer can be made on the viability of edge fueling, one must investigate much more carefully how exactly neutrals enter the plasma, i.e., wall reflection of cx neutrals may allow somewhat deeper penetration. Also ionization and charge exchange data for hydrogen is probably not known to within 20% or 30% and, therefore, could make a difference.

The 90% power point shown in both Figs. VI-3 and VI-4 indicate that 90% of the fusion power produced by the reactor is done so in the volume enclosed by the radius to that point, i.e., $r_{90\%} \simeq 205$ cm for UWMAK-II. From Fig. VI-4 one can see, as expected, that 90% of the alphas are born within this radius also. The code assumes that these alphas thermalize immediately and the division of the alpha energy between the ions and electrons is computed and used as source terms. No alpha drift orbit averaging is done to account for energy deposition in locations other than the radius at which the alpha was born. This is probably not too bad for a high density ($n \sim 10^{14}$ #/cm^3) large radius plasma such as UWMAK-II. Also the energy partition was calculated using classical rates[20] and no anomalous slowing down processes were accounted for in the distribution of the energy between electrons and ions. From a surface and materials point of view this implies that alphas diffusing into the scrape-off zone are at the ion temperature at the separatrix.

Figure VI-5 also shows the electron and ion temperatures in the core and divertor regions. As can be seen, $T_e \simeq T_i$ (due to the high

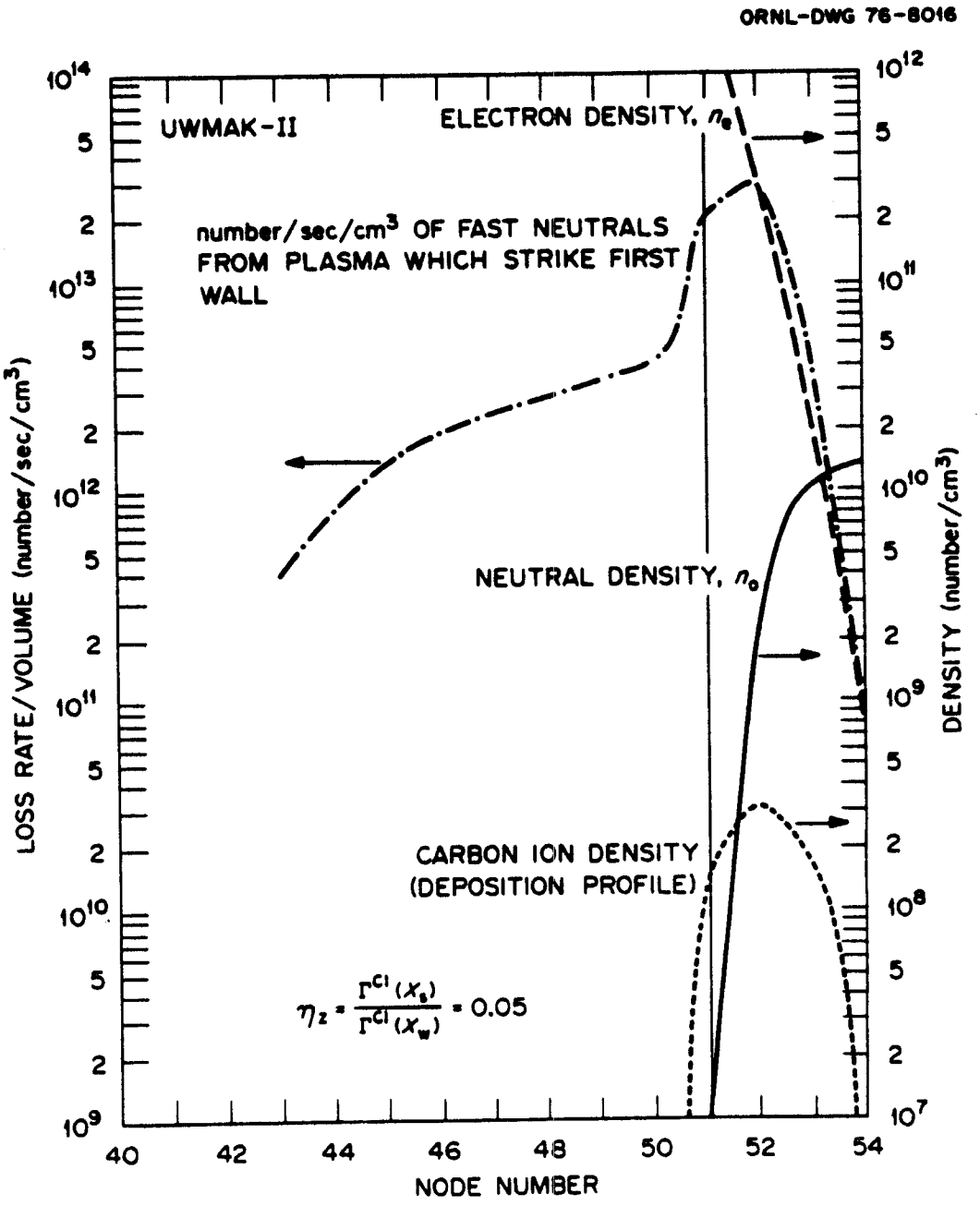
ORNL-DWG 76-8016
UWMAK-II
ELECTRON DENSITY, n_e
number/sec/cm^3 OF FAST NEUTRALS FROM PLASMA WHICH STRIKE FIRST WALL
NEUTRAL DENSITY, n_o
CARBON ION DENSITY (DEPOSITION PROFILE)
$\eta_z = \frac{\Gamma^{CI}(x_s)}{\Gamma^{CI}(x_w)} = 0.05$
LOSS RATE/VOLUME (number/sec/cm^3)
DENSITY (number/cm^3)
NODE NUMBER
40
42
44
46
48
50
52
54

Figure VI-4

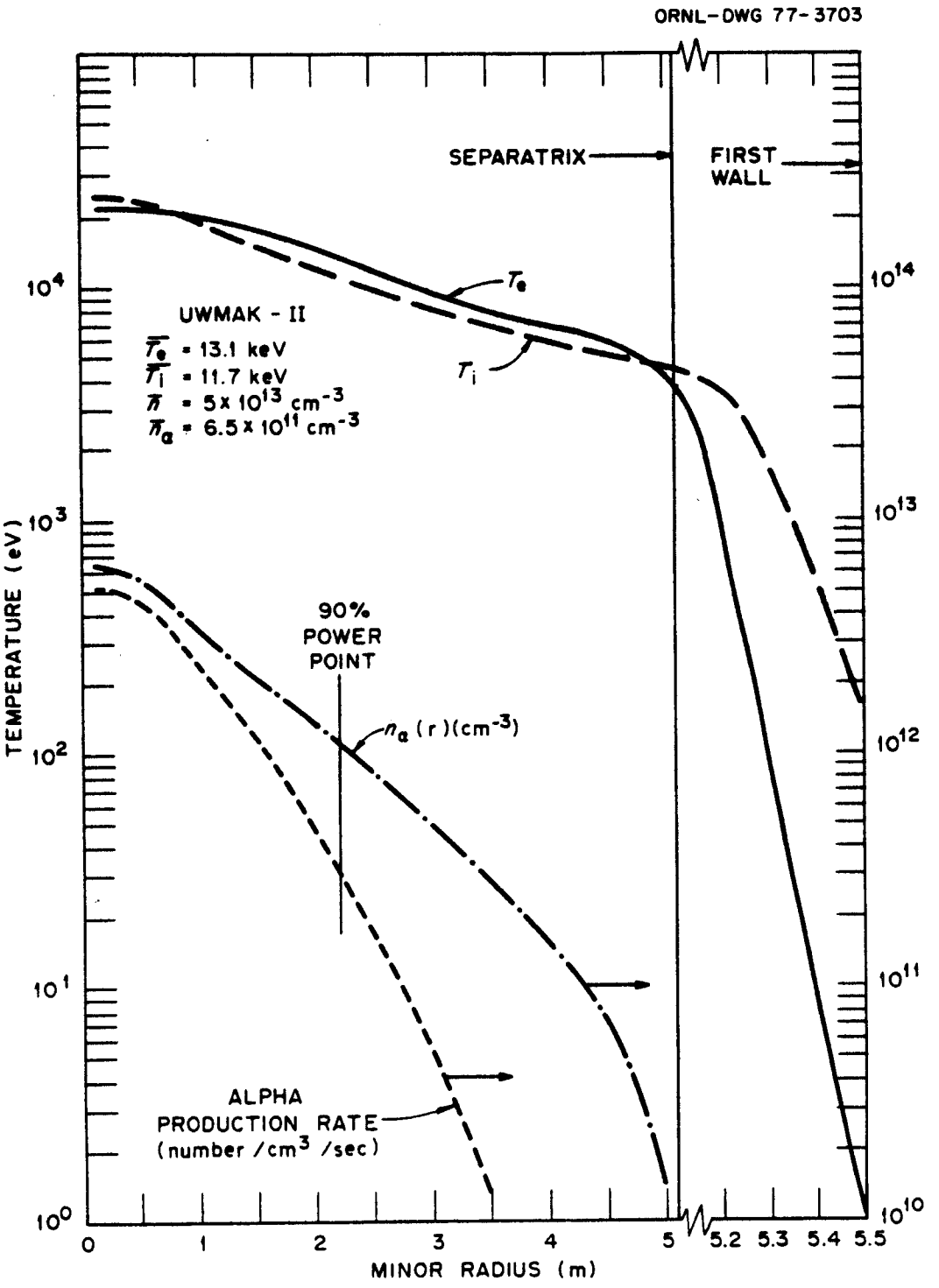
ORNL-DWG 77-3703
SEPARATRIX
FIRST WALL
UWMAK - II
$\bar{T}_e$ = 13.1 keV
$\bar{T}_i$ = 11.7 keV
$\bar{n}$ = 5 x 10^13 cm^-3
$\bar{n}_\alpha$ = 6.5 x 10^11 cm^-3
T_e
T_i
90% POWER POINT
n_α (r) (cm^-3)
ALPHA PRODUCTION RATE (number /cm^3 /sec)
TEMPERATURE (eV)
MINOR RADIUS (m)

Figure VI-5

densities) over most of the core region. As no impurities were assumed present, the radiation losses, which usually are responsible for most of the electron temperature degradation near the plasma edge in present day devices, were negligible and as a consequence the edge temperature remains reasonably high. The primary cooling effects are: 1) thermal conduction across the separatrix to the cooler divertor electrons,* and 2) the requirement to heat the electrons and ions which are produced due to the pellet source. The difference, $T_e - T_i$, in the divertor zone is due to both the sheath electron cooling effect at the collector plates and the low density which reduces the electron-ion collisional equilibration rate. One might suspect that anamalous mechanisms may be present in the divertor zone to enhance the equilibration process, but none were assumed for the work presented here. This problem constitutes a further area of study in divertor zone physics.

The characteristics of the divertor zone itself are quite striking. For example, the density drops from 2×10^{12} #/cm^3 at the separatrix to 2×10^{11} in roughly 15 cm and would have dropped even faster had we not recycled some of the plasma as cold neutral gas coming off of the first wall. This will be seen more explicitly in the UWMAK-III figures. The electron temperature ten-folds down from the separatrix value also in about 10 to 15 cm while T_i does so in 30

*Remember from Chapter V that the electrons cool quickly due to the electrostatic sheath at the collectors.

to 35 cm. The ions, of course, cool only by effusion cooling—the hottest leave the quickest.

The edge (separatrix) density is rather low (5×10^{12} #/cm^3). This is due to the fact that in our model the trapped ion mode predominates over most of this region. This can be seen (see Appendix A) by noting that $D_{TI} \propto T_e^{7/2} (\nabla n)^2/n^3$ and even though T_e drops, it does not come down by enough to beat the $1/n^3$ dependence. The only factors that prevent the density from being eaten away further are: 1) the density gradient begins to flatten, and 2) the cold fuel (pellet) source $\propto(1-.5(r/a)^2)$. How then does the profile evolve from its initial condition to the equilibrium state as shown in Figs. VI-3–5? An answer to this question is shown in Fig. VI-6 which shows how the plasma density evolved from its initial conditions in a time span of 338 msec. The important point to note is that the profile shape changes first and then once the "fundamental spatial eigenmode" is found, the whole profile adjusts up or down to agree with the source rates. Since the equations are nonlinear, one can only use the words "eigenmode" in the broadest of terms because the shape of the profile does change somewhat depending on the overall density due to the density dependence of the transport coefficients. The behavior shown in Fig. VI-6 for the density also applies to the temperature profiles, but is not quite so severe since T_e and T_i only drop by 10 from center to edge, while n changes by 10^2.

The basic characteristics constituting the numerical modeling of the plasma behavior in UWMAK-II have now been given. The plasma

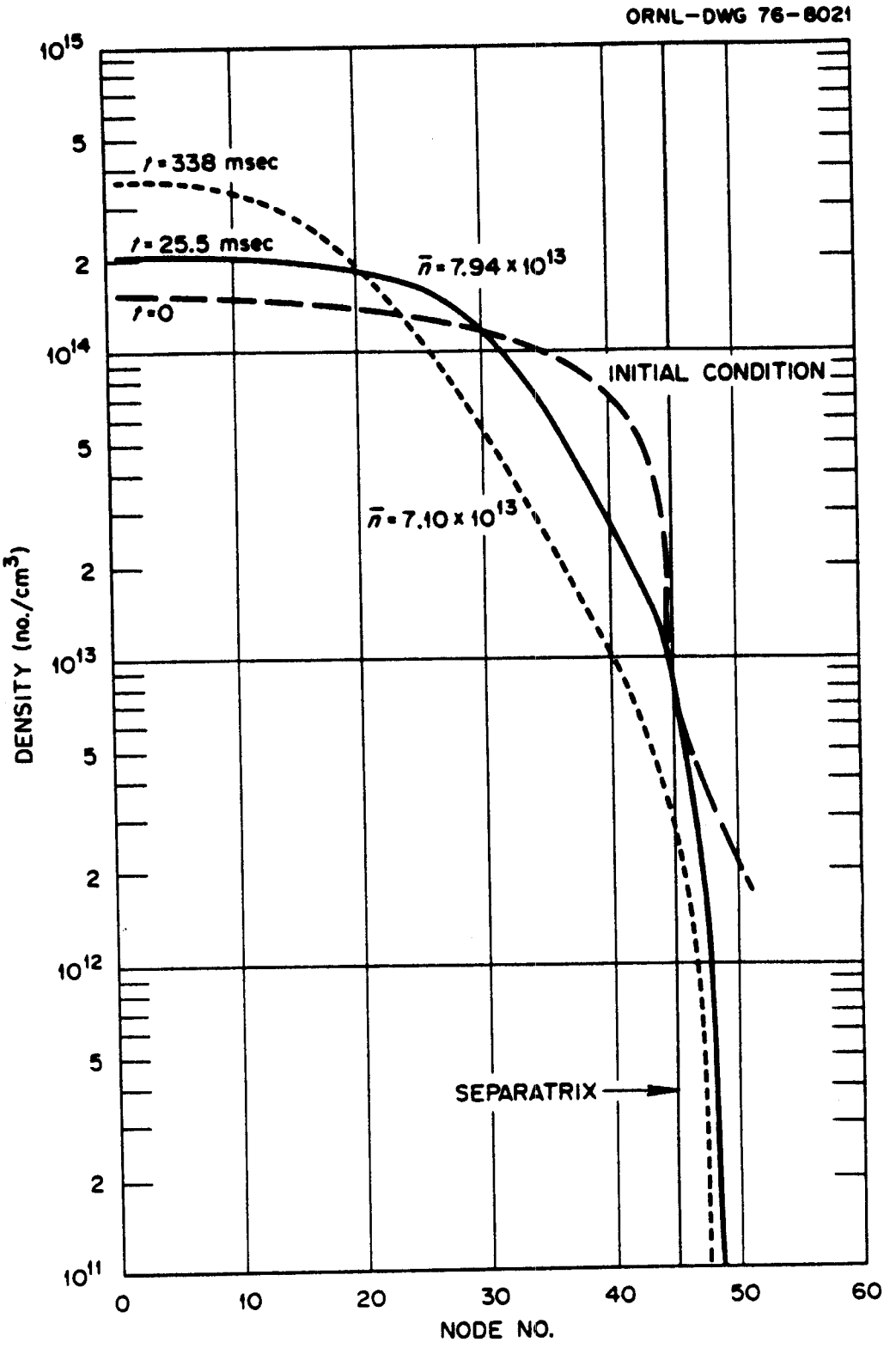
ORNL-DWG 76-8021
DENSITY (no./cm³)
NODE NO.
t = 338 msec
t = 25.5 msec
t = 0
n̄ = 7.94 x 10¹³
n̄ = 7.10 x 10¹³
INITIAL CONDITION
SEPARATRIX

Figure VI-6

characteristics which resulted from the model have also been described and displayed graphically. In addition, a typical temporal evolution of one of the plasma variables (i.e., density) was detailed in order to demonstrate that the "normal mode" type of profile behavior can be expected even though the problem is inherently nonlinear.

Before moving on to UWMAK-III, there are a couple of points, alluded to earlier, which must be discussed. These points have to do with the tokamak physics which seem to most sensitively affect the plasma operation. To begin this discussion, let us start with a short discourse on the transport coefficients which were assumed.

The transport coefficients (see Appendix A) were chosen to reflect the energy and particle loss rates due to theoretically predicted microinstability modes. The existence of these modes has never been conclusively demonstrated in any of the present day fusion devices. Thus, they are a guess. Why guess these particular modes? The main reason is to test for profile effects (i.e., shapes) which might allow us to verify the presence of these instabilities in the tokamaks themselves. Secondly, the theoretical predictions indicate pessimistically high transport scalings and one wishes to know whether or not one has a chance to have a fusion power reactor in the presence of such scaling laws. One can numerically experiment with different heating and fueling profiles to see if the loss rates due to these modes can be (theoretically) reduced. We do much the same thing when

we take neoclassical transport coefficients* so there is nothing wrong with doing so using other types of scaling laws. Thirdly, the trapped particle scaling laws are easily referenceable (WASH-1295) and one can, therefore, more easily compare results from one person's transport code to another's.

It should be emphasized, however, that there is nothing sacred about the values for the diffusion coefficients in WASH-1295. They have usually been determined from a quasilinear theory where a guess had to be made at some point as to how much energy was present in the modes. At this point in time, a guess is all that there is, so the values in WASH-1295 could easily be factors of 10 to 100 too large or they could be "exactly" as quoted. No one yet knows. In any case, we have assumed the full values as quoted in WASH-1295 and when one does this, several startling factors appear.

1. With trapped particle mode scaling, the edge (separatrix) temperature and density can affect the central plasma properties.

2. When a divertor is present at the plasma edge the density can be held quite low ($< 10^{13}$) unless a large pellet source or large neutral recycling from the divertor chamber is implemented. A low edge density encourages the trapped particle modes to develop and decreases the particle and energy confinement time. Unless one can bring the

*There is no evidence that present day reactors behave neoclassically either. ORMAK does lend itself to being modeled using neoclassical ion thermal conductivity, but χ_e and D are not neoclassical.[21]

edge temperatures down or raise the edge density in order to increase the collisionality, most of the plasma edge would be under the influence of the trapped ion mode in a UWMAK-II type of device.

3. In connection with what was said above, the plasma source rate inside the core region has been found to be a critical factor in determining the transport processes. The reasons are obvious. First, it is the primary mechanism for keeping temperature down in the absence of radiative processes and, secondly, by affecting the density and temperature, one can affect the transport coefficients, which in turn determine the particle and energy confinement times, which in turn determine whether or not one can have a "steady state," ignited fusion reactor.

Having made the above points based on observations of UWMAK-II modeling, we can now look at UWMAK-III and compare the differences.

Case II: UWMAK-III

When the UWMAK-II reactor design was complete, an assessment was made as to whether or not one would really want to try and build such a large device. The answer which resulted was no. The reasons are obvious: 1) it is a low β device and, therefore, has a low energy density; and 2) due to this low β, it is physically large and, therefore, requires large materials costs. To try and reduce the nuclear island portion of a fusion power plant cost, it was deemed adivsable to try to go to a physically smaller system. This was done in UWMAK-III and its details are reported elsewhere.[22] A unique

feature in UWMAK-III was an attempt to try to place the divertor particle collection chambers outside the toroidal field coils. This allowed the TF coils to be physically smaller and, of course, lowered the magnetic field energy density and, therefore, cost of the system. A copy of the relevant section of the UWMAK-III report is reproduced as Appendix C. Figures VI-7, 8, and 9 describe the essential characteristics of UWMAK-III as reported.[22] Again, however, the divertor research reported herein had not been completed at the time of issuance of the UWMAK-III report. Thus, the divertor characteristics quoted do not exactly agree with those to be presented here. For the UWMAK-III report, approximate boundary conditions were applied at the plasma edge to simulate the divertor's presence. The conditions were in the nature of gradient conditions, i.e.,

$$\frac{1}{n}\frac{dn}{dr} = -\frac{1}{\Delta_n}\,,\ \frac{1}{T_e}\frac{dT_e}{dr} = -\frac{1}{\Delta_e}\,,\ \frac{1}{T_i}\frac{dT_i}{dr} = -\frac{1}{\Delta_i}$$

These kinds of conditions, of course, are valid only when the plasma is in a steady state, i.e., the values one uses for Δ_n, Δ_e, and Δ_i all would change as a function of time as the discharge evolves. The reader is referred to the UWMAK-III report for further details.

Figures VI-7 amd VI-8 contain data on UWMAK-III extracted from the report. An important point to notice is that analysis of the reactor's (equilibrium) operating point was carried out using a

Plasma Parameters for UWMAK-III*

	Space-Time	Point Model
Mean ion temperature (keV)	11.4	18.4
Mean electron temperature (keV)	11.9	22.9
Mean ion density (cm^{-3})	7.9×10^{13}	6.46×10^{13}
Mean electron density (cm^{-3})	8.1×10^{13}	6.86×10^{13}
Mean alpha density	8.8×10^{11}	1.9×10^{12}
Plasma current (MA)	15.6	15.7
Stability factor at plasma edge, q(a)	2.7	2.69
Plasma width (m)	2.7	2.7
Plasma height (m)	5.4	5.4
Radius of equivalent volume circular plasma (m)	3.83	---
Major radius (m)	8.1	8.1
Axial toroidal magnetic field (kG)	40	40
Plasma volume (m^3)	2370	2360
Electron poloidal beta, β_θ^e	0.69	1.05
Total poloidal beta, β_θ	1.65	2.3
Total toroidal beta, β_Φ	.058	.083
Energy content of plasma (GJ)	1.32	1.63
Wall surface area (m^2)	1600	1600
Particle confinement time (sec)	0.547	3.33
Energy confinement time (sec)	1.64	1.66
$\bar{n}_e \tau_E$	1.33×10^{14}	1.14×10^{14}
Fractional burnup, f_b	0.83%	5.9%
Voltage around torus (volts)	0.059	---

*As taken from Ref. [22].

Figure VI-7

Power Parameters*

Energy per Fusion (MeV)	21.7
Thermal Power During Burn (MW)	5000
Average Power Density in Plasma (MW/m^3)	1.72
14 MeV Neutron Production Rate (sec^{-1})	1.44×10^{21}
Power to Wall (MW)	71.3
Radiation (MW)	63.2
Particles (MW)	8.1
Surface Wall Loading (MW/m^2)	0.44
Power to Divertor (MW)	725

Fueling Parameters

Tritium (Deuterium) Consumption Rate	1.94×10^{21}/sec
Tritium Burnup Rate	.62 kg/day
Deuterium Burnup Rate	.413 kg/day
Particle Leakage Rate ($D + T + \alpha$)	3.44×10^{23}/sec
Fueling Rate	
Deuterium	49.8 kg/day
Tritium	74.7 kg/day

*As taken from Ref. [22].

Figure VI-8

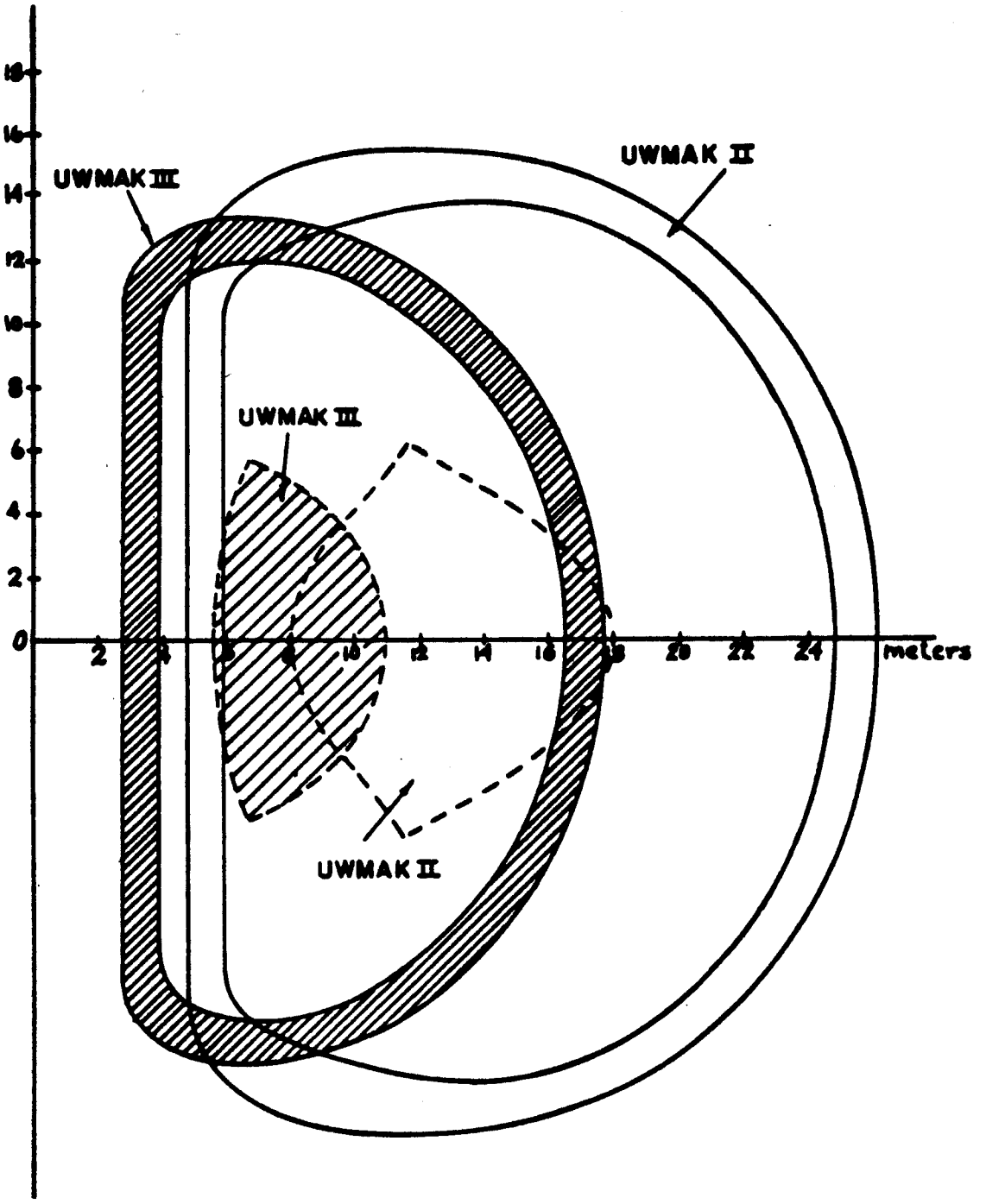
UWMAK III
UWMAK II
UWMAK III
UWMAK II
0
2
4
6
8
10
12
14
16
18
20
22
24
meters

Figure VI-9

"point" code* and a 1-D code. As can be seen, there are marked differences particularly between the particle confinement times and the average temperatures. The reasons for these differences have mainly to do with what assumptions were made (or implicitly made) in the derivation of the point model. The details of how this was done and where exactly the discrepancies lie will be discussed after the 1-D results are reviewed.

Looking at Fig. VI-10 we see the density appears very much like UWMAK-II. The minor radius of the reactor is smaller in UWMAK-III and, therefore, in order to achieve the same thermal output, we had to go to higher densities. Higher densities and smaller size imply a larger density gradient and, in fact, the particle confinement time for UWMAK-III was .4 seconds as taken from my analysis which is shorter by almost a factor of two from that of UWMAK-II. Figure VI-11 shows the temperatures and again nothing significantly different occurs here from what was seen in UWMAK-II. In fact, all the profiles appear qualitatively the same.

The first wall was set closer to the separatrix ($r_w - r_s \simeq 30$ cm) than in UWMAK-II, but 30 cm was still adequate to allow the density to e-fold down enough to "decouple" the wall from the plasma. The point illustrated in the UWMAK-III drawings is the net effect of the 10% recycling of plasma (collected in the divertor) back as neutrals. As

*A point code or point reactor model is one where the spatial profile dependence of the transport equation has been integrated out usually by assuming some spatial profile for n, T_e, T_i, etc.

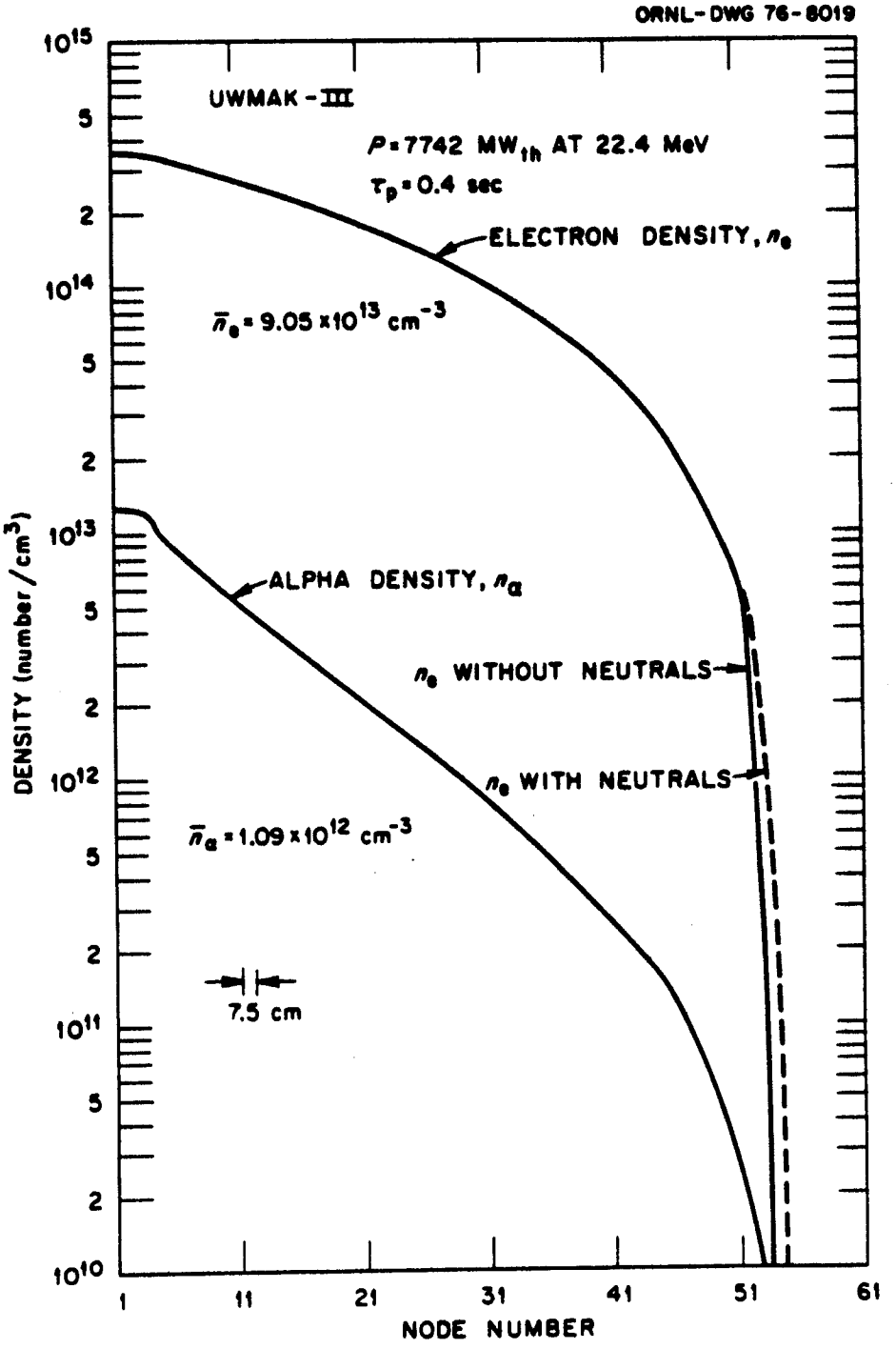
ORNL-DWG 76-8019
UWMAK-III
P = 7742 MW$_{th}$ AT 22.4 MeV
τ_p = 0.4 sec
ELECTRON DENSITY, n_e
$\bar{n}_e$ = 9.05 x 10^{13} cm^{-3}
ALPHA DENSITY, n_α
n_e WITHOUT NEUTRALS
n_e WITH NEUTRALS
$\bar{n}_\alpha$ = 1.09 x 10^{12} cm^{-3}
7.5 cm
DENSITY (number/cm^3)
NODE NUMBER
10^{15}
5
2
10^{14}
5
2
10^{13}
5
2
10^{12}
5
2
10^{11}
5
2
10^{10}
1
11
21
31
41
51
61

Figure VI-10

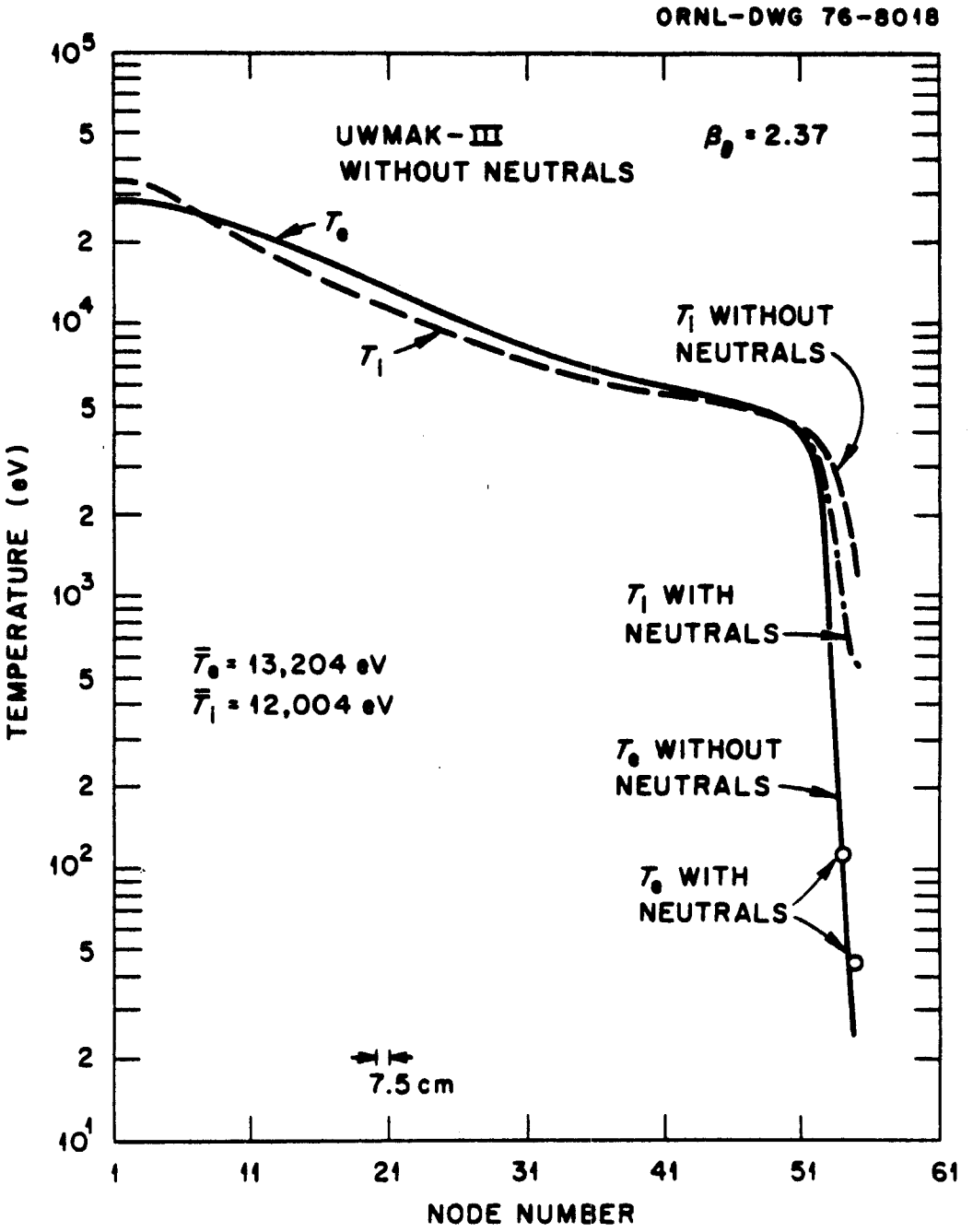
ORNL-DWG 76-8018
UWMAK-III
WITHOUT NEUTRALS
β_θ = 2.37
T_e
T_i
T_i WITHOUT NEUTRALS
T_i WITH NEUTRALS
T_e WITHOUT NEUTRALS
T_e WITH NEUTRALS
$\bar{T}_e$ = 13,204 eV
$\bar{T}_i$ = 12,004 eV
7.5 cm
TEMPERATURE (eV)
NODE NUMBER
10^5
5
2
10^4
5
2
10^3
5
2
10^2
5
2
10^1
1
11
21
31
41
51
61

Figure VI-11

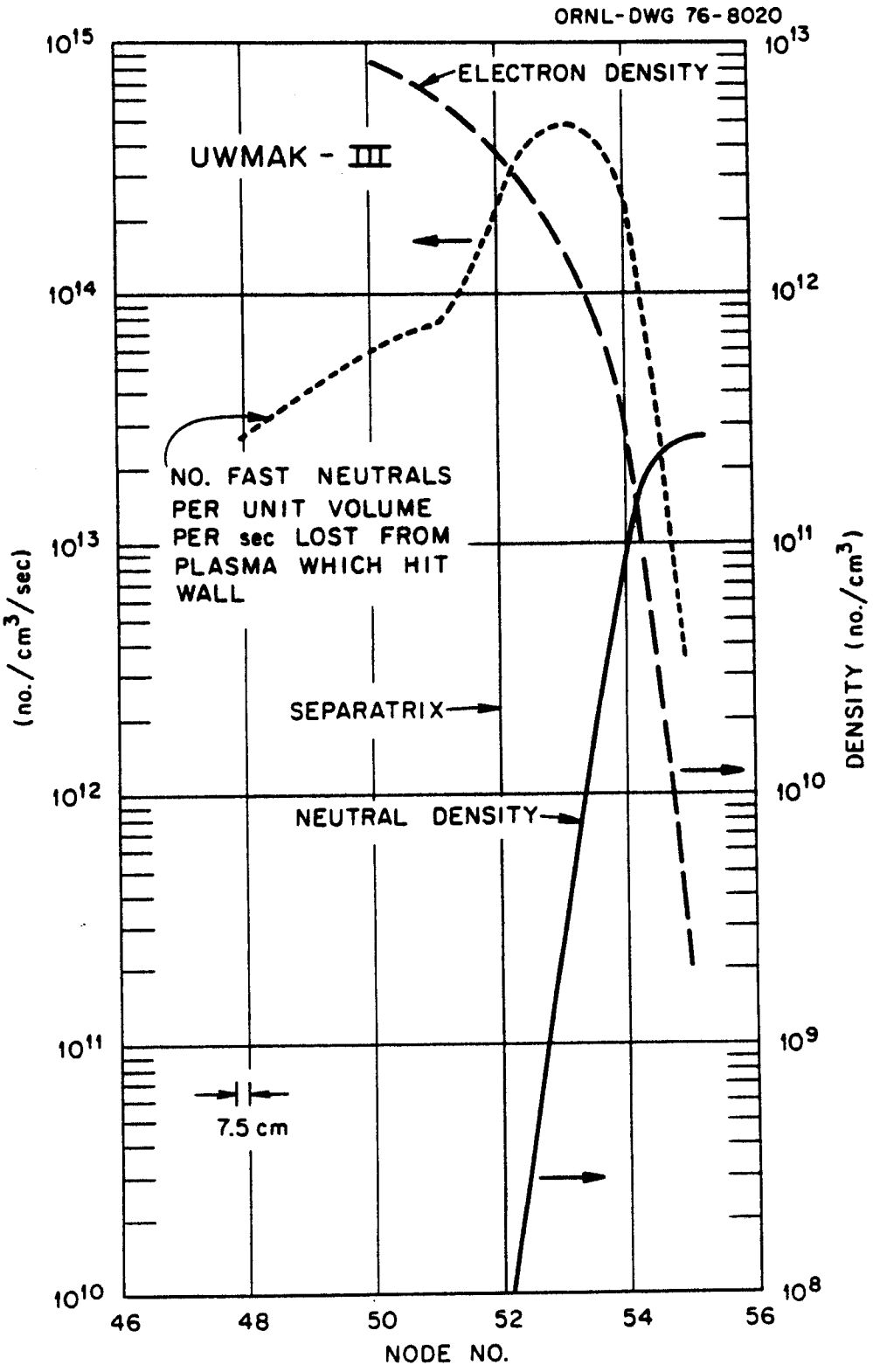
ORNL-DWG 76-8020
UWMAK - III
ELECTRON DENSITY
NO. FAST NEUTRALS PER UNIT VOLUME PER sec LOST FROM PLASMA WHICH HIT WALL
SEPARATRIX
NEUTRAL DENSITY
7.5 cm
(no./cm³/sec)
DENSITY (no./cm³)
NODE NO.
10¹⁵
10¹⁴
10¹³
10¹²
10¹¹
10¹⁰
10¹³
10¹²
10¹¹
10¹⁰
10⁹
10⁸
46
48
50
52
54
56

Figure VI-12

can be seen in Fig. VI-10, the divertor zone seems to "screen" the hydrogen neutrals very effectively so that the net effect is an increased divertor zone density without a noticeable increase in plasma core density.* The temperature decrease due to the neutrals is most pronounced in the ion temperature in the divertor zone. This ion temperature degradation is due to charge exchange. A smaller degradation may occur if one incorporated a wall reflection model for the neutrals,[23] but this was not done in the analysis presented here.

Again, as in UWMAK-II, the plasma "equilibrium" was sensitive to both the divertor (which wants to keep the separatrix density low) and to the cold pellet fueling rate. In fact, the plasma size (i.e., minor radius) also was a sensitive factor. When the minor radius was taken to be much smaller than 3.8 meters we were unable to find a steady state ignited plasma. It must be noted, however, that if we had assumed that the transport coefficients were smaller than those in WASH-1295, then we could have found an ignited plasma of smaller size. In fact, asking by what fraction must one multiply the transport coefficients (due to trapped particle modes as quoted in WASH-1295) in order to have an ignited reactor of a given size is an equally valid way of approaching the problem. We merely chose instead to see how small a device one could make under the influence of the

*Obviously, if the divertor will screen hydrogen, it will also screen carbon and iron too!

exact scalings reported in WASH-1295 even though, as we have said before, it is doubtful that these coefficients are valid quantitatively to within a factor of 10 to 100.

Case III: Experimental Power Reactor

An experimental power reactor (EPR) is supposed to be the fusion device immediately preceeding a full-scale demonstration plant. Several conceptual design studies have been made of such a reactor.[3] None of these studies have included a divertor. To remedy this oversight a divertor transport calculation has been made using the basic design parameters proposed by the Oak Ridge National Laboratory plasma engineering group.[24]

The main plasma parameters of interest are listed below:

Minor plasma radius, a (cm)	220
Major plasma radius, R_0 (cm)	675
Mean radius to wall, A_w (cm)	250
Toroidal field on axis, B_{T0} (kG)	48
Total toroidal plasma current, I (amps)	7.2×10^6
Thermal power output at 22.4 MeV, P_{th} (MW)	520

The ORNL study group only used a point model to ascertain the plasma characteristics. When a 1-D code is applied, including a divertor, the following plasma parameters are obtained:

Mean electron temperature, $\bar{T}_e$ (eV)	7400
Mean ion temperature, $\bar{T}_i$ (eV)	7100
Mean electron density, $\bar{n}_e$ (#/cm^3)	8×10^{13}
Mean beta poloidal, $\bar{\beta}_\theta$	1.22
Particle confinement time, τ_p (sec)	1.3

The plasma profiles obtained are shown in Figs. VI-13 and VI-14. They appear qualitatively similar to those found for the UWMAK reactors. The peak density is slightly higher than for UWMAK-II and it does not drop to quite so low a value at the separatrix. The average density is higher than in UWMAK-II and the average temperatures are lower. Due to the higher separatrix density, the shielding efficiency of the EPR divertor, η_z, is higher than in UWMAK-II.

Another feature of interest which is shown specifically for the EPR case is a plot of how the transport properties vary across the plasma. Figure VI-15 shows the values of D, χ_e, and χ_i. Since $D \gamma/k_r^2$ [γ = linear growth rate of the mode (function of $k_\perp$ and k_r), k_r is the "radial" wave number, and $(\pi/k_r)^{-1}$ is taken in this case as the distance between mode rational surfaces*], the dip near the q = 2 surface is explained by a change in the value of k_r used to compute D and χ. The drop in D and χ_i as one gets closer to the center of the plasma tends to create peaked profiles. This is a characteristic of the trapped particle modes in particular and, in fact, D or χ which is

*Near the plasma edge, k_r is taken as π/Δ where Δ = distance from mode rational surface to separatrix.

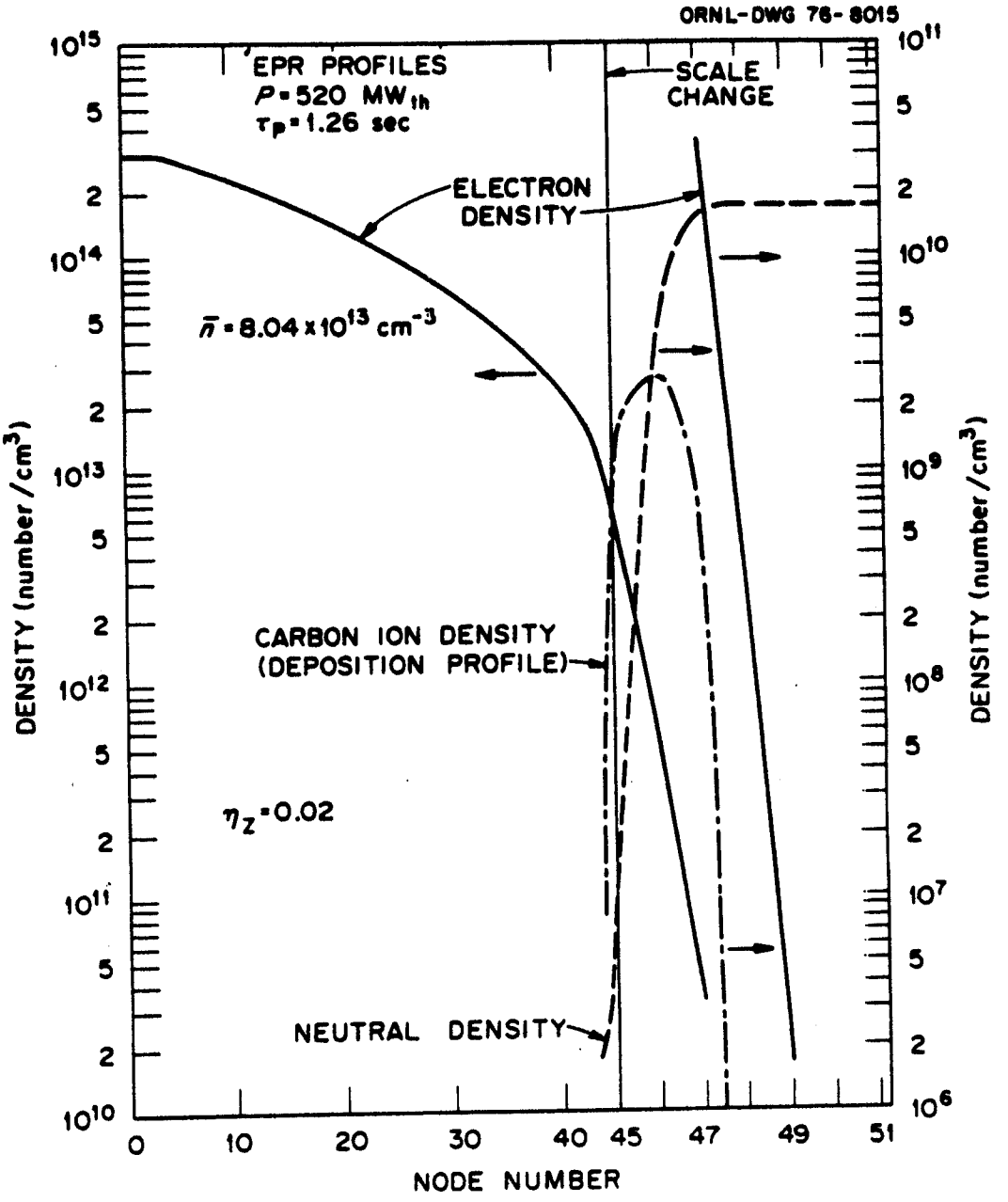
ORNL-DWG 76-8015
EPR PROFILES
P = 520 MWth
τp = 1.26 sec
SCALE CHANGE
ELECTRON DENSITY
n̄ = 8.04 x 10^13 cm^-3
CARBON ION DENSITY (DEPOSITION PROFILE)
ηz = 0.02
NEUTRAL DENSITY
DENSITY (number/cm^3)
DENSITY (number/cm^3)
NODE NUMBER
0
10
20
30
40
45
47
49
51

Figure VI-13

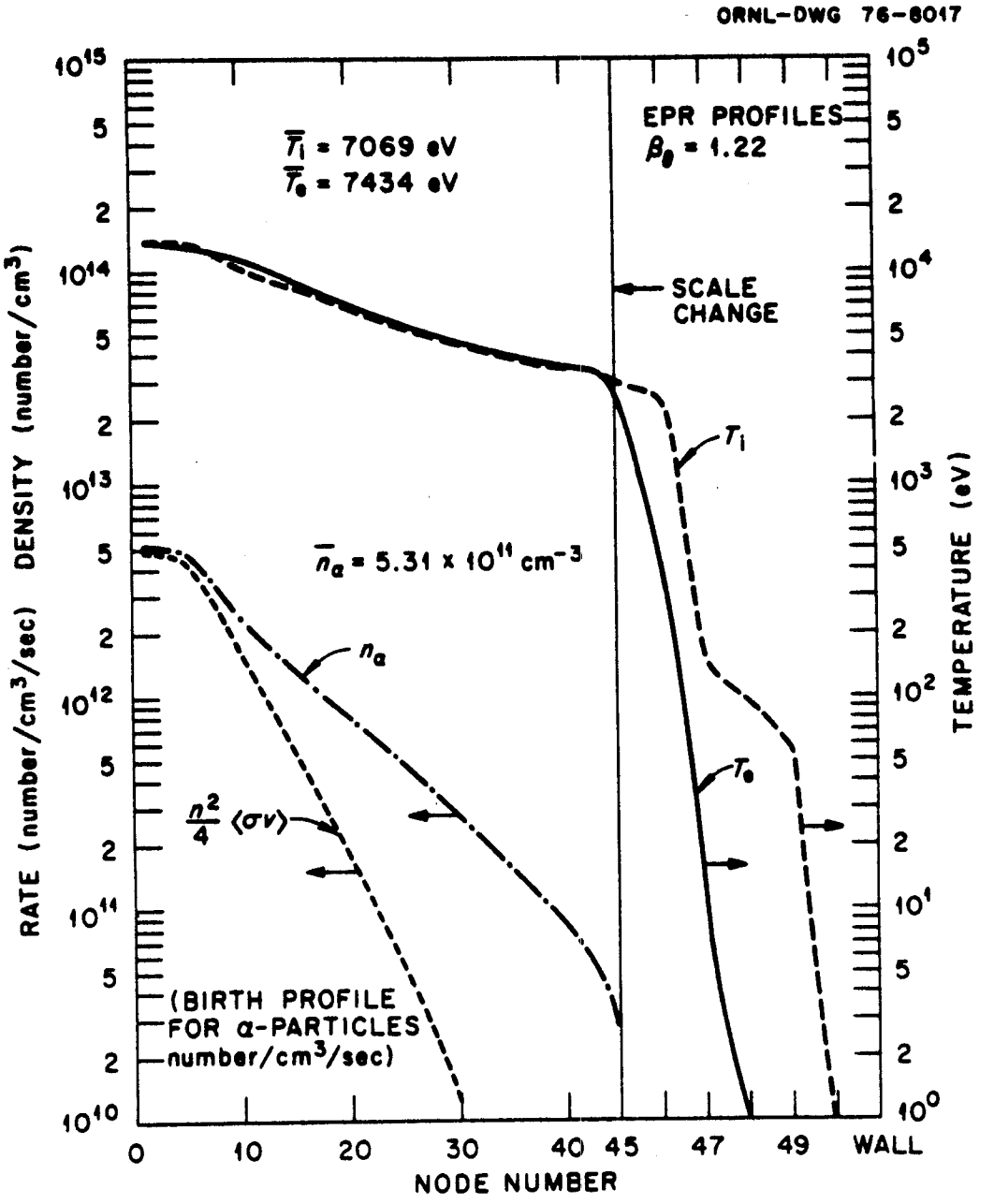
ORNL-DWG 76-6017
EPR PROFILES
β_θ = 1.22
$\bar{T}_i$ = 7069 eV
$\bar{T}_e$ = 7434 eV
SCALE CHANGE
T_i
$\bar{n}_\alpha = 5.31 \times 10^{11}$ cm^{-3}
n_α
T_e
$\frac{n^2}{4}\langle\sigma v\rangle$
(BIRTH PROFILE FOR α-PARTICLES number/cm^3/sec)
RATE (number/cm^3/sec) DENSITY (number/cm^3)
TEMPERATURE (eV)
NODE NUMBER
WALL

Figure VI-14

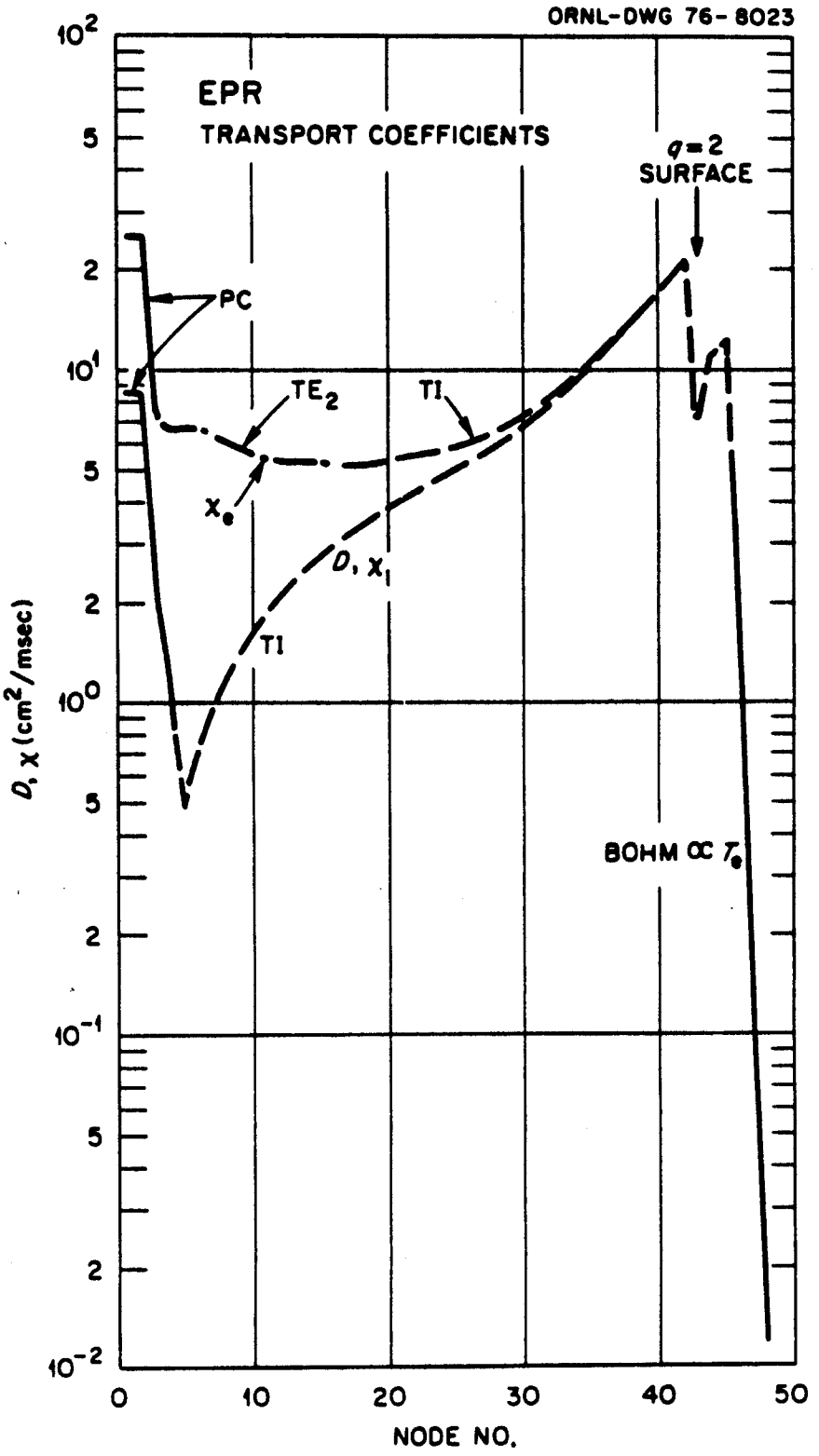
ORNL-DWG 76-8023
EPR
TRANSPORT COEFFICIENTS
q=2
SURFACE
PC
TE2
TI
Xe
D, X1
TI
BOHM ∝ Te
D, X (cm²/msec)
NODE NO.
10²
5
2
10¹
5
2
10⁰
5
2
10⁻¹
5
2
10⁻²
0
10
20
30
40
50

Figure VI-15

proportional to (density)$^{-1}$ will exhibit a density peaking.

A final note on the EPR profiles is that they are not equilibrium profiles. They have a decay constant of roughly 200 seconds and as most EPR designs only need "equilibrium" which lasts that long, this example may be considered suitable.

Summary

All three reactor designs have now been described and their profiles presented. The divertor's presence is felt due to the nature of its producing a low particle density at the separatrix. This low density in the presence of trapped particle modes (or any other) which scales as 1/n produces very peaked profiles for n and T. The cold (pellet) fuel deposition rate profile plus neutral recyling at the plasma edge are the only methods for holding the density at an equilibrium level in the presence of 1/n transport scaling. One can thus see a direction to go in increasing the particle confinement time. A careful recyling, combined with a pellet deposition profile peaked near the separatrix, will increase the edge density, lower D, χ, etc., and thus increase τ_p. This will lighten the pumping load in the divertor collection chambers. From the experience gained in using the code, it seems clear that once the trapped particle modes "get a foothold," so to speak, on the plasma, that it is very difficult to turn them off using pellets unless one can create a very inverted deposition profile. This may shut the reactor down (de-ignite) if not handled carefully. A possibility exists in the idea of recycling more of the plasma collected by the divertor back to the plasma edge

as neutrals. If this can be done carefully enough, the edge density could be raised. The raising of the edge density then slows down the transport rate and fewer ions leave—so even fewer have to be returned to keep n up!

The above scenario is what one might try to do <u>if</u> the plasma transport were governed by coefficients $\propto 1/n$. The real reason for desiring a longer particle confinement time is twofold. First, longer confinement means a higher fractional burnup or more power per fuel "loading." Second, the vacuum pumping rates required to handle the divertor throughput can be very large, not to mention the need to handle some reasonably large fraction of the alpha power.

In this regard, no mention has been made of the divertor particle collectors or how the energy flux to the divertor should be handled. The reason for this is that neither of these problems have been solved, even conceptually, in a satisfactory manner. One can refer to the literature,[25] but no one claims to really have a solution. If some form of lithium collector is used and kept from saturating and vaporizing, this will pump most of the D and T. It is not clear, however, that we want to pump <u>all</u> the D and T; we really only want to pump the higher Z materials and let the D and T recycle. If we had to collect all the D and T, separate it, form it into pellets, and reinject it, it would seem to require a rather costly outlay of funds.

In fact, with the small fractional burn-ups associated with the UWMAK reactors, one is faced with a very large tritium inventory[1] mainly in the divertor collectors! This is unappealing. The UWMAK-III reactor design has tried putting the particle collection chamber outside the toroidal field coils. This allows cryopumps to be used and permits larger collection areas. It is not clear that this can be made a mechanically viable concept, but is under further study.

With the coverage of these models and a brief discussion of what the problems seem to be <u>if</u> large particle loss rates are present in the plasma, one can get some idea of the problems associated with having a divertor. Nct all the solutions are at hand, but one sees ways of going about alleviating some of the problem areas. It is encouraging to see that one can obtain ignited reactor systems using trapped particle mode scalings. These scalings are very pessimistic and hopefully even if their dependencies on T_e, n, ∇n, etc. are correct, their magnitudes may be reduced from the values calculated in WASH-1295.[26] This would make things even more promising.

CHAPTER VI

Bibliography

[1] Ref. [6], Chapter I.

[2] Ref. [7], Chapter I.

[3] Ref. [8], Chapter I.

[4] S. E. Attenberger and D. G. McAlees in, "Proc. of Second Topical Meeting on the Technology of Controlled Nuclear Fusion," Richland, Wash. (Sept. 1976), sponsored by ANS, MFD, Division of ERDA, and EPRI (to be published).

[5] L. G. Kelly, Handbook of Numerical Methods and Applications, Addison-Wesley, Mass., 1967), Chapt. 1.

[6] Ref. [26], Chapter II.

[7] Carnahan et al., Applied Numerical Methods, (John Wiley and Sons, New York, 1969).

[8] S. Milora and C. Foster, private communication on pellet injection experiments on ORMAK.

[9] Ref. [25], Chapter V.

[10] J. Donhowe, private communication on sputtering work at Univ. of Wisconsin.

[11] E. Sucov, Westinghouse and R. Cherdak, Burns and Roe, private communication on divertor trapping.

[12] Ref. [11], Chapter V.

[13] B. A. Truvnikov, translation of Ph.D. thesis, 1958, AEC-tr-4073 (June 1960).

[14] Ref. [25], Chapter V; also C. Audenaerda, private communication on synchrotron radiation with reference to his Ph.D. thesis at Univ. of Utrecht (1976).

[15] J. F. Clarke, private communication on photon transport.

[16] Ref. [6], Chapter I.

[17] W. A. Houlberg, FDM-103, Nuc. Eng. Dept., Univ. of Wisconsin, Madison, WI (May 1974); see also S. Inoue and K. Itoh, IPPJ-249 (June 1976).

[18] Ref. [19], Chapter V.

[19] W. A. Houlberg, private communication.

[20] W. A. Houlberg, in Ref. [17].

[21] H. C. Howe, private communication on ORMAK scaling; see also Ref. [19] in Chapter II.

[22] Ref. [7], Chapter I.

[23] H. C. Howe, private communication on using reflection model in ORMAK modeling; see also Ref. [19], Chapter II.

[24] D. G. McAlees et al., ORNL/TM-5573 (Oct. 1976).

[25] Ref. [6], Ref. [7], and Ref. [13], Chapter I.

[26] Ref. [30], Chapter II.

CHAPTER VII

Conclusion

Since a great deal of somewhat diverse material has been covered in the preceding chapters, it is perhaps worthwhile to consolidate that information before trying to draw any conclusions.

In Chapter I we noted with some optimism that a poloidal divertor has been successfully operated on a tokamak (JFT-2a), and that a bundle divertor appears to be successfully working on DITE. Neither experiment appears to have run into any unusual MHD effects. In addition, divertor configurations have been run on other types of devices (stellerators, FM1) with reasonably good results; this is also encouraging.

Chapter II presented the perplexing subject of impurities and their control. The evidence to date tends to indicate that, from an energy loss point of view, one may prefer a low z wall material or liner for large fusion reactors if the chemical sputtering can be maintained within reasonable bounds, and if the material can maintain some semblance of structural integrity at high temperatures.

The elaborate and subtle question of exactly what the "edge" conditions will be (or should be) in a fusion reactor was also discussed in Chapter II. The conclusion was that no definite answer can be given at this time due to the fact that there are a number of theoretically possible operating schemes available for tokamak operation. Each scheme carries with it its own set of assumptions and requirements. A

number of scenarios are viable from a reactor standpoint. Whether or not all of these schemes will appear equally attractive from an electrical power producing point of view is hard (and probably too soon) to tell.

The MHD problems plaguing tokamak reactors were briefly reviewed in Chapter III and the conclusion was drawn that one may have some theoretical reasons for concern due to the sharp curvature needed to produce the x-type null points in a poloidally diverted reactor. This concern settles more around the fact that one must have a strong pulling force on the plasma near these null points and unless the nulls are "hard," one may be able to find perturbations which could produce instabilities. Only experiment will likely answer this question. It was clearly noted in Chapter III that impurities coming in at the plasma edge would tend to narrow the current density profile and cause, in some instances, a "shearless" layer to form inside the plasma volume. This may cause MHD stability problems.

Chapter IV began addressing the problem of plasma transport in the divertor region of a tokamak reactor. Several models which used only the particle continuity equation with some simplifying assumptions as to what were the ionization rates, electron temperature and ion temperature profiles were solved. These models tended to indicate that density fell very rapidly in the divertor zone unless the plasma could be either mirror trapped in the divertor zone or unless one could produce (at the very least) a warm electron plasma of

higher density ($n_e > 5 \times 10^{11}$) in the divertor zone by some external means. The only other feature of interest from these models was the observation that the density near the separatrix was, in large measure, independent of the boundary conditions present at the first wall. This fact was to be used in the more advanced one-dimensional numerical simulation schemes.

In Chapter V the detailed formulation of the particle and energy balance equations was presented. Suitable boundary conditions were discussed and shown explicitly. The entire set of model equations to handle the parallel particle and energy loss in the divertor zone was presented and their probable physical consequences discussed.

The solutions (i.e., density and temperature profiles) to the coupled set of nonlinear transport equations were presented for three different large tokamak reactor designs. All of the assumptions made in obtaining the solutions were outlined (there are, by necessity, many) and their consequences were quantitatively evaluated where possible.

The conclusions which can be drawn from the results of Chapter VI are the following:

1) The density and electron temperature drop sharply in the divertor zone, but stay slightly higher than what would have been expected in using the simple models outlined in Chapter IV. This is due to the L(r) effect in $\Gamma_{\parallel}(r)/L(r)$.

2) The electron temperature drops much faster than the ion temperature due to the sheath behavior at the particle collector

plates. (This assures that there is no anomalous electron-ion temperature equilibration mechanism present in this low density zone.)

3) With the assumption that 10% of all the plasma collected by the divertor is recycled as cold H_2 neutrals, one finds the largest contributor to the impurity sputtering is the fast charge exchange neutrals. Most of these neutrals come from the region near the separatrix.

4) The impurity ion deposition profile, assuming 20 eV carbon atoms (leaving the wall isotropically), was calculated. This calculation indicated that more than 90% of these atoms were ionized (deposited) in the divertor zone. Most all of these will be heated and stream to the particle collector plates before they can undergo much cross field diffusion.

5) The effects of these impurities on the plasma energy balance were not taken into account. However, since the mean residency time of an impurity in the divertor zone is very small, its impact on the electron energy balance should be small compared to the effects produced by impurities which enter the hot plasma core region.

6) The characteristics of these reasonably large (low β) plasmas with divertors present are the following:

$$\frac{n_e(r=0)}{n_e(\text{separatrix})} \simeq 10^2$$

$$\frac{T_i(r=0)}{T_i(\text{sep})} \simeq \frac{T_e(r=0)}{T_e(\text{sep})} \simeq 10$$

$$\tau_p \equiv \frac{\bar{n}V}{\Gamma_i(\text{sep})A} \simeq \theta(1 \text{ sec})$$

where many of these numbers are equally sensitive to the assumed cross field transport coefficients as they are to the presence of the divertor.

8) The two criteria which tend to affect the characteristics of the plasma core region most (under the assumed use of the trapped particle scaling laws) are: i) the boundary conditions on the plasma at the separatrix (i.e., a divertor or no divertor) and ii) the deposition profile of the cold fuel ions (i.e., pellet injection profile).

9) A comparison was made in UWMAK-III of the particle confinement times obtained from a point reactor model with those obtained from a one-dimensional transport model. The τ_p from a point model is usually a factor of 5 to 10 too long. This is easily explained by the fact that in order to attain an energy balance, i.e., maintain a given energy confinement time, the point model assumes that each particle that leaves carries out 3/2 $\bar{T}_i$ or 3/2 $\bar{T}_e$ which is clearly not what happens. Particles leave the edge with the local edge temperatures which may be factors of 5 or more below the average plasma temperatures. Thus, for the same τ_E, the real τ_p must be much smaller. This is not surprising, but does indicate that the fractional burnup is lower and particle collection schemes will have to be able to handle a much higher particle throughput. This also implies large fueling rates! The work done here corroborates this observation.

The above factors pretty much complete the observational picture taken using a divertor model ($\Gamma_{\parallel}/L(r)$) on a one-dimensional cylindrical transport code. There are several extensions which must be made to this model before meaningful results can be found for more near-term tokamak reactors. The "enhancement factors" must be in the following areas:

1) A complete time dependent impurity stripping and diffusion code must be incorporated in order to realistically weigh the impurity effects and ascertain what effects may limit the behavior during start-up.

2) A realistic assessment must be made of how the impurities, which are sputtered from the particle collector plates that are housed in a region somewhat remote from the plasma core, are ionized in the incident plasma stream, and affect the plasma energy balance.

3) The recycled neutrals and neutral-wall reflection coefficients should be included [1] to see how much the neutral spectrum is hardened due to neutral reflections at the walls.

4) While the formalism to include secondary electron emission is included in Chapter V, it was not explicitly used in any of the above calculations. This must be included in the future.

5) Some care should be taken in extrapolating these results to non-round cross section devices, if one believes that there will be some overriding physical phenomena present other than a decrease in the transport coefficients due to the reduction in the fraction of trapped particles (compared to a circular cross section plasma of the

same total volume and major radius). Also, if one believes there are other terms present in the transport equations due to non-round geometry effects, then one must be cautious in interpreting the results presented herein.

6) A careful treatment must be made of how the resistivity and electron-ion temperature equilibration terms may be affected by micro-instability turbulence. The equations for η and ΔQ_{ei} used in this research were neoclassical in nature with a correction in the resistivity for the local collisionality ($\nu_{eff}(r)/\omega_{be}(r)$). There may be at least a conceptual inconsistency in using some neoclassical terms side by side with coefficients whose validity is based upon the presence of turbulence.

All in all, one can see that a number of important problem areas have yet to be included. In particular, impurity transport must somehow be resolved. With the previously stated caveats, one can only say that it appears initially that divertors on large tokamak reactors may be feasible, and that dissipative trapped particle mode diffusion does not prohibit ignition in large radius devices for any reasonable impurity confinement times.

The work presented here should not be interpreted as the operating plan for a tokamak with a poloidal divertor. There are many scenarios possible for a tokamak discharge other than the few presented here. The results should be viewed as a "first cut" in trying to self-consistently model the plasma "edge" boundary conditions. It appears that the effects of a material limiter could be included

semi-quantitatively within the context of this divertor model and work on doing just that is now being pursued.

As a final note, one must try to address the question of how a divertor might affect the economic feasibility of a tokamak reactor. This is difficult to assess so early in the development of real divertors. Nevertheless, one can point out where some of the costs will lie without putting an explicit price tag on them and it is probably just and right to do so.

First, the major cost difference between a reactor with a poloidal divertor versus one without a poloidal divertor may not be in the additional cost of coils to produce the required magnetic field configuration although one can argue that certainly some additional room is needed which may push the TF coils to a larger size and adversely influence the cost. For a fusion reactor to be profitable from a power producing point of view, it will have to operate at high β values ($\beta > .06$) and to do so with reasonable q values and aspect ratios, one finds that the equilibrium B_v field required to hold the plasma will already be on the same order as the field produced by the plasma current alone. Thus, the separatrix will always be somewhere nearby and only small changes in coil positions and/or currents will be needed to drive a null in the total poloidal field inside the plasma containment shell, and, therefore, produce a divertor configuration.

If trapped particle modes produce the transport, then tremendous throughputs of particles and energy will be incident upon the divertor

"collector plates." The handling of this throughput with high efficiency is certainly pushing the state-of-the-art in the particle collection business, and will no doubt be very expensive. This throughput, a large part of which is unburnt fuel, implies a large tritium content in the divertor system unless one can reprocess the unburnt fuel quickly into pellets (or whatever!) for reinjection. The cost of the facilities to reprocess this unburnt fuel back into pellets, etc., may also be a large cost of a divertor. If the trapped particle modes do not appear and if neoclassical diffusion governs the particle and energy flux out of the machine, then the pumping problem will be considerably reduced. However, the whole scenario of plasma behavior would be completely different from that shown in the examples of Chapter VI, and a reassessment of divertor operation and costs would have to be made.

Any power producing ($> 1000\ MW_{th}$) device will of necessity be expensive and somewhat elaborate. Tokamaks are no exception and due to their low power densities ($\lesssim$ few watts/cm^3) will have to be larger than comparable fission devices. The state-of-the-art in tokamak reactor development is waiting upon the solution of two major problems: 1) plasma scaling and 2) development of materials with better structural properties in the presence of high neutron fluences. The added cost and complexity of a divertor should not in this author's opinion adversely influence, cost-wise, the development patterns of fusion reactors given the solutions to 1) and 2) above.

CHAPTER VII

Bibliography

[1] Ref. [19], Chapter II; see also O. S. Oen and M. T. Robinson in Solid State Physics Division Annual Progress Report for the period ending December 31, 1974, ORNL-5028.

APPENDIX A

Transport Coefficients Used in 1-D Computer Code

The coefficients represented on the following pages were taken from WASH-1295, "Status and Objectives of Tokamak Systems for Fusion Research," edited by S. O. Dean.

At each spatial position in the plasma, each of the following transport coefficients were evaluated. The maximum coefficient was chosen in each spatial region and used for the next time step. When the trapped particle modes were stabilized, the diffusion and electron thermal conductivity was assumed to behave pseudoclassically and the ion-thermal conductivity was taken to be neoclassical.

Transport Coefficients:

Pseudoclassical (PC)

$$\chi_e^{PC} = C_0 \, \nu_{ei} \, \rho_{e\theta}^2$$

$$D^{PC} = \frac{1}{3} \chi_e^{PC}$$

where

C_0 = constant from 4 to 10

$\rho_{e\theta}$ = electron gyroradius in the poloidal field

ν_{ei} = electron-ion (90°) collision frequency

Dissipative Trapped Electron Mode (TEM):

$$\chi_e^{TEM} = A \frac{m_i}{m_e} \left(\frac{r}{T_e} \frac{dT_e}{dr}\right)^2 \frac{\rho_{e\theta} \nu_{ei}}{1 + \frac{\nu_{ei}}{\nu_0}}$$

$$D^{TEM} = \frac{1}{A} \chi_e^{TEM}$$

$$= \chi_i^{TEM} \text{ (assumed)}$$

where

$A = r/R_0$ = aspect ratio (local)

R_0 = major radius of torus

$$\nu_0 \equiv \theta \frac{A^{1/4}}{R_0} \sqrt{\frac{T_e}{m_i}} \sqrt{\left|\frac{d \ell n\, n}{d \ell n\, T_e}\right|}$$

$$\theta \equiv \frac{r}{qR_0} \frac{d \ell n\, q}{d \ell n\, r} \sim \frac{B_\theta}{B} \sim \frac{1}{qA} \text{ (shear)}$$

Dissipative Trapped-Ion Mode (TIM):

$$D^{TIM} = \chi_e^{TIM} = \chi_i^{TIM}$$

$$= \frac{1}{A^{5/2}} \frac{\rho_e^2 \left(v_{th}^e\right)^2}{\nu_{ei}} \frac{\left(\frac{d \ell n\, n}{dr}\right)^2}{\left(1 + \frac{T_e}{T_i}\right)^2}$$

where

ρ_e = electron gyroradius

v_{th}^e = electron thermal velocity = $\sqrt{\frac{2T_e}{m_e}}$

Trapped Particle Interchange Mode:

$$D^{TPI} = \chi_i^{TPI} = \chi_e^{TPI}$$

$$= \frac{1}{A^{3/4}} \frac{T_e}{eB} \frac{(\Delta r)^2}{r} \left| \frac{1}{n} \frac{dn}{dr} \right|$$

where

(Δr) = radial localization width $< \left| \frac{1}{n} \frac{dn}{dr} \right|^{-1}$

Bohm (drift wave turbulence):

$$D^{Bohm} = \epsilon_B \left(\frac{1}{16} \frac{T_e}{eB} \right) = 6.25 \times 10^6 \, \epsilon_B \frac{T_e(eV)}{B(Gauss)} \frac{cm^2}{sec}$$

where

$\epsilon_B = 1 \Rightarrow$ Bohm diffusion

and usually

$1 > \epsilon_B > .001$

APPENDIX B

Estimation of Impurity Residency Time in Divertor Zone

The calculations to be performed here are intended to show two features. The first calculation is intended to show that the ratio of the time it takes an ionized impurity in the divertor zone to leave along the field line to the time it takes it to diffuse across the field into the plasma core region is very small. The second calculation then estimates on what time scale one can expect an impurity ion to be heated and leave versus the time to ionize up to a higher charge state. Specific examples will be given using carbon as the impurity.

Calculation #1

To estimate the time it would take an impurity (assumed collisional) to diffuse along a $\vec{B}$ field line a distance $L_\parallel$, one uses*

$$\tau_\parallel = \frac{(L_\parallel)^2}{D_\parallel}$$

and

$$D_\parallel = \nu_z(\lambda^z_{mfp})^2 = (v^z_{th})^2/\nu_z$$

$$v^z_{th} \equiv \sqrt{2kT_z/m_z} \tag{B.3}$$

$$\nu_z \simeq \nu_{zi} \simeq \frac{1.0 \times 10^{-6}\, n_i(cm^{-3}) \left[\frac{\ell n\, \Lambda}{15}\right] F_{zi}}{[T_i(eV)]^{3/2}} \ sec^{-1} \tag{B.4}$$

where

$$F_{zi} \equiv z^2 \frac{A_i^{3/2}}{A_z^2}\left(1 + \frac{A_z}{A_i}\right) \tag{B.5}$$

*If λ^z_{mfp} becomes comparable to $L_\parallel$, then $\tau_\parallel$ as given by (B.1) is incorrect and one should use instead $\tau_\parallel = L_\parallel/v^z_{th}$.

For $A_i = 2.5$, $A_z = 12$, $F_{zi} \simeq 1.9\ z^2$.

The estimate of the time it would take an impurity to diffuse across the magnetic field some distance $L_\perp$ is given by

$$\tau_\perp = \frac{(L_\perp)^2}{D_\perp} \tag{B.6}$$

and it will be assumed that $D_\perp$ is some multiple, C, of the classical value

$$D_\perp \simeq C\ \nu_{zi}\ \rho_{Lz}^2 \tag{B.7}$$

$$\rho_{Lz} = \sqrt{2m_z kT_z}/z\ |e|\ B \tag{B.8}$$

The ratio of concern is

$$\frac{\tau_\parallel}{\tau_\perp} = C\ \left(\frac{L_\parallel}{L_\perp}\frac{\nu_{zi}}{\omega_{bz}}\right)^2 \tag{B.9}$$

and

$$\omega_{bz} = \rho_{Lz}/v_{th}^z = 9.6 \times 10^3\ z\ B(\text{gauss})/A_z \tag{B.10}$$

Taking as a pessimistic example

$T_i \simeq 100$ eV

$n_i \simeq 10^{12}$ cm^{-3}

$B \simeq 3 \times 10^4$ gauss

$z = 1$ (once ionized carbon)

$A_i = 2.5$

$A_z = 12$

one easily finds that

$$\frac{\tau_{\parallel}}{\tau_{\perp}} = 6.3 \times 10^{-9}\, C \left(\frac{L_{\parallel}}{L_{\perp}}\right)^2 \qquad \text{(B.11)}$$

Let us further assume that C = 1000, i.e., the cross field diffusion is 1000 times the classical value. Then ask the question: for what ratio of $L_{\parallel}$ to $L_{\perp}$ will $\tau_{\parallel}/\tau_{\perp} = 1$. The answer is

$$\frac{L_{\parallel}}{L_{\perp}} = \frac{1}{\sqrt{6.3 \times 10^{-6}}} \approx 400$$

If the distance to the particle collectors is 20 meters, then all the carbon ions deposited within 5 cm of the separatrix stand an even chance of diffusing into the plasma core rather than leaving along the field line.

The approximation used to evaluate ν_{zi} was that T_z, the impurity temperature, was much less than T_i. Obviously as the plasma ions and electrons collide with the impurity ions, they will on the average give up some of their energy and thus heat the impurity atom making it less collisional and thus $D_{\parallel}$ for the impurity increases making the ratio $\tau_{\parallel}/\tau_{\perp}$ even smaller. Also the calculation performed here does not include the possibility of an electic field along the field lines which Meade claims may be present.[1] This field, if it extends any reasonable distance along the field lines, could help to draw out the impurities.

To obtain an estimate of how long it takes a cold (once ionized) impurity to heat up versus the time to strip it to a higher energy level, one performs the second calculation indicated earlier.

Calculation #2

The impurity-fuel ion equilibration time is given by [2]

$$\tau_{zi}^{eq} \simeq \frac{5 \times 10^5}{z^2} \frac{A_z}{\sqrt{A_i}} \frac{[T_i(eV)]^{3/2}}{n_i(cm^{-3})} \text{ sec} \qquad (B.12)$$

which for the example considered here gives

$$\tau_{zi}^{eq} \simeq \frac{4 \times 10^{-3}}{z^2} \text{ sec} \qquad (B.13)$$

This shows that as the impurity is stripped up the equilibration time decreases very rapidly, i.e., once the impurity has stripped to Z = 3 equilibration time with the ions is reduced by $\simeq 10$. This equilibration time, which is also roughly the time scale for the impurity to escape by merely flowing along the field lines at $\simeq \sqrt{T_i/m_z}$ must be compared to the ionization and recombination time scales so as to estimate the "damage" which the impurity produces in the divertor zone.

Estimating the electron temperature to be also at 100 eV gives ionization rates ($\langle \sigma v \rangle$) for carbon ions of from 2×10^{-8} cm^3/sec for C^{II} to C^{III} to 2.5×10^{-9} cm^3/sec for C^{IV} to C^{V}. With $n_e \simeq 10^{12}$ cm^{-3}, this implies characteristic times for ionization of from

$$\tau_{iz}(C^{II} \rightarrow C^{III}) \simeq \frac{1}{(10^{12})(2 \times 10^{-8})} \simeq 5 \times 10^{-5} \text{ sec} \qquad (B.14)$$

to

$$\tau_{iz}(C^{IV} \rightarrow C^{V}) \simeq 4 \times 10^{-4} \text{ sec} \qquad (B.15)$$

Comparing (B.13) for Z = 3, which is C^{IV} to τ_{iz} given by (B.15), we see that

$$\frac{(B.15)}{(B.13)} \simeq 1$$

which suggest that a carbon ion in a 100 eV, 10^{12} cm^{-3} plasma will strip to roughly a $Z \simeq 3$ charge state in about the time it takes to heat to $\simeq$ 100 eV. A 100 eV carbon ion could travel a distance $L_{\|}$ = 20 meters in a time $\tau_s \simeq 7 \times 10^{-4}$ sec which is comparable to the ionization and equilibration times.

One may then conclude on semi-quantitative grounds that carbon may strip up to a $Z \simeq 3$ or 4 state, and heat in 10^{-3} sec, and, as long as it is not depositing too close to the separatrix, it should leave along the field line rather than diffuse into the plasma core region

Obviously this calculation is invalidated if the impurity cross field diffusion in the divertor zone is much more than 10^3 times the classical value.

References

[1] D. A. Meade, private communication.

[2] G. Schmidt, Physics of High Temperature Plasmas, (Academic Press, New York, 1966).

APPENDIX C

This appendix consists of a reproduction of Section III-A of UWMAK-III report, FDM-150, Fusion Technology Program, Nuclear Engineering Department, University of Wisconsin, Madison, Wisconsin. The preponderance of the magnetic field design work in this section was performed by Dr. T. Yang.

III. Divertor and Vacuum Pumping

III-A. Divertor Magnetic Field Design

UWMAK-III utilizes a double-null poloidal divertor in order to protect the first wall from charged particle bombardment and the consequent buildup of impurities in the plasma. The divertor also possesses the desirable property of establishing a boundary for the magnetically confined plasma and, with proper programming of the divertor and transformer currents during startup, can produce an expanding magnetic limiter. The large stored poloidal magnetic energy in the reactor size plasmas requires that the plasma current be brought to its full value rather slowly (~15 seconds). In order to maintain reasonable values of q, the MHD stability factor, during this time, it is necessary to have a small plasma initially and let the radius expand during the current rise, keeping the current density approximately constant. The programmed divertor is a way of doing this without having metallic surfaces in contact with the plasma.

The UWMAK-I[1] and UWMAK-II[2] divertors were designed using a filamentary model[1] to calculate the flux surfaces. This model is acceptable for determining approximate values for the divertor currents and their locations. The next level of sophistication is to use a free boundary MHD equilibrium code where the divertor currents play a crucial role in determining the MHD equilibrium. This has been done for UWMAK-III and is described in Section II-A of this report. In this section, we describe the magnetic field geometry in the scrape-off zone and discuss how particles get to the collectors. Section III-B describes the vacuum pumping system and Section III-C describes the particle collectors.

The UWMAK-I and UWMAK-II divertors used a flowing liquid lithium film to collect the particles. These plates were placed inside the toroidal field magnets, as shown in Fig. III-A-1 for UWMAK-II. The major drawback, especially for UWMAK-II, was that the power density on the collectors was large because of the small transverse dimension of the plasma beam at the collector. The heat transfer problems caused by this were tremendous. This problem becomes worse for a smaller size reactor of the same power level. Furthermore, space becomes a problem when the plasma is vertically elongated as in UWMAK-III. (See Fig. III-A-2).

We decided in UWMAK-III to design the divertor with the particle collectors outside the toroidal field coils. This allows us to fan the field lines and reduce the power density on the collectors. Furthermore, it allows us to place the cryopumps in close proximity to the collectors for maximum pumping efficiency. Combining this with the relatively small flow conductance back through the slots to the plasma, we expect that there will be little back-streaming of neutrals and impurities.

The particles get from the plasma to the collectors by following magnetic field lines into the fringing region of the toroidal field coils. These field lines get "caught" in the poloidal component of the fringing toroidal field and pass through the gaps.

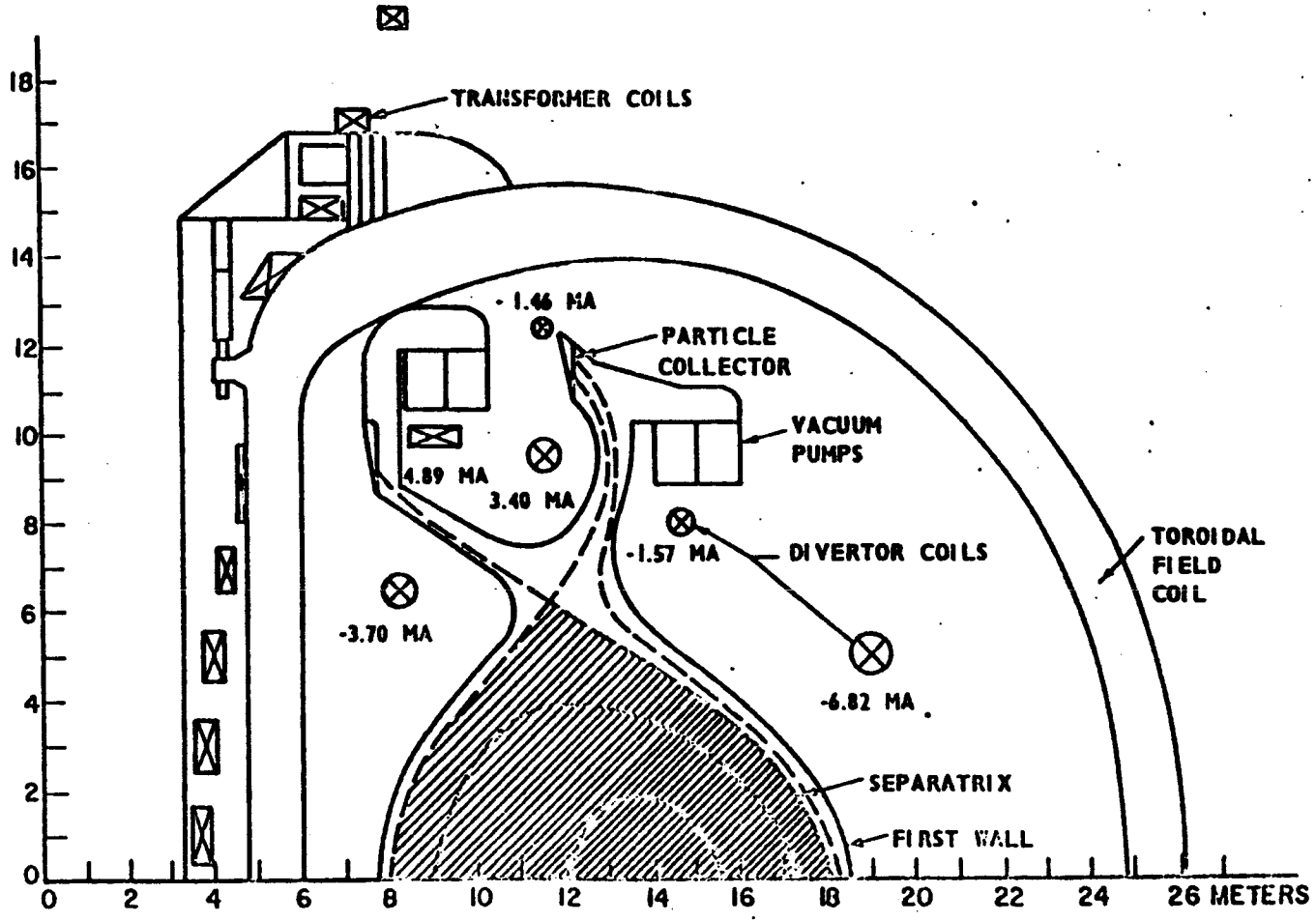

UWMAK - II POLOIDAL DIVERTOR

FIGURE III-A-1

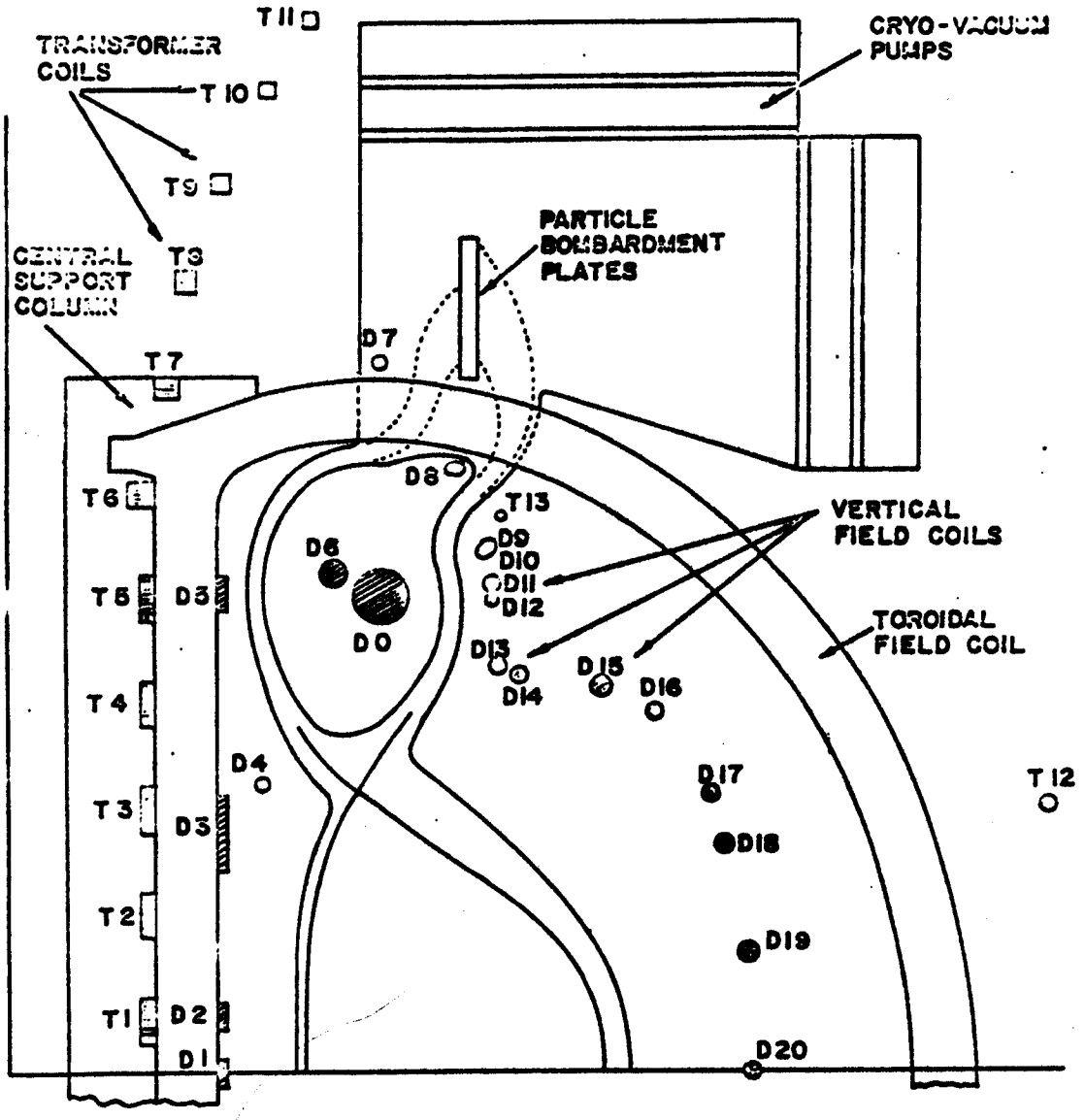

FIGURE III-A-3 - UWMAK-III Poloidal Divertor

CROSS SECTION VIEW OF UWMAK III

FIGURE III-A-2

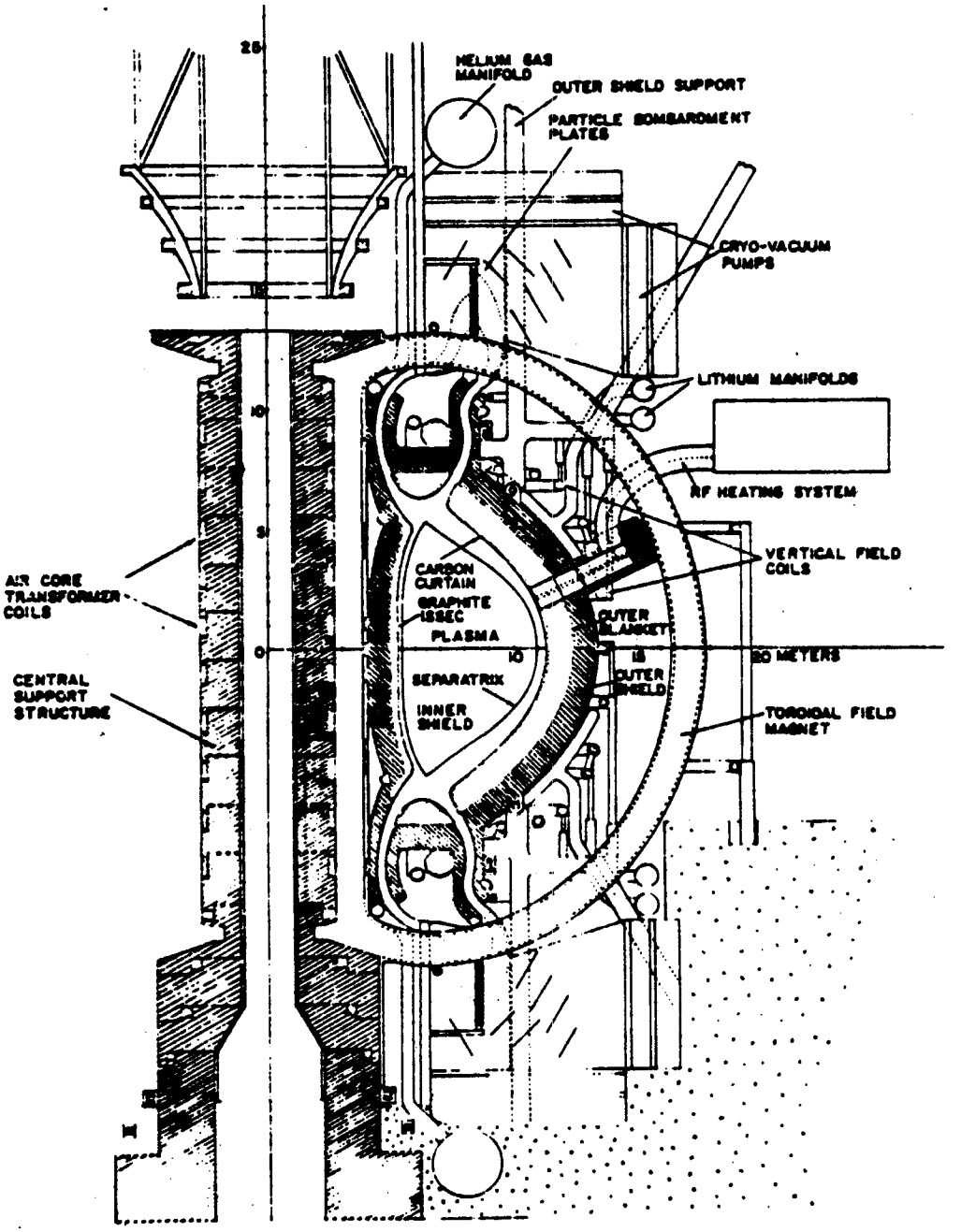

To see how this occurs, consider first a discrete coil cylindrical solenoid as shown in Fig. III-A-4. Around each coil there is a separatrix. Field lines (A) inside the separatrix encircle their respective coil; some of them will intercept the coil structure because of the finite dimensions of the windings. Field lines (B) inside the solenoid but outside the separatrix deflect outwards near the gap but return to the interior of the solenoid. Some of them intercept the coil structure only if the separatrix also intercepts the structure.

Let us now introduce an external magnetic field transverse to the solenoid axis. The resulting flux plot near the coils is shown qualitatively in Fig. III-A-5. All field lines (B) are now carried towards the coils and eventually pass through the gaps if the separatrix lies outside the coil dimensions. If these field lines are carrying particles, as in the scrape-off zone of a divertor, then the particles get through the gaps and do not bombard the surfaces of the coil.

Let us now apply these rather "idealized" concepts to the tokamak reactor where we have discrete toroidal field coils and an axisymmetric poloidal field. Near the TF coils the poloidal field is outwards in some locations and inwards at others. The resultant path of field lines which originates in the scrape-off zone near the plasma is shown qualitatively in Fig. III-A-6 from three different perspectives. The UWMAK-III divertor utilizes this behavior of the magnetic field to carry particles through the gaps between the TF coils to the particle collectors.

The surfaces of the magnets will experience direct charged particle bombardment if the separatrix around the coils intercepts the surface or if the particles can cross-field drift (due to curvature and ∇B drifts) to field lines that intercept the surface. The latter effect is not considered to be important since the particles can only drift a distance of the order of the gyroradius while traversing a distance along the field lines equal to the radius of curvature of the field. The fields are strong (toroidal field = 4T, poloidal field ~1T) and the gyroradius is small ($\lesssim$ 1 cm) so this effect can be ignored. Calculation of the location of separatrix requires extensive 3D field line computer calculations. This has not yet been done for UWMAK-III, but we are preparing to do this work. We have done similar calculations for UWMAK-I[3] and II; in those cases, the coils were protected except near the inner leg of the "D". This leads us to believe the method described will work for UWMAK-III. If the coils suffer some charged particle bombardment, one can place particle collectors on the surface of the magnets, or at other strategic locations, to protect the magnets from erosion and heat input.

The location of the particle collector plates is shown in Fig. III-A-2 and III-A-3. This is based on the assumption that the coils are protected by the magnetic field against bombardment. This arrangement requires two collectors back-to-back to receive the flux from the inner and outer scrape-off zones. The particles from the inner scrape-off zone pass by the supports for the portion of the blanket and shield directly above and below the plasma.

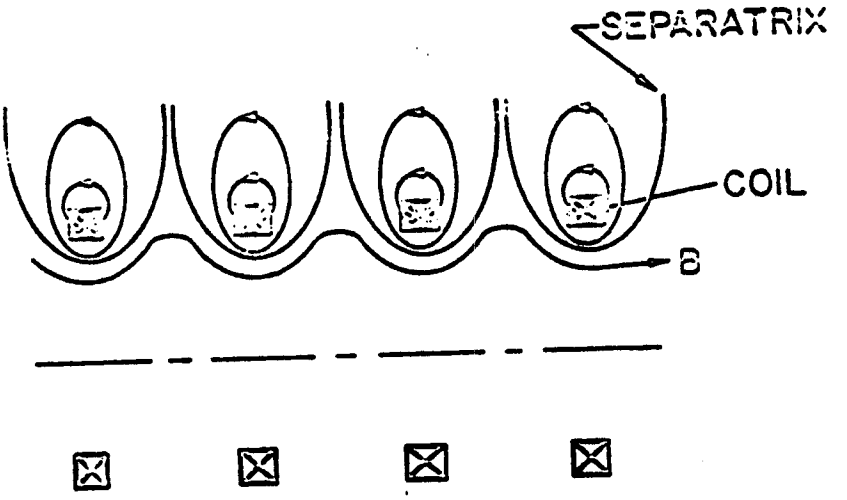

Fig. III – A – 4

Magnetic Field of a Solenoid

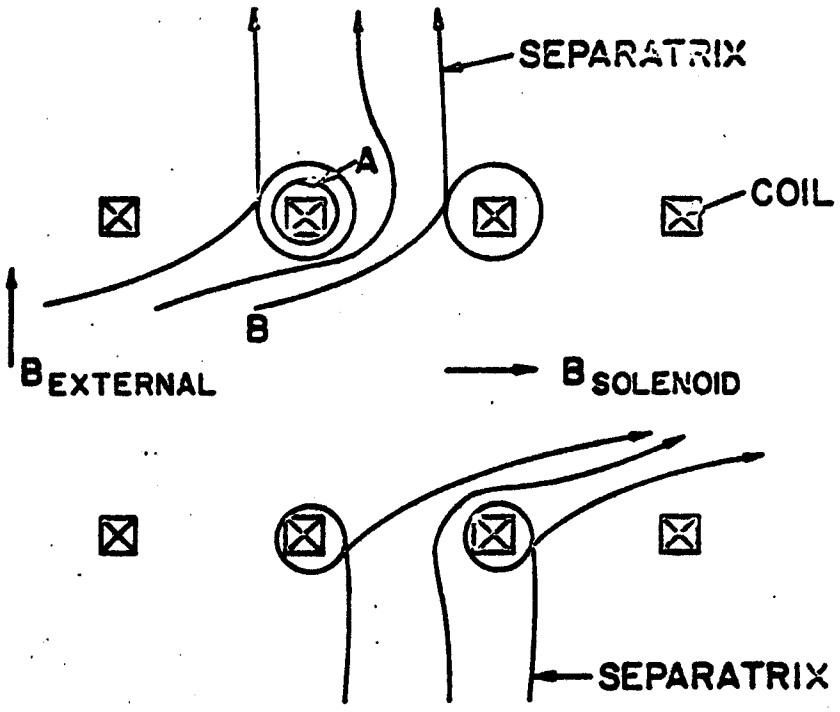

Fig. III - A - 5

Effect of a Transverse Field

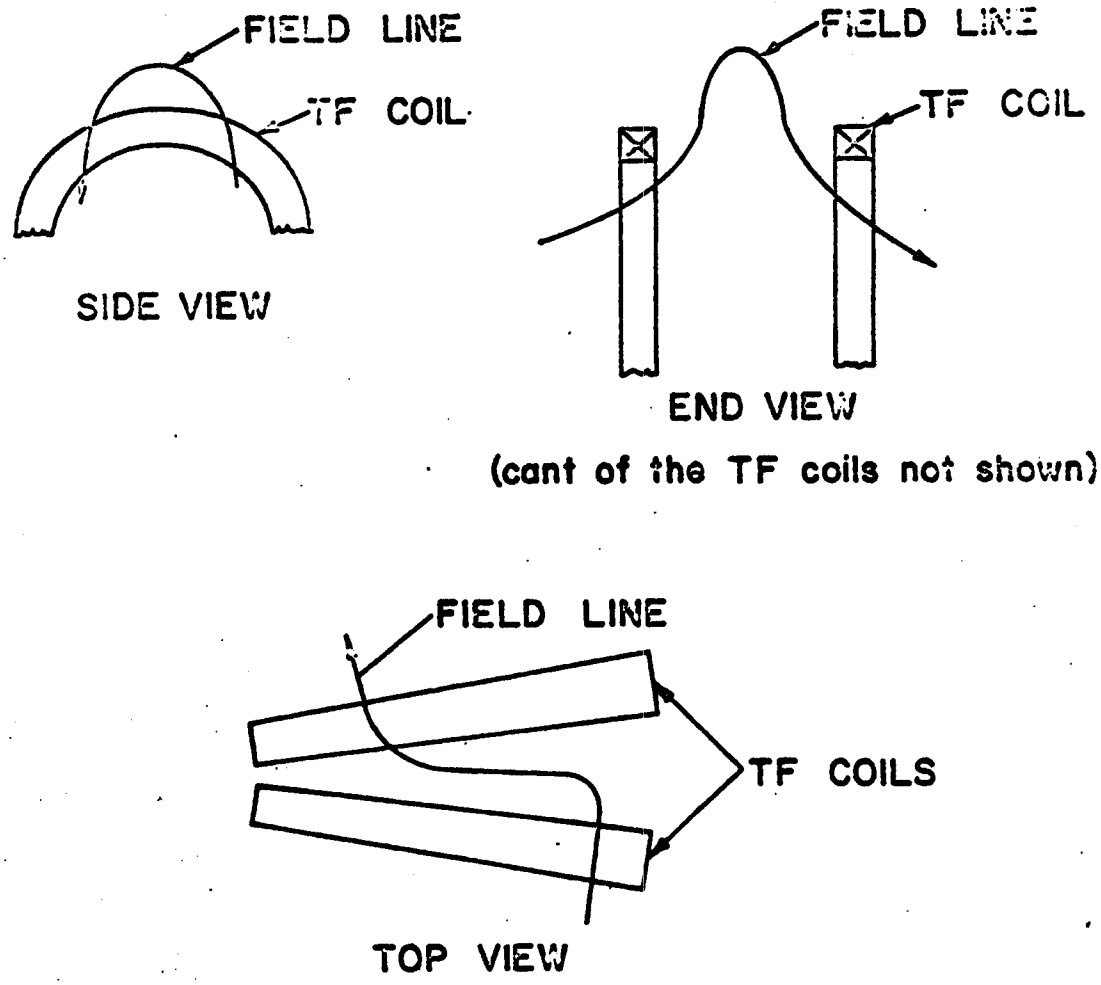

Fig. III - A - 6

Diverted Field Line Near TF Coils

These supports are guarded against charged particle bombardment by two parallel currents as shown in Fig. III-A-7. The line currents create a separatrix and thereby divert the field around the supports as shown in Fig. III-A-8. The required current to guard the supports is 1.9 MA per support. Because of the location behind the blanket and shield, this can be a superconducting current.

References for Section III-A

1. B. Badger et al., "UWMAK-I, A Wisconsin Toroidal Fusion Reactor Design," UWFDM-68, Vol. I, Dept. of Nuclear Engineering, Univ. of Wisconsin.

2. B. Badger, et al., "UWMAK-II, A Conceptual Tokamak Reactor Design," UWFDM-112, Dept. of Nuclear Engineering, Univ. of Wisconsin.

3. T. F. Yang, "A Direct Energy Conversion Scheme for a Tokamak with a Poloidal Divertor," Bull. of the APS, 18, 1303 (1973).

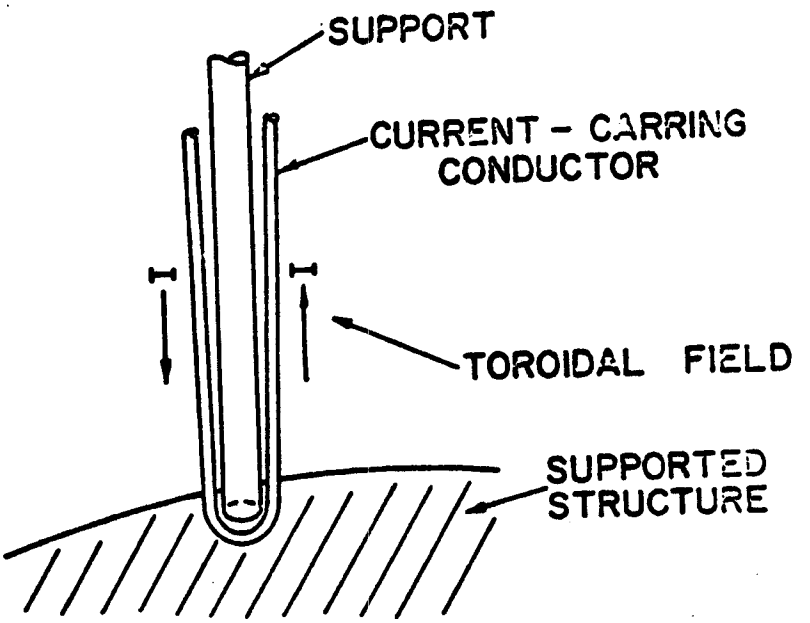

Fig. III-A-7

Magnetic Guarding of the Support

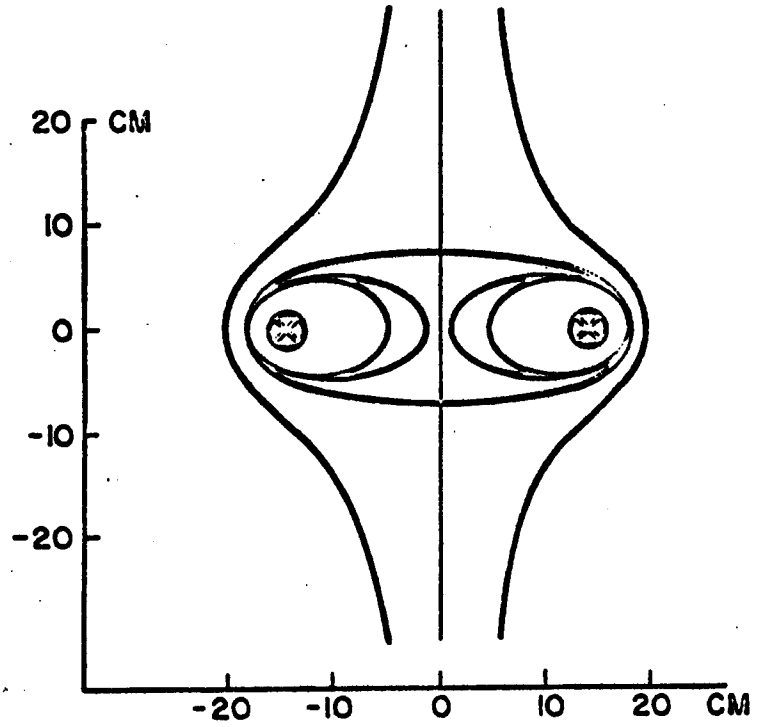

Fig. III-A-8

Magnetic Guarding of Supports

APPENDIX D

Localized Mode MHD Stability Criteria

The basic references for this section are the articles by: 1) Glasser, Greene, and Johnson, MATT-1068, August 1974, and 2) L. S. Solov'ev, Reviews of Plasma Physics, Vol. 6, pp. 239-331, Consultants Bureau, New York, 1975.

1) Solov'ev's necessary criterion for localized interchange stability using the ideal MHD equations is:

$$D_I^S \equiv \Omega \left\langle \frac{B^2}{|\nabla v|^2} \right\rangle + \left\langle \frac{\vec{J} \cdot \vec{J}}{|\nabla v|^2} \right\rangle \left\langle \frac{\vec{B} \cdot \vec{B}}{|\nabla v|^2} \right\rangle - S \left\langle \frac{\vec{J} \cdot \vec{B}}{|\nabla v|^2} \right\rangle - \left\langle \frac{\vec{J} \cdot \vec{B}}{|\nabla v|} \right\rangle^2 - \frac{S^2}{4} < 0 \text{ for stability} \tag{D.1}$$

2) Glasser, Green and Johnson's equivalent expression for ideal modes is

$$D_I^{GGJ} \equiv D_I^S + (P')^2 \left\langle \frac{B^2}{|\nabla v|^2} \right\rangle \left\langle \frac{1}{B^2} \right\rangle < 0 \text{ for stability} \tag{D.2}$$

where

$$\Omega \equiv I'\Phi'' - J'\chi'' \tag{D.3}$$

$$S \equiv \chi'\Phi'' - \Phi'\chi'' = q'/(\chi')^2 \tag{D.4}$$

and the angular brackets $\langle \ \rangle$ imply averaging over the volume between two neighboring ψ surfaces. In the context of this appendix,

J = toroidal current flux

I = poloidal current flux

Φ = toroidal magnetic flux

χ = poloidal magnetic flux (called ψ in Chapter III)

The prime ($'$) indicates d/dV where $V(\psi)$ is the volume enclosed by a given ψ surface.

Glasser, et al. also derive a necessary criterion for local interchange stability of resistive modes, i.e., $\eta \neq 0$. The form of this criterion is

$$D_R^{GGJ} = D_I^{GGJ} + (H - \tfrac{1}{2})^2 < 0 \text{ for stability} \qquad (D.5)$$

where

$$H \equiv - \left[\left\langle \frac{\vec{J} \cdot \vec{B}}{|\nabla v|^2} \right\rangle - \frac{\langle \vec{J} \cdot \vec{B} \rangle}{\langle B^2 \rangle} \left\langle \frac{B^2}{|\nabla v|^2} \right\rangle \right] \qquad (D.6)$$

The author was unsuccessful in his attempt to discern why (D.2) did not agree with (D.1).

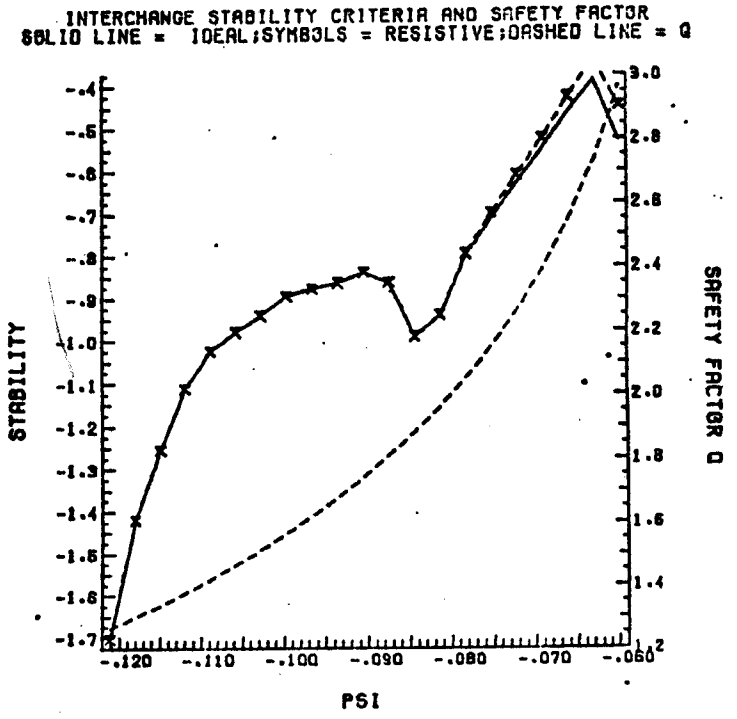

Figure D-1

APPENDIX E

Reproduction of Nuclear Fusion Letter by A. T. Mense, G. A. Emmert, and J. D. Callen, Nuc. Fusion 15, 703 (1975).

To illustrate results obtained from the code, Fig.2 shows, on a log-log scale, "snapshots" of $n(r)$ at successive time intervals during the convergence process. Figure 3 shows the last stages, on an expanded linear time scale. The source parameters used were the same as those in the first (20-keV) example given earlier, with $t_p = 0.5\ t_0$, $R = 3$ m.

By examining the figure, it can be seen that this more accurate calculation yields converged densities not far from those estimated from Eq.(4). Furthermore, for the example given, the assumption of weak interaction of the neutral beam particles with each other is confirmed; using published cross-sections σ_{00} for strong atom-atom interactions and defining an interaction probability p as the integral of $n(r)\sigma_{00}$ from the outer surface of the sphere up to the point in question, p remains $\ll 1$ until the last few nanoseconds. At this time, the beams have nearly reached their full convergence, so that subsequent scattering or collisional self-ionization effects would be expected to have too little time to act to appreciably influence the final density. Thus, convergence should proceed to completion essentially as calculated, provided the background particle density is kept reasonably low (say $< 10^{-6}$ torr, for this example). However, at peak convergence cascading collisional self-ionization would be expected to rapidly ionize the neutral cloud. In Fig.2, values of p are indicated, as estimated from published cross-sections [8].

One curiosity seen in Fig.2 is the momentary sharp "spike" in density that occurs at the exact centre. This spike is a result of the smallness of the uncertainty associated with the longitudinal position of the target cloud [Eq.(3)]. It would be expected that in an actual system geometrical inaccuracies in the source system would substantially weaken the spiking tendency. The dotted curve shown in Fig.2 is a rough estimate of this effect for the case where the inaccuracies in source positioning at radius R are about ± 0.5 cm.

On the basis of the above calculations, and in view of advances in high-current pulsed-neutral-beam technology, we believe that the convergence-bunching technique here described could have important applications in fusion power research. Among these is the possibility, mentioned earlier, of creating high-beta or field-reversed states in intense magnetic fields on a nano-second time scale. Some such states would appear to be intrinsically inaccessible via conventional methods where plasma build-up times are long compared to particle transit-times. Other possibilities for utilizing the high peak power densities and high instantaneous momentum fluxes that would be associated with such converging beams will no doubt emerge as the technique is brought to practical realization.

The importance of properly assessing the magnitude of neutral-neutral interactions was pointed out to one of us (RFP) by R.S. Pease, and the authors are indebted to him for this and other helpful comments.

REFERENCES

[1] POST, R.F., FOWLER, T.K., KILLEEN, J., MERIN, A.A., Phys. Rev.Lett. 31 (1973) 280.

[2] LEVENTTEV, O.A., KALMYKOV, A.A., in Electrostatic and Electromagnetic Plasma Confinement and the Phenomenology of Relativistic Electron Beams, (Proc.Conf.N.Y. Acad. of Sciences, NY, 1974), Paper 10.

[3] WINTERBERG, F., in Annals of the New York Academy (Proc.Conf. on Electrostatic and Electromagnetic Plasma Confinement and the Phenomenology of Relativistic Electron Beams, NY, 1974).

[4] BERKNER, K.H., et al., in Ion Sources and Formation of Ion Beams, (Proc.2nd Symp.Berkeley, CA, 1974), Paper VI-12.

[5] SUDAN, R.N., HUMPHRIES, S., FRIEDMAN, A., Bull.Am.Phys. Soc. 19 (1974) 871.

[6] BATES, D.R., GRIFFING, G.W., Proc.Phys.Soc. (Lond.) A66 (1953) 961.

(Letter received 16 July 1975)

MIRROR MICROINSTABILITIES IN DIVERTORS

A.T. MENSE, G.A. EMMERT (Nuclear Engineering Department, University of Wisconsin, Madison, Wis.), J.D. CALLEN (Thermonuclear Division, Oak Ridge National Laboratory, Oak Ridge, Tenn., United States of America)

As impurity control in tokamaks appears to be one of the most pressing problems in present-day plasma research [1], much thought and some calculation has gone into its eventual attainment. One proposed method is through the use of a divertor [2]. There are many unknowns associated with a divertor's presence on a tokamak. Lacking any experimental observations, one may propose a myriad of models to illustrate different potential problem areas. The problem addressed here is the possibility that the plasma in the divertor region is unstable to mirror microinstabilities and how this may affect plasma transport in this region.

In the operation of a divertor there exists a region (bounded on one side by a magnetic separatrix and on the other by the liner or first wall of the reactor) in which the magnetic field lines are diverted from the local vicinity of the plasma and are channelled into some type of particle collection chamber. This region of diverted B-field lines has been labelled appropriately a scrape-off region [2]. Plasma feeds this zone by diffusion across the field lines from the plasma core and in turn leaves the zone (mostly) by following field lines to the collection region. Cross-sections of

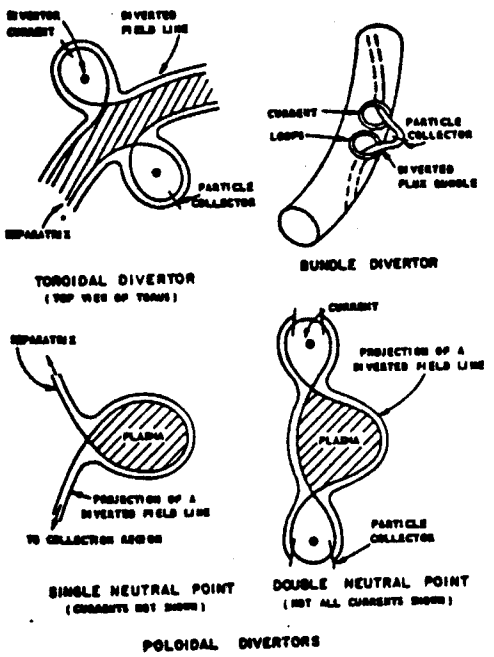

FIG. 1. Some proposed divertors for toroidal devices.

some proposed models are shown in Fig. 1. The mean thickness characterizing the plasma density "drop-off" perpendicular to the field lines is determined by a balance between the cross-field diffusion with coefficient $D_\perp$ and the parallel flow to the collectors on a time scale $\tau_\parallel$. For the model of a poloidal divertor that we consider here, this thickness is given approximately by [3]

$$\lambda \sim \sqrt{D_\perp \tau_\parallel}$$

For the purposes of this letter, $D_\perp$ (in the divertor region) will be taken to be some fraction of the Bohm value $[10^8\ (T_e/1\ \text{keV})/(16\ B/1\ \text{kG})\,\text{cm}^2/\text{s}]$. The electron temperature T_e is to be determined self-consistently from energy balance equations. This choice reflects a belief, substantiated by some experimental observations [4], that low-frequency turbulence (say drift waves) may be present in the divertor and the Bohm-type scaling of $D_\perp$. With this choice for $D_\perp$, one needs to ascertain what $\tau_\parallel$ might be. The low-frequency turbulence will not affect $\tau_\parallel$ because all except the short-wavelength (compared to the ion gyroradius) forms of these waves cannot change the magnetic moment of the particle. Therefore, particle collisions and/or high-frequency turbulence ($\omega \gtrsim \Omega_i$ instabilities) will determine parallel transport times.

Since the distance through which plasma must flow along field lines to reach the divertor collector region is quite long (2 to 10 m in possible next-generation devices, 50 m in future large-scale fusion reactors), a lower limit on $\tau_\parallel$ is the time it takes the plasma to flow there at the speed v_i, i.e.,

$$\tau_{\parallel\,\min} \sim L/v_i$$

where L is the mean distance to be travelled to the collector plates and

$$v_i = (\max\,(T_e,\ T_i)/m_i)^{1/2}$$
$$= 3.1 \times 10^7 \left[\frac{\max\,(T_e,\ T_i)}{A}\right]^{1/2}\ \text{cm/s}$$

for ions of A amu. For illustrative purposes, we consider two numerical examples: 1) a next-generation tokamak with divertor, and 2) a fusion power reactor. One notes that for case 1, $\lambda_{\min} \sim \sqrt{D_\perp \tau_{\parallel\min}} \sim 1/2$ cm and for case 2, $\lambda_{\min} \sim 2$ cm.

Since the thermal velocity of the electrons is much higher than that of the ions, there will be an electrostatic sheath at the collectors. Most electrons will be electrostatically contained in their parallel motion by this sheath. Since only the faster electrons will penetrate the sheath and be collected, the energy lost per electron is greater than $(3/2)\,T_e$. Consequently, the electrons are cooled in the scrape-off zone. The ions, however, are attracted by the sheath; the ion energy lost is $\sim (3/2)\,T_i$ per particle so there is no substantial ion cooling in the scrape-off zone. Consequently, one expects T_e to drop below T_i in the scrape-off zone.

The poloidal configurations considered in this letter (see Fig. 1) are such that the plasma, once in the (outer) divertor zone, must move through a region of higher magnetic field ($B \sim 1$ R) in order to reach the collectors. In these cases, there may be some magnetic confinement as in a mirror machine. The magnetic mirror ratio is less than 2:1 along the field line so that the mirror is fairly weak. One sees that at least half the plasma in the scrape-off region would not be "trapped" by the mirror; it would flow out in a time $\tau_{\parallel\min}$. The maximum time that the remaining mirror-confined plasma could be trapped would be of the order of the 90° scattering time [5], the time for ions to be scattered into the loss cone:

$$\tau_{i\max} \sim \tau_{ii} \sim \frac{3 \times 10^{-3} A^{1/2} (T_i/1\ \text{keV})^{3/2}}{[n_e/10^{13}\,\text{cm}^{-3}]Z^3}\ \text{sec}$$

As can be seen from $\lambda \sim \sqrt{D_\perp \tau_\parallel}$, the density drop-off thickness can vary by as much as a factor of $\sqrt{\tau_{\parallel\max}/\tau_{\parallel\min}} \sim 10$ (case 1) and ~ 100 (case 2).

depending upon the appropriate parallel flow time [6].

In addition to the classical processes discussed above, plasma instabilities can decrease the minimum flow time. Specifically, since the mirror-confined plasma has a loss-cone, it is susceptible to all the usual loss-cone-driven microinstabilities [7]. The four most important loss-cone-driven instabilities for this case are: (1) the Post-Rosenbluth convective loss-cone instability [8]; (2) the absolute loss-cone instabilities [9]; (3) the negative-energy loss-cone modes [10]; and (4) the drift-cone modes [11]. Before discussing these modes in detail, one needs to estimate some parameters of this mirror-confined plasma. First, one needs to know the ratio of the ion gyro-radius, ρ_i, to the plasma inhomogeneity scale lengths. For case 1, $\rho_i \sim 1$ cm and case 2, $\rho_i \sim 0.7$ cm. Thus, it appears that the scrape-off thickness is from 5 (case 1) to 3 (case 2) ion gyro-radii in width. The characteristic inhomogeneity scale length along a magnetic field line is $L_{\nu\beta} \sim qR_0$, where $q = r B_T/R_0 B_p$ is the MHD-stability factor and R_0 the plasma major radius. For case 1, $L_{\nu\beta} \sim 420$ cm and case 2, $L_{\nu\beta} \sim 3000$ cm. Therefore, $L_{\nu\beta}/\rho_i \sim 4200$ for case 1 and 4300 for case 2. This is essentially an infinite, homogeneous plasma for loss-cone instability calculations where $\lambda_\beta \sim \rho_i \sqrt{m_i/m_e} \sim (40 - 70)\,\rho_i$.

The last three of the four loss-cone instabilities listed above are standing-wave (or absolute) modes that are typically found to be radially localized within a few gyro-radii. The drift-cone mode [11] has been shown to be present and unstable for radial scale lengths as short as one or two ion gyro-radii [12]. The negative-energy modes are finite-medium forms of the absolute loss-cone and drift-modes [7], which are most easily derived in infinite-medium theory. In general, for $L \gg \lambda_\perp$ as appears to be the case here, these standing wave instabilities are all unstable for $\omega_{pi} \geq \Omega_i$, (i.e. $n_i > 3.3 \times 10^{10}$ cm^{-3}, for $B = 25$ kG) where ω_{pi} is the ion plasma frequency and Ω_i is the ion gyro-frequency. (These modes generally require $T_{\perp e} < T_{\perp i}$, which seems reasonable to expect; however, n_i may drop below a few 10^{10} cm^{-3} if the above instabilities begin to appear and affect $\tau_\parallel$. Thus, these modes may stabilize somewhere between the separatrix and the wall). When this density threshold is exceeded the mode growth rates range from a few percent (for absolute loss-cone modes) to large fractions (for drift-cone modes) of the ion gyro-frequency. The non-linear consequences of the modes are apparently to enhance the pitch-angle scattering which causes the loss-cone to be filled in on a time scale of a few growth times [13]. If one presumes a modest growth rate of 0.01 Ω_i and requires 10 growth times for significant effects, then the loss-cone fill-in time is $\tau_{inst} \sim 10^3\,\Omega_i^{-1} \sim 5$ to 10 μs. For the divertor scrape off region considered here $\tau_{inst} \ll \tau_{\parallel\,min}$. This indicates that the instability could cause sufficient scattering to keep the loss-cone filled with particles and thus make $\tau_\parallel$ only a few times τ_{min}, at most.

In addition to the standing-wave modes discussed in the preceding paragraph, there are the convective loss-cone instabilities, which can give rise to significantly enhanced ("quasi-classical") scattering [14] into the loss cone by virtue of the long-range polarization fields of the ions in the convectively unstable plasma. The polarization fields around individual "test" ions extend only a few Debye lengths ($\lambda_D \ll \rho_i$) perpendicular to the field line, but they extend all the way to the mirror "throat" region along the lines, i.e. in essence, we have a zero of the parallel dielectric coefficient. For the divertor scrape-off region where we expect $\omega_{pe} < \Omega_e$ (i.e. $n_e < 6 \times 10^{13}$ cm^{-3} for case 1; $n < 9 \times 10^{13}$ cm^{-3} for case 2) and a fairly sharp loss cone, the effective collision frequency for scattering into the loss cone is given approximately by [14]

$$\nu_{eff} \simeq \frac{1}{\tau_{ii}} \left(\frac{\tau_i}{\tau_e}\right)^{3/2} \left(\frac{m_e}{m_i}\right)^{1/2} \frac{\exp\,(2\ \mathrm{Im}\,k_\parallel L)}{\mathrm{Im}\,k_\parallel L\,\ln\Lambda}$$

where

$$\mathrm{Im}\,k_\parallel \sim \frac{0.1}{\rho_i}\frac{\omega_{pe}}{\Omega_e}\ \mathrm{cm}^{-1}$$

$$\sim 9.5 \left(\frac{m_e}{m_i}\right)^{1/2} \left(\frac{n/10^{13}\,\mathrm{cm}^{-3}}{T_i\ /\ 1\ \mathrm{keV}}\right)^{1/2}\ \mathrm{cm}^{-1}$$

For the parameters used above one finds for case 1 ($\mathrm{Im}\,k_\parallel = 0.09$ cm^{-1},

$$\omega_{pe} \sim .1\,\Omega_e,\ L_{\nu\beta} = 420\ \mathrm{cm}) \quad \nu_{eff}\,\tau_{ii} \sim 10^{73}$$

and for case 2

$$(\mathrm{Im}\,k_\parallel = .01\ \mathrm{cm}^{-1},\ \omega_{pe} \sim .1\,\Omega_e,\ L_{\nu\beta} = 3000\ \mathrm{cm})$$

$$\nu_{eff}\,\tau_{ii} \sim 10^{21}$$

These are absurdly large because the parallel growth length is of the order of a few hundredths of $L_{\nu\beta}$ in both cases. In such a situation, one expects [14] ν_{eff} to be no larger than the ion bounce frequency $\omega_{bi} \sim v_{Ti}/L_{\nu\beta}$, since otherwise the instability is filling the loss-cone before the plasma even knows it has one. We thus conclude for the divertor scrape-off region that $\tau_\parallel \sim \omega_{bi}^{-1} \sim L/v_{Ti}$, which is equal to $\tau_{\parallel\,min}$ to within a factor of $\sqrt{\max\,(T_e, T_i)/T_i}$.

The derivations of the loss-cone-driven modes in mirror-confined plasmas [7, 12, 14] have not taken shear into account since it is unimportant in open-ended systems. However, in tokamaks,

TABLE I. DIVERTOR CHARACTERISTICS

Case 1 *(Next Generation Device)	Case 2 **(Fusion Reactor)
Hydrogen	Mass = 2.5 amu
B_T = 25 kgauss	B_T = 30.8 kgauss
T_e = .2 keV } Diverter	T_e = 7 keV
T_i = .33 keV }	T_i = 9 keV
L = 1000 cm	L = 6000 cm
q = 3.0	q = 2.3
R_o = 140 cm	R_o = 1300 cm
a = 450 cm	a = 500 cm
n = 5 x 10^{11} cm^{-3} (@ separatrix)	n = 10^{11} - 5 x 10^{12} cm^{-3}
$D_\perp = \frac{1}{10} D_{Bohm}$ = 5.0 x 10^3 cm^2/sec	$D_\perp = \frac{1}{50} D_{Bohm}$ = 2.8 x 10^4 cm^2/sec
$\tau_{H\ min}$ = 56 μsec	$\tau_{H\ min}$ = 100 μsec
$\tau_{H\ max}$ = 11 msec	$\tau_{H\ max}$ = .3 to 13 sec
λ_{min} = .5 cm	λ_{min} = 2 cm
ρ_i = .1 cm	ρ_i = .7 cm
$L_{VB} \sim qR_o \sim$ 420cm ~ 4200 ρ_i	$L_{VB} \sim qR_o \sim$ 3000 cm ~ 4300 ρ_i
$\omega_{pi} > \Omega_i \Rightarrow n_i > 3.3 \times 10^{10} cm^{-3}$	$\omega_{pi} > \Omega_i \Rightarrow n_i > 2.0 \times 10^{10} cm^{-3}$
$\omega_{pe} < \Omega_e \Rightarrow n_e < 6.1 \times 10^{13} cm^{-3}$	$\omega_{pe} < \Omega_e \Rightarrow n_e < 9.2 \times 10^{13} cm^{-3}$
Ω_i = 2.4 x 10^8 rad/sec	Ω_i = 1.18 x 10^8 rad/sec
f = 38.2 MH_z	f = 18.8 MH_z
λ_{De} = .015 cm	λ_{De} = .2 to .03 cm
Im $k_{\|}$ = .09 cm^{-1}	Im $k_{\|}$ = .005 to .033 cm^{-1}

*Parameters taken from Ref. [18].

**Parameters taken from Ref. [19]

the magnetic field is sheared in the minor-radius direction, with a typical scale length

$$\frac{1}{L_s} \sim \frac{1}{qR_o} \frac{r}{q} \frac{\partial q}{\partial r} \leq \frac{1}{10r}$$

and it is worth considering the effects of shear on these modes. The effective parallel wavelength of a mode in a sheared magnetic field is given by [15]

$$k_{\|} = k_z + k_y \frac{x}{L_s}$$

where k_y, k_z are the local y, z components of the wave propagation and x is the distance from the modal surface investigated. For a mode radially localized to a width δx, the effective k over the region of interest is

$$k_{\|} \sim k_z\left[1 + \frac{k_y \delta x}{k_z L_s}\right]$$

For the microinstabilities discussed above

$$\delta x \geq \rho_i, \sqrt{m_i/m_e} > k_y \rho_i > 1 \text{ and } k_z L_s \sim \frac{L_s}{40\ \rho_i}$$

Thus, for a typical shear length of, say, 1000 cm, the effect of shear on the effective parallel wavelength is quite small. It should be noted that if, in addition to the shear, there is significant fanning of the magnetic field lines as in minimum-B mirror systems, then these loss-cone-driven instabilities might be more significantly affected by the magnetic topology [16]. Shear may also affect $D_\perp$ [17].

In summary, we have found that while the scrape-off region in a divertor may appear to contain a mirror-confined plasma, the plasma so confined seems to be unstable to a large variety of micro-instabilities driven by the free energy associated

with the loss-cone distribution. The net result of the instabilities apparently would be to reduce the expected $\tau_{\parallel\,max} \sim \tau_{\parallel}$ to a value very close to the free flow value of $L/v_{\parallel}$. Thus, the best estimate of the parallel flow time is probably $\tau_{\parallel} \sim \tau_{\parallel\,min}$, which implies a relatively thin density "drop-off" thickness of only a few centimetres or less. As such, the hopes of having an effective "screening" divertor diminish, i.e. the probability of ionizing an incoming neutral in the scrape-off zone is very small.

ACKNOWLEDGEMENTS

The authors are grateful to G. G. Kelley (ORNL) and J. Schmidt (PPPL) for illuminating discussions on properties of divertors.

This work was sponsored jointly by USAEC and Wisconsin Electric Utilities Research Foundation (A. T. M., G. A. E.) and by the USAEC under contract with Union Carbide Corporation (J. D. C.).

REFERENCES

[1] MENSE, A.T., Univ. of Wisconsin (Madison), Nuclear Engr. Dept. Fusion Design Memo, FDM-100, Apr. 1974; Also see HOGAN, J.T., CLARKE, J.F., J. Nucl. Mat. 53 (1974) 1.

[2] EMMERT, G.A., MENSE, A.T., DONHOWE, J.M., Proc. 1st Top. Meeting on Technology of Controlled Thermonuclear Fusion (April 1974), San Diego. Also see J. Nucl. Mat. 53 (1974) 39.
KITSUNEZAKI, A., MAEDA, H., SHIMOMURA, Y., TOSHIKAWA, M., 3rd Int. Symp. Toroidal Plasma Confinement, Garching 1973, paper G-2.
COLVEN, C., GIBSON, A., SCOTT, P.E., 5th Europ. Conf. Controlled Fusion and Plasma Physics 1, Grenoble (1972) 6.
PDX, The Poloidal Divertor Experiment, paper 47, Joint EURATOM-US Workshop on Large Tokamak Designs, Culham (May 1974).

[3] MENSE, A.T., EMMERT, G.A., Bull. Am. Phys. Soc. 18 (1973) 1365; MENSE, A.T., Ph. D. Diss. Nuclear Engr. Dept., Univ. of Wis., 1975 (to be published).

[4] SCHMIDT, J.A., private communication about FM-1.

[5] BRAGINSKII, S.I., in Reviews of Plasma Physics 1, Consultants Bureau, New York (1965) 219.

[6] This calculation ignores the effect of sheaths at collecting plates and secondary emission of electrons at collecting plates due to ion bombardment.

[7] For synopsis of the modes see: HORTON, C.W., Jr., CALLEN, J.D., ROSENBLUTH, M.N., Phys. Fluids 14 (1971) 2019; BALDWIN, D.E., et al., in Plasma Physics and Controlled Fusion Research, 2, (Proc. 4th Int. Conf. Madison, 1971), IAEA, Vienna (1971) 735; CALLEN, J.D., Ph.D. Thesis, MIT, CSR T-68-3 (1968).

[8] ROSENBLUTH, M.N., POST, R.F., Phys. Fluids 8 (1965) 547.

[9] McCUNE, J.E., CALLEN, J.D., Plasma Physics 12 (1969) 315 and references therein; BERK, H.L., et al., in Plasma Physics and Controlled Fusion Research 2, IAEA, (Vienna, 1968) 151; also see Ref.[7].

[10] BERK, H.L., PEARLSTEIN, L.D., CALLEN, J.D., HORTON, C.W., ROSENBLUTH, M.N., Phys. Rev. Lett. 22 (1969) 876; see also Ref.[7].

[11] POST, R.F., ROSENBLUTH, M.N., Phys. Fluids 9 (1966) 730; MIKHAILOVSKII, A.B., Nucl. Fusion 5 (1965) 125.

[12] CORDEY, J.G., KUO-PETRAVIC, L.G., PETRAVIC, M., Nucl. Fusion 8 (1968) 163; see also Ref.[7].

[13] See, for example: BYERS, J.A., GREWAL, M., Phys. Fluids 13 (1970) 1819.

[14] BALDWIN, D.E., CALLEN, J.D., Phys. Rev. Lett. 28 (1972) 1688.

[15] See, for example: DAVIDSON, J.N., KAMMASH, T., Nucl. Fusion 8 (1968) 203.

[16] BALDWIN, D.E., Phys. Fluids 17 (1974) 1346.

[17] Drift waves are sensitively affected by shear, thus the scrape-off region may be thinner owing to a reduction of $D_{\perp}$.

[18] MEADE, D.M., et al., in Plasma Physics and Controlled Nuclear Fusion Research (Proc. 5th Int. Conf. Tokyo, 1974) 1, IAEA, Vienna (1975) 606.

[19] BADGER, B., et al., UWFDM-68, University of Wisconsin, March 1974.

(Letter received 2 April 1975
Final version received 13 June 1975)

A POSSIBLE CAUSE OF ELECTRON BEAM PINCHES NEAR A TARGET

J. G. LINHART

It has been suggested that a "super-pinch" might develop on an intense electron beam as a result of its passage through some discontinuity, such as a conducting target [1].

Some evidence of this has been found recently [2, 3] and it seems, therefore, appropriate to describe the phenomenon in a greater detail than has been done in Ref. [1].

Let us start with a single-particle analogy. When an electron and a positron collide, it is probable that they will annihilate each other with subsequent emission of γ-radiation (Fig. 1).

There is a similar process in classical physics known as the transition radiation [4, 5]. Let us describe an extreme example of this process, i.e. what happens when an electron -e (or a tight bunch of charges of one sign) impinges (at right angles) on a metallic boundary (Fig. 2). The description of this process can be made in terms of an image charge +e approaching -e from the opposite direction. If the speed of the electron is v, then the speed of +e will be $v_+ = -v$. When -e meets +e at the boundary L, the electric fields between +e and

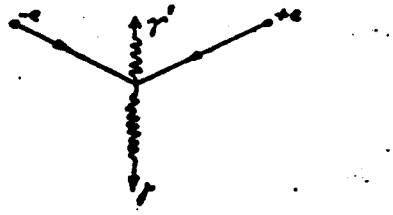

FIG. 1. e-p annihilation. Two γ-quanta are emitted.

APPENDIX F

Computer Listing of Divertor References as of June 1976

Print 1/5/1-16
DIALOG Search File12: INSPEC-PHYSICS 70-76 ISS 16 (COPR. I.E.E.)

894087 A7635209
A TOKAMAK-DIVERTOR EXPERIMENT IN THE DC OCTOPOLE
PRATER, R., FREEMAN, R.L., HAMADA, Y., MOELLER, C., OHKAWA, T., TAMANO, T. ; GENERAL ATOMIC CO., SAN DIEGO, CA, USA
; IAEA
5TH INTERNATIONAL CONFERENCE ON PLASMA PHYSICS AND CONTROLLED NUCLEAR FUSION RESEARCH 291-7 1975
I 11-15 NOV. 1974 IAEA TOKYO, JAPAN
PUBL: IAEA VIENNA, AUSTRIA
DESCRIPTORS: PLASMA CONFINEMENT, PLASMA PROBES
IDENTIFIERS: DC OCTOPOLE, FLUX CONFIGURATION, AXISYMMETRIC DIVERTORS, CONDUCTIVITY ELECTRON TEMPERATURE, PLASMA ENERGY DENSITY, MAGNETIC PROBES, PLASMA CURRENT DISTRIBUTION, TOKAMAK DIVERTOR EXPERIMENT
SECTION CLASS CODES: A6560, A6570
UNIFIED CLASS CODES: LGNAEB, LGRACV
AN OHMIC CURRENT HAS BEEN INDUCTIVELY DRIVEN IN THE D.C. OCTOPOLE. THE RESULTING FLUX CONFIGURATION RESEMBLES THAT OF A TOKAMAK WITH AXISYMMETRIC DIVERTORS. THE PEAK CURRENT IS 4 KA IN A TOROIDAL FIELD OF 450 G. THE DENSITY ON THE AXIS IS 4•10/SUP 11/ CM/SUP -3/ AND THE CONDUCTIVITY ELECTRON TEMPERATURE IS 27 EV. BECAUSE THE PLASMA ENERGY DENSITY IS LOW, MAGNETIC PROBES CAN BE INSERTED INTO THE PLASMA FOR MEASUREMENTS OF THE PLASMA CURRENT DISTRIBUTION. MAGNETIC PROBE TRACES THAT ARE QUIET AND REPRODUCIBLE AT ALL POSITIONS INDICATE THAT THE PLASMA HAS OBTAINED A STABLE EQUILIBRIUM. THE INITIAL STAGE OF THE DISCHARGE IS VERY SENSITIVE TO ERROR MAGNETIC FIELDS (4 REFS)

893935 A7635055
THE EFFECTS OF IMPURITIES AND MAGNETIC DIVERTORS ON HIGH-TEMPERATURE TOKAMAKS
MEADE, D.M., FURTH, H.P., RUTHERFORD, P.H., SEIDL, F.G.P., DUCHS, D.F. ; PLASMA PHYS. LAB., PRINCETON UNIV., PRINCETON, NJ, USA
; IAEA
5TH INTERNATIONAL CONFERENCE ON PLASMA PHYSICS AND CONTROLLED NUCLEAR FUSION RESEARCH 605-21 1975
I 11-15 NOV. 1974 IAEA TOKYO, JAPAN
PUBL: IAEA VIENNA, AUSTRIA
DESCRIPTORS: PLASMA TRANSPORT PROCESSES, PLASMA CONFINEMENT
IDENTIFIERS: MAGNETIC DIVERTORS, TOKAMAK PLASMA TRANSPORT CODE, IMPURITY INFLUX, STRIPPING, RADIATION, DIFFUSION, HEAT TRANSPORT, ADIABATIC COMPRESSION, DIVERTOR BOUNDARY CONDITIONS, IMPURITY CONTROL, NEUTRAL BEAM HEATING, CHARGE EXCHANGE
SECTION CLASS CODES: A6515, A6560
UNIFIED CLASS CODES: LGEACL, LGNAEB
A ONE-DIMENSIONAL TOKAMAK PLASMA TRANSPORT CODE HAS BEEN ADAPTED TO INCLUDE IMPURITY INFLUX, STRIPPING, RADIATION, AND DIFFUSION, AS WELL AS THE USUAL PROCESSES OF HYDROGEN PLASMA AND HEAT TRANSPORT, RECYCLING AT THE BOUNDARY, AND MULTI-GENERATION CHARGE-EXCHANGE. NEUTRAL-BEAM HEATING, ADIABATIC COMPRESSION, AND DIVERTOR BOUNDARY CONDITIONS ARE

User 720 (Item 1 of 16) Date:26oct76

INCLUDED AS OPTIONAL FEATURES. ILLUSTRATIVE COMPUTATIONS ARE GIVEN FOR PRESENT-DAY AND NEXT-GENERATION TOKAMAKS. THE PROBLEMS OF IMPURITY CONTROL ARE DISCUSSED, AND TWO TECHNICAL APPROACHES ARE EXAMINED IN GREATER DETAIL: THE TRANSIENT COLD-PLASMA SHIELD, AND THE POLOIDAL DIVERTOR (18 REFS)

887188 A7630324
A MAGNETOHYDRODYNAMIC THEORY OF DIVERTORS
BOOZER, A.H. ; PLASMA PHYS. LAB., PRINCETON UNIV., PRINCETON, NJ, USA
; EUROPEAN PHYS. SOC.
7TH EUROPEAN CONFERENCE ON CONTROLLED FUSION AND PLASMA PHYSICS 20 1975
I 1-5 SEPT. 1975 EUROPEAN PHYS. SOC. LAUSANNE, SWITZERLAND
PUBL: ECOLE POLYTECHNIQUE FEDERALE DE LAUSANNE LAUSANNE, SWITZERLAND
DESCRIPTORS: MAGNETOHYDRODYNAMICS, PLASMA CONFINEMENT
IDENTIFIERS: MAGNETOHYDRODYNAMIC THEORY OF DIVERTORS, ZERO ION TEMPERATURE, ION GYRORADIUS, ELECTRON TEMPERATURE, TOKAMAK
SECTION CLASS CODES: A6560, A6530
UNIFIED CLASS CODES: LGNAEB, LGHAEN
A TWO-FLUID MHD DIVERTOR MODEL IS STUDIED WITH ZERO ION TEMPERATURE. THE ELECTRONS ARE SHOWN TO LEAVE THE DIVERTOR MUCH CLOSER TO THE MAIN PLASMA BODY THAN THE IONS. THE DIVERTOR WIDTH IS FOUND COMPARABLE TO THE ION GYRORADIUS CALCULATED WITH THE ELECTRON TEMPERATURE (1 REFS)

DIALOG Search File12: INSPEC-PHYSICS 70-76 ISS 16 (COPR. I.E.E.)

852442 A7608875
MERCIER STABILITY OF NON-CIRCULAR CROSS-SECTION CONFIGURATIONS
GALVAO, R.M.O. ; DEPT. OF NUCLEAR ENGNG., MIT, CAMBRIDGE, USA
NUCL. FUSION (AUSTRIA) VOL.15, NO.5 785-92 OCT. 1975
CODEN: NUFUAU
DESCRIPTORS: PLASMA INSTABILITY, PLASMA CONFINEMENT
IDENTIFIERS: MERCIER STABILITY, PLASMA COLUMN, MAGNETIC CONFINEMENT CONFIGURATIONS, POLOIDAL DIVERTORS, TOROIDAL DIFFUSE PINCH, BELL SHAPED CURRENT DENSITY PROFILE, MHD EQUILIBRIUM, PLASMA STABILITY, HERRNEGGER MASCHKE SOLUTIONS, LOCALISED FLUTE MODES, NORMAL-D CROSS SECTION, PLASMA COLUMN CROSS SECTION, INVERTED-D
SECTION CLASS CODES: A6540, A6560, A6530
UNIFIED CLASS CODES: LGKAFF, LGNAEB, LGHAEN
THE INSTABILITY OF A PLASMA COLUMN AGAINST FLUTE MODES LOCALISED INSIDE THE COLUMN IS STUDIED FOR A BELL-SHAPED CURRENT-DENSITY PROFILE; MAGNETIC CONFINEMENT CONFIGURATIONS WHICH CAN BE USED WITH POLOIDAL DIVERTORS ARE CONSIDERED. THE IDEAL MHD-EQUILIBRIUM IS DESCRIBED BY MEANS OF THE HERRNEGGER-MASCHKE SOLUTIONS OF THE EQUILIBRIUM EQUATIONS. A TOROIDAL DIFFUSE PINCH CONFIGURATION IS EXAMINED: THE STABILITY CONDITIONS FOR A CROSS-SECTION RESEMBLING A NORMAL D ARE SIMILAR TO THOSE FOR AN INVERTED D CROSS-SECTION; THESE CROSS-SECTIONS ARE PREFERABLE TO A RECTANGULAR CROSS-SECTION IF THE PLASMA COLUMN IS GREATLY ELONGATED VERTICALLY (27 REFS)

799471 A7561553
OBSERVATION OF EQUILIBRIUM AND DISRUPTIVE INSTABILITY IN A DIVERTOR-TOKAMAK CONFIGURATION IN THE DC OCTOPOLE
PRATER, R., HAMADA, Y., FREEMAN, R., MOELLER, C., TOMANO, T., OHKAWA, T. ; GENERAL ATOMIC CO., SAN DIEGO, CA, USA
PHYS. REV. LETT. (USA) VOL.34, NO.23 1432-5 9 JUNE 1975
CODEN: PRLTAO
DESCRIPTORS: MAGNETOHYDRODYNAMICS, PLASMA INSTABILITY, PLASMA CONFINEMENT
IDENTIFIERS: DISRUPTIVE INSTABILITY, MAGNETOHYDRODYNAMIC EQUILIBRIUM, TOKAMAK WITH POLOIDAL DIVERTORS, DC OCTOPOLE
SECTION CLASS CODES: A6540, A6560
UNIFIED CLASS CODES: LGKAFF, LGNAEB
MAGNETOHYDRODYNAMIC EQUILIBRIUM PROPERTIES OF A PLASMA, WITH CHARACTERISTICS SIMILAR TO THOSE OF A TOKAMAK WITH POLOIDAL DIVERTORS, HAVE BEEN DETERMINED, USING A D.C. OCTOPOLE. A CURRENT-DISRUPTIVE INSTABILITY IS OBSERVED WHEN THE SAFETY FACTOR IS LOW (11 REFS)

757868 A7532499, B7517980, C7510790
A FUSION POWER PLANT
MILLS, R.G.
REPORT NO.: MATT-1050 ISSUED BY: PRINCETON UNIV., N.J., USA
CONTRACT NO.: AT(11-1)-3073

User 720 (Item 4 of 16) Date:26oct76 3189

AUG. 1974
DESCRIPTORS: FUSION REACTORS, PLASMA CONFINEMENT, NUCLEAR POWER STATIONS, NUCLEAR REACTOR MATERIALS, NUCLEAR REACTOR OPERATION, DIVERTORS, ENVIRONMENTAL ENGINEERING, SAFETY, MAINTENANCE ENGINEERING
IDENTIFIERS: OPERATING CYCLE OF FUSION POWER PLANT, REACTOR MATERIALS, HEAT TRANSFER SYSTEMS, MAINTENANCE OF REACTOR, REPAIR OF REACTOR OVERHAUL OF REACTOR, FUSION POWER PLANT, TECHNICAL FEATURES, ADVANTAGES, PLASMA FUSION PRINCIPLES, PLASMA CONTROL, DIVERTER, VACUUM SYSTEM, FUEL INJECTION, MAGNETICS, ENERGY CONVERSION SYSTEMS, HAZARDS, ENVIRONMENTAL COMPATIBILITY
SECTION CLASS CODES: A4640, B5220, A6560, C7854, A4630, B1263
UNIFIED CLASS CODES: HMGAAP, LGNACX, TEEAAG, VMKGAA, HMEAAZ, ADGDAL
AVAILIABILITY: NTIS, SPRINGFIELD, VA. 22151, USA
THE TECHNICAL FEATURES AND ADVANTAGES OF ELECTRIC POWER PLANTS BASED ON PLASMA FUSION PRINCIPLES ARE DISCUSSED. THE CHARACTERISTICS OF PLASMAS AND THE PROBLEMS OF PLASMA CONTROL ARE ANALYZED. THE OPERATING CYCLE OF A FUSION POWER PLANT IS EXPLAINED. THE SUBJECTS DISCUSSED INCLUDE THE FOLLOWING: (1) THE DIVERTER AND VACUUM SYSTEM, (2) FUEL INJECTION, (3) MAGNETICS, (4) CHOICE OF MATERIALS FOR THE REACTOR, (5) HEAT TRANSFER AND ENERGY CONVERSION SYSTEMS, (6) HAZARDS, (7) ENVIRONMENTAL COMPATIBILITY, AND (8) MAINTENANCE, REPAIR, AND OVERHAUL OF THE REACTOR

DIALOG Search File12: INSPEC-PHYSICS 70-76 ISS 16 (COPR. I.E.E.)

744962 A7524569, B7513766
THE PROBLEMS OF DIVERTORS
TENNEY, F.H. : PRINCETON UNIV., N.J., USA
; AMERICAN NUCLEAR SOC
TRANS. AM. NUCL. SOC. (USA) VOL. 19 7 OCT. 1974
CODEN: TANSAO
CONF: AMERICAN NUCLEAR SOCIETY 1974 WINTER MEETING. (SUMMARIES) 27-31 OCT. 1974 AMERICAN NUCLEAR SOC WASHINGTON, D.C., USA
DESCRIPTORS: FUSION REACTORS
IDENTIFIERS: DIVERTORS, MAGNETICALLY CONFINED FUSION REACTOR, VERY LOW NEUTRAL PRESSURE, HIGH PLASMA EDGE TEMPERATURE, LIMITING MAGNETIC SURFACE, CONFINING FIELD, SEPARATRIX SURFACE, SCRAPEOFF PLASMA
SECTION CLASS CODES: A4640, B5220
UNIFIED CLASS CODES: HMGAAP
THE DIVERTOR CONCEPT WAS DEVELOPED TO SOLVE THREE PROBLEMS THAT WERE ENVISIONED FOR A STEADY-STATE MAGNETICALLY CONFINED FUSION REACTOR: NAMELY, HOW TO MAINTAIN A STEADY FLOW OF MATERIAL OUT OF THE CONFINED PLASMA AND INTO VACUUM PUMPS WHILE MAINTAINING A VERY LOW NEUTRAL PRESSURE BETWEEN THE PLASMA AND THE WALLS OF THE VACUUM VESSEL, HOW TO MAINTAIN A HIGH PLASMA EDGE TEMPERATURE, AND HOW TO REDUCE THE FLOW OF IMPURITIES FROM THE WALLS INTO THE REACTING PLASMA. IN SUCH A FUSION REACTOR THE PLASMA IS TO BE CONFINED IN A SPECIAL MAGNETIC FIELD WHICH CLOSES ON ITSELF IN SUCH A MANNER AS TO DEFINE A SET OF NESTED, CLOSED (TOROIDAL) MAGNETIC SURFACES THAT DO NOT INTERSECT ANY MATERIAL WALLS. THE DIVERTOR, BY VIRTUE OF ITS OWN COILS, PRODUCES A LIMITING MAGNETIC SURFACE OF THE CONFINING FIELD, CALLED THE SEPARATRIX SURFACE, OUTSIDE OF WHICH THE MAGNETIC SURFACES DO INTERSECT MATERIAL WALLS. PLASMA THAT PASSES OUTWARD ACROSS THE SEPARATRIX SURFACE, CALLED THE SCRAPEOFF PLASMA, CAN FLOW EASILY ALONG THE DIVERTED MAGNETIC FIELD LINES TO WALLS DISTANT FROM THE REACTING PLASMA. THE SCRAPEOFF PLASMA CONSTITUTES THE BOUNDING MEDIUM FOR THE PLASMA INSIDE THE SEPARATRIX SURFACE

740881 A7525210
KINETIC THEORY OF PLASMA SCRAPE-OFF IN A DIVERTOR TOKAMAK
HINTON, F.L., HAZELTINE, R.D. ; UNIV. TEXAS, AUSTIN, USA
PHYS. FLUIDS (USA) VOL.17 NO.12 2236-40 DEC. 1974
CODEN: PFLDAS
DESCRIPTORS: PLASMA CONFINEMENT, PLASMA TRANSPORT PROCESSES
IDENTIFIERS: PLASMA SCRAPE OFF, KINETIC THEORY, DIVERTOR TOKAMAK, PLASMA TRANSPORT, POLOIDAL DIVERTOR
SECTION CLASS CODES: A6560, A6515
UNIFIED CLASS CODES: LGNAEB, LGEACL
A KINETIC THEORY MODEL IS USED TO STUDY PLASMA TRANSPORT IN A TOKAMAK WITH A POLOIDAL DIVERTOR (5 REFS)

724007 A7512275
FIRST-WALL PROTECTION

User 720 (Item 7 of 16) Date:26oct76 3190

MCCRACKEN, G.M. : UKAEA, ABINGDON, ENGLAND
: IAEA
NUCL. FUSION (AUSTRIA) SPEC. SUPPL 471-8 1974 CODEN: NUFUAU
CONF: WORKSHOP ON FUSION REACTOR DESIGN PROBLEMS 29 JAN. - 15 FEB. 1974 IAEA ABINGDON, BERKS., ENGLAND
DESCRIPTORS: FUSION REACTORS, RADIATION PROTECTION, NEUTRON EFFECTS
IDENTIFIERS: FIRST WALL PROTECTION, INDIVIDUAL PARTICLE INTERACTIONS, SURFACE EFFECTS UNDER PULSED OPERATION, GAS BLANKETS, DIVERTORS
SECTION CLASS CODES: A4640
UNIFIED CLASS CODES: HMGAAP
THE DISCUSSION OF FIRST-WALL PROTECTION HAS BEEN DIVIDED INTO FOUR SECTIONS: (I) SURVEY OF INDIVIDUAL PARTICLE INTERACTIONS: (II) SURFACE EFFECTS UNDER PULSED OPERATION; (III) GAS BLANKETS; AND (IV) DIVERTORS. THE AUTHOR IS CONCERNED PRIMARILY WITH INDIVIDUAL PARTICLE REACTIONS AT THE FIRST WALL AND WITH MEANS OF PROTECTING THE WALL FROM EROSION

719223 A7509507
BUNDLE DIVERTORS AND TOPOLOGY
TAYLOR, J.B.
REPORT NO.: CLM-R-132 ISSUED BY: UKAEA, ABINGDON, BERKS., ENGLAND
FEB. 1974
DESCRIPTORS: TOPOLOGY, TOKAMAK DEVICES, PLASMA CONFINEMENT
IDENTIFIERS: BUNDLE DIVERTORS, TOPOLOGY, MAGNETIC SURFACES, TOPOLOGICALLY IMPOSSIBLE
SECTION CLASS CODES: A6580, A1110
UNIFIED CLASS CODES: LGSAZW, DBCEMD
AVAILIABILITY: HMSO, LONDON, ENGLAND
IT IS POINTED OUT THAT A PERFECT :BUNDLE DIVERTOR:, COMPOSED OF MAGNETIC SURFACES, IS TOPOLOGICALLY IMPOSSIBLE

DIALOG Search File12: INSPEC-PHYSICS 70-76 ISS 16 (COPR. I.E.E.)

699734 A7474801, B7440369
THE USE OF EFFUSORS TO IMPROVE DIVERTOR PERFORMANCE
HUSSEINY, A.A., IMPINK, A.J., JR., SABRI, Z. ; CARNEGIE-MELLON UNIV., PITTSBURGH, PA., USA
; AMERICAN NUCLEAR SOC., USAEC
1ST TOPICAL MEETING ON THE TECHNOLOGY OF CONTROLLED NUCLEAR FUSION (ABSTRACTS ONLY RECEIVED) 90 1974
16-18 APRIL 1974 AMERICAN NUCLEAR SOC., USAEC SAN DIEGO, CALIF., USA
PUBL: AMERICAN NUCLEAR SOC. HINSDALE, ILL., USA
DESCRIPTORS: FUSION REACTORS, PLASMA CONFINEMENT
IDENTIFIERS: EFFUSORS, DIVERTORS, THERMOMOLECULAR EFFUSION, PLASMA MACHINE, HONEYCOMB DOUBLE WALL STRUCTURE, DUCTS, FIRST WALL, POROUS MATERIALS, STEADY STATE TORCIDAL FUSION DEVICE
SECTION CLASS CODES: A4640, B5220, A6560
UNIFIED CLASS CODES: HMGAAP, LGNAEB
THE AUTHORS HAVE INVESTIGATED THE POSSIBILITY OF AUGMENTING THE FUNCTION OF PRESENT DIVERTORS BY THE USE OF AN EFFUSOR. THE CONVENTIONAL WALL OF THE PLASMA MACHINE IS REPLACED IN THIS SITUATION BY AN EFFUSOR IN THE FORM OF A HONEYCOMB DOUBLE WALL STRUCTURE EMBODIED WITH DUCTS TO CONVEY NATURAL GASES. THE FIRST WALL IS TO BE FABRICATED FROM POROUS MATERIALS COMPATIBLE WITH THE HIGH TEMPERATURE AND NEUTRONIC ENVIRONMENT OF THE PLASMA DEVICE. INTEGRATING AN EFFUSOR OF THIS TYPE IS A STEADY STATE TOROIDAL FUSION DEVICE IS NOT EXPECTED TO POSE LIMITATIONS ON THE BLANKET DESIGN OR TO CAUSE DISTURBANCE OF EITHER THE PLASMA OR THE MAGNETIC FIELD CONFIGURATIONS (2 REFS)

699708 A7478288, B7440343
TECHNICAL PROBLEMS IN LARGE NUCLEAR FUSION EXPERIMENTS
SEIDEL, E.R. ; MAX-PLANCK-INST. PLASMAPHYSIK, GARCHING, MUNCHEN, GERMANY
. KERNTECHNIK (GERMANY) VOL.16, NO.7 289-95 JULY 1974
CODEN: KERTAA
DESCRIPTORS: FUSION REACTORS, PLASMA DEVICES, PLASMA CONFINEMENT, STELLARATORS
IDENTIFIERS: NUCLEAR FUSION EXPERIMENTS, PLASMA PHYSICS CONDITIONS, FUSION REACTORS, PLASMA PARAMETERS, PLASMA DIMENSIONS, REACTOR CONDITIONS, DIVERTORS, FUEL, LARGE VOLUME MAGNETIC FIELD COILS, PLASMA WALL INTERACTION
SECTION CLASS CODES: A4640, B5220
UNIFIED CLASS CODES: HMGAAP
AFTER EXPLAINING THE MOST IMPORTANT PLASMA PHYSICS CONDITIONS FOR THE REALIZATION OF FUSION REACTORS, THE PLASMA PARAMETER OF SOME FUSION EXPERIMENTS IN OPERATION, UNDER CONSTRUCTION OR IN THE PLANNING STAGE ARE COMPARED WITH THE PLASMA DIMENSIONS. COMPLEX TECHNOLOGICAL PROBLEMS ARISE WITH INCREASING APPROACH TO THE REACTOR CONDITIONS AND THEIR SOLUTION MAY BE IMPORTANT ALSO FOR THE TECHNICAL REALIZATION OF A FUSION REACTOR. AS AN EXAMPLE, THE EFFECTS OF FORCES OF LARGE-VOLUME MAGNETIC FIELD COILS AND THE USE OF DIVERTORS TO REDUCE THE PLASMA-WALL INTERACTION AND TO REMOVE BURNTUP FUEL ARE DESCRIBED (26 REFS)

DIALOG Search File12: INSPEC-PHYSICS 70-76 ISS 16 (COPR. I.E.E.)

647054 A7444360
MULTIPOLE TOKAMAK EQUILIBRIA WITH FINITE BETA
FENEBERG, W., LACKNER, K. ; MAX-PLANCK-INST. PLASMAPHYS., GARCHING, MUNCHEN, GERMANY
; EUROPEAN PHYS. SOC., ACAD. SCI., USSR, ET AL
6TH EUROPEAN CONFERENCE ON CONTROLLED FUSION AND PLASMA PHYSICS. VOL.I 209-12 1973
30 JULY - 4 AUG. 1973 EUROPEAN PHYS. SOC., ACAD. SCI., USSR, ET AL MOSCOW, USSR
PUBL: JOINT INST. NUCL. RES. MOSCOW, USSR
DESCRIPTORS: PLASMA CONFINEMENT, TOKAMAK DEVICES
IDENTIFIERS: MULTIPOLE TOKAMAK EQUILIBRIA, PLASMA CONFIGURATIONS, TRIANGULAR DEFORMATIONS, STABILITY WITH MAGNETIC DIVERTORS, FINITE BETA, ELLIPTIC DEFORMATIONS
SECTION CLASS CODES: A6560
UNIFIED CLASS CODES: LGNAEB
A METHOD IS DESCRIBED FOR THE COMPUTATION OF PLASMA CONFIGURATIONS WITH VARIOUS CURRENT PROFILES AND FINITE POLOIDAL BETA, HELD IN EQUILIBRIUM BY GIVEN EXTERNAL CURRENTS. APPLICATIONS TO CONFIGURATIONS COMBINING THE ELLIPTIC AND TRIANGULAR DEFORMATIONS DESIRABLE FOR STABILITY WITH MAGNETIC DIVERTORS ARE GIVEN (6 REFS)

402607 A7246745
ESTIMATION OF SCATTERING CENTER IN A DIVERTOR TYPE PLASMA SOURCE
TOYAMA, H., KURODA, T., HORIKOSHI, G. ; NAGOYA UNIV., JAPAN
PHYS. LETT. A (NETHERLANDS) VOL.39A NO.4 287-8 22 MAY 1972 CODEN: PYLAAG
DESCRIPTORS: PLASMA, DEVICES, PLASMA, CONFINEMENT
IDENTIFIERS: SCATTERING CENTRE RADIUS, DIVERTOR TYPE PLASMA SOURCE, PARTICLE TRAJECTORY, STATIONARY TORUS MACHINE
SECTION CLASS CODES: A1424
NUMERICAL CALCULATIONS OF THE PARTICLE TRAJECTORY IN A DIVERTOR TYPE PLASMA SOURCE SHOW THAT THE RADIUS OF THE SCATTERING CENTER IS PROPORTIONAL TO (MASS)/SUP 1/4/ (2 REFS)

User 720 (Item 15 of 16) Date:26oct76 3192

Print 11/5/1-24
DIALOG Search File12: INSPEC-PHYSICS 70-76 ISS 16 (COPR. I.E.E.)

926583 A7657505
VACUUM AND WALL PROBLEMS IN PRECURSOR REACTOR TOKAMAKS
COHEN, S.A. ; PLASMA PHYS. LAB., PRINCETON UNIV., PRINCETON, NJ, USA
; AMERICAN VACUUM SOC.
J. VAC. SCI. AND TECHNOL. (USA) VOL.13, NO.1 449-62 JAN.-FEB. 1976 CODEN: JVSTAL
CONF: PROCEEDINGS OF THE 22ND NATIONAL SYMPOSIUM OF THE AMERICAN VACUUM SOCIETY 28-31 OCT. 1975 AMERICAN VACUUM SOC. PHILADELPHIA, PA, USA
DESCRIPTORS: TOKAMAK DEVICES, PLASMA CONFINEMENT, VACUUM APPARATUS, SURFACE TREATMENT, REVIEWS
IDENTIFIERS: TOKAMAK DEVICES, DISCHARGE CHARACTERISTICS, IMPURITY EFFECTS, VACUUM SYSTEM, MAGNETIC FIELD INDUCED STRAINS, EDDY CURRENTS, PHONON BOMBARDMENT, SURFACE CLEANING PROCEDURES, PRINCETON LARGE TORUS, POLOIDAL DIVERTOR EXPERIMENT, ENERGETIC PARTICLE BOMBARDMENT
SECTION CLASS CODES: A6580, A7860, A6560, A0634
UNIFIED CLASS CODES: LGSAZW, NVRZAG, LGNAEB, BGGEAR
OPERATION OF THE TOKAMAK DEVICES IS REVIEWED WITH DETAILS OF THE DISCHARGE CHARACTERISTICS AND IMPURITY EFFECTS. THE VACUUM SYSTEM REQUIREMENT OUTLINED FOR THE PRINCETON LARGE TORUS AND POLOIDAL DIVERTOR EXPERIMENT WERE INFLUENCED BY THE MAGNETIC FIELD INDUCED STRAINS AND EDDY CURRENTS, ENERGETIC PARTICLE AND PHONON BOMBARDMENT. IN SITU SURFACE CLEANING PROCEDURES ARE DISCUSSED. IN THE TFTR ADDITIONAL PROBLEMS WERE DUE TO THE USE OF LARGE QUANTITIES OF TRITIUM AND LARGE BEAM POWERS (78 REFS)

904928 A7644717
PLASMA BEHAVIOUR NEAR A SEPARATRIX MAGNETIC SURFACE IN THE JFT-2A TOKAMAK
MAEDA, H., SHIMOMURA, Y., KITSUNEZAKI, A., OHTSUKA, H., NAGAMI, M., FUNAHASHI, A., MATOBA, T., KASAI, S., TAKEUCHI, H., TAKAHASHI, K., KUMAGAI, K., TOKUTAKE, T., NAGASHIMA, T., UEDA, N., YOSHIKAWA, M. ; JAPAN ATOMIC ENERGY RES. INST., TOKAI, IBARAKI, JAPAN
NUCL. FUSION (AUSTRIA) VOL.16, NO.1 148-9 FEB. 1976 CODEN: NUFUAU
DESCRIPTORS: TOKAMAK DEVICES
IDENTIFIERS: SEPARATRIX MAGNETIC SURFACE, JFT-2A TOKAMAK, PLASMA BEHAVIOUR, DIVERTOR REGION, ENERGY FLUXES, PLASMA COLUMN, PARTICLE FLUXES
SECTION CLASS CODES: A6560
UNIFIED CLASS CODES: LGNAEB
DESCRIBES PLASMA BEHAVIOUR NEAR THE DIVERTOR REGION, ESPECIALLY PARTICLE AND ENERGY FLUXES ALONG THE SEPARATRIX MAGNETIC SURFACE AT A PLASMA CURRENT BELOW 20 KA WHEN THE MAIN PLASMA COLUMN IS FREE FROM NEGATIVE SPIKE INSTABILITIES (2 REFS)

User 720 (Item 1 of 24) Date:26oct76

904363 A7644119
HELIOTRON AS A STEADY FUSION REACTOR
IIYOSHI, A., UO, K. ; PLASMA PHYS. LAB., FACULTY OF ENGNG., UNIV. OF KYOTO, GOKASHO, UJI, JAPAN
: IAEA
5TH INTERNATIONAL CONFERENCE ON PLASMA PHYSICS AND CONTROLLED NUCLEAR FUSION RESEARCH 619-30 1975
III 11-15 NOV. 1974 IAEA TOKYO, JAPAN
PUBL: IAEA VIENNA, AUSTRIA
DESCRIPTORS: FUSION REACTORS, PLASMA CONFINEMENT
IDENTIFIERS: STEADY FUSION REACTOR, HELIOTRON, OPTIMUM GEOMETRY, ROTATIONAL TRANSFORM, MAGNETIC FIELD CONFIGURATION, BUILT IN DIVERTOR
SECTION CLASS CODES: A4640, A6560
UNIFIED CLASS CODES: HMGAAP, LGNAEB
THE PAPER DEALS WITH A HYPOTHETICAL STEADY FUSION REACTOR BASED ON THE HELIOTRON. THE MAGNETIC-FIELD CONFIGURATION USED IS THE L=2 HELICAL HELIOTRON FIELD WITH NO TOROIDAL COILS. THIS MODEL PROVIDES THE SIMPLEST STRUCTURE OF HELIOTRON REACTOR WITH A BUILT-IN DIVERTOR. BY CHOOSING THE OPTIMUM GEOMETRY OF THE HELICAL COIL, A LARGE ROTATIONAL TRANSFORM AND A STRONG SHEAR ARE OBTAINED. FOR AN ESTIMATED MAXIMUM BETA OF 0.1=0.2, DIFFUSION REMAINS NEAR THE PLATEAU REGIME OF NEOCLASSICAL THEORY. HELIOTRONS TEST REACTOR MODELS FOR BOTH PHYSICAL AND TECHNOLOGICAL FEASIBILITY ARE DISCUSSED. CHARACTERISTICS OF THE HELIOTRON DIVERTOR ARE DISCUSSED WITH REGARD TO STEADY OPERATION (16 REFS)

900747 A7639898
TRANSPORT AND DIVERTOR STUDIES IN THE FM-1 SPHERATOR
ANDO, K., EJIMA, S., DAVIS, S., HAWRYLUK, R., HSUAN, H., MEADE, D., OKABAYASHI, M., SAUTHOFF, N., SCHMIDT, J., SINNIS, J. ; PLASMA PHYS. LAB., PRINCETON UNIV., PRINCETON, NJ, USA
: IAEA
5TH INTERNATIONAL CONFERENCE ON PLASMA PHYSICS AND CONTROLLED NUCLEAR FUSION RESEARCH 103-14 1975
II 11-15 NOV. 1974 IAEA TOKYO, JAPAN
PUBL: IAEA VIENNA, AUSTRIA
DESCRIPTORS: FUSION REACTORS, PLASMA CONFINEMENT, PLASMA TRANSPORT PROCESSES, PLASMA HEATING
IDENTIFIERS: DIVERTOR, FM-1 SPHERATOR, TOROIDAL FUSION DEVICES, TRANSPORT, LOWER HYBRID HEATING, DRIFT WAVE TURBULENCE, TRAPPED ELECTRON REGIME
SECTION CLASS CODES: A6560, A6550, A6515, A4640
UNIFIED CLASS CODES: LGNAEB, LGMAET, LGEACL, HMGAAP
FUNDAMENTAL PROBLEMS OF TOROIDAL FUSION DEVICES HAVE BEEN INVESTIGATED IN THE FM-1 SPHERATOR. THESE SUBJECTS INCLUDE THE TRANSPORT DUE TO DRIFT-WAVE TURBULENCE IN THE TRAPPED-ELECTRON REGIME, POLOIDAL DIVERTOR AND IMPURITIES, AND LOWER HYBRID HEATING (16 REFS)

DIALOG Search File12: INSPEC-PHYSICS 70-76 ISS 16 (COPR. I.E.E.)

894092 A7635214
FREE-BOUNDARY MHD-EQUILIBRIA
SUZUKI, Y., KAMEARI, A., NINOMIYA, H., MASUZAKI, M., TOYAMA, H. ; JAPAN ATOMIC ENERGY RES. INST., IBARAKI, JAPAN
; IAEA
5TH INTERNATIONAL CONFERENCE ON PLASMA PHYSICS AND CONTROLLED NUCLEAR FUSION RESEARCH 411-20 1975
I 11-15 NOV. 1974 IAEA TOKYO, JAPAN
PUBL: IAEA VIENNA, AUSTRIA
DESCRIPTORS: PLASMA CONFINEMENT, MAGNETOHYDRODYNAMICS
IDENTIFIERS: COMPUTATIONAL METHODS, PLASMA EQUILIBRIUM, DIVERTOR HOOPS, FREE BOUNDARY MHD EQUILIBRIA, SHELL LESS TOKAMAK, TOROID, NONCIRCULAR CROSS SECTION
SECTION CLASS CODES: A6560, A6530, A6540
UNIFIED CLASS CODES: LGNAEB, LGHAEN, LGKAFF
THREE PROCEDURES ARE PRESENTED FOR A SYSTEMATIC DESIGN OF THE MAINTAINING FIELDS OF LARGE SHELL-LESS TOKAMAKS WITH CIRCULAR OR NON-CIRCULAR PLASMA CROSS-SECTION. THESE STEPS ARE CLOSELY RELATED TO THE FREE-BOUNDARY PROBLEMS OF MHD-EQUILIBRIA, AND FOR TWO OF THEM NEW COMPUTATIONAL METHODS ARE DEVELOPED. ONE IS TO CALCULATE THE MAINTAINING FIELDS FOR AN AXISYMMETRIC TOROIDAL MHD-EQUILIBRIUM WITH THE GIVEN PLASMA PARAMETERS WHICH ARE REQUIRED BY EXPERIMENTAL AIMS, AND THE OTHER IS TO SOLVE THE PLASMA EQUILIBRIUM PROBLEM UNDER THE GIVEN MAINTAINING FIELDS FOR THE CASE WITHOUT THE SHELL. AN APPLICATION OF THESE METHODS TO A LARGE SHELL-LESS TOKAMAK WITH DIVERTOR HOOPS IS DESCRIBED (4 REFS)

894077 A7635199
RESEARCH ON A TOKAMAK WITH AN AXISYMMETRIC DIVERTOR AND IMPURITY PROBLEMS IN TOKAMAK DEVICES
YOSHIKAWA, M., TAZIMA, T., SHIMOMURA, Y., KITSUNEZAKI, A., MAEDA, H., INOUE, K., NAGASHIMA, T., TOKUTAKE, T., OHTSUKA, H., NAGAMI, M., TANAKA, M., KUNIEDA, S., FUNAHASHI, A., KAWAKAMI, T., TAKAHASHI, K., MATOBA, T., AZUMI, M., SHOJI, T., ANNO, K., KUMAGAI, K., KASAI, S., OHGA, T., TAKEUCHI, H., TANI, T., ARAI, T., MORI, S. ; JAPAN ATOMIC ENERGY RES. INST., IBARAKI, JAPAN
; IAEA
5TH INTERNATIONAL CONFERENCE ON PLASMA PHYSICS AND CONTROLLED NUCLEAR FUSION RESEARCH 17-29, 31 1975
I 11-15 NOV. 1974 IAEA TOKYO, JAPAN
PUBL: IAEA VIENNA, AUSTRIA
DESCRIPTORS: PLASMA CONFINEMENT
IDENTIFIERS: AXISYMMETRIC DIVERTOR, IMPURITY PROBLEMS, TOKAMAK DEVICES, PLASMA CONFINEMENT, PLASMA EQUILIBRIUM, SEPARATRIX MAGNETIC SURFACE, IMPURITY DENSITY DISTRIBUTIONS, RADIATION LOSSES
SECTION CLASS CODES: A6560
UNIFIED CLASS CODES: LGNAEB
EXPERIMENTAL AND THEORETICAL RESEARCH WORK ON IMPURITY PROBLEMS IN TOKAMAK PLASMA CONFINEMENT CARRIED OUT AT JAERI IS DESCRIBED. INITIAL EXPERIMENTS IN A TOKAMAK WITH AN AXISYMMETRIC DIVERTOR INDICATE THAT A POSITIONALLY STABLE PLASMA EQUILIBRIUM ENCLOSED IN A SEPARATRIX MAGNETIC SURFACE IS

User 720 (Item 5 of 24) Date:26oct76 3194

OBTAINED AND THAT THE GROSS BEHAVIOUR OF THE PLASMA IS RATHER SIMILAR TO THAT OF CONVENTIONAL TOKAMAK PLASMAS. THEORETICAL STUDIES ON IMPURITY PROBLEMS ARE MADE IN IMPURITY DENSITY DISTRIBUTIONS, RADIATION LOSSES, AND TIME EVOLUTION OF IMPURITY CONTENT; THEY INDICATE THAT THE RELEVANT PROBLEMS HAVE TO BE STUDIED SERIOUSLY BEFORE A LARGE TOKAMAK DEVICE OF THE NEXT GENERATION CAN BE DESIGNED (13 REFS)

887186 A7630322
THE DIVERTOR EXPERIMENT ON THE HELIOTRON-D DEVICE
UO, K., MOTOJIMA, O., IIYOSHI, A., MORIMOTO, S. ; FACULTY OF ENGNG., KYOTO UNIV., GOKASHO, UJI, JAPAN
; EUROPEAN PHYS. SOC.
7TH EUROPEAN CONFERENCE ON CONTROLLED FUSION AND PLASMA PHYSICS 18 1975
I 1-5 SEPT. 1975 EUROPEAN PHYS. SOC. LAUSANNE, SWITZERLAND
PUBL: ECOLE POLYTECHNIQUE FEDERALE DE LAUSANNE LAUSANNE, SWITZERLAND
DESCRIPTORS: TOKAMAK DEVICES, PLASMA CONFINEMENT
IDENTIFIERS: DIVERTOR EXPERIMENT, HELIOTRON-D DEVICE, INTRINSIC MAGNETIC LIMITER, MAGNETIC FIELD CONFIGURATION, HELICAL HELIOTRON, COMPUTER CALCULATION, SEPARATRIX REGION, TOKAMAK
SECTION CLASS CODES: A6560, A6580
UNIFIED CLASS CODES: LGNAEB, LGSAZW
THE HELIOTRON-D DEVICE HAS AN INTRINSIC MAGNETIC LIMITER AND A BUILT-IN DIVERTOR BECAUSE OF THE CHARACTERISTICS OF THE MAGNETIC FIELD CONFIGURATION OF THE HELICAL HELIOTRON. THE COMPUTER CALCULATION OF THE SEPARATRIX REGION AND THE EXPERIMENTAL RESULTS WHICH CONFIRM THESE CHARACTERISTICS ARE REPORTED (8 REFS)

DIALOG Search File12: INSPEC-PHYSICS 70-76 ISS 16 (COPR. I.E.E.)

887175 A7630311
ON PLASMA SCRAPE-OFF IN AXIALSYMMETRIC DIVERTOR
GRATZL, H.
REPORT NO.: JUL-1208 ISSUED BY: KERNFORSCHUNGSANLAGE, JULICH, GERMANY
JUNE 1975
DESCRIPTORS: PLASMA CONFINEMENT
IDENTIFIERS: TORSIONAL GUIDING CENTRE, HOT IONS, COLD ELECTRONS, DRIFT ORBITS, AXIALSYMMETRIC DIVERTOR, POLOIDAL LARMOR RADIUS, PLASMA SCRAPE OFF LAYER, MAGNETICALLY UNTRAPPED IONS
SECTION CLASS CODES: A6560
UNIFIED CLASS CODES: LGNAEB
IN A TORSIONAL GUIDING CENTRE PLASMA WITH HOT IONS AND COLD ELECTRONS AT SURFACE, THE PLASMA SCRAPE-OFF LAYER IS COMPUTED FROM THE DRIFT ORBITS OF MAGNETICALLY UNTRAPPED IONS THAT DO NOT REACH THE COLLECTOR PLATES OF AN AXIALSYMMETRIC DIVERTOR. THE SCRAPE-OFF THICKNESS IS OF THE POLOIDAL LARMOR RADIUS (R/SUB P/) ORDER

887046 A7630176
EXTRACTION OF IMPURITIES FROM A TOKAMAK
CONSOLI, T., LEGARDEUR, R., TONON, G.F. ; DEPT. DE PHYSIQUE DU PLASMA ET DE LA FUSION CONTROLEE. SERVICE IGN. CEN. GRENOBLE, FRANCE
; EUROPEAN PHYS. SOC.
7TH EUROPEAN CONFERENCE ON CONTROLLED FUSION AND PLASMA PHYSICS 139 1975
I 1-5 SEPT. 1975 EUROPEAN PHYS. SOC. LAUSANNE, SWITZERLAND
PUBL: ECOLE POLYTECHNIQUE FEDERALE DE LAUSANNE LAUSANNE, SWITZERLAND
DESCRIPTORS: PLASMA FLOW, PLASMA CONFINEMENT, TOKAMAK DEVICES
IDENTIFIERS: TOKAMAK, ELECTRODYNAMICAL DIVERTOR, NEUTRAL ATOMS, LOW DENSITY PLASMA CORONA, HOT PLASMA CORE, E X B-FORCE, LOW DENSITY PLASMA FLOW, EXTERNAL PLASMA INJECTORS, IMPURITY EXTRACTION
SECTION CLASS CODES: A6530, A6560
UNIFIED CLASS CODES: LGHADL, LGNAEB
IN THE ELECTRODYNAMICAL DIVERTOR DESCRIBED, THE NEUTRAL ATOMS EMITTED BY THE WALL AFTER BEING IONIZED IN THE LOW DENSITY PLASMA CORONA SURROUNDING THE DENSE AND HOT PLASMA CORE, ARE EXPELLED BY AN E X B FORCE. THIS DIVERTOR MAY BE MADE MORE EFFICIENT IF A LOW DENSITY PLASMA FLOW IS MAINTAINED AND CONTROLLED BETWEEN THE LINER AND THE LIMITER BY MEANS OF EXTERNAL PLASMA INJECTORS (6 REFS)

876943 A7625845
DIVERTOR EXPERIMENT IN THE HELIOTRON-D DEVICE
MOTOJIMA, O., HYOSHI, A., UO, K. ; PLASMA PHYS. LAB., FACULTY OF ENGNG., KYOTO UNIV., GOKASHO, UJI, JAPAN
NUCL. FUSION (AUSTRIA) VOL.15, NO.6 985-90 DEC. 1975

User 720 (Item 8 of 24) Date:26oct76 3195

CODEN: NUFUAU
DESCRIPTORS: PLASMA CONFINEMENT, PLASMA TRANSPORT PROCESSES, FUSION REACTORS
IDENTIFIERS: HELIOTRON-D DEVICE, MAGNETIC LIMITER, HELICAL CONDUCTOR, DIVERTOR LAYER, PLASMA CONFINEMENT, DIVERTOR LIKE MAGNETIC FIELD CONFIGURATION, PLASMA ISOLATION, PLASMA DIFFUSION, TOROIDAL DEVICE
SECTION CLASS CODES: A6560, A6515, A4640
UNIFIED CLASS CODES: LGNAEB, LGEACL, HMGAAP
EXPERIMENTAL EVIDENCE OF THE EFFECTIVENESS OF A MAGNETIC LIMITER HAS BEEN OBTAINED IN THE HELIOTRON-D. THE FUNDAMENTAL PROPERTIES OF A BUILT-IN DIVERTOR ARE STUDIED. IN A DIVERTOR-LIKE MAGNETIC-FIELD CONFIGURATION, THE PLASMA IS OBSERVED TO BE ISOLATED STABLY FROM THE HELICAL CONDUCTOR. IT IS OBSERVED THAT THE PLASMA DIFFUSES THROUGH THE DIVERTOR LAYER, WHOSE THICKNESS IS ESTIMATED EXPERIMENTALLY (14 REFS)

857667 A7608867, B7607507
MHD-SYNCHRONOUS POWER GENERATION USING DIVERTOR-FUSION REACTOR PLASMA
DENNO, K. : NEWARK COLL. OF ENGNG., NEWARK, NJ, USA
: IEEE, PLASMA SCI. SOC.
2ND INTERNATIONAL CONFERENCE ON PLASMA SCIENCE. (ABSTRACTS ONLY RECEIVED) 132 1975
14-16 MAY 1975 IEEE, PLASMA SCI. SOC. ANN ARBOR, MICH., USA
PUBL: IEEE NEW YORK, USA
DESCRIPTORS: MAGNETOHYDRODYNAMIC CONVERTORS, FUSION REACTORS, ELECTRIC POWER GENERATION
IDENTIFIERS: APPLIED MAGNETIC FIELD, DIVERTOR MAIN FIELD, COUPLED MHD EQUATION, CONFINED CURRENT DENSITY DISTRIBUTION, SYNCHRONOUS MACHINE THEORY, MHD GENERATION, SYNCHRONOUS POWER GENERATION, DIVERTOR FUSION REACTOR PLASMA
SECTION CLASS CODES: B5440, A6530, A4640, B5220
UNIFIED CLASS CODES: EVGAAF, LGHAEN, HMGAAP
THE AUTHOR DISCUSSES THE DEVELOPMENT OF MHD-SYNCHRONOUS ELECTRIC POWER GENERATOR WHICH COULD BE REALIZED BY EFFECTIVE UTILIZATION OF THE DIVERTOR-FUSION REACTOR PLASMA AS A WORKING FLUID, THUS REMOVING THE NEED OF FOSSIL FUEL. THE APPLIED MAGNETIC FIELD COULD BE AN INTEGRAL PART OF THE DIVERTOR MAIN FIELD, MODIFIED TO IMPOSE A POWERFUL TRANSVERSE COMPONENT ON THE PLASMA AND ELIMINATING ANY SERIOUS PERTURBATION WITH RESPECT TO THE REACTOR MAIN MAGNETIC FIELD. SOLUTIONS OF THE COUPLED MHD EQUATION RESULTED IN EXPRESSIONS FOR THE CONFINED CURRENT DENSITY DISTRIBUTION WITHIN THE DIVERTOR FUSION PLASMA. CONVENTIONAL SYNCHRONOUS MACHINE THEORY IS USED TO CALCULATE VARIOUS DESIGNS AND PERFORMANCE COMPONENTS OF THE MHD-SYNCHRONOUS GENERATOR AND THE DEVELOPMENT OF ITS EQUIVALENT CIRCUIT IN LUMPED PARAMETERS FORM

DIALOG Search File12: INSPEC-PHYSICS 70-76 ISS 16 (COPR. I.E.E.)

841020 A7601452
MIRROR MICROINSTABILITIES IN DIVERTORS
MENSE, A.T., EMMERT, G.A., CALLEN, J.D. ; DEPT. OF NUCLEAR ENGNG., UNIV. OF WISCONSIN, MADISON, WI, USA
NUCL. FUSION (AUSTRIA) VOL.15, NO.4 703-7 AUG. 1975
CODEN: NUFUAU
DESCRIPTORS: PLASMA CONFINEMENT, PLASMA INSTABILITY
IDENTIFIERS: TOKAMAKS, DIVERTOR, MINOR MICROINSTABILITIES, PLASMA TRANSPORT, IMPURITY CONTROL
SECTION CLASS CODES: A6560, A6540
UNIFIED CLASS CODES: LGNAEB, LGKADB
IMPURITY CONTROL IN TOKAMAKS MAY BE IMPLEMENTED BY THE USE OF A DIVERTOR. THE PLASMA IN THE DIVERTOR REGION MAY HOWEVER, BE UNSTABLE TO MINOR MICROINSTABILITIES WHICH MAY AFFECT PLASMA TRANSPORT IN THIS REGION (19 REFS)

831243 A7580939
A NEW MAGNETIC SYSTEM OF TOKAMAK FOR A DIVERTOR AND STATIONARY OPERATION
OSHIYAMA, H. ; FACULTY OF INDUSTRIAL ARTS, KYOTO TECH. UNIV., KYOTO, JAPAN
J. PHYS. SOC. JAP. (JAPAN) VOL.39, NO.1 263-4 JULY 1975
CODEN: JUPSAU
DESCRIPTORS: TOKAMAK DEVICES
IDENTIFIERS: TOKAMAK, DIVERTOR, STATIONARY OPERATION, MODIFIED QUADRUPOLE MAGNETIC FIELD, MAGNETIC SURFACES, FIELD PARAMETERS, BIOT SARARTS LAW, SCRAPE OFF FLUX
SECTION CLASS CODES: A6580
UNIFIED CLASS CODES: LGSAZ#
A NEW MAGNETIC SYSTEM OF TOKAMAK FOR A DIVERTOR AND FOR OPERATING TOKAMAK STATIONARILY BY USING THE MODIFIED QUADRUPOLE MAGNETIC FIELD IS PROPOSED. NUMERICAL CALCULATIONS OF THE SYSTEM USING BIOT-SAVART:S LAW SHOW THAT THE SUITABLE MAGNETIC SURFACES AND THE SCRAPE-OFF FLUX EXIST BY CHOSING THE FIELD PARAMETERS (3 REFS)

790913 A7557940
A HOT-PLASMA INJECTOR USING A DIVERTOR BASED ON THE MAGNETIC-NEUTRAL-POINT DISCHARGE
OKAMURA, S., OHYABU, N., KAWASHIMA, N. ; INST. OF SPACE AND AERONAUTICAL SCI., UNIV. OF TOKYO, TOKYO, JAPAN
NUCL. FUSION (AUSTRIA) VOL.15, NO.2 207-12 APRIL 1975
CODEN: NUFUAU
DESCRIPTORS: PLASMA DEVICES
IDENTIFIERS: HOT PLASMA INJECTOR, MAGNETIC NEUTRAL POINT DISCHARGE, DIVERTOR, PLASMA CURRENT, ELECTROSTATIC DOUBLE PROBES, DIFFUSING PLASMA IONS, ELECTROSTATIC DOUBLE PROBES, FUSION REACTOR
SECTION CLASS CODES: A6580
UNIFIED CLASS CODES: LGSAZW
THE FEASIBILITY OF A HOT PLASMA INJECTOR USING A DIVERTOR BASED ON A MAGNETIC NEUTRAL POINT DISCHARGE IS STUDIED

User 720 (Item 12 of 24) Date:26oct76 3196

EXPERIMENTALLY. AN INTENSE PLASMA CURRENT IS INDUCED ALONG A CIRCULAR MAGNETIC NEUTRAL LINE OF THE DIVERTOR, AND THE PLASMA IS HEATED AND INJECTED INWARD TO THE CENTRAL REGION. THE PLASMA DIFFUSING ALONG THE MAGNETIC FIELD LINES IS MEASURED BY A TIME-OF-FLIGHT METHOD USING A PAIR OF ELECTROSTATIC DOUBLE PROBES, AND IT IS SHOWN THAT THE AVERAGE ENERGY OF THE DIFFUSING PLASMA IONS IS 200 EV AND THE TOTAL AMOUNT OF INJECTED PARTICLES IS 6*10/SUP 16/ PARTICLES PER SHOT. THE POSSIBLE USE OF THE DIVERTOR INJECTOR IN A FUSION REACTOR IS DISCUSSED (10 REFS)

787704 A7554054
MEASUREMENT OF PLASMA FLOW VELOCITY INTO THE DIVERTOR OF THE FM-1 SPHERATOR BY USING ION ACOUSTIC WAVE PROPAGATION
HSUAN, H., OKABAYASHI, M., EJIMA, S. ; PLASMA PHYS. LAB., PRINCETON UNIV., PRINCETON, NJ, USA
NUCL. FUSION (AUSTRIA) VOL.15, NO.2 191-4 APRIL 1975
CODEN: NUFUAU
DESCRIPTORS: PLASMA FLOW, PLASMA DIAGNOSTICS
IDENTIFIERS: PLASMA FLOW VELOCITY, DIVERTOR, FM-1 SPHERATOR, ION ACOUSTIC WAVE PROPAGATION, PLASMA SHEATH MODEL, POLOIDAL DIVERTOR DEVICES
SECTION CLASS CODES: A6570, A6530, A6540
UNIFIED CLASS CODES: LGRAZN, LGHADL, LGKADB
THE PLASMA FLOW VELOCITY INTO THE DIVERTOR CHAMBER OF THE FM-1 SPHERATOR IS DETERMINED BY MEASURING THE PROPAGATION VELOCITY OF ION ACOUSTIC WAVES. THE OBSERVED DEPENDENCE OF PLASMA FLOW INTO THE DIVERTOR IS CONSISTENT WITH THE PLASMA SHEATH MODEL, WHICH IS NOW FREQUENTLY USED FOR DESIGNING POLOIDAL DIVERTOR DEVICES (7 REFS)

DIALOG Search File12: INSPEC-PHYSICS 70-76 ISS 16 (COPR. I.E.E.)

764672 A7540982
VACUUM PROBLEMS IN PLASMA PHYSICS AND CONTROLLED NUCLEAR FUSION
PREVOT, F. ; CEN, FONTENAY-AUX-ROSES, FRANCE
; INTERNAT. UNION FOR VACUUM SCI., TECHNIQUE AND APPLICATIONS
JAP. J. APPL. PHYS. (JAPAN) SUPPL.2, PT.1 225-31 1974
CODEN: JJAPA5
CONF: PROCEEDINGS OF THE 6TH INTERNATIONAL VACUUM CONGRESS 25-29 MARCH 1974 INTERNAT. UNION FOR VACUUM SCI., TECHNIQUE AND APPLICATIONS KYOTO, JAPAN
DESCRIPTORS: NUCLEAR FUSION, FUSION REACTORS, VACUUM TECHNIQUES, PLASMA CONFINEMENT
IDENTIFIERS: NEUTRAL MOLECULES, VESSEL SIZE, /SUP 3/H HANDLING, WALL MATERIAL, VACUUM PROBLEMS, PLASMA PHYSICS, CONTROLLED NUCLEAR FUSION, PLASMA, NEUTRAL GAS, INTERNAL PUMP, NEUTRAL ATOMS, PLASMA POLLUTION BY HIGH Z ATOM INDUCED EMISSION , THERMONUCLEAR REACTORS, PUMPING SPEED, SAFETY PROBLEMS, NEUTRON ACTIVATION, BAKING, SURFACE PROCESSING, PUMPING, AUXILIARY EQUIPMENT, MAGNETIC DIVERTOR, PROTECTIVE LAYER OF COLD PLASMA, ENERGY BALANCE
SECTION CLASS CODES: A4640, A6580, A0634
UNIFIED CLASS CODES: HMGAAP, LGSAZW, BGGEAR
THE FIRST IMPORTANT ASPECT IS THE EXISTANCE OF THE PLASMA ITSELF WHICH IS AT THE SAME TIME A LARGE SOURCE OF NEUTRAL GAS AND A POWERFUL INTERNAL PUMP. INTERACTION BETWEEN NEUTRAL GAS AND PLASMA IS VERY DIFFERENT WHETHER THE PLASMA IS TRANSPARENT OR OPAQUE TO NEUTRAL ATOMS OR MOLECLES. THE SECOND IMPORTANT ASPECT IS THE INFLUENCE OF THE WALLS ON PLASMA POLLUTION BY HIGH Z ATOM INDUCED EMISSION. THESE TWO PHENOMENA PLAY AN IMPORTANT ROLE IN THE ENERGY BALANCE OF BOTH LABORATORY PLASMAS AND FUTURE THERMONUCLEAR REACTORS. CONCERNING THE VACUUM SYSTEM OF THERMONUCLEAR REACTOR, THE ENORMOUS SIZE OF THE VESSEL AND PUMPING SPEED REQUESTED AND SOME SAFETY PROBLEMS INHERENT TO TRITIUM HANDLING AND NEUTRON ACTIVATION MUST BE SPECIALLY MENTIONED. SEVERAL SOLUTIONS HAVE BEEN PROPOSED AND PARTIALLY TESTED IN PRESENT EXPERIMENTS: CHOICE OF THE MATERIAL OF THE WALL, BAKING AND SURFACE PROCESSING, PUMPING AND AUXILIARY EQUIPMENTS, MAGNETIC DIVERTOR AND PROTECTIVE LAYER OF COLD PLASMA (22 REFS)

724321 A7512593
THE IMPURITY PROBLEM IN QUASI-STEADY-STATE TOROIDAL PLASMA EXPERIMENTS AND FUSION REACTORS
DUCHS, D., HAAS, G., PFIRSCH, D., VERNICKEL, H. ; MAX-PLANCK INST. PLASMAPHYSIK, GARCHING MUNCHEN, GERMANY ; IAEA
NUCL. FUSION (AUSTRIA) SPEC. SUPPL 409 1974 CODEN: NUFUAU
CONF: WORKSHOP ON FUSION REACTOR DESIGN PROBLEMS 29 JAN. - 15 FEB. 1974 IAEA ABINGDON, BERKS., ENGLAND
DESCRIPTORS: FUSION REACTORS, PLASMA TRANSPORT PROCESSES
IDENTIFIERS: FIRST WALL EROSION, QUASI STEADY STATE TOROIDAL PLASMA EXPERIMENT, FUSION REACTORS, PLASMA CONTAMINATION, DIVERTOR, IMPURITIES, NEOCLASSICAL DIFFUSION

User 720 (Item 16 of 24) Date:26oct76 3197

SECTION CLASS CODES: A6515, A4640
UNIFIED CLASS CODES: LGEACL, HMGAAP
THE PROBLEM OF PLASMA CONTAMINATION BY THE MATERIAL RELEASED FROM THE FIRST WALL IS DISCUSSED. IN A FIRST APPROXIMATION THE IMPURITY BUILT UP IN THE PLASMA CAN BE DESCRIBED BY A SIMPLE DIFFERENTIAL EQUATION. THE SOLUTION OF THIS EQUATION FOR VARIOUS ASSUMPTIONS SHOW: (A) IF NO DIVERTOR IS BUILT INTO THE FUSION DEVICE, THE TOLERABLE CONCENTRATION OF IMPURITIES IN THE PLASMA OF =10/SUP -2/ IS REACHED IN A TIME SLIGHTLY LESS THAN ONE CONFINEMENT TIME TAU OF THE PLASMA IONS, EVEN IF ONLY SPUTTERING IS TAKEN INTO ACCOUNT. (B) FOR A FUSION DEVICE WITH DIVERTOR, THE WALL BOMBARDMENT WILL BE REDUCED TO A FRACTION EPSILON OF THAT WITHOUT DIVERTOR, EPSILON BEING A FEW TIMES 10/SUP -2/ AT BEST. IF THE NEOCLASSICAL DIFFUSION OF IMPURITIES TOWARD THE CENTRE OF THE DISCHARGE ALSO HOLDS IN THE SCREENING LAYER THERE WILL BE PRACTICALLY NO SCREENING EFFECT: THUS THE BURNING TIME IS INCREASED ONLY TO TAU/EPSILON

724320 A7512592
THE IMPURITY PROBLEM IN STEADY-STATE TOROIDAL DEVICES
TAYLOR, J.B. ; UKAEA, ABINGDON, ENGLAND ; IAEA
NUCL. FUSION (AUSTRIA) SPEC. SUPPL 403-7 1974 CODEN: NUFUAU
CONF: WORKSHOP ON FUSION REACTOR DESIGN PROBLEMS 29 JAN. - 15 FEB. 1974 IAEA ABINGDON, BERKS., ENGLAND
DESCRIPTORS: FUSION REACTORS, PLASMA TRANSPORT PROCESSES
IDENTIFIERS: STEADY STATE TOROIDAL DEVICE, FUSION REACTOR, PLASMA DIFFUSION, IMPURITY CONCENTRATION, DIVERTOR
SECTION CLASS CODES: A6515, A4640
UNIFIED CLASS CODES: LGEACL, HMGAAP
THE IMPURITY CONCENTRATION IN A STEADY-STATE DEVICE IS ESTIMATED. THE EXTREME DIFFICULTY OF MAINTAINING ADEQUATE PURITY, EVEN WITH A DIVERTOR, IS ILLUSTRATED (2 REFS)

DIALOG Search File12: INSPEC-PHYSICS 70-76 ISS 16 (COPR. I.E.E.)

691397 A7474800, 87437786
A POLOIDAL DIVERTOR FOR UWMAK-I TOKAMAK REACTOR
EMMERT, G.A., MENSE, A.T., DONHOWE, J.M. ; UNIV. WISCONSIN, MILWAUKEE, USA
; AMERICAN NUCLEAR SOC., USAEC
1ST TOPICAL MEETING ON THE TECHNOLOGY OF CONTROLLED NUCLEAR FUSION (ABSTRACTS ONLY RECEIVED) 88-9 1974
16-18 APRIL 1974 AMERICAN NUCLEAR SOC., USAEC SAN DIEGO, CALIF., USA
PUBL: AMERICAN NUCLEAR SOC. HINSDALE, ILL., USA
DESCRIPTORS: FUSION REACTORS, TOKAMAK DEVICES, PLASMA CONFINEMENT
IDENTIFIERS: POLOIDAL DIVERTOR, UWMAK-I TOKAMAK REACTOR, PLASMA BOUNDARY, FIRST WALL, WALL EROSION, ENERGETIC CHARGED PARTICLE BOMBARDMENT, CHARGED PARTICLE COLLECTORS
SECTION CLASS CODES: A4640, B5220, A6560
UNIFIED CLASS CODES: HMGAAP, LGNAEB
THE WISCONSIN TOKAMAK REACTOR DESIGN (UWMAK-I) INCORPORATES A POLOIDAL DIVERTOR TO ESTABLISH A PLASMA BOUNDARY AWAY FROM THE FIRST WALL AND TO REDUCE WALL EROSION BY ENERGETIC CHARGED PARTICLE BOMBARDMENT AND THE SUBSEQUENT RELEASE OF IMPURITIES INTO THE PLASMA. THE DIVERTOR WHICH IS OF THE POLOIDAL TYPE TO PRESERVE THE AXISYMMETRIC PROPERTY OF THE TOKAMAK AND TO PROVIDE MAXIMUM AREA FOR THE CHARGED PARTICLE COLLECTORS IS DESCRIBED (5 REFS)

647051 A7444357
AN AXISYMMETRIC DIVERTOR IN A TOKAMAK WITH A TEAR DROPLIKE CROSS SECTION (DIVA)
YOSHIKAWA, M., SHIMOMURA, Y., MAEDA, H., KITSUNEZAKI, A., MORI, S. ; JAPAN ATOMIC ENERGY RES. INST., TOKAI
; EUROPEAN PHYS. SOC., ACAD. SCI., USSR, ET AL
6TH EUROPEAN CONFERENCE ON CONTROLLED FUSION AND PLASMA PHYSICS. VOL.I 173-6 1973
30 JULY - 4 AUG. 1973 EUROPEAN PHYS. SOC., ACAD. SCI., USSR, ET AL MOSCOW, USSR
PUBL: JOINT INST. NUCL. RES. MOSCOW, USSR
DESCRIPTORS: TOKAMAK DEVICES, PLASMA CONFINEMENT
IDENTIFIERS: AXISYMMETRIC DIVERTOR, TOKAMAK, PLASMA CONFINEMENT, TEAR DROP LIKE CROSS SECTION, DIVA
SECTION CLASS CODES: A6560
UNIFIED CLASS CODES: LGNAEB
A TOKAMAK DEVICE (DIVA) WITH AN AXISYMMETRIC DIVERTOR HAS A TEAR DROP-LIKE CROSS SECTION WITH A MAJOR RADIUS OF 60 CM AND AN AVERAGE ASPECT RATIO OF 5.5. THE TOROIDAL FIELD IS 10 KG. THE PLASMA CONFINEMENT IN SUCH A TOKAMAK IS STUDIED AS WELL AS THE EFFECT OF A DIVERTOR ON THE CONFINED PLASMA (1 REFS)

631780 A7432346
DESIGN OF A TOKAMAK DEVICE WITH AN AXISYMMETRIC DIVERTOR (DIVA)
KITSUNEZAKI, A., MAEDA, H., SHIMOMURA, Y., YOSHIKAWA, M. ;

User 720 (Item 19 of 24) Date:26oct76 3198

JAPAN ATOMIC ENERGY RES. INST., TOKAI
; EUROPEAN PHYS. SOC
3RD INTERNATIONAL SYMPOSIUM ON TOROIDAL PLASMA CONFINEMENT G2/1PP. 1973
26-30 MARCH 1973 EUROPEAN PHYS. SOC GARCHING, GERMANY
PUBL: MAX-PLANCK-INST. PLASMAPHYS. GARCHING, GERMANY
DESCRIPTORS: TOKAMAK DEVICES
IDENTIFIERS: DESIGN, TOKAMAK DEVICE, AXISYMMETRIC DIVERTOR, TEARDROP LIKE CROSS SECTION
SECTION CLASS CODES: A6580
UNIFIED CLASS CODES: LGSAZW
A TOKAMAK DEVICE WITH AN AXISYMMETRIC DIVERTOR (DIVA) CURRENTLY UNDER DESIGN IS DESCRIBED. THE PLASMA HAS A TEARDROP-LIKE CROSS SECTION WITH A MAJOR RADIUS OF 60 CM AND AN ASPECT RATIO OF 5.5 (8 REFS)

576397 A7375401
ELECTRON INJECTION THROUGH THE DIVERTER IN A HELIOTRON
ZYKOV, V.G., KARPUKHIN, V.I., LONIN, YU.F., RUDNEV, N.I., TOLOK, V.T. ; PHYSICOTECH. INST., ACAD. SCI., KHAR:KOV, UKRAINIAN SSR
ZH. TEKH. FIZ. (USSR) VOL.43, NO.2 287-93 FEB. 1973 CODEN: ZTEFA3
TRANS OF: SOV. PHYS.-TECH. PHYS. (USA) VOL.18, NO.2 188-91 AUG. 1973 CODEN: SPTPA3
DESCRIPTORS: ELECTRON BEAMS, PLASMA DEVICES, PLASMA PRODUCTION
IDENTIFIERS: ELECTRON INJECTION, DIVERTOR, HELIOTRON, ELECTRON BEAMS, MAGNETIC SLOTS, DIVERTOR MAGNETIC SURFACE, COAXIAL CYLINDERS
SECTION CLASS CODES: A6550
UNIFIED CLASS CODES: LGMACP
EXPERIMENTS ARE DESCRIBED ON THE INJECTION OF ELECTRON BEAMS THROUGH THE MAGNETIC SLOTS OF A DIVERTER INTO THE MAIN CHAMBER OF A HELIOTRON DEVICE. THE POINT ELECTRON BEAM IS CONVERGED BY THE DIVERTER MAGNETIC FIELD INTO A (HOLLOW) CYLINDER IN THE MAIN CHAMBER, THE DIAMETER OF THE CYLINDER BEING APPROXIMATELY EQUAL TO THE DIAMETER OF THE DIVERTER MAGNETIC SURFACE. THE CYLINDER IS FOUND TO CONSIST OF TWO COAXIAL CYLINDERS (4 REFS)

DIALOG Search File12: INSPEC-PHYSICS 70-76 ISS 16 (COPR. I.E.E.)

494208 A7320656
A LOCAL DIVERTOR FOR A TOKAMAK
COLVEN, C., GIBSON, A., STOTT, P.E. ; UKAEA, ABINGDON, ENGLAND
; EUROPEAN PHYS. SOC
5TH EUROPEAN CONFERENCE ON CONTROLLED FUSION AND PLASMA PHYSICS. VOL.II 6 1972
21-25 AUG. 1972 EUROPEAN PHYS. SOC GRENOBLE, FRANCE
PUBL: CENTRE D:ETUDES NUCLEAIRES GRENOBLE, FRANCE
DESCRIPTORS: TOKAMAK DEVICES, PLASMA CONFINEMENT
IDENTIFIERS: LOCAL DIVERTOR, TOKAMAK, FIELD PERTURBATION, PLASMA CENTRE, TOROIDAL FIELD
SECTION CLASS CODES: A6580, A6560
UNIFIED CLASS CODES: LGSACC, LGNAEB
A NEW TYPE OF LOCAL DIVERTOR FOR A TOKAMAK IS DESCRIBED. THE DIVERTOR CAUSES A FIELD PERTURBATION AT THE PLASMA CENTRE WHICH IS LESS THAN 1PERCENT OF THE TOROIDAL FIELD

484193 A7314535
INVESTIGATION OF THE STABILITY OF THE MOVEMENT OF A PLASMA STREAM IN THE MAGNETIC FIELD OF A DIVERTOR
ZYKOV, V.G., KARPUKHIN, V.I., RUDNEV, N.I., TOLOK, V.T.
FIZ. PLAZMY AND PROBL. UPR. TERMOYAD. SINT. (USSR) NO. 3 213-20 1972 CODEN: FPPUAP
DESCRIPTORS: PLASMA STABILITY, PLASMA FLOW, ION DENSITY
IDENTIFIERS: STABILITY, MOVEMENT, PLASMA STREAM, MAGNETIC FIELD, DIVERTOR, VACUUM ENCLOSURE, DIVERTOR COILS, PLASMA DENSITY, VELOCITY, DIVERTOR OUTLET
SECTION CLASS CODES: A6530, A6540
UNIFIED CLASS CODES: LGHAGS, LGKAZS
LANGUAGE: RUSSIAN
THE DIVERTOR WAS BUILT ONTO A VACUUM ENCLOSURE OF LENGTH 52 CM AND DIAMETER 10 CM. THE DIVERTOR COILS WERE POWERED BY A 400 KJ CONDENSOR BATTERY AND GAVE FIELDS OF CONTROLLED STRENGTH FROM 0.1 TO 18 KOE. THE PLASMA DENSITY AND VELOCITY WERE MEASURED AT THE DIVERTOR OUTLET AND SHOWN TO BE 2*10/SUP 13/ CM/SUP -3/ AND 10/SUP 7/ CM/S RESPECTIVELY. PLASMA DISTRIBUTIONS ACROSS THE ENCLOSURE CROSS SECTION ARE ILLUSTRATED OVER THE WHOLE RANGE OF OPERATING VARIABLES, AND IT IS SHOWN THAT THE DIVERTOR EFFECTIVELY STABILISES THE MOTION OF THE PLASMA THROUGH THE ENCLOSURE (15 REFS)

User 720 (Item 23 of 24) Date:26oct76 3199

Print 16/5/1-3
DIALOG Search File13: INSPEC-ELEC & COMPUT 70-76 IS-16 (COPR. I.E.E.)

722776 A7509150, B7507245
A 2100 MW(E) FUSION POWER PLANT
TENNEY, F.H. ; PRINCETON UNIV., N.J., USA
; IAEA
NUCL. FUSION (AUSTRIA) SPEC. SUPPL 17-25 1974 CODEN: NUFUAU
CONF: WORKSHOP ON FUSION REACTOR DESIGN PROBLEMS 29 JAN. - 15 FEB. 1974 IAEA ABINGDON, BERKS., ENGLAND
DESCRIPTORS: FUSION REACTORS, TOKAMAK DEVICES
IDENTIFIERS: PLASMA FUSION, DT BURNING TOKAMAK REACTION, FLIBE T BREEDING, 2100 MW(E) FUSION POWER PLANT, BLANKET STRUCTURAL MATERIAL, POLOIDAL FIELD DIVERTOR
SECTION CLASS CODES: A4640, B5220
UNIFIED CLASS CODES: HMGAAP
A :FIRST GENERATION: 2100 MW(E) FUSION POWER PLANT USING A DT-BURNING TOKAMAK REACTION IS DESCRIBED. SOME REACTOR PARAMETERS ARE: 10.5 M MAJOR RADIUS; 3.25 M MINOR RADIUS; 14.6 MA DISCHARGE CURRENT; Q=2.0; B=6T. HELIUM COOLING IS USED THROUGHOUT. TRITIUM IS BRED IN FLIBE. THE BLANKET STRUCTURAL MATERIAL IS A NICKEL-IRON ALLOY, PE-16. OPERATION OF THE REACTOR WITH ITS POLOIDAL FIELD DIVERTOR IS DESCRIBED (1 REFS)

562587 A7360641, B7337216
CONCEPTUAL DESIGN OF A TOKAMAK REACTOR
ABDOU, M.A., BOOM, R.W., CARBON, M.W., CONN, R.W., DONHOWE, J.M., EL-GUEBALY, L.A., EMMERT, G.A., FORSEN, H.K., HOULBERG, W.A., KAMPERSCHROER, J.H., KERST, D.W., KULCINSKI, G.L., MAYNARD, C.W., MCALEES, D.G., MENSE, A.T., SANGER, P.A., STEWART, W.E., SZE, D.K., WINTER, W.R., YANG, T.A., YOUNG, W.C.
; UNIV. WISCONSIN, MADISON, USA
; TEXAS ATOMIC ENERGY RES. FOUND., AMERICAN NUCLEAR SOC., ATOMIC ENERGY COMM., IEEE, UNIV. TEXAS
TEXAS SYMPOSIUM ON THE TECHNOLOGY OF CONTROLLED THERMONUCLEAR FUSION EXPERIMENTS AND THE ENGINEERING ASPECTS OF FUSION REACTORS. (ABSTRACTS ONLY RECEIVED) 45 1972
20-22 NOV. 1972 TEXAS ATOMIC ENERGY RES. FOUND., AMERICAN NUCLEAR SOC., ATOMIC ENERGY COMM., IEEE, UNIV. TEXAS AUSTIN, TEX., USA
PUBL: UNIV. TEXAS AUSTIN, TEX., USA
DESCRIPTORS: FUSION REACTORS, TOKAMAK DEVICES
IDENTIFIERS: CONCEPTUAL DESIGN, TOKAMAK REACTOR, SCOPING DESIGN, PLASMA, CONTROL, DIVERTOR, BLANKET, SHIELD, HEAT REMOVAL SYSTEM, TOROIDAL MAGNET, LIMITING STRESS EFFECTS, HAZARDS, LOW BETA TOKAMAK, QUASI STEADY STATE OPERATION
SECTION CLASS CODES: A6580, A4640, B5220
UNIFIED CLASS CODES: LGSACC, HMGAAP
A SCOPING DESIGN HAS BEEN CARRIED OUT TO DETERMINE THE TECHNOLOGICAL PROBLEMS ASSOCIATED WITH THE LOW BETA TOKAMAK APPROACH TO REACTORS. THIS SYSTEM IS ENVISIONED TO OPERATE QUASI STEADY STATE PRODUCING ABOUT 1000 MW(TH) USING STAINLESS STEEL AND A WALL LOADING OF 0.85 MW/M/SUP 2/. VARIOUS SYSTEM ASPECTS OF THE DESIGN ARE DESCRIBED INCLUDING THE PLASMA AND

User 720 (Item 1 of 3) Date:26oct76

ITS CONTROL; A DIVERTOR AND START-UP MAGNET SYSTEM; A BLANKET, SHIELD AND HEAT REMOVAL SYSTEM; TOROIDAL MAGNET DESIGN AND LIMITING STRESS EFFECTS; AND AN ANALYSIS OF SYSTEM HAZARDS

286204 A7147931, B7128804

THE TORSATRON WITHOUT TOROIDAL FIELD COILS AS A POSSIBLE SOLUTION THE DIVERTOR PROBLEM

GOURDON, C., MARTY, D., MASCHKE, E., TOUCHE, J. ; EURATOM-CEA, FONTENAY-AUX-ROSE, FRANCE
; NAT. NUCLEAR ENERGY COMMITTEE

4TH EUROPEAN CONFERENCE ON CONTROLLED FUSION AND PLASMA PHYSICS 35 1970
31 AUG-4 SEP 1970 NAT. NUCLEAR ENERGY COMMITTEE ROME, ITALY
PUBL: NAT. NUCLEAR ENERGY COMMITTEE ROME, ITALY
DESCRIPTORS: PLASMA DEVICES, PLASMA CONFINEMENT
IDENTIFIERS: TORSATRON, DIVERTOR PROBLEM, STELLARATOR CONFIGURATION, HELICAL CONDUCTORS, ASPECT RATIO
SECTION CLASS CODES: A1424, B4220

A STELLARATOR TYPE CONFIGURATION, WITH ONLY HELICAL CONDUCTORS AND NO TOROIDAL FIELD COILS IS INVESTIGATED BY NUMERICAL CALCULATIONS INTERESTING PROPERTIES ARE FOUND FOR THE CONFIGURATIONS WITH HIGHER ASPECT RATIO (R/A=10) (T UP TO 4, AND P/L/SUB S/=1). THIS CONFIGURATION (TORSATRON) IS PARTICULARLY WELL SUITED FOR THE CONSTRUCTION OF A DIVERTOR

APPENDIX G

Estimation of Wall Reabsorption Effect of Secondary Electrons Due to Finite Angle of Incidence of Magnetic Field

Let the angle which the magnetic field ($\vec{B}$) makes with the particle collection plate be α. The secondary electron is "emitted" from the plate with a velocity vector v_0 which makes an angle θ with the collector plate. For simplicity $\vec{B}$ and $\vec{v}$ are assumed in the same plane and that plane is normal to the collector plate. Thus the angle between $\vec{v}_0$ and $\vec{B}$ is θ-α. The following dynamic quantities can then be found.

$$v_{\parallel} = v \cos(\theta-\alpha) = \text{speed parallel to B field}$$

$$v_{\perp} = v \sin(\theta-\alpha)$$

Let $\vec{a}$ be an acceleration vector which is presumed normal to the collector plate. Therefore,

$$a_{\parallel} = a \cos(\pi/2 - \alpha)$$

$$v_{\parallel} = v_{\parallel_0} + a_{\parallel} t$$

where $v_{\parallel_0}$ is the projection of $\vec{v}_0$ or $\vec{B}$.

$s_{\parallel} = (v_{\parallel_0} + a_{\parallel}/2\ t)t$ = distance electron travels along B field is in time t.

$s_{\perp} = s_{\parallel} \tan \alpha$ = distance from position $s_{\parallel}$ on field line to wall as measured normal to $\vec{B}$ field line.

If $s_{\perp}$ > electron gyroradius (ρ_e), then electrons cannot be recaptured by the wall.

To estimate the fraction of secondary electrons emitted from the collector plate which are not recaptured due to the electron gyrating back onto the plate one must calculate how far along the field line ($s_\parallel$) the electron would have traveled in a cyclotron period ($\tau_c = 2\pi/\omega_c$) and then whether or not the gyroradius of the electron at that place is larger than $s_\perp$, the distance to the wall. If $\rho_e < s_\perp$, then the electron escapes and contributes to the secondary emission coefficient. The fraction which escapes are those with velocity vectors whose angle to the collector plate are less than some value θ_c, i.e., for an emission source function $s(\theta)$ one finds

$$f_{esc} = \text{fraction escape} = \frac{\int_0^{\theta_c} s(\theta)d\theta}{\int_0^{\pi} s(\theta)d\theta} = \frac{\theta_c}{\pi} \text{ for isotropic emission}$$

The angle θ_c is determined as follows:

$$s_\parallel = (v_{\parallel 0} + \frac{a_\parallel}{2}\tau_c)\tau_c \cos(\theta-\alpha)$$

$$s_\perp = s_\parallel \tan\alpha$$

$$= (v_0 + a\tau_c/2 \cos(\pi/2 - \alpha))\tau_c \cos(\theta-\alpha)\tan\alpha$$

Using $\tau_c = 2\pi/\omega_c = 2\pi\rho_e/v_\perp$, one finds that the requirement $\rho_e \leq s_\perp$ becomes

$$\tan(\theta-\alpha) < A(\alpha)\tan\alpha$$

where

$$A(\alpha) \equiv \left[\frac{v_0 + \frac{\pi a}{\omega_c}\cos(\frac{\pi}{2} - \alpha)}{v_0 + \frac{2\pi a}{\omega_c}\sin(\frac{\pi}{2} - \alpha)}\right] 2\pi$$

The angle θ_c becomes

$$\theta_c = \alpha + \tan^{-1} \{A(\alpha) \tan \alpha\}$$

and the fraction escaping becomes

$$f_{esc} = \frac{\alpha + \tan^{-1} \{A(\alpha) \tan \alpha\}}{\pi}$$

Clearly the limiting cases are easily verified. If $\alpha = 0$, which corresponds to the $\vec{B}$ field being tangential to the collector plate, then we would expect $f_{esc} = 0$. This is easily verified since $\tan 0 = 0$. A second limiting case is when $\alpha = \pi/2$ (i.e., $\vec{B}$ normal to plate); here one finds

$$f_{esc} = \frac{\theta_c}{\pi} = \frac{\frac{\pi}{2} + \tan^{-1} \{A(\frac{\pi}{2}) \tan (\frac{\pi}{2})\}}{\pi} = 1$$

which is expected.

It is clearly seen that as long as good control of the angle of incidence of the $\vec{B}$ field line to the collector plate is maintained the effective electron emission coefficient

$$\langle \beta \rangle_{eff} \equiv f_{esc} \langle \beta \rangle$$

can be made as small as desired, e.g., $\alpha = 5°$

$$A(\alpha) = 2\pi \left[\frac{1 + .274x}{1 + 6.25928x}\right] \quad \text{where} \quad x = \frac{a/v_0}{\omega_c}$$

$x = 0$ $\quad A(5°) = 2\pi \quad \theta_c \approx .6$ radius $\quad f_{esc} = .188 \approx \frac{1}{5}$

$x = \infty$ $\quad A(5°) = .27485 \quad \theta_c \approx .1$ radius $\quad f_{esc} = .035 \approx \frac{1}{28}$.

ORNL-DWG 77-8817

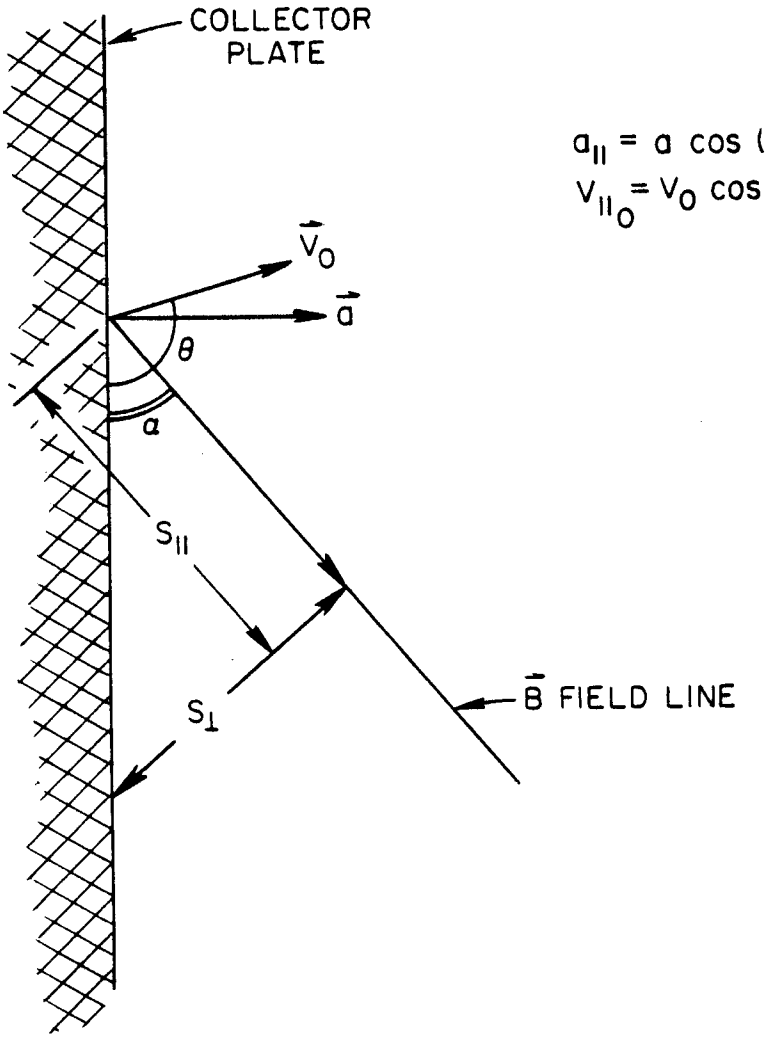

$$a_{||} = a \cos(\pi/2 - \alpha)$$
$$V_{||_0} = V_0 \cos(\theta - \alpha)$$

Figure G-1